

A Thesis Submitted for the Degree of PhD at the University of Warwick

Permanent WRAP URL:

<http://wrap.warwick.ac.uk/148071>

Copyright and reuse:

This thesis is made available online and is protected by original copyright.

Please scroll down to view the document itself.

Please refer to the repository record for this item for information to help you to cite it.

Our policy information is available from the repository home page.

For more information, please contact the WRAP Team at: wrap@warwick.ac.uk

Rhodium complexes of NHC-based pincer ligands: Catalysis and reactions through rings



Caroline Maria Storey

A thesis submitted in partial fulfilment of the requirements for
the degree of Doctor of Philosophy in Chemistry

University of Warwick

Department of Chemistry

July 2019

Table of Contents

Acknowledgements	5
Declaration of Collaborative and Published Work	7
Abbreviations list	8
Abstract	10
Chapter 1. Introduction	
1.1 Overview of the history of pincer ligands	11
1.2 <i>N</i> -heterocyclic carbenes	13
1.3 NHC-based pincer ligands and their complexes	16
1.3.1 Structural diversity	16
1.3.2 Proligand synthesis	19
1.3.3 Complexes of NHC-based pincer ligands	20
1.3.4 Decomposition pathways	25
1.3.5 Structural dynamics and ligand flexibility	27
1.3.6 Applications of NHC-based pincer complexes	31
1.4 Aims and objectives	35
1.5 References	36
Chapter 2. Synthesis and coordination chemistry of macrocyclic CNC pincer proligands	43
2.1 Introduction	44
2.1.1 Macrocyclic NHC-based ligands	44
2.1.2 Previous work in the Chaplin group	47
2.2 Proligand synthesis	51
2.3 Synthesis of palladium chloride complexes – 6-n	55
2.4 Effectiveness of Ag(I), Cu(I) and Ni(II) transfer agents	60
2.4.1 Synthesis of nickel chloride complex – 7-12	60
2.4.2 Transmetallation studies	62
2.5 Synthesis and characterisation of copper complexes	66
2.5.1 Copper(I) bromide adducts – 8-n	66
2.5.2 Copper(I) BAr ^F ₄ complexes – 9-n	68
2.6 Synthesis of rhodium complexes	71
2.6.1 Rhodium ethylene complexes – 11-n	71
2.6.2 Rhodium carbonyl complexes – 10-n	73
2.7 References	78

Chapter 3. Catalytic terminal alkyne coupling reactions	81
3.1 Introduction	82
3.2 Pre-catalyst substitution reactions	87
3.3 Terminal alkyne dimerisation	89
3.3.1 Homocoupling in CH ₂ Cl ₂	89
3.3.2 Organic preparation of <i>gem</i> -enyne – 18a	92
3.3.3 Kinetic investigations into alkyne dimerisation	93
3.3.4 Catalytic intermediates	95
3.3.5 Dimerisation mechanism	99
3.3.6 Homodimerisation in 1,2-difluorobenzene	100
3.3.7 Discussion of selectivity	103
3.4 Catalytic formation of bicyclo[4.2.0]octa-1,5,7-trienes	107
3.4.1 Scope of the reaction	107
3.4.2 Kinetic investigations	111
3.4.3 Mechanistic proposal	112
3.4.4 Supporting evidence: <i>Fac-mer</i> ligand isomerism	113
3.4.5 Supporting evidence: Intermediacy of metallocyclopentadienes	114
3.4.6 Supporting evidence: Bimetallic intermediates	118
3.4.7 Comparison with macrocyclic analogue	121
3.4.8 Summary of findings	121
3.5 References	122
Chapter 4. Terminal alkyne coupling reactions through a ring	125
4.1 Introduction	126
4.1.1 Overview of interlocked architectures	126
4.1.2 Methods of synthesising rotaxanes and catenanes	127
4.1.3 Previous work in the Chaplin group	130
4.2 Homocoupling of <i>tert</i> -butyl alkyne	133
4.2.1 Synthesis and characterisation of enyne complexes	133
4.2.2 Kinetic investigations	136
4.3 Homocoupling of 3,5-di(<i>tert</i> -butyl)phenyl alkyne	139
4.3.1 Synthesis and characterisation of Rh(III) intermediates	139
4.3.2 Synthesis and characterisation of interlocked enynes	142
4.3.4 Kinetic investigations and mechanistic implications	147
4.4 Homocoupling of a terminal alkyne with a trityl stoppering group	150
4.4.1 Preparation of trityl alkyne - 16m	150
4.4.2 Homocoupling catalysed by 11-Me	152
4.4.3 Homocoupling through rings	153
4.5 Reactivity of interlocked complexes	158
4.5.1 Dethreading studies	158

4.5.2	Exploiting the selectivity switch	161
4.5.3	Reactions with hydrogen	163
4.6	References	168
Chapter 5. Experimental		170
5.1	General considerations	170
5.2	Compounds prepared in Chapter 2	171
5.3	Compounds prepared in Chapter 3	195
5.4	Compounds prepared in Chapter 4	220
5.5	Crystallographic data	243
5.6	References	249
Chapter 6. Summary of Findings		250

Acknowledgements

First and foremost, I must thank my supervisor, Adrian Chaplin, for not only giving me the opportunity to conduct this research, but also for his continued excitement, enthusiasm and drive. I am grateful for all your help over the past four years and for pushing me to achieve things I never thought possible.

In completing this thesis, I thank the spectroscopic support staff who have helped throughout my postgraduate studies. In particular, thanks must be given to Phil Aston and Jim Morrey who went above and beyond; from running air sensitive mass spec samples at the drop of a hat to sifting through countless hard drives to retrieve raw mass spec data without complaint. Ivan Prokes, you are an NMR wizard and I cannot thank you enough for your endless support and patience with regards to NMR analyses. Thanks also go to Tobias Krämer who's computational insights have aided in understanding the mechanistic pathways investigated throughout this project.

To the Shipmen, my adoptive family, you have always kept me asking myself the question - *what would Jon Beadle do?* Thank you for welcoming me into your office and providing an outlet in which to vent group frustrations. My PhD wouldn't have been the same without you.

Chaplin group you were a nightmare, I hope you all fail ... ***Just kidding!***

Firstly, to Tom and Gemma, one thing is for certain, you brought new life and laughs into the group. Thank you for all the fun times over the years. Your friendship has definitely got me through some tough times and is something I will always treasure. Baptiste, or should I say Baptise, the forgotten middle child, thank you first for the many lifts to and from group activities, but more importantly thank you for the laughs along the way. Japan would not have been as pleasurable without you as my travel companion. So that leaves me to say "It's finished, see you tomorrow", "You can't stay here, people stuck" and in the words of Korean Billy "it's been boss, La". I wish you all the best for the rest of your time at Warwick and good luck with the write up. It has also been a pleasure to supervise an extremely talented masters student through a challenging research project and in turn adopt a little sister in Amy. You are smarter and tougher than you'll ever know, good luck in your PhD superstar.

To the Chaplin group postdocs, past and present, Thibault, Lucero and Sam, your extensive knowledge, experience and advice are attributes I continue to cherish. Sam, you in particular have given me the confidence to pursue a career in academia and for that I am infinitely grateful. Ruth and Rhiann, it feels like a long time ago that you welcomed me into the group with open arms. Ladies nights really helped me settle in at Warwick and I owe it to you both. Representing phenomenal WIS and leading by example you always gave me something to strive towards and for that I thank you.

Matthew 'pops' Gyton, I am so grateful for all your hard work on our joint projects and for your endless efforts preparing all those compounds that never made it out of the bin because they're not what we want. Who'd have thought there would be so many issues just adding two carbons, eh? Seriously though, thank you for all your help over the years, you are truly the kind of postdoc I strive to become.

JEK, putting it simply, I couldn't have asked for a better PhD brother. You have really kept me sane these past four years. We have been through some ups and downs together and there is no one I'd have rather ridden this rollercoaster with. I have some of the fondest memories of our time at Warwick. I can't sum up my appreciation fully on this page, but I'll see you in Manchester!

Riche – You have been my rock. Thank you for all the proof reading and presentation feedback you have given me over the years, as well as listening to me rant about my problems constantly, I owe you big time. I could go on forever about how you have enriched my life over the last 4 years but that will just inflate your massive ego, so instead I'll just say thanks.

Outside of chemistry, I'd like to thank my fantastic housemates, Kryssi, Caitlyn and Steph, I'm appreciative for the constant reminder of the importance of having fun. Finally, thanks, of course, go to my mum and dad without who I could not have dreamt of starting this PhD let alone finishing it. Your endless love and support has been so important to me and for that I cannot thank you enough.

Declaration of Collaborative and Published Work

This thesis is submitted to the University of Warwick in support of my application for the degree of Doctor of Philosophy. It has been composed by myself and has not been submitted in any previous application for any degree.

The work presented (including data generated and data analysed) was carried out by the author except in the cases outlined below:

- Kinetics modelling for the annulation reaction (Chapter 3) as well as, crystallographic analysis of all compounds, for which solid-state structures are described, was conducted by Dr Adrian Chaplin, Associate Professor, University of Warwick.
- The computational investigations of the mechanistic pathways of terminal alkyne dimerisation and the geometry optimisation of complex **30** were conducted by Dr Tobias Kraemer, University of Maynooth.
- Characterisation of complexes **10-Me**, **11-Me**, **19-12** and **32-12** were performed by Dr Rhiann Andrew, PhD graduate, University of Warwick.
- Synthesis and characterisation of complexes **22-12** and **28**, variable temperature kinetics measurements for the formation of complexes **19-n**, **32-n** and **33-16** and low temperature NMR data collected of **22-14** and **22-16** were conducted by Dr Matthew Gyton, Postdoctoral Researcher, University of Warwick.

Parts of this thesis have been published by the author:

1. R. E. Andrew; C. M. Storey; A. B. Chaplin, *Dalton Trans.* **2016**, 45, 8937 – 8944.
2. S. L. Apps; R. E. Alflatt; B. Leforestier; C. M. Storey; A. B. Chaplin, *Polyhedron*, **2018**, 143, 57 – 61.
3. C. M. Storey; H. P. Cook; A. B. Chaplin "Complexes of NHC-Based CEC Pincer Ligands: Structural Diversity and Applications" in *Pincer Compounds: Chemistry and Applications*, Ed. D. Morales-Morales, Elsevier, Amsterdam, 1st edn, **2018**, ch 8, pp 173 – 189.
4. C. M. Storey; M. R. Gyton; R. E. Andrew; A. B. Chaplin, *Angew. Chem. Int. Ed.* **2018**, 57, 12003 – 12006.

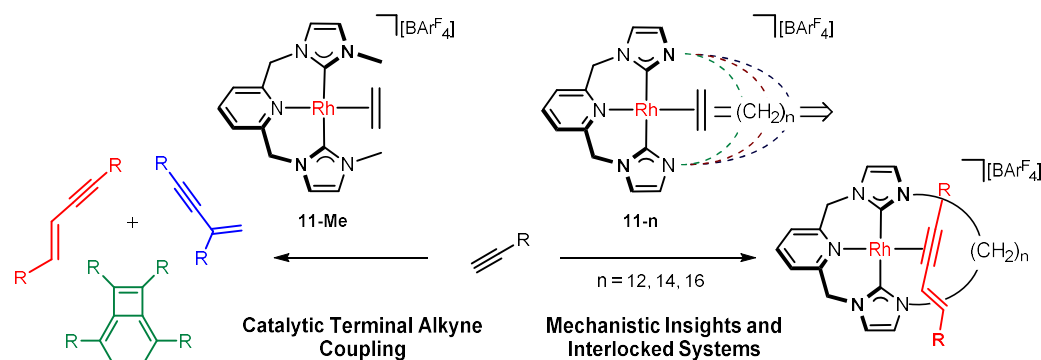
Abbreviations

Ar	Aryl
Ar'	3,5-Di(<i>tert</i> butyl)phenyl
Ar*	4,4,4-Tris(<i>p-tert</i> butyl)phenyl)butyl
Ar ^F	3,5-Bis(trifluoromethyl)phenyl
br	Broad
Bz	Benzyl
calcd	Calculated
CCDC	Cambridge crystallographic data centre
COD	1,5-Cyclooctadiene
COSY	Correlation spectroscopy
Cy	Cyclohexyl
DCC	<i>N, N'</i> -Dicyclohexylcarbodiimide
DiFB	1,2-Difluorobenzene
Dipp	2,6-Di(isopropyl)phenyl
DFT	Density functional theory
DME	Dimethoxyethane
DMF	Dimethylformamide
DMSO	Dimethylsulfoxide
eq	Equivalents
ESI	Electrospray ionisation
Et	Ethyl
<i>fac</i>	Facial
FPT	Freeze-pump-thaw
fwhm	Full width half maximum
<i>Gem</i>	Geminal
HMDS	Hexamethyldisilylamide
HMDSO	Hexamethyldisiloxane
HMBC	Heteronuclear multiple bond correlation
HMPA	Hexamethylphosphoramide
HR	High resolution
HSQC	Heteronuclear single bond quantum coherence

IR	Infrared
LDA	Lithium diisopropylamide
LR	Low resolution
Me	Methyl
<i>Mer</i>	Meridional
Mes	2,4,6-Trimethylphenyl (mesity)
MIM	Mechanically interlocked molecule
MS	Mass spectrometry
Ms	Mesyl
m/z	Mass to charge ratio
NBD	Norbornadiene
NBE	Norbornene
NHC	<i>N</i> -heterocyclic carbene
NOESY	Nuclear Overhauser effect spectroscopy
ph	Phenyl
py	Pyridyl
<i>t</i> Bu	Tertiary butyl
TBE	Tertiary butyl ethylene
THF	Tetrahydrofuran
THP	Tetrahydropyran
TLC	Thin layer chromatography
TMEDA	<i>N, N, N', N'</i> -Tetramethylethane-1,2-diamine
TMS	Tetramethylsilane
Tol	Tolyl
<i>t</i> _{1/2}	Half life
VT	Variable temperature
XRD	X-ray diffraction
Xyl	1,5-Dimethylphenyl

Abstract

N-heterocyclic carbenes (NHCs) are robust and versatile ancillary ligands for a wide range of metals. Incorporation of these strong σ -donors into *mer*-tridentate pincer frameworks confers greater thermal stability, representing an amalgamation of favourable ligand design principles that underpin many advances being made in contemporary organometallic chemistry and catalysis. This project aims to develop understanding of the mechanistic organometallic chemistry of terminal alkyne coupling reactions promoted by rhodium complexes of NHC-based pincer ligands, with the hope of exploiting this methodology in the formation of mechanically interlocked structures of macrocyclic variants of differing ring size.



Following development of a mild copper-based transmetallation procedure, rhodium(I) ethylene complexes of a series of NHC-based pincer ligands were prepared (*viz.* **11-n**; $n = \text{Me}, 12, 14, 16$). The acyclic complex **11-Me** was found to be a highly effective pre-catalyst for the head-to-tail dimerisation of aryl alkynes to afford *gem*-enynes under mild conditions and curiously their subsequent annulation into bicyclo[4.2.0]octa-1,5,7-trienes. Through *in situ* reaction monitoring using NMR spectroscopy, kinetic studies and computational modelling, the mechanism and factors which influence the selectivity of the alkyne dimerisation reaction were probed. Terminal alkyne coupling of bulky alkynes through the macrocyclic annuli of **11-n** ($n = 12, 14, 16$) are associated with increased selectivity for *E*-enynes products, which were formed exclusively in the case of $n = 12$ and 14 , as a consequence of the unique ligand topology. Using these and related results the prospects for synthesising interlocked assemblies, comprising an NHC-based pincer macrocycle and an entrapped hydrocarbon axle, have been critically assessed.

Chapter 1 – Introduction

1.1 Overview of the history of pincer ligands

Pincer ligands benefit from predictable modular binding of three donating groups around a metal center in a meridional coplanar fashion.¹ The κ^3 -chelating nature of these ligand architectures confers high thermal stability and their inherent modularity makes them highly tunable scaffolds. These characteristics have enabled pincer ligands to find a wide variety of applications across the fields of coordination chemistry and homogeneous catalysis.¹⁻⁵

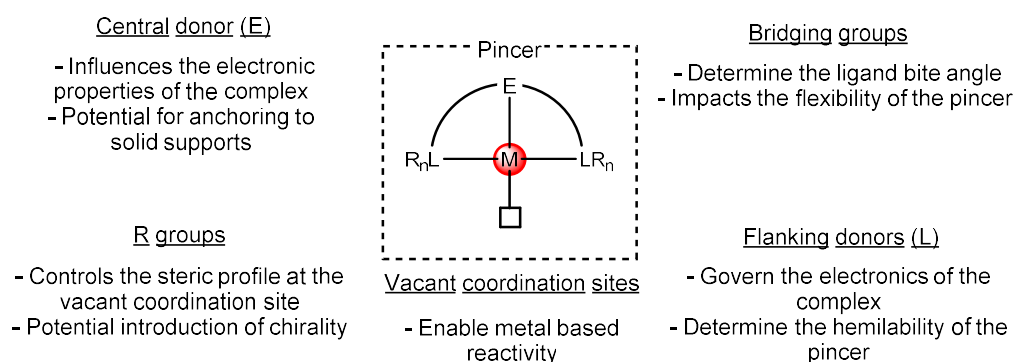
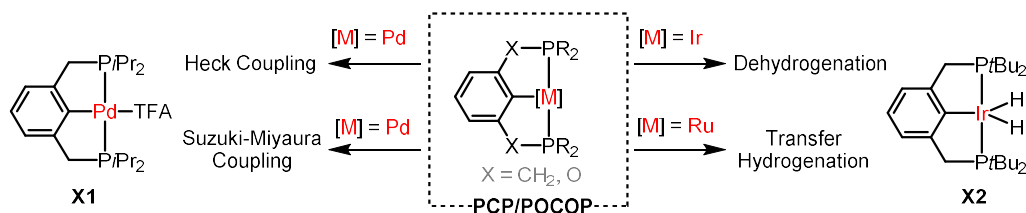


Figure 1.1.1. Pincer architectures

The first pincer complexes were reported in the late 1970's by Shaw, who described the synthesis of a range of transition metal complexes of a PCP pincer ligand.⁶ This seminal report was followed soon after by studies from Kaska, and van Koten, with the latter coining the term *pincer*.^{7,8} However, it wasn't until the now archetypal PCP ligands were re-examined in the 1980's that their extreme thermal resilience was realised.⁵ It is this characteristic that has provided the foundation for their successful application in catalysis (Scheme 1.1.1). In particular, palladium PCP complexes have been found to promote a range of C–C bond-forming reactions, including Heck and Suzuki-Miyaura variants. For instance, **X1**, which is stable at 140 °C for 300 hours, catalyses the Heck coupling of methylacrylate and either iodo- or bromobenzene with remarkably high turnover numbers (TON = 500,000 and 132,900, respectively).⁹ Using a phosphinito analogue (POCOP), bearing anisyl substituents, even higher TONs (up to 980,000) were achieved.¹⁰⁻¹² Similar palladium POCOP catalysts (R = Ph) have also been shown to catalyse the Suzuki-Miyaura coupling of a range of aryl halides with phenyl boronic acid (TON = 92,000).¹³



Scheme 1.1.1. Catalytic applications of phosphorous-based pincers

Group 9 PCP pincer complexes also display extremely high thermal stability, with some Rh examples stable for up to a week at 150 °C.¹⁴ Whilst these rhodium complexes performed poorly in catalytic dehydrogenation, highlighted by poor turnover frequencies (*cf.* TOF = 1.8 h⁻¹), the related iridium complex **X2** was effective in the dehydrogenation of cyclooctane in the presence of a sacrificial hydrogen acceptor, *viz.* *tert*-butylethylene (TBE) (TOF = 720 h⁻¹).^{14–16} Adaptation of these complexes has also enabled them to promote acceptorless dehydrogenation reactions.^{17,18} Other noble metal-based phosphine pincers have been used in catalytic transformations. Van Koten, for example, found that ruthenium PCP pincer complexes display extremely high catalytic activity (TON = 27,000) in the transfer hydrogenation of ketones (*e.g.* cyclohexanone) to their corresponding alcohols in the presence of a hydrogen donor (*e.g.* *i*PrOH) and a KOH co-catalyst.¹⁹ The high thermal stability of these complexes allows them to withstand forcing reaction conditions over prolonged reaction times, ensuring catalyst longevity and therefore overall performance.

The high tunability of pincer architectures allows for the rational design and development of metal coordination spheres tailored specifically for their intended application. Indeed, the advent of NHC ligands has led to the establishment of NHC-based pincers which are becoming increasingly prominent. Following a brief overview of the history of monodentate NHC ligands, their pincer variants will compose the remainder of this chapter.

1.2 N-Heterocyclic carbenes

N-heterocyclic carbenes (NHCs) are widely employed ligands in contemporary organometallic chemistry and catalysis, with the most common imidazolylidene and imidazolinyldine variants stronger σ -donors and weaker π -acceptors than more traditional alkyl phosphines (Figure 1.2.1).²⁰ Compared with phosphines, complexes of NHC ligands are characterised by shorter M–L bond lengths and substituents that point inwards and therefore encroach further into the metal coordination sphere.^{20–22}

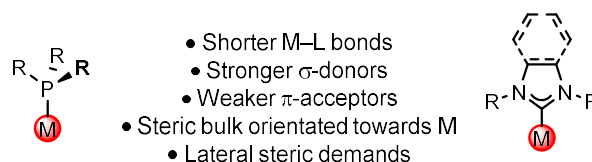
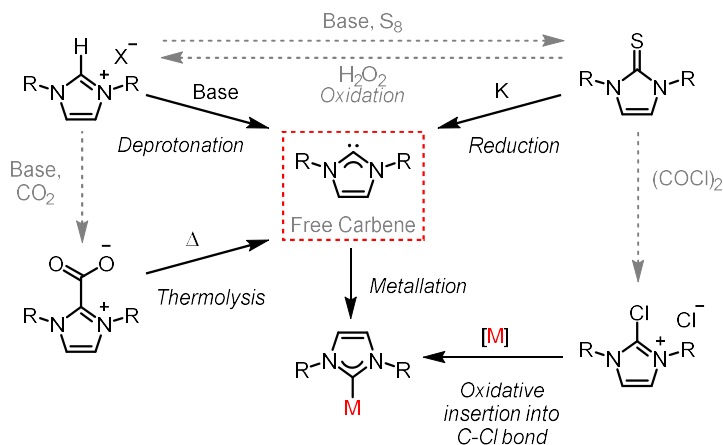


Figure 1.2.1. Comparison of phosphine and NHC ligands

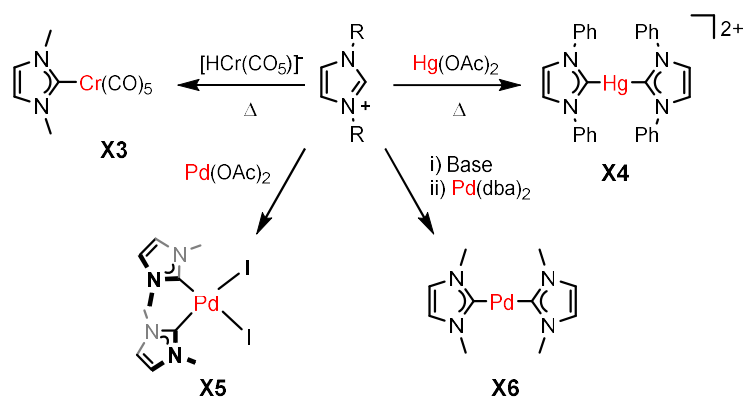
The formation of NHC complexes is typically achieved through coordination of the ‘free’ carbene, either isolated or generated *in situ*. These are commonly accessed through deprotonation of the associated azolium salt (Scheme 1.2.1), which can be purchased or readily prepared from commercial materials.^{23,24} The most prevalent syntheses of these proligands involves the double alkylation of a chosen imidazole precursor. In general, this is realised stepwise; with the first alkylation requiring deprotonation of the NH group followed by a second nucleophilic substitution with an alkyl halide to generate the bis-substituted imidazolium salt.²³ As the halide salts, these proligands are particularly hygroscopic which can pose challenges in handling and purification.²⁵ Overcoming these difficulties, the carbenic centre can be protected using trapping reactions with CO₂ or S₈, to form the air and moisture stable imidazolium carboxylates and imidazoethiones respectively.^{26,27} The free carbene can then be accessed from these species either through reductive desulfurisation of the imidazole-2-thione using potassium or *via* decarboxylative thermolysis of the NHC·CO₂ species (Scheme 1.2.1).^{28,29} Alternately, imidazole-2-thiones can be returned to their respective imidazolium salts using a peroxide oxidising agent or chlorinated to form chloro-imidazolium salts using oxalyl chloride.^{30,31} The ability of these chloro-imidazolium salts to act as masked carbene precursors has been demonstrated by Fürstner *et al.* who showed that reaction with [Pd(PPh₃)₄]

or a mixture of $[\text{Ni}(\text{COD})_2]$ and PPh_3 produced $[\text{M}(\text{NHC})(\text{PPh}_3)\text{Cl}_2]$ complexes in good yields (61 – 87%).³²



Scheme 1.2.1. Methods of accessing NHCs

Predating the isolation of the first free NHC considerably,³³ the first well-defined NHC complexes were reported independently by Wanzlic³⁴ and Öfele in 1968;³⁵ each prepared by direct metalation of imidazolium proligands to generate Cr(0) and Hg(II) complexes **X3** and **X4**, respectively (Scheme 1.2.2). However, it wasn't until a seminal report by Herrmann in 1995 that the prowess of NHC ligands was truly realised.³⁶ Recognising the issues associated with traditional phosphine-based catalysts employed in Heck coupling reactions,³⁷ Herrmann developed NHC-based analogues **X5** and **X6** which showed significantly enhanced catalytic performance. Using Heck coupling as the primary example, kinetic studies showed enhanced catalytic performance of **X5** compared with the phosphine counterparts even for deactivated aryl bromides ($\text{TOF} = 15,000 \text{ h}^{-1}$) and aryl chlorides, despite a prolonged induction period. Furthermore, TONs in excess of 250,000 could be achieved using **X6**, whilst direct phosphine counterparts gave varied results depending on the phosphine and substrate employed. Even following substantial reaction optimisation, the Heck coupling of 4-bromobenzonitrile with ethyl acrylate using $[\text{Pd}(\text{Ptol}_3)_2]$ only achieved a maximum TON of 134,000 and performed particularly poorly in the coupling of activated aryl chlorides ($\text{TON} = 51$) due to catalyst decomposition under the forcing reaction conditions (150°C).^{36,38–41}



Scheme 1.2.2. Early NHC complexes

Inspired by this pioneering work, the use of NHCs as robust ancillary ligands in homogeneous catalysis blossomed.^{21,42–44} Grubbs' catalysts **X7** and **X8**, now synonymous with alkene metathesis,⁴⁵ and the 'PEPPSI' catalyst **X9**, which catalyses a plethora of traditional C–C coupling reactions,^{46–48} are archetypal examples (Figure 1.2.2), but NHC complexes have been employed in an array of pivotal organic transformations.^{48–51} Prepared through oxidative addition of biphenylene to the parent Au(I) species, the Au(III) complex **X10**, for instance, has recently been found to act as a hard Lewis-acid centre promoting Michael additions with high fidelity.⁵²

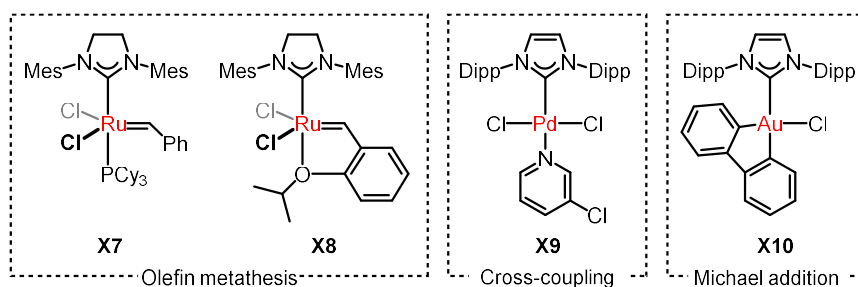


Figure 1.2.2. Representative NHC-based homogeneous (pre)catalysts

This privileged ligand class has grown to encompass both monodentate and polydentate variants, with CEC pincer variants a particularly prominent line of enquiry.⁵³

1.3 NHC-based pincer ligands and their complexes

1.3.1 Structural diversity

Although CEC ligand architectures had been described previously,⁵⁴ the first tridentate NHC pincer complexes were reported independently by the groups of Crabtree and Danopoulos in 2001.^{55,56} These investigations focused primarily on the preparation of palladium(II) halide complexes of pyridyl- and lutidyl-based bis(imidazol-2-ylidene) pincer ligands (**Aα** and **Bα** respectively) and followed shortly thereafter by the isosteric carbon centred phenyl- and xylyl-based bis(imidazol-2-ylidene) analogues (**Aca** and **Bca** respectively).⁵⁷ Over the intervening 18 years, the structural diversity of NHC pincer complexes has broadened considerably (Figure 1.3.1). A wide array of structural modifications to the central donor (E), pincer scaffold (**A-H**) and the NHC groups (**α-t**), as well as different flanking substituents (R), has significantly expanded the scope of this burgeoning ligand class.

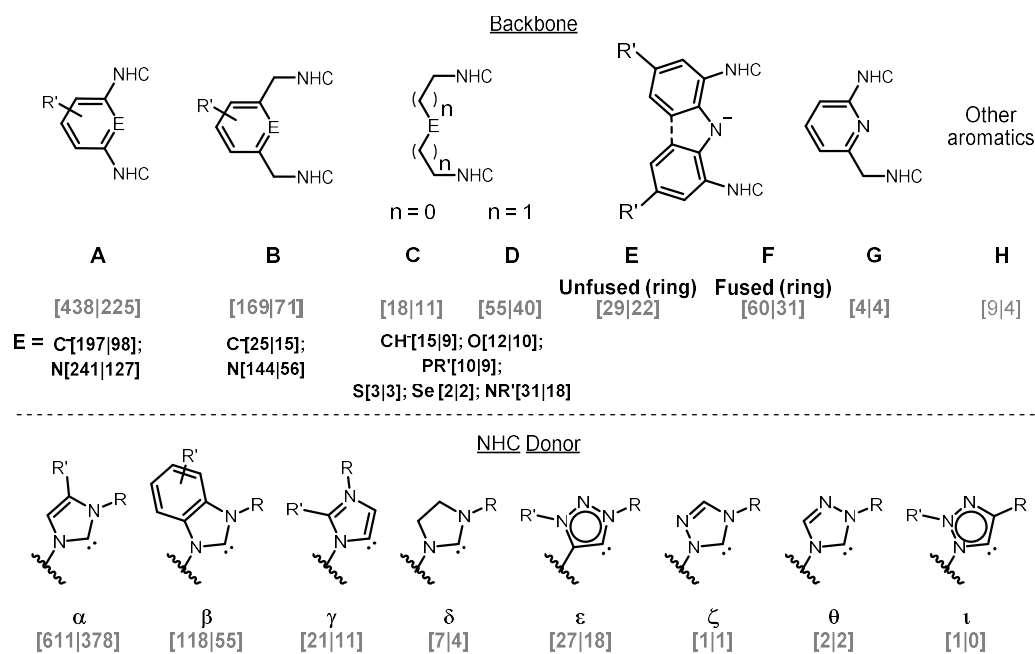
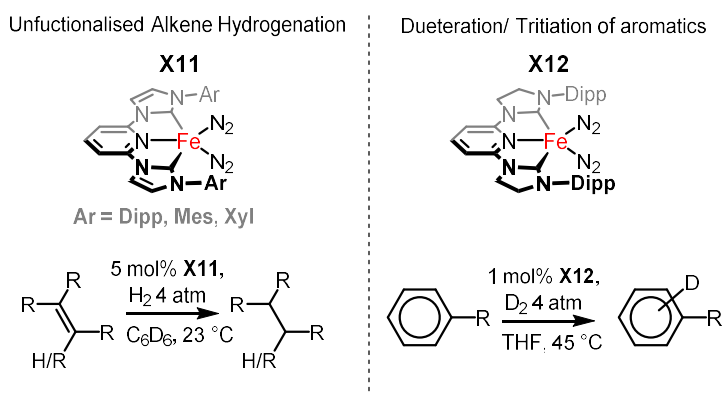


Figure 1.3.1. Scope of CEC-based pincer ligands [number of well-defined κ^3 -complexes | crystal structures deposited in the CSD]

A recent evaluation of the literature[‡] found that the majority of described CEC pincer complexes feature the well-established imidazolylidene (α) and benzimidazolylidene (β) appendages (611 and 118 complexes, respectively). Curiously, unlike their unsaturated counterparts and the prevalence of monodentate equivalents, only seven examples of saturated imidazolinylidene containing pincers (δ) have been isolated and characterised to date.^{58–61} Aiming to exploit the enhanced σ -donating capacity of these groups, Chirik developed $A_N\delta$ complex **X12** for application in the hydrogenation of sterically crowded alkenes (Scheme 1.3.1).^{60,62} As part of this work, **X12** was serendipitously discovered to promote H-D exchange reactions between H_2 and the deuterated solvent (C_6D_6). This reactivity was exploited to enable selective deuteration or tritiation of aromatics. Highlighting the differences in NHC donor capacity, similar reactivity is not observed for the $A_N\alpha$ analogue **X11** (Scheme 1.3.1).



Scheme 1.3.1. Reactions of $A_N\alpha$ and $A_N\delta$ pincer complexes

Several different approaches have been employed in the literature to evaluate the donor strength of NHCs, and the widely agreed trend in overall donor character (both σ -donating and π -accepting) follows the order; 1,2,4-triazol-5-ylidene (ζ) = 1,3,4-triazol-5-ylidene (θ) < benzimidazol-2-ylidene (β) < imidazol-2-ylidene (α) < imidazolin-2-ylidene (δ) \leq 1,2,3-triazol-5-ylidene (ϵ/ι) < imidazol-4-ylidene (γ), *ceteris paribus*.^{63–67} Whilst these trends are useful, they are based predominantly on the study of monodentate examples and thus do not encompass deviations in the electronic properties of these ligands caused by

[‡] Based on a comprehensive structure-based search up until June 2019, conducted using a combination of SciFinder® and the Cambridge Structural Database (CSD)

distortions away from ideal binding geometries. Small perturbations have been reported to considerably impact the donor characteristics of NHC ligands owed to reductions in orbital overlap.⁶⁸

An emerging branch of the CEC ligand class involves flanking mesoionic NHC donors: imidazol-4-ylidenes (**γ**, 3%) and 1,2,3-triazol-5-ylidenes (**δ** and **ι**, 4%).^{69–73} During the complexation of bis(imidazolylidene) pincers, coordination through the ‘abnormal’ C4 position can compete with traditional C2 binding,^{74–77} thus alkyl blocking groups are often employed to encourage this unconventional ligation. Indicative of the stronger ligating character of these terminal donors, Albrecht *et al.* have described a series of Rh(CCC) complexes in which a significant rate enhancement in intramolecular CH bond activation is observed for the **Cγ** complexes *versus* the conventional **Cα** equivalents.⁷⁸

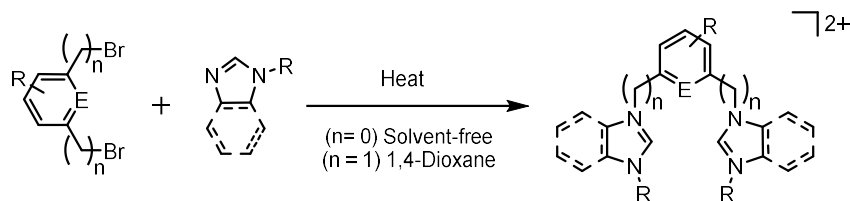
Diversification of central donor (E) is another structural modification that has also been explored for CEC pincer complexes. The aforementioned search of the literature[†] identified nitrogen as the most prominent central donor found in the commonly employed pyridine and lutidine backbones (**A_N**, **B_N** and **G**), but also in less well-established amine (**D**) and amido-based scaffolds (**E – F**). Incorporation of anionic diarylamido (**E**) and carbazole (**F**) units results in very strongly donating pincer ligands that are of interest for applications involving the transition metal promoted activation of inert chemical bonds (*e.g.* C–C and C–H). Pincers **C** and **D** highlight the capacity for incorporation of a more diverse range of heteroatoms into the backbone. Notably, the use of flexible backbones with central oxygen and sulfur donors can enable useful hemilabile coordination and thus provide access to an additional vacant coordination site during catalytic transformations (*vide infra*).

Despite the aforementioned structural variations, traditional **Aα** and **Bα** ligands remain the most widely investigated in the literature (up until 06.2019),[†] representing over half of the total number of isolated complexes to date (607 of 782 compounds) and accounting for 73% of the total XRD structures deposited in the CSD (296 of 408 structures).[†] On the whole, whilst the scope of CEC pincers

has significantly broadened over the past two decades, full exploitation of this diversity has yet to be realised.

1.3.2 Proligand synthesis

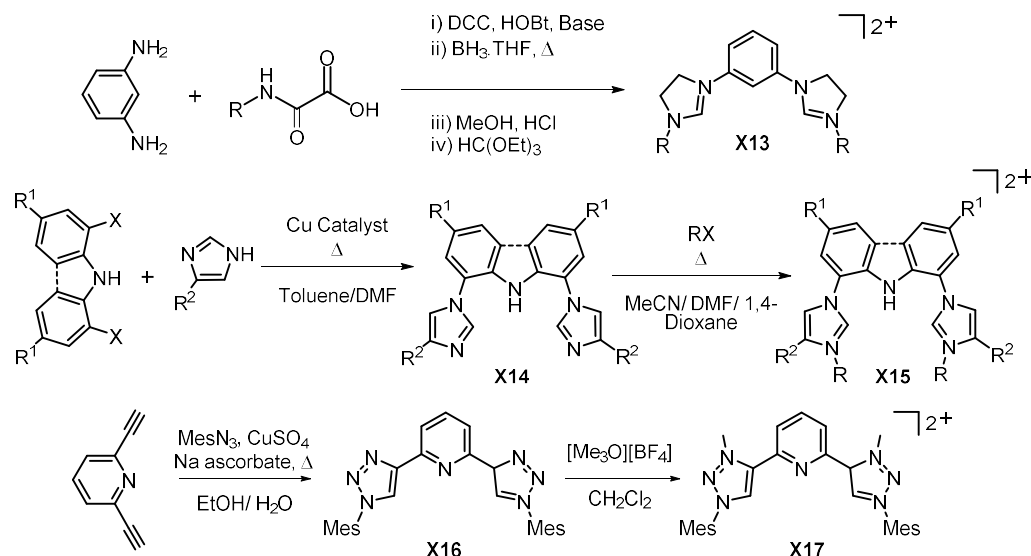
The prominence of bis(imidazolylidene) (**α**) and bis(benzimidazolylidene) (**β**) functionalised pincers is reconciled by straightforward preparative procedures involving commercially available or accessible reagents. The synthesis of CEC proligands typically follows analogous procedures to those employed for their non-chelating azolium counterparts (*vide supra*). For instance, the synthesis of type-**A** and **B** proligands is most commonly achieved by alkylation of functionalised imidazoles with bis(bromo) or bis(bromomethyl) arenes. These straightforward one-pot reactions enable the bis(imidazolium) salts to be formed in yields in excess of 95% (Scheme 1.3.2).^{79–82} Reflecting the high-energetic barriers associated with aromatic substitutions (S_NAr) relative to aliphatic systems, the formation of type-**A** proligands requires significantly more forcing conditions and longer reaction times compared with methylene bridged type-**B** structures.



Scheme 1.3.2. Synthesis of **A** and **B** proligands

Exploiting the contrasting energies associated with alkyl vs aryl substitutions, different NHC units can be sequentially introduced to either side of the asymmetric 2-bromo-6-bromomethylpyridine central donor to afford mixed NHC systems of **G** ligands.⁸³ Moreover, through adaption of this general procedure less common acyclic CEC proligands (**C** and **D**) have been accessed.^{84,85} Recently, following its employment in the formation of **A_Nδ** complex **X12**,⁶⁰ a report by Asay *et al.*, extended this methodology to the preparation of the first examples of **B_Nδ** and **B_Cδ** ligands and their related complexes.^{86,87} These studies dispute the idea that the incorporation of saturated imidazolinyldine donors (**δ**) into pincer architectures requires particularly laborious multi-step syntheses (*cf.* **X13**,

Scheme 1.3.3); an impression that may have contributed to the relative paucity of these systems to date.^{59,61}



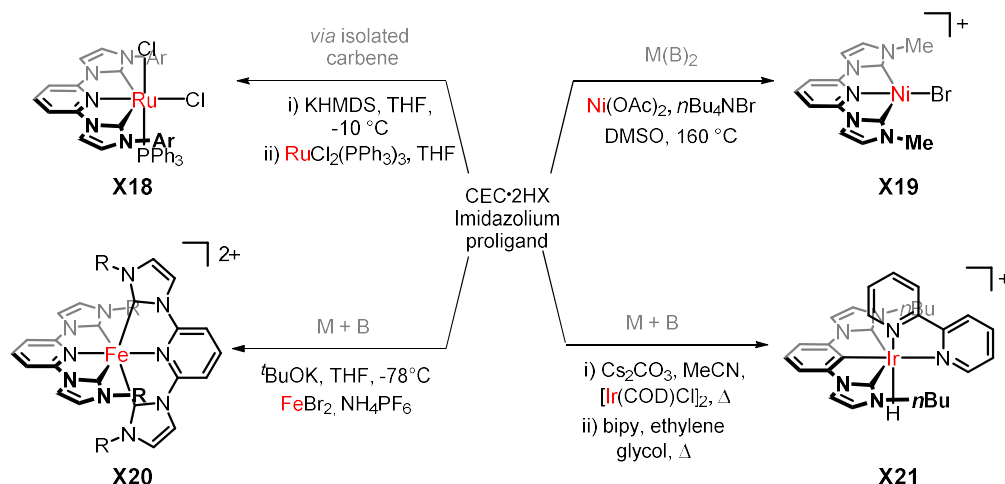
Scheme 1.3.3. Synthesis of CEC pincer prolignands

In contrast, the emerging class of anionic amido-centred scaffolds, **E** and **F**, are prepared through a markedly different methodology (*e.g.* **X15**, Scheme 1.3.3); employing a copper-catalysed Ullman-type coupling followed by alkylation at the N3 position of the imidazole unit to form the desired imidazolium salt in yields of up to 90%.^{88–90} Of contemporary interest is the use of mesoionic 1,2,3-triazolium donors (**ε** and **ι**), which can be introduced into pincer moieties using copper catalysed alkyne-azide cycloaddition ‘click’ reactions followed by alkylation using Meerwein’s salt (Scheme 1.3.3).⁹¹ Complimentary reaction pathways involving either the reaction of the alkyne functionalised central scaffold with two equivalents of a simple azide or the reverse, using an azide backbone with two equivalents of alkyne, have allowed access to both triazole isomers **ε** and **ι**, respectively (*cf.* **X17**).^{91,92} Already utilised in the synthesis of **A**, **D** and **F** ligands, this procedure could provide the foundation for further expansion of this ligand class.^{72,93}

1.3.3 Complexes of NHC-based pincer ligands

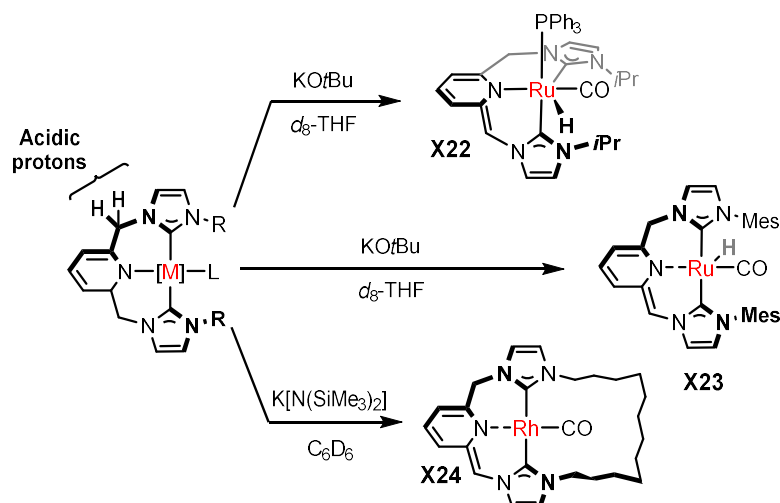
Complexation through reaction of the isolated carbene with an appropriate metal precursor is conceptually the simplest method and indeed has found practical application, for example in the synthesis of **X18** (Scheme 1.3.4).⁹⁴ However, the

inherent high reactivity of the 'free' carbene makes this pathway practically challenging. Indeed, the number of isolated CEC pincer carbenes described in the literature is limited to just a few examples,^{84,95–101} hindering the universal applicability of this methodology. Avoiding the difficulties associated with carbene isolation, low temperature deprotonation of the azolium proligand in the presence of a chosen metal fragment is an alternate pathway to CEC complexes such as **X20** (Scheme 1.3.4).



Scheme 1.3.4. Previously reported complexation methods involving free carbenes

Direct complexation of the *in situ* generated carbene to a metal centre in this way is also not always straightforward due to the strongly basic conditions required to deprotonate the pre-carbenic centre of the associated azolium proligand (pK_a 21 – 24).¹⁰² As a result, this methodology is not well suited to ligands containing acidic functionalities, such as the methylene bridges in type-**B** pincer morphologies. Mirroring PEP analogues,^{103–109} this deprotonation results in dearomatisation of the ligand backbone (Scheme 1.3.5). Whilst dearomatisation typically renders the resulting complexes unstable,¹¹⁰ these systems have the potential to offer niche metal-ligand cooperative activity in certain catalytic processes; *viz.* **X22** in imine hydrogenation and **X23** in ester hydrolysis and CO₂ hydrogenation.^{75,111,112}

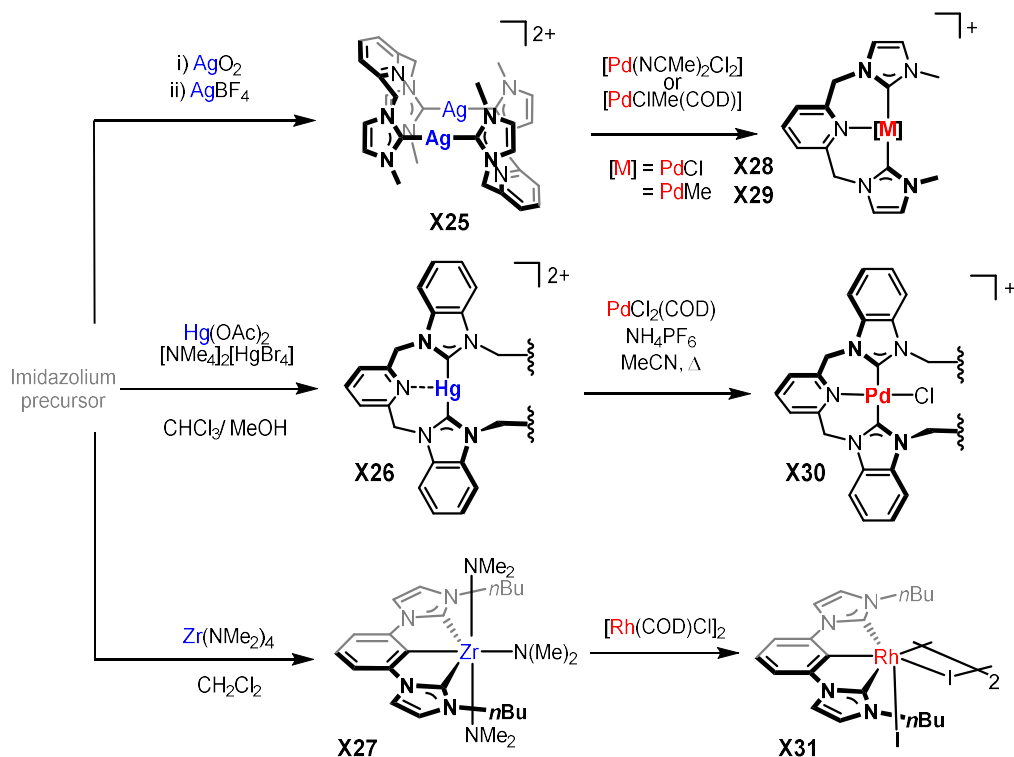


Scheme 1.3.5. Deprotonation of methylene linkages to form dearomatised pincers

Avoiding these functional group incompatibility issues, alternate ‘accessible syntheses’ have been developed, which employ milder, equilibrium conditions involving a weak external bases (*e.g.* $\text{CO}_3^{2-}/\text{NEt}_3$) or internal bases (*e.g.* $\text{M}[\text{OAc}]$, M_2O or $[\text{M}]\text{NR}_2$) along with elevated temperatures to achieve complexation.¹¹³ The utility of these reaction conditions have been demonstrated in the synthesis of **X19**, where reaction of the **Anα** proligand with the basic metal precursor $\text{Ni}(\text{OAc})_2$ in the presence of a bromide source ($n\text{Bu}_4\text{NBr}$) led to the formation of **X19**. Likewise, refluxing a solution of an **Anα** imidazolium salt, CsCO_3 and $[\text{Ir}(\text{COD})\text{Cl}]_2$ followed by a ligand exchange reaction afforded **X21**, demonstrating the utility of these equilibrium controlled ‘accessible syntheses’.¹¹⁴

Milder conditions can also be achieved through transfer of the NHC donors from one metal centre to another in a transmetallation reaction (Scheme 1.3.6). Targeting metals with weak carbene-metal bonds which can be readily displaced by the preferred metal fragment, carbene transfer reactions are driven by favourable thermodynamics, aided by the formation of insoluble metal halides. Undeniably the most commonly explored NHC-transfer agents are silver-based systems,¹¹⁵ which are typically formed through reaction of the chosen azolium salt with Ag_2O . Whilst these silver complexes can be isolated, they are typically generated *in situ* and used directly in the synthesis of the desired NHC complex.^{81,116,117} Numerous silver CEC complexes have been prepared and isolated in the literature,^{118,119} with the nature of the anion an important

experimental variable. For instance, whereas Ag(I) CEC halide complexes primarily form homobimetallic species (CEC-(AgX)₂),¹²⁰ those featuring more weakly coordinating anions often adopt dimeric structures (*viz.* **X25**).¹²¹ In some cases, these species also show reversible Ag-C bond cleavage in solution rapidly interconverting between both dimeric isomers (*syn*- and *anti*-) as well as the mononuclear species, illustrating the weak metal interactions and facile dissociation of these complexes.^{118,121-123}

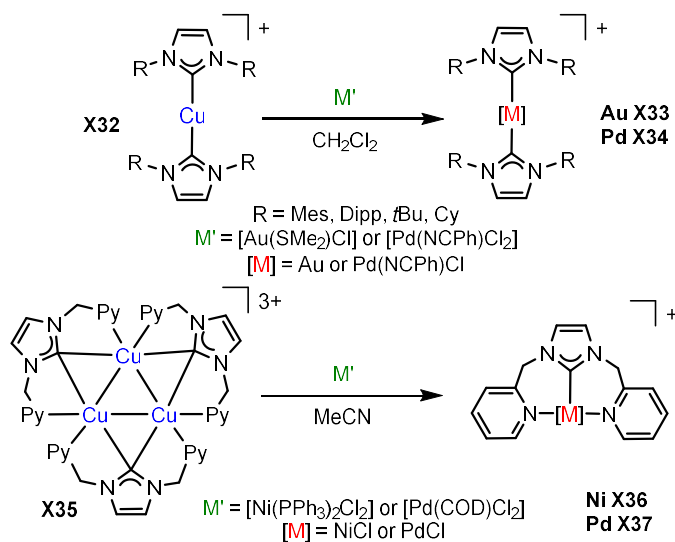


Scheme 1.3.6. Transmetalation of CEC pincer ligands

Silver transmetalation has been successfully employed for many NHC-based pincer ligands, exemplified in the transfer of the **Aα** ligand from the dimeric silver complex **X25** to palladium, forming **X28** and **X29** in 81% and 86% yield respectively (Scheme 1.3.6).^{86,121,124} Whilst the relative simplicity of these reactions has no doubt contributed to their prominence, the inherent light sensitivity and redox activity of silver(I) complexes, along with the difficulty in removing silver containing by-products, has stimulated investigations into alternative transfer agents.

The formation of CCC complexes typically requires triple deprotonation or sp^2 CH bond or CX activation to achieve the targeted tridentate coordination of the pincer. In this context, zirconium CCC transfer agents have shown potential; conveniently accessed by reaction of the proligand with $[Zr(NMe_2)_4]$, subsequent transmetallation from **X27** to **X31** has been demonstrated.¹²⁵ Another example comes from the Wright group who have described the direct mercuration of the $\text{AN}\beta$ -based macrocycle forming **X26** which can be reacted with $[PdCl_2(COD)]$ to generate **X30** in 57% yield.¹²⁶

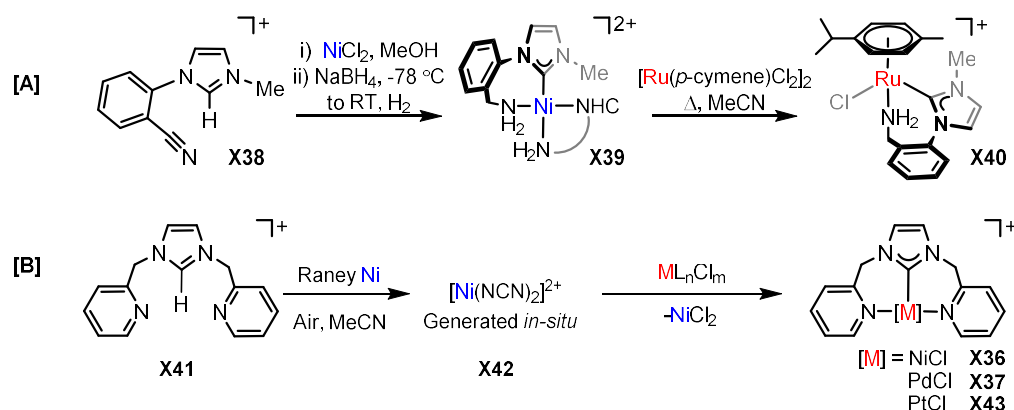
Over the past decade the use of Cu(I) in transmetallation reactions has advanced considerably, as highlighted in a recent review by Cazin *et al.*,¹²⁷ but examples of CEC complexes of copper remain scarce (10 examples).^{93,128–131} The first copper transmetallation strategy was reported in 2009 and involved the transfer of a simple monodentate imidazolylidene moiety to both sulfur (to form the NHC-thione) and ruthenium.¹³² Since then this methodology has been developed extensively by Cazin *et al.* and applied in the synthesis of a range of late transition metal complexes of monodentate carbenes, including; cyclo(alkyl)amino carbenes (CAACs), abnormal carbenes and mesoionic carbenes (MICs).^{127,133} Of note, adaptation of this methodology using a range of bis(NHC) copper complexes **X32** has allowed access to a range of homo- and heteroleptic gold and palladium complexes (Scheme 1.3.7).^{134,135}



Scheme 1.3.7 Selected examples of Cu(I) NHC transfer agents

Copper transmetallation reactions are not limited to monodentate carbenes and examples have emerged describing the use of copper(I) compounds in the transmetallation of polydentate NHC-based ligands. Work by Chen *et al.*, for instance demonstrated the use of the trimeric **X35**, bearing three NCN pincer moieties, in the formation of monomeric group 10 complexes **X36** and **X37** (Scheme 1.3.7).¹³⁶

NHC-based nickel(II) complexes have also been used as carbene transfer agents to access a range of late transition metal complexes, albeit to a lesser extent than their coinage metal counterparts. Selected examples of nickel transmetallation of multidentate NHC ligands are highlighted below in Scheme 1.3.8.^{137,138}



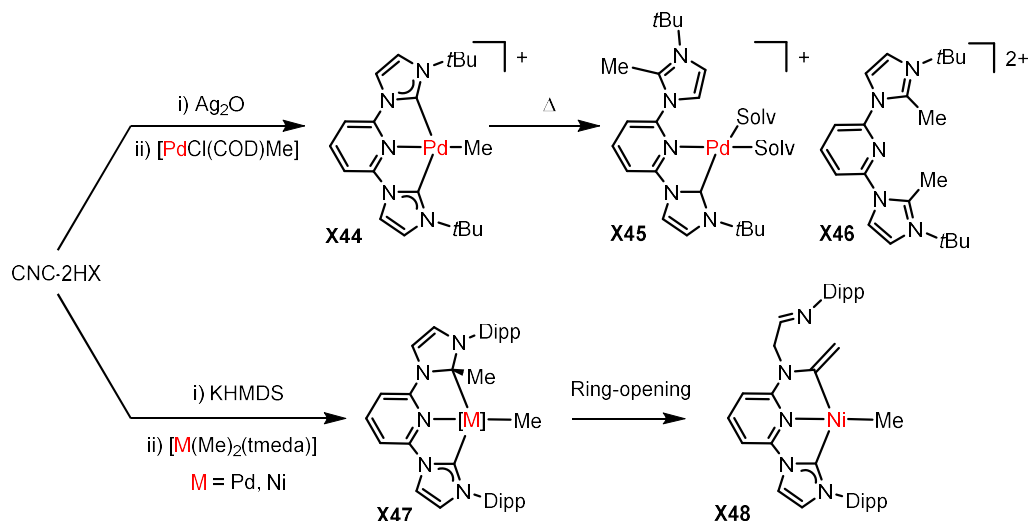
Scheme 1.3.8. Previous examples of nickel complexes used as carbene transfer agents

Interestingly, evaluation of the effectiveness of copper and nickel transfer agents in the synthesis of **X36** and **X37** indicates that in these cases **X41** outperforms **X35**.¹³⁸ However, in spite of the abundance of Ni CEC complexes in the literature, their use as transfer agents was unprecedented before this work (Chapter 2).¹²¹

1.3.4 Decomposition pathways

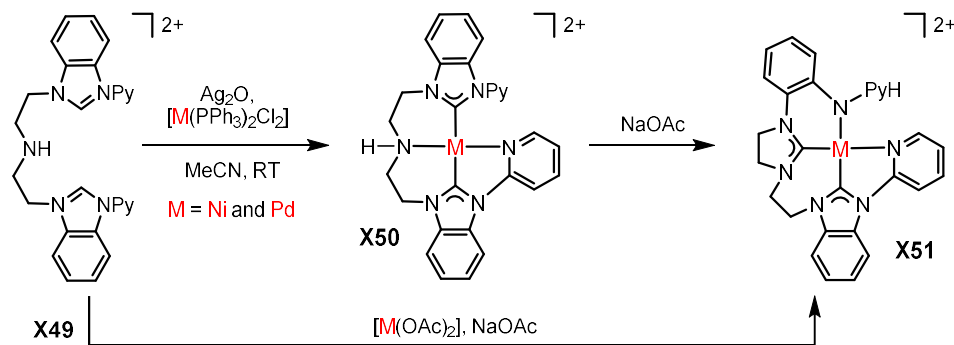
Despite high thermal stability relative to monodentate counterparts, NHC-based pincers have been shown to decompose *via* a number of different pathways. For instance, CEC complexes bearing alkyl ligands are susceptible to reductive cleavage of the M–NHC bond. Palladium CNC methyl complexes (*e.g.* **X44**) can undergo reductive elimination at elevated temperatures to form the pendant methyl imidazolium palladium(0) complex **X45** alongside bis(imidazolium) salt **X46**, palladium black and several other unidentified decomposition

products.^{116,117} In more sterically encumbered analogues, the methyl group instead migrates to the C2 carbon generating the palladium bound carbanion species **X47**.¹³⁹ The rate and nature of this decomposition is also influenced by the metal centre; whereas the palladium complex saw no further decomposition, the nickel congener underwent NHC ring opening to give **X48** (Scheme 1.3.9).¹⁰⁰



Scheme 1.3.9. Decomposition pathways of CEC pincers

In addition to these reductive decompositions, ligand rearrangement reactions have also been described (Scheme 1.3.10).¹⁴⁰ For instance, during the investigation into the coordination chemistry of pentadentate proligand **X49**, four coordinate complexes **X50** were shown to undergo an unexpected ligand rearrangement in the presence of excess Na(OAc) to form a new NCCN complex **X51**. The mechanism for this process has been proposed as a C–N bond cleavage and C–N bond formation step facilitated by the deprotonation of the central secondary amine donor. However, similar reactivity has not been described for analogous complexes absent pyridine appendages.^{84,141–143}



Scheme 1.3.10. Ligand rearrangement reaction of CNCN complex

1.3.5 Structural dynamics and ligand flexibility

Initially introduced into the pincer backbone for improved solubility,¹⁴⁴ the presence of methylene spacers in CEC pincer ligands (type-**B**) permits adoption of more ideal metal coordination geometries compared to type-**A** analogues, as evidenced by their respective bite angles (172° **B**; 154° **A**).[‡] Comfortably adopting conformations with carbenic donors lying directly *trans*-disposed to one another, type-**B** complexes typically bear flanking substituents that ultimately encroach further into the metal coordination sphere (Figure 1.3.2). Yawing of the NHC donor in type-**A** scaffolds has been shown to extend M–C bond lengths, reduce metal-ligand orbital overlap and by extension dampen π -acceptor character.⁶⁸ As a result, perturbations in NHC binding enforced by the pincer profile can augment the electronic properties at the metal centre.

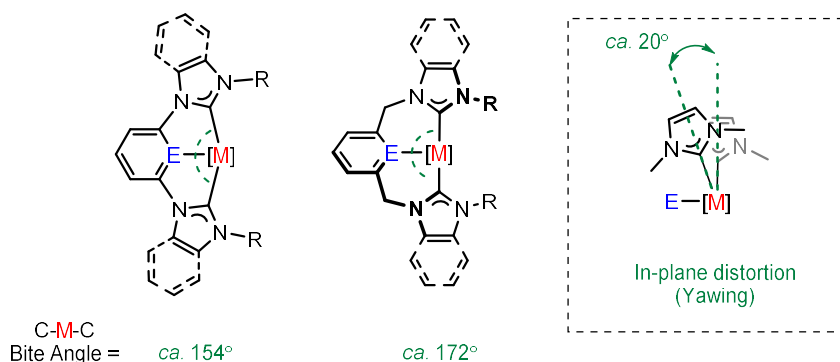
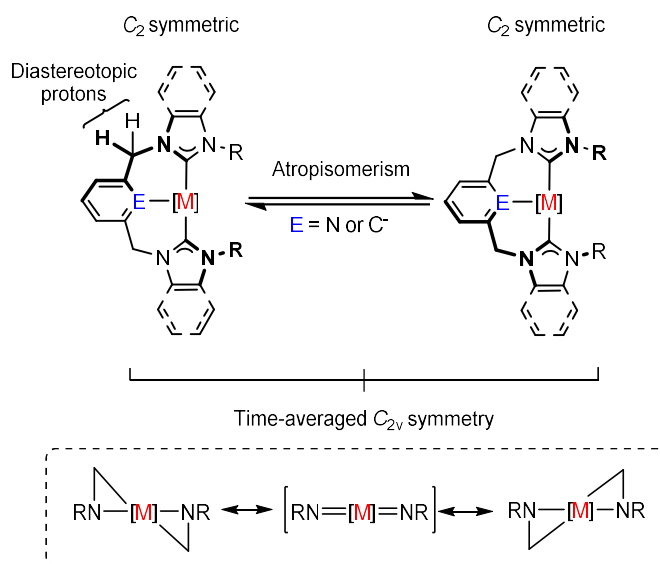


Figure 1.3.2. Coordination geometries of type-**A** and type-**B** pincers

Whereas type-**A** bearing complexes adopt a broadly planar coordination sphere, the methylene bridges in **B** systems introduce additional flexibility to the backbone which manifests itself in a characteristic buckling of the ligand framework. Twisting of the central aromatic ring and associated puckering of the methylene linkers results in the distal wingtip substituents (R) being projected to opposing sides of the coordination plane. As a result, formation of square-planar **B** complexes typically leads to two distinct C_2 symmetric atropisomers (Scheme 1.3.11). However, in solution it is not uncommon for these compounds to be appreciably dynamic, interconverting between the two chiral conformers and displaying time-averaged C_{2v} symmetry on the NMR timescale.

Seminal investigations into this phenomena were conducted using Pd(II) complexes (**X52**, Figure 1.3.3). Using variable temperature ^1H NMR spectroscopy

the barriers for interconversion were determined to be *ca.* ΔG^\ddagger 50 kJmol⁻¹ for lutidine-centred pincers (E = N) and *ca.* ΔG^\ddagger 70 kJmol⁻¹ for the xylene-centred counterparts (E = C⁻), for both α and β donors.^{145,146} Supported by DFT calculations, the more facile atropisomerism observed for the lutidine-centred pincers was attributed to a mechanism involving complete or partial dissociation of the central nitrogen donor. In support of this hypothesis, the rate of atropisomerism was faster in the presence of coordinating counter anions, which promote this reversible dissociation.¹⁴⁶



Scheme 1.3.11. Atropisomerism of type-**B** pincer ligands

In addition, variations in solvent as well as wingtip substituents have also been shown to have a measurable impact on the energetic barrier and therefore the rate of fluxionality.⁸² Whereas varying between *n*-alkyl and macrocyclic substituents has been shown to have very little impact on the energetic barrier,¹⁴⁷ work by Danopoulos *et al.* showed that more sterically demanding aromatic flanking substituents (R = Mes or Dipp) significantly diminish the rate of this process.¹⁴⁸ This is presumably due to steric clashes between the terminal N-appendages which destabilise the C_s symmetric transition state evoked during their interconversion (Scheme 1.3.11).

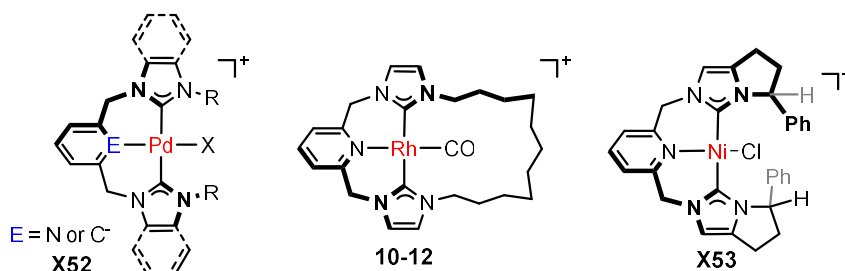


Figure 1.3.3. Systems in which atropisomerism has been investigated

More recently, these solution dynamics have been interrogated in the Chaplin group using macrocyclic type-**B** Rh(I) carbonyl complex **10-12** (Chapter 2.1.2). Furthermore, preparation of a single atropisomer has been achieved through the incorporation of chiral appendages to the carbene wingtips in the form of fused cyclopentyl rings (*viz.* **X53**, Figure 1.3.3).¹⁴⁹ Removal of the structural dynamics associated with this ligand architecture introduces the potential for application in asymmetric catalysis.

The increased flexibility of type-**B** pincer frameworks also introduces uncertainty regarding the coordination geometry, with the methylene bridges evoking a higher propensity for adopting a facial coordination mode. The absence of a constrained aromatic ring system and the presence of flexible methylene linkers allows the ligand freedom to ligate both meridionally and facially on minor changes to the complex structure.^{112,150} The ability to assume facial coordination is of particular note for aliphatic **C** and **D** pincers which feature a flexible sp³ hybridised linker (E = CH₂,^{71,151–153} O,¹⁵⁴ NH,^{143,155,156} and P^{157,158}); exemplified by **X56** and **X57**, bearing an ether tethered **Doα** ligand. Although the **Doα** ligand is flexible and contains a hemilabile ether linkage, **X56** showed limited activity towards olefin metathesis.¹⁵⁴

The ability of CNC pincers to adopt alternative coordination geometries has been explicitly investigated by the Chaplin group using the Mo(CO)₃ fragment.¹⁵⁹ The synthesis of two NHC pincer complexes of varying backbone composition (**Anα** (**X55**) and **Bnα** (**X54**)) showed opposing coordination geometries, *mer* and *fac* respectively. Probing this divergence using DFT calculations of truncated models of these pincer complexes revealed a negligible difference in energy between the isomers of the flexible **Bnα** ligand, with a slight energetic preference for the

experimentally observed *fac*-isomer ($\Delta G_{fac,mer} = -0.5 \text{ kJmol}^{-1}$), whereas a substantial preference for the *mer*-isomer was confirmed for the planar **A α** ligand ($\Delta G_{fac,mer} = +42.6 \text{ kJmol}^{-1}$).

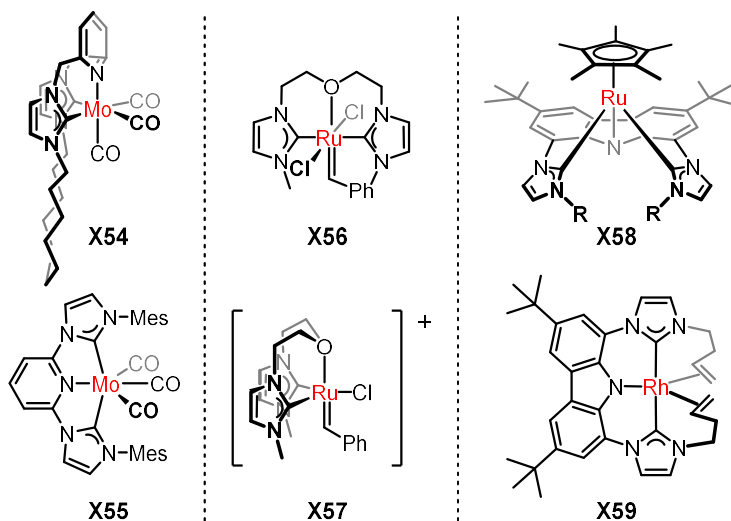
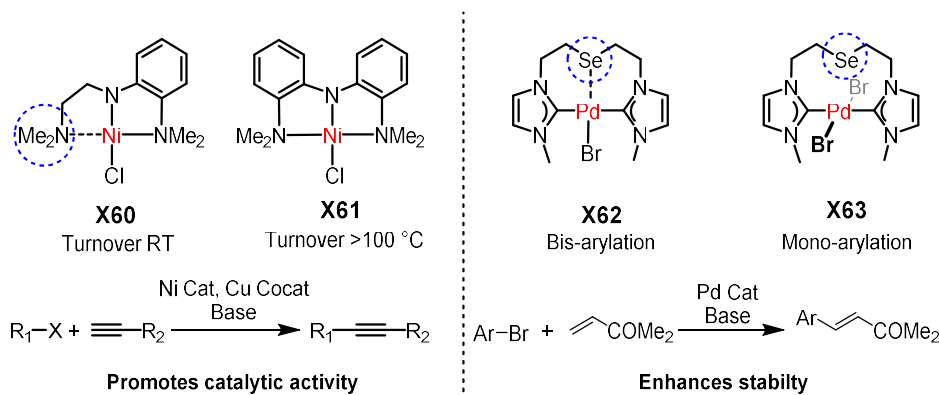


Figure 1.3.4. Examples of divergent coordination modes of CEC pincer ligands

Contrasting the flexibility of **B** ligands, the non-bridged **A** scaffolds and the tricyclic carbazole ligands **F**, are conformationally rigid and lead almost exclusively to *mer*-coordination. The lone exception is ruthenium complex **X58** bearing the anionic **F α** ligand.¹⁶⁰ In this structure, the sterically demanding facial capping Cp* ligand enforces facial coordination of the type-**F** pincer. In the absence of the conformational constraints imposed by the Cp* ancillary, the pincer binds to rhodium in **X59** in the expected *mer*-configuration. This rhodium complex is further notable for π -coordination of the terminal alkene substituents and adoption of a trigonal bipyramidal geometry (Figure 1.3.4).¹⁶¹

Although conferring chemical and thermal robustness, the high fixity of pincer architectures restricts the number and position of available coordination sites on the bound transition metal. The presence of hemilabile donors can overcome this issue, enabling temporary access to an additional coordination site on dissociation. This type of reactivity has the potential to increase the scope of reactions which can be promoted by pincer complexes,^{162–166} but has yet to be exploited in catalysts bearing CEC ligands. The potential of hemilabile coordination is illustrated by the contrasting catalytic activity of nickel(II) NNN complexes **X60** and **X61** (Scheme 1.3.12).^{167,168} Sonogashira cross-coupling reactions catalysed by **X61** required relatively forcing reaction conditions (100

°C), whereas reactions using **X60** proceeded at room temperature. Detailed kinetic experiments and inhibition studies supported rate limiting decoordination of the primary amine donor reconciling the low activity of **X61**.

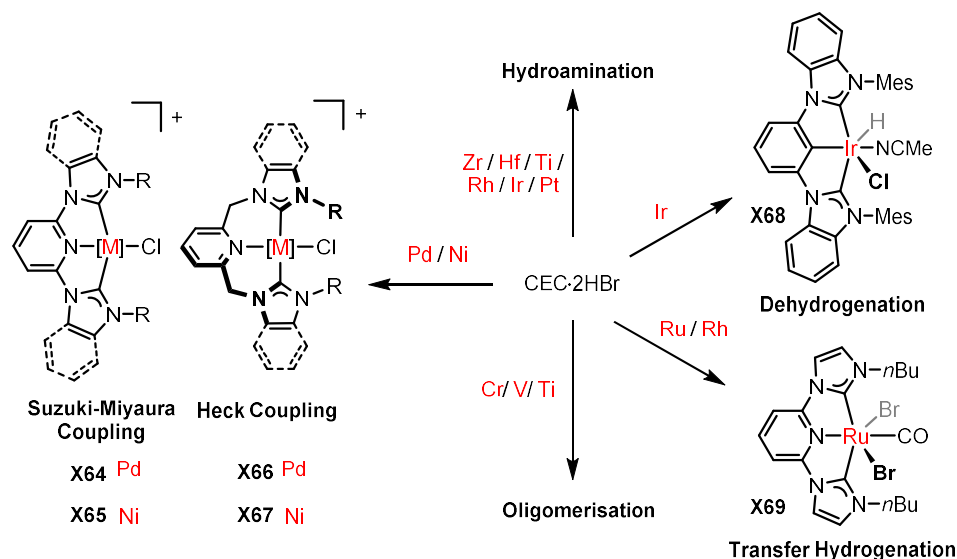


Scheme 1.3.12. Examples of complexes bearing hemilabile pincer ligands

Recently palladium CEC complexes featuring a central selenoether linkage that has the propensity to effortlessly change denticity between pincer (tridentate; **X62**) and *pseudopincer* (bidentate; **X63**) arrangements, have been reported.¹⁶⁹ It is this characteristic that the authors suggest accounts for enhanced complex stability and reactivity. However, a positive mercury drop test and the visible presence of nanoparticles in the reactions directly contradict this assertion and instead advocate a transformation that is promoted heterogeneously by colloidal palladium. Similar results were observed for an analogous amino-centred **Dα** palladium complex, thus supporting the latter assertion.⁸⁴

1.3.6 Applications of NHC-based pincer complexes

The contemporary interest in NHC-based pincer complexes can largely be linked with their successful application in homogeneous catalysis. Indeed, the majority of CEC complexes reported in the literature have been prepared for evaluation in catalytic reactions, with those of platinum group metals being the most heavily investigated (63%).[‡] Emulating the chemistry of PEP pincers (*vide supra*), CEC complexes have also found application in keystone organic transformations. In particular, Pd and Ni complexes **X64** – **X67** are effective pre-catalysts for C–C bond forming Suzuki-Miyaura and Heck reactions (Scheme 1.3.13).^{55,57,81,170–176}



Scheme 1.3.13. CEC pincer complexes in catalysis

For the palladium examples highlighted, flexible **Bn α** variants proved the most active, with **X66** displaying an average TOF approaching 1000 h⁻¹ at 165 °C.^{55,57} Subsequent work by White and co-workers identified a similar trend when investigating the coupling between 4-bromoacetophenone and *n*-butylacrylate using a range of **An α** and **Bn α** ligands with different wingtip substituents.⁸¹ Generally greater catalytic activity was reported for **B** derivatives, and for those bearing bulkier wingtip substituents – with the highest average TOF of 3640 h⁻¹.⁸¹ Curiously, the opposite trend was observed for the corresponding nickel complexes, with complexes of the rigid type-**A** ligands being the most efficacious, and moreover, outperforming heavier palladium congeners.^{89,172,173}

Contrasting phosphine counterparts, the iridium **Ac β** complex **X68** was found to be a poor dehydrogenation catalyst in the presence of sacrificial hydrogen acceptors norbornene (NBE) and TBE (TONs = 10 and 1, respectively).^{177,178} However, **X68** saw significantly improved activity in acceptorless dehydrogenations (TOF = 12 h⁻¹, 150 °C).¹⁷⁹ The hydrogenation of alkenes has been previously highlighted for **X11**,⁶² and indeed the most active CEC catalysts are of the first-row metals, with cobalt CNC complexes decidedly active in the hydrogenation of tri-substituted and sterically congested alkenes and alkynes.^{180–182} Of the non-earth abundant CEC hydrogenation catalysts

ruthenium complexes are the most notable, with **X69** catalysing the transfer hydrogenation of cyclohexanone with a TON of 126,000.¹⁸³

Anchoring a complex onto a solid support requires the presence of a pendant tethering functionality, appendages which are easily introduced into CEC pincer scaffolds either *via* the central donor (*cf.* **X70** and **X71**; Figure 1.3.5) or through the wingtip substituents (*cf.* **X72**).^{184–187} Marrying the desirable characteristics of homogeneous catalysis with the ease of catalyst recovery and purification associated with heterogeneous catalysis, this is an area of contemporary interest.^{185,186} For instance, **X70** outperforms its homogeneous counterpart in the catalytic hydrogenation of CO₂ (TON = 18,000) owed to its enhanced longevity and immobilised complexes **X71** and **X72** retain catalytic activity over at least 12 recycling events.^{184–186}

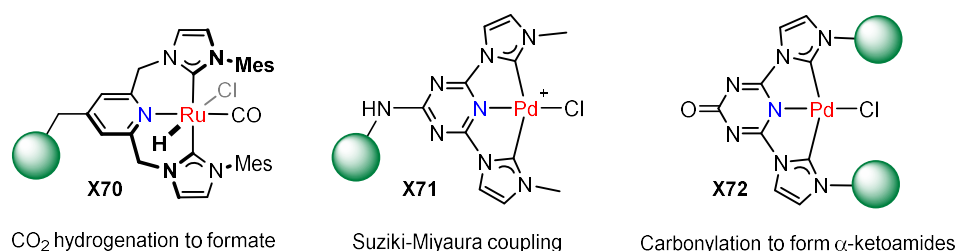


Figure 1.3.5. CEC pincer complexes attached to solid supports

Alongside their application in catalysis, an increasing number of CEC complexes are being recognised as having interesting photophysical properties. Resembling the benchmark ruthenium bis(terpyridine) complex, ruthenium complexes of planar type-**A** CNC pinners are the most prevalent in this field (34 examples; Figure 1.3.6).[‡] For instance, both homoleptic complex **X73** and heteroleptic complex **X74** have been reported to show microsecond ³MLCT excited state lifetimes,¹⁸⁸ four orders of magnitude greater than the related bis(terpyridine) systems. Whilst similar complexes bearing mesoionic triazolium carbenes (ϵ) remain photochemically active (*viz.* **X74**), examples featuring flexible type-**B** ligands are not. Moreover, other late transition metal systems each with interesting green (Os(II); **X75**),¹⁸⁹ blue (Pt(II))¹⁹⁰ and near-UV (Ir(III))¹⁹¹ emission bands have also been described.

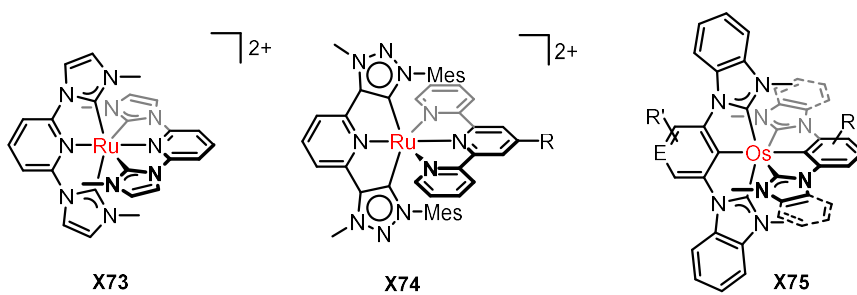
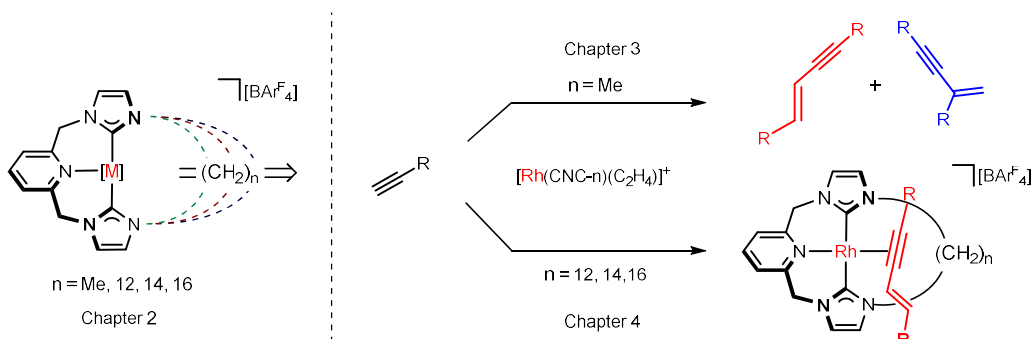


Figure 1.3.6 CEC complexes with photoluminescence behaviour

1.3 Aims and objectives

This project aims to develop understanding of the mechanistic organometallic chemistry of terminal alkyne coupling reactions promoted by rhodium CNC complexes, with the hope of exploiting this methodology in the formation of mechanically interlocked structures of macrocyclic analogues with varying ring sizes ($n = 12, 14, 16$).

To this end, following the synthesis of the full series of NHC-based pincer proligands, the first objective is the development of a mild transmetallation procedure to enable the preparation of rhodium(I) complexes bearing a kinetically labile ethylene ligand; synthons for the inherently reactive three coordinate, formally 14 valence electron, $\{\text{Rh}(\text{CNC})\}^+$ fragments.



The ability of these well-defined complexes to promote terminal alkyne coupling reactions will then be evaluated, using the acyclic analogue as a model system to first establish the underlying mechanism and factors that influence selectivity. This reactivity will then be used as a reference point to establish the role of the macrocyclic ring in influencing the homocoupling reactions of bulky alkynes, with a view of mechanically entrapping the enyne products within the ligand topology.

1.4 References

- 1 E. Peris and R. H. Crabtree, *Chem. Soc. Rev.*, 2018, **47**, 1959–1968.
- 2 C. M. Storey, H. P. Cook and A. B. Chaplin, in *Pincer Compounds*, Elsevier, 2018, pp. 173–189.
- 3 M. A. W. Lawrence, K.-A. Green, P. N. Nelson and S. C. Lorraine, *Polyhedron*, 2018, **143**, 11–27.
- 4 D. Pugh and A. A. Danopoulos, *Coord. Chem. Rev.*, 2007, **251**, 610–641.
- 5 D. Morales-Morales, *Pincer Complexes: Applications in Catalysis*, Sociedad Química de México, 2004, vol. 48.
- 6 C. J. Moulton and B. L. Shaw, *J. Chem. Soc., Dalt. Trans.*, 1976, 1020–1024.
- 7 S. Nemeh, C. Jensen, E. Binamira-Soriaga and W. C. Kaska, *Organometallics*, 1983, **2**, 1442–1447.
- 8 G. van Koten, K. Timmer, J. G. Noltes and A. L. Spek, *J. Chem. Soc., Chem. Commun.*, 1978, 250–252.
- 9 M. Ohff, A. Ohff, M. E. van der Boom and D. Milstein, *J. Am. Chem. Soc.*, 1997, **119**, 11687–11688.
- 10 D. Morales-Morales, C. Grause, K. Kasaoka, R. Redón, R. E. Cramer and C. M. Jensen, *Inorg. Chim. Acta*, 2000, **300–302**, 958–963.
- 11 D. Morales-Morales, R. Redón, C. Yung and C. M. Jensen, *Chem. Commun.*, 2000, 1619–1620.
- 12 F. Miyazaki, K. Yamaguchi and M. Shibasaki, *Tetrahedron Lett.*, 1999, **40**, 7379–7383.
- 13 R. B. Bedford, S. M. Draper, P. Noelle Scully and S. L. Welch, *New J. Chem.*, 2000, **24**, 745–747.
- 14 M. Gupta, C. Hagen, R. J. Flesher, W. C. Kaska and C. M. Jensen, *Chem. Commun.*, 1996, 2083–2084.
- 15 M. Gupta, W. C. Kaska and C. M. Jensen, *Chem. Commun.*, 1997, 461–462.
- 16 M. Gupta, C. Hagen, W. C. Kaska, R. E. Cramer and C. M. Jensen, *J. Am. Chem. Soc.*, 1997, **119**, 840–841.
- 17 W. Xu, G. P. Rosini, K. Krogh-Jespersen, A. S. Goldman, M. Gupta, C. M. Jensen and W. C. Kaska, *Chem. Commun.*, 1997, 2273–2274.
- 18 F. Liu and A. S. Goldman, *Chem. Commun.*, 1999, 655–656.
- 19 P. Dani, T. Karlen, R. A. Gossage, S. Gladiali and G. van Koten, *Angew. Chem. Int. Ed.*, 2000, **39**, 743–745.
- 20 R. Tonner, G. Heydenrych and G. Frenking, *Chem. – An Asian J.*, 2007, **2**, 1555–1567.
- 21 M. N. Hopkinson, C. Richter, M. Schedler and F. Glorius, *Nature*, 2014, **510**, 485–496.
- 22 S. Díez-González and S. P. Nolan, *Coord. Chem. Rev.*, 2007, **251**, 874–883.
- 23 L. Benhamou, E. Chardon, G. Lavigne, S. Bellemin-Laponnaz and V. César, *Chem. Rev.*, 2011, **111**, 2705–2733.
- 24 X. Bantreil and S. P. Nolan, *Nat. Protoc.*, 2011, **6**, 69–77.
- 25 M. Hans, J. Lorkowski, A. Demonceau and L. Delaude, *Beilstein J. Org. Chem.*, 2015, **11**, 2318–2325.
- 26 S. Naumann and M. R. Buchmeiser, *Catal. Sci. Technol.*, 2014, **4**, 2466–2479.
- 27 D. Tapu, Z. McCarty, L. Hutchinson, C. Ghattas, M. Chowdhury, J. Salerno and D. VanDerveer, *J. Organomet. Chem.*, 2014, **749**, 134–141.
- 28 A. Tudose, A. Demonceau and L. Delaude, *J. Organomet. Chem.*, 2006, **691**, 5356–5365.
- 29 F. E. Hahn and M. C. Jahnke, *Angew. Chem. Int. Ed.*, 2008, **47**, 3122–3172.
- 30 J. G. Schantl, in *Advances in Heterocyclic Chemistry*, Academic Press, 2010, vol. 99, pp. 185–207.
- 31 D. M. Wolfe and P. R. Schreiner, *Eur. J. Org. Chem.*, 2007, **2007**, 2825–2838.

- 32 D. Kremzow, G. Seidel, C. W. Lehmann and A. Fürstner, *Chem. Eur. J.*, 2005, **11**, 1833–1853.
- 33 A. J. Arduengo, R. L. Harlow and M. Kline, *J. Am. Chem. Soc.*, 1991, **113**, 361–363.
- 34 H.-W. Wanzlick and H.-J. Schönherr, *Angew. Chem. Int. Ed.*, 1968, **7**, 141–142.
- 35 K. Öfele, *J. Organomet. Chem.*, 1968, **12**, 42–43.
- 36 W. A. Herrmann, M. Elison, J. Fischer, C. Köcher and G. R. J. Artus, *Angew. Chem. Int. Ed.*, 1995, **34**, 2371–2374.
- 37 W. A. Herrmann, C. Broßmer, K. Öfele, M. Beller and H. Fischer, *J. Organomet. Chem.*, 1995, **491**, 1–4.
- 38 A. Spencer, *J. Organomet. Chem.*, 1984, **270**, 115–120.
- 39 R. F. Heck, *Acc. Chem. Res.*, 1979, **12**, 146–151.
- 40 R. F. Heck, *Pure Appl. Chem.*, 1978, **50**, 691–701.
- 41 A. Spencer, *J. Organomet. Chem.*, 1983, **258**, 101–108.
- 42 P. L. Arnold and I. J. Casely, *Chem. Rev.*, 2009, **109**, 3599–3611.
- 43 N. Kuhn and A. Al-Sheikh, *Coord. Chem. Rev.*, 2005, **249**, 829–857.
- 44 Z. N. Gafurov, A. O. Kantyukov, A. A. Kagilev, A. A. Balabayev, O. G. Sinyashin and D. G. Yakhvarov, *Russ. Chem. Bull.*, 2017, **66**, 1529–1535.
- 45 C. Samojłowicz, M. Bieniek and K. Grela, *Chem. Rev.*, 2009, **109**, 3708–3742.
- 46 E. A. B. Kantchev, C. J. O'Brien and M. G. Organ, *Angew. Chem. Int. Ed.*, 2007, **46**, 2768–2813.
- 47 C. Valente, S. Çalimsiz, K. H. Hoi, D. Mallik, M. Sayah and M. G. Organ, *Angew. Chem. Int. Ed.*, 2012, **51**, 3314–3332.
- 48 G. C. Fortman and S. P. Nolan, *Chem. Soc. Rev.*, 2011, **40**, 5151–5169.
- 49 S. Díez-González, N. Marion and S. P. Nolan, *Chem. Rev.*, 2009, **109**, 3612–3676.
- 50 J. D. Egbert, C. S. J. Cazin and S. P. Nolan, *Catal. Sci. Technol.*, 2013, **3**, 912–926.
- 51 S.-T. Liu, C.-I. Lee, C.-F. Fu, C.-H. Chen, Y.-H. Liu, C. J. Elsevier, S.-M. Peng and J.-T. Chen, *Organometallics*, 2009, **28**, 6957–6962.
- 52 C.-Y. Wu, T. Horibe, C. B. Jacobsen and F. D. Toste, *Nature*, 2015, **517**, 449–454.
- 53 R. E. Andrew, L. González-Sebastián and A. B. Chaplin, *Dalton Trans.*, 2016, **45**, 1299–1305.
- 54 J. C. C. Chen and I. J. B. Lin, *J. Chem. Soc., Dalt. Trans.*, 2000, 839–840.
- 55 E. Peris, J. Mata, J. A. Loch and R. H. Crabtree, *Chem. Commun.*, 2001, 201–202.
- 56 A. A. D. Tulloch, A. A. Danopoulos, G. J. Tizzard, S. J. Coles, M. B. Hursthouse, R. S. Hay-Motherwell and W. B. Motherwell, *Chem. Commun.*, 2001, 1270–1271.
- 57 S. Gründemann, M. Albrecht, J. A. Loch, J. W. Faller and R. H. Crabtree, *Organometallics*, 2001, **20**, 5485–5488.
- 58 M. Asay, M. Quezada-Miriel, J. R. Ochoa-Sanfelice and D. Martinez-Otero, *J. Organomet. Chem.*, 2018, **859**, 10–17.
- 59 L. González-Sebastián and A. B. Chaplin, *Inorg. Chim. Acta*, 2017, **460**, 22–28.
- 60 R. Pony Yu, D. Hesk, N. Rivera, I. Pelczer and P. J. Chirik, *Nature*, 2016, **529**, 195–199.
- 61 R. J. Rubio, G. T. S. Andavan, E. B. Bauer, T. K. Hollis, J. Cho, F. S. Tham and B. Donnadieu, *J. Organomet. Chem.*, 2005, **690**, 5353–5364.
- 62 R. P. Yu, J. M. Darmon, J. M. Hoyt, G. W. Margulieux, Z. R. Turner and P. J. Chirik, *ACS Catal.*, 2012, **2**, 1760–1764.
- 63 H. V. Huynh, Y. Han, R. Jothibas and J. A. Yang, *Organometallics*, 2009, **28**, 5395–5404.
- 64 Q. Teng and H. V. Huynh, *Dalton Trans.*, 2017, **46**, 614–627.
- 65 L. Mercks, G. Labat, A. Neels, A. Ehlers and M. Albrecht, *Organometallics*, 2006, **25**, 5648–5656.
- 66 M. Süßner and H. Plenio, *Chem. Commun.*, 2005, 5417–5419.
- 67 A. R. Chianese, A. Kovacevic, B. M. Zeglis, J. W. Faller and R. H. Crabtree, *Organometallics*, 2004, **23**, 2461–2468.
- 68 J.-N. Luy, S. A. Hauser, A. B. Chaplin and R. Tonner, *Organometallics*, 2015, **34**,

- 5099–5112.
- 69 G. Kleinhans, M. M. Hansmann, G. Guisado-Barrios, D. C. Liles, G. Bertrand and D. I. Bezuidenhout, *J. Am. Chem. Soc.*, 2016, **138**, 15873–15876.
- 70 G. Kleinhans, G. Guisado-Barrios, D. C. Liles, G. Bertrand and D. I. Bezuidenhout, *Chem. Commun.*, 2016, **52**, 3504–3507.
- 71 A. Krüger, A. Neels and M. Albrecht, *Chem. Commun.*, 2010, **46**, 315–317.
- 72 L. C. Tolley, I. Strydom, W. J. Louw, M. A. Fernandes, D. I. Bezuidenhout and G. Guisado-Barrios, *ACS Omega*, 2019, **4**, 6360–6374.
- 73 G. Kleinhans, G. Guisado-Barrios, E. Peris and D. I. Bezuidenhout, *Polyhedron*, 2018, **143**, 43–48.
- 74 A. A. Danopoulos, N. Tsoureas, J. A. Wright and M. E. Light, *Organometallics*, 2004, **23**, 166–168.
- 75 G. A. Filonenko, E. Cosimi, L. Lefort, M. P. Conley, C. Copéret, M. Lutz, E. J. M. Hensen and E. A. Pidko, *ACS Catal.*, 2014, **4**, 2667–2671.
- 76 W. Zuo and P. Braunstein, *Organometallics*, 2012, **31**, 2606–2615.
- 77 W. Zuo and P. Braunstein, *Dalton Trans.*, 2012, **41**, 636–643.
- 78 A. Krüger, L. J. L. Häller, H. Müller-Bunz, O. Serada, A. Neels, S. A. Macgregor and M. Albrecht, *Dalton Trans.*, 2011, **40**, 9911–9920.
- 79 D. Serra, P. Cao, J. Cabrera, R. Padilla, F. Rominger and M. Limbach, *Organometallics*, 2011, **30**, 1885–1895.
- 80 A. M. Magill, D. S. McGuinness, K. J. Cavell, G. J. Britovsek, V. C. Gibson, A. J. P. White, D. J. Williams, A. H. White and B. W. Skelton, *J. Organomet. Chem.*, 2001, **617–618**, 546–560.
- 81 D. J. Nielsen, K. J. Cavell, B. W. Skelton and A. H. White, *Inorg. Chim. Acta*, 2006, **359**, 1855–1869.
- 82 F. E. Hahn, M. C. Jahnke and T. Pape, *Organometallics*, 2007, **26**, 150–154.
- 83 A. R. Naziruddin, C.-L. Kuo, W.-J. Lin, W.-H. Lo, C.-S. Lee, B.-J. Sun, A. H. H. Chang and W.-S. Hwang, *Organometallics*, 2014, **33**, 2575–2582.
- 84 J. Houghton, G. Dyson, R. E. Douthwaite, A. C. Whitwood and B. M. Kariuki, *Dalton Trans.*, 2007, 3065–3073.
- 85 F. M. Nachtigall, Y. E. Corilo, C. C. Cassol, G. Ebeling, N. H. Morgon, J. Dupont and M. N. Eberlin, *Angew. Chem. Int. Ed.*, 2008, **47**, 151–154.
- 86 M. Asay, M. Quezada-Miriel, J. R. Ochoa-Sanfelice and D. Martinez-Otero, *J. Organomet. Chem.*, 2018, **859**, 10–17.
- 87 M. Quezada-Miriel, J. R. Ochoa-Sanfelice, S. Mendoza-Tellez, D. Martinez-Otero and M. Asay, *Dalton Trans.*, 2018, **47**, 17382–17391.
- 88 W. B. Cross, C. G. Daly, R. L. Ackerman, I. R. George and K. Singh, *Dalton Trans.*, 2011, **40**, 495–505.
- 89 W. Wei, Y. Qin, M. Luo, P. Xia and M. S. Wong, *Organometallics*, 2008, **27**, 2268–2272.
- 90 M. Moser, B. Wucher, D. Kunz and F. Rominger, *Organometallics*, 2007, **26**, 1024–1030.
- 91 B. Schulze, D. Escudero, C. Friebe, R. Siebert, H. Görls, U. Köhn, E. Altuntas, A. Baumgaertel, M. D. Hager, A. Winter, B. Dietzek, J. Popp, L. González and U. S. Schubert, *Chem. Eur. J.*, 2011, **17**, 5494–5498.
- 92 S. N. Sluijter, T. J. Korstanje, J. I. van der Vlugt and C. J. Elsevier, *J. Organomet. Chem.*, 2017, **845**, 30–37.
- 93 D. I. Bezuidenhout, G. Kleinhans, G. Guisado-Barrios, D. C. Liles, G. Ung and G. Bertrand, *Chem. Commun.*, 2014, **50**, 2431.
- 94 A. A. Danopoulos, S. Winston and W. B. Motherwell, *Chem. Commun.*, 2002, 1376–1377.
- 95 D. Pugh, J. A. Wright, S. Freeman and A. A. Danopoulos, *Dalton Trans.*, 2006, 775–782.
- 96 E. M. Matson, G. Espinosa Martinez, A. D. Ibrahim, B. J. Jackson, J. A. Bertke and A.

- R. Fout, *Organometallics*, 2015, **34**, 399–407.
- 97 D. S. McGuinness, J. A. Suttill, M. G. Gardiner and N. W. Davies, *Organometallics*, 2008, **27**, 4238–4247.
- 98 D. S. McGuinness, V. C. Gibson, D. F. Wass and J. W. Steed, *J. Am. Chem. Soc.*, 2003, **125**, 12716–12717.
- 99 D. S. McGuinness, V. C. Gibson and J. W. Steed, *Organometallics*, 2004, **23**, 6288–6292.
- 100 D. Pugh, A. Boyle and A. A. Danopoulos, *Dalton Trans.*, 2008, 1087.
- 101 J. A. Wright, A. A. Danopoulos, W. B. Motherwell, R. J. Carroll, S. Ellwood and J. Saßmannshausen, *Eur. J. Inorg. Chem.*, 2006, **2006**, 4857–4865.
- 102 T. L. Amyes, S. T. Diver, J. P. Richard, F. M. Rivas and K. Toth, *J. Am. Chem. Soc.*, 2004, **126**, 4366–4374.
- 103 D. Milstein, *Philos. Trans. R. Soc. A Math. Phys. Eng. Sci.*, 2015, **373**, 20140189–20140189.
- 104 Y. Wang, B. Zheng, Y. Pan, C. Pan, L. He and K.-W. Huang, *Dalton Trans.*, 2015, **44**, 15111–15115.
- 105 M. Hernández-Juárez, J. López-Serrano, P. González-Herrero, N. Rendón, E. Álvarez, M. Paneque and A. Suárez, *Chem. Commun.*, 2018, **54**, 3843–3846.
- 106 M. Feller, Y. Diskin-Posner, L. J. W. Shimon, E. Ben-Ari and D. Milstein, *Organometallics*, 2012, **31**, 4083–4101.
- 107 E. Ben-Ari, G. Leitus, L. J. W. Shimon and D. Milstein, *J. Am. Chem. Soc.*, 2006, **128**, 15390–15391.
- 108 L. Schwartsburd, M. A. Iron, L. Konstantinovski, E. Ben-Ari and D. Milstein, *Organometallics*, 2011, **30**, 2721–2729.
- 109 G. A. Filonenko, E. Cosimi, L. Lefort, M. P. Conley, C. Copéret, M. Lutz, E. J. M. Hensen and E. A. Pidko, *ACS Catal.*, 2014, **4**, 2667–2671.
- 110 R. E. Andrew and A. B. Chaplin, *Inorg. Chem.*, 2015, **54**, 312–322.
- 111 G. A. Filonenko, D. Smykowski, B. M. Szyja, G. Li, J. Szczygieł, E. J. M. Hensen and E. A. Pidko, *ACS Catal.*, 2015, **5**, 1145–1154.
- 112 M. Hernández-Juárez, J. López-Serrano, P. Lara, J. P. Morales-Cerón, M. Vaquero, E. Álvarez, V. Salazar and A. Suárez, *Chem. Eur. J.*, 2015, **21**, 7540–7555.
- 113 D. J. Nelson, *Eur. J. Inorg. Chem.*, 2015, **2015**, 2012–2027.
- 114 L.-H. Chung, H.-S. Lo, S.-W. Ng, D.-L. Ma, C.-H. Leung and C.-Y. Wong, *Sci. Rep.*, 2015, **5**, 1–13.
- 115 H. M. J. Wang and I. J. B. Lin, *Organometallics*, 1998, **17**, 972–975.
- 116 D. J. Nielsen, A. M. Magill, B. F. Yates, K. J. Cavell, B. W. Skelton and A. H. White, *Chem. Commun.*, 2002, 2500–2501.
- 117 D. J. Nielsen, K. J. Cavell, B. W. Skelton and A. H. White, *Inorg. Chim. Acta*, 2002, **327**, 116–125.
- 118 A. Biffis, M. Cipani, C. Tubaro, M. Basato, M. Costante, E. Bressan, A. Venzo and C. Graiff, *New J. Chem.*, 2013, **37**, 4176–4184.
- 119 F. E. Hahn, C. Radloff, T. Pape and A. Hepp, *Chem. Eur. J.*, 2008, **14**, 10900–10904.
- 120 R. S. Simons, P. Custer, C. A. Tessier and W. J. Youngs, *Organometallics*, 2003, **22**, 1979–1982.
- 121 R. E. Andrew, C. M. Storey and A. B. Chaplin, *Dalton Trans.*, 2016, **45**, 8937–8944.
- 122 B. P. Morgan, G. A. Galdamez, R. J. Gilliard, Jr. and R. C. Smith, *Dalton Trans.*, 2009, 2020–2028.
- 123 C. Radloff, H.-Y. Gong, C. Schulte to Brinke, T. Pape, V. M. Lynch, J. L. Sessler and F. E. Hahn, *Chem. Eur. J.*, 2010, **16**, 13077–13081.
- 124 A. A. Danopoulos, A. A. D. Tulloch, S. Winston, G. Eastham and M. B. Hursthouse, *Dalton Trans.*, 2003, 1009–1015.
- 125 R. J. Rubio, G. T. S. Andavan, E. B. Bauer, T. K. Hollis, J. Cho, F. S. Tham and B. Donnadieu, *J. Organomet. Chem.*, 2005, **690**, 5353–5364.
- 126 K. Meyer, A. F. Dalebrook and L. J. Wright, *Dalton Trans.*, 2012, **41**, 14059–14067.

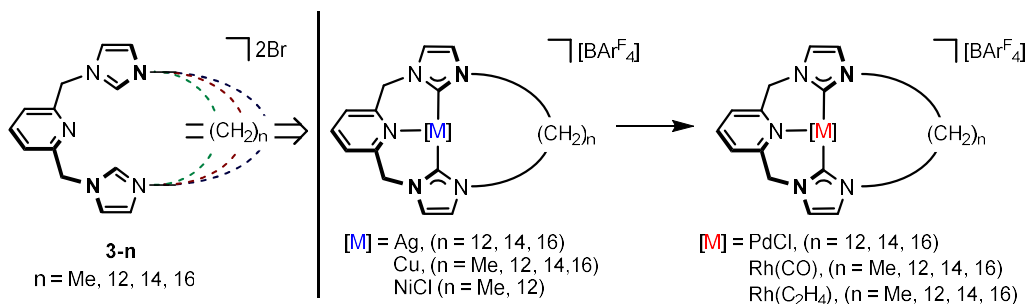
- 127 F. Nahra, A. Gómez-Herrera and C. S. J. Cazin, *Dalton Trans.*, 2017, **46**, 628–631.
- 128 D. Domyati, S. L. Hope, R. Latifi, M. D. Hearn and L. Tahsini, *Inorg. Chem.*, 2016, **55**, 11685–11693.
- 129 D. Domyati, R. Latifi and L. Tahsini, *J. Organomet. Chem.*, 2018, **860**, 98–105.
- 130 Q.-X. Liu, J. Yu, X.-J. Zhao, S.-W. Liu, X.-Q. Yang, K.-Y. Li and X.-G. Wang, *CrystEngComm*, 2011, **13**, 4086.
- 131 T. Lu, J.-Y. Wang, L.-X. Shi, Z.-N. Chen, X.-T. Chen and Z.-L. Xue, *Dalton Trans.*, 2018, **47**, 6742–6753.
- 132 G. Venkatachalam, M. Heckenroth, A. Neels and M. Albrecht, *Helv. Chim. Acta*, 2009, **92**, 1034–1045.
- 133 Y. D. Bidal, O. Santoro, M. Melaimi, D. B. Cordes, A. M. Z. Slawin, G. Bertrand and C. S. J. Cazin, *Chem. Eur. J.*, 2016, **22**, 9404–9409.
- 134 M. R. L. Furst and C. S. J. Cazin, *Chem. Commun.*, 2010, **46**, 6924–6925.
- 135 O. Santoro, F. Lazreg, D. B. Cordes, A. M. Z. Slawin and C. S. J. Cazin, *Dalton Trans.*, 2016, **45**, 4970–4973.
- 136 C. Chen, H. Qiu and W. Chen, *J. Organomet. Chem.*, 2012, **696**, 4166–4172.
- 137 W. W. N. O, A. J. Lough and R. H. Morris, *Organometallics*, 2009, **28**, 6755–6761.
- 138 B. Liu, X. Liu, C. C. Chen, C. C. Chen and W. Chen, *Organometallics*, 2012, **31**, 282–288.
- 139 A. A. Danopoulos, N. Tsoureas, J. C. Green and M. B. Hursthouse, *Chem. Commun.*, 2003, 756–757.
- 140 C.-F. Yang, T. Lu, X.-T. Chen and Z.-L. Xue, *Chem. Commun.*, 2018, **54**, 7830–7833.
- 141 R. E. Douthwaite, J. Houghton and B. M. Kariuki, *Chem. Commun.*, 2004, 698–699.
- 142 T. Lu, C.-F. Yang, C. A. Steren, F. Fei, X.-T. Chen and Z.-L. Xue, *New J. Chem.*, 2018, **42**, 4700–4713.
- 143 G. A. Filonenko, M. J. B. Aguila, E. N. Schulpen, R. van Putten, J. Wiecko, C. Müller, L. Lefort, E. J. M. Hensen and E. A. Pidko, *J. Am. Chem. Soc.*, 2015, **137**, 7620–7623.
- 144 J. A. Loch, M. Albrecht, E. Peris, J. Mata, J. W. Faller and R. H. Crabtree, *Organometallics*, 2002, **21**, 700–706.
- 145 F. E. Hahn, M. C. Jahnke, V. Gomez-Benitez, D. Morales-Morales and T. Pape, *Organometallics*, 2005, **24**, 6458–6463.
- 146 J. R. Miecznikowski, S. Gründemann, M. Albrecht, C. Mégret, E. Clot, J. W. Faller, O. Eisenstein and R. H. Crabtree, *Dalton Trans.*, 2003, 831–838.
- 147 S. Saito, I. Azumaya, N. Watarai, H. Kawasaki and R. Yamasaki, *Heterocycles*, 2009, **79**, 531–548.
- 148 A. A. Danopoulos, D. Pugh and J. A. Wright, *Angew. Chem. Int. Ed.*, 2008, **47**, 9765–9767.
- 149 K. Yoshida, S. Horiuchi, T. Takeichi, H. Shida, T. Imamoto and A. Yanagisawa, *Org. Lett.*, 2010, **12**, 1764–1767.
- 150 M. Hernández-Juárez, M. Vaquero, E. Álvarez, V. Salazar and A. Suárez, *Dalton Trans.*, 2013, **42**, 351–354.
- 151 K. Farrell, H. Müller-Bunz and M. Albrecht, *Organometallics*, 2015, **34**, 5723–5733.
- 152 J. A. Cabeza, M. Damonte, P. García-Álvarez and E. Pérez-Carreño, *Chem. Commun.*, 2013, **49**, 2813–2815.
- 153 A. Krüger, L. J. L. Häller, H. Müller-Bunz, O. Serada, A. Neels, S. A. Macgregor and M. Albrecht, *Dalton Trans.*, 2011, **40**, 9911–9920.
- 154 C. L. Lund, M. J. Sgro and D. W. Stephan, *Organometallics*, 2012, **31**, 580–587.
- 155 C. Y. Chan and P. J. Barnard, *Dalton Trans.*, 2015, **44**, 19126–19140.
- 156 M. R. Norris, S. E. Flowers, A. M. Mathews and B. M. Cossairt, *Organometallics*, 2016, **35**, 2778–2781.
- 157 S. E. Flowers and B. M. Cossairt, *Organometallics*, 2014, **33**, 4341–4344.
- 158 C. Gradert, J. Krahmer, F. D. Sönnichsen, C. Näther and F. Tuczek, *Eur. J. Inorg. Chem.*, 2013, **2013**, 3943–3955.
- 159 S. L. Apps, R. E. Alflatt, B. Leforestier, C. M. Storey and A. B. Chaplin, *Polyhedron*,

- 2018, **143**, 57–61.
- 160 E. Jürgens and D. Kunz, *Eur. J. Inorg. Chem.*, 2017, **2017**, 233–236.
- 161 Y. Tian, E. Jürgens and D. Kunz, *Chem. Commun.*, 2018, **54**, 11340–11343.
- 162 G. M. Adams and A. S. Weller, *Coord. Chem. Rev.*, 2018, **355**, 150–172.
- 163 A. J. M. Miller, *Dalton Trans.*, 2017, **46**, 11987–12000.
- 164 E. Poverenov, M. Gandelman, L. J. W. Shimon, H. Rozenberg, Y. Ben-David and D. Milstein, *Organometallics*, 2005, **24**, 1082–1090.
- 165 A. Luquin, N. Castillo, E. Cerrada, F. L. Merchan, J. Garrido and M. Laguna, *Eur. J. Org. Chem.*, 2016, **2016**, 789–798.
- 166 A. G. Nair, R. T. McBurney, D. B. Walker, M. J. Page, M. R. D. Gatus, M. Bhadbhade and B. A. Messerle, *Dalton Trans.*, 2016, **45**, 14335–14342.
- 167 O. Vechorkin, D. Barmaz, V. Proust and X. Hu, *J. Am. Chem. Soc.*, 2009, **131**, 12078–12079.
- 168 P. M. Pérez García, P. Ren, R. Scopelliti and X. Hu, *ACS Catal.*, 2015, **5**, 1164–1171.
- 169 R. Rishu, B. Prashanth, D. Bawari, U. Mandal, A. Verma, A. R. Choudhury and S. Singh, *Dalton Trans.*, 2017, **46**, 6291–6302.
- 170 S. Zhang, X. Li, H. Sun, O. Fuhr and D. Fenske, *J. Organomet. Chem.*, 2016, **820**, 41–45.
- 171 K. Inamoto, J. Kuroda, K. Hiroya, Y. Noda, M. Watanabe and T. Sakamoto, *Organometallics*, 2006, **25**, 3095–3098.
- 172 S. Wang, F. Ren, Y. Qiu and M. Luo, *J. Organomet. Chem.*, 2015, **788**, 27–32.
- 173 K. Inamoto, J. Kuroda, E. Kwon, K. Hiroya and T. Doi, *J. Organomet. Chem.*, 2009, **694**, 389–396.
- 174 T. Tu, H. Mao, C. Herbert, M. Xu and K. H. Dötz, *Chem. Commun.*, 2010, **46**, 7796–7798.
- 175 M. Xu, X. Li, Z. Sun and T. Tu, *Chem. Commun.*, 2013, **49**, 11539–11541.
- 176 K. D. M. MaGee, G. Travers, B. W. Skelton, M. Massi, A. D. Payne and D. H. Brown, *Aust. J. Chem.*, 2012, **65**, 823–833.
- 177 A. R. Chianese, A. Mo, N. L. Lampland, R. L. Swartz and P. T. Bremer, *Organometallics*, 2010, **29**, 3019–3026.
- 178 A. R. Chianese, S. E. Shaner, J. A. Tendler, D. M. Pudalov, D. Y. Shopov, D. Kim, S. L. Rogers and A. Mo, *Organometallics*, 2012, **31**, 7359–7367.
- 179 A. R. Chianese, M. J. Drance, K. H. Jensen, S. P. McCollom, N. Yusufova, S. E. Shaner, D. Y. Shopov and J. A. Tendler, *Organometallics*, 2014, **33**, 457–464.
- 180 R. P. Yu, J. M. Darmon, C. Milsman, G. W. Margulieux, S. C. E. Stieber, S. DeBeer and P. J. Chirik, *J. Am. Chem. Soc.*, 2013, **135**, 13168–13184.
- 181 K. Tokmic, C. R. Markus, L. Zhu and A. R. Fout, *J. Am. Chem. Soc.*, 2016, **138**, 11907–11913.
- 182 K. Tokmic and A. R. Fout, *J. Am. Chem. Soc.*, 2016, **138**, 13700–13705.
- 183 M. Poyatos, J. A. Mata, E. Falomir, R. H. Crabtree and E. Peris, *Organometallics*, 2003, **22**, 1110–1114.
- 184 M. Bahadori, S. Tangestaninejad, M. Moghadam, V. Mirkhani, A. Mechler, I. Mohammadpoor-Baltork and F. Zadehahmadi, *Microporous Mesoporous Mater.*, 2017, **253**, 102–111.
- 185 Y. Qian, J. So, S.-Y. Jung, S. Hwang, M.-J. Jin and S. Shim, *Synthesis*, 2019, **51**, 2287–2292.
- 186 H. Lo and C. Copéret, *ChemCatChem*, 2019, **11**, 430–434.
- 187 S. S. Islam, R. A. Molla, S. Ta, N. Yasmin, D. Das and S. M. Islam, *J. Organomet. Chem.*, 2019, **882**, 18–25.
- 188 D. G. Brown, N. Sanguantrakun, B. Schulze, U. S. Schubert and C. P. Berlinguette, *J. Am. Chem. Soc.*, 2012, **134**, 12354–12357.
- 189 R. G. Alabau, B. Eguillor, J. Esler, M. A. Esteruelas, M. Oliván, E. Oñate, J.-Y. Tsai and C. Xia, *Organometallics*, 2014, **33**, 5582–5596.
- 190 X. Zhang, A. M. Wright, N. J. DeYonker, T. K. Hollis, N. I. Hammer, C. E. Webster and

- E. J. Valente, *Organometallics*, 2012, **31**, 1664–1672.
- 191 N. Darmawan, C.-H. Yang, M. Mauro, M. Raynal, S. Heun, J. Pan, H. Buchholz, P. Braunstein and L. De Cola, *Inorg. Chem.*, 2013, **52**, 10756–10765.

Chapter 2. Synthesis and coordination chemistry of macrocyclic CNC pincer prolignands

This chapter describes the preparation and coordination chemistry of two novel NHC-based macrocyclic prolignands, comprising a flexible bis(imidazolium)lutidine backbone and either a tetradecamethylene (**3-14**) or hexadecamethylene tether (**3-16**) with particular focus given to the synthesis of palladium(II) and rhodium(I) derivatives. The former complete a homologous family of pincer complexes of the form $[\text{Pd}(\text{CNC}-n)\text{Cl}][\text{BAR}^{\text{F}_4}]$ (**6-n**, $n = \text{Me}, 8, 10, 12, 14, 16$), which have been systematically interrogated in solution and in the solid-state to enable more comprehensive structure-property relationships to be drawn. To advance the coordination chemistry of this ligand class, particularly with a view to isolating analytically pure samples of labile rhodium(I) ethylene derivatives, transmetallation reactions of silver(I), copper(I) and nickel(II) complexes of the previously reported CNC-12 macrocycle have also been investigated. Copper(I) complexes proved to be effective carbene transfer agents and were employed in the preparation of the synthetically challenging target $[\text{Rh}(\text{CNC}-n)(\text{C}_2\text{H}_4)][\text{BAR}^{\text{F}_4}]$ complexes **11-n** ($n = \text{Me}, 12, 14, 16$).



Publications resulting from the work described in this chapter:

1. R. E. Andrew, C. M. Storey, A. B. Chaplin, *Dalton Trans.* **2016**, 45, 8937–8944
2. C. M. Storey, M. R. Gyton, R. E. Andrew, A. B. Chaplin, *Angew. Chem. Int. Ed.* **2018**, 57, 12003–12006
3. C. M. Storey, M. R. Gyton, R. E. Andrew, A. B. Chaplin, *Manuscript in preparation.*

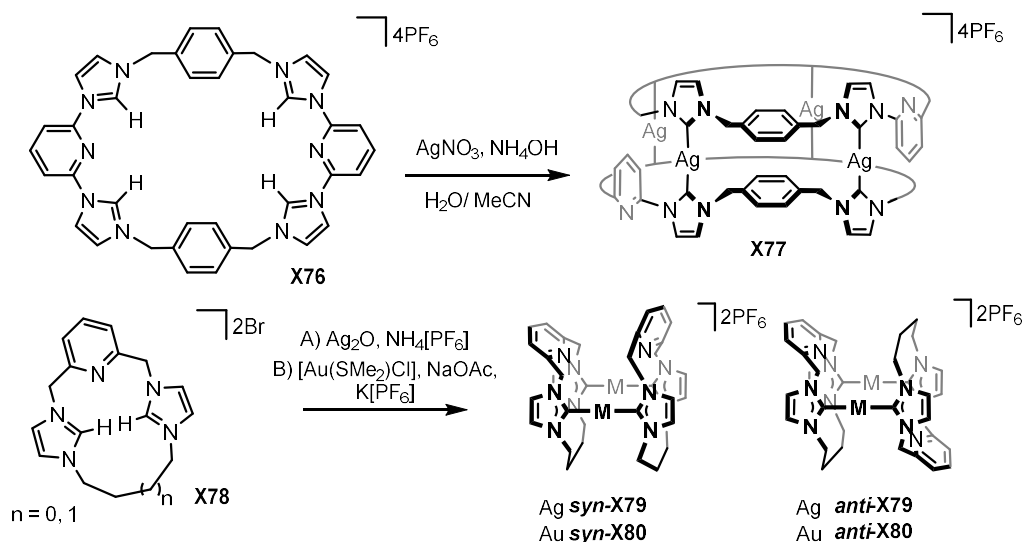
2.1 Introduction

2.1.1 Macrocyclic NHC-based ligands

Macrocyclic ligand scaffolds offer a plethora of opportunities owing to their unique steric profiles and the topological constraints they impose on the coordinated metal center. It is widely accepted that extending acyclic ligand scaffolds into macrocyclic equivalents brings about an increase in the kinetic and thermodynamic stability of their metal complexes; commonly termed the macrocyclic effect.¹ This enhanced stability has undoubtedly fueled research into the use of macrocyclic complexes in catalysts,^{2–4} and materials chemistry.^{5,6} Given the prominence of NHC-based pincers outlined in Chapter 1, it is unsurprising that these moieties have been successfully incorporated into a variety of macrocyclic architectures.^{7–9}

The synthesis of NHC-based macrocyclic complexes can be achieved through metal-templated ring closing reactions of suitably functionalised monodentate derivatives. Reported literature examples however, are limited to relatively small tetradentate macrocycles, which in some cases require the use of highly toxic reagents, *viz.* diphosgene.^{7,8,10} Despite challenges associated with competing oligomerisation side-reactions, the synthesis and subsequent coordination of preformed polyNHC macrocyclic proligands is a more prevalent approach, and allows for a more diverse variety of macrocyclic structures.

Whilst featuring functionalities that distinctly resemble those of CEC pincers, the majority of reported complexes of NHC-based macrocycles are adducts of coinage metals Ag(I) and Au(I).^{9–15} These metals favour linear coordination geometries and as such almost exclusively form multinuclear metallocycles (Scheme 2.1.1).



Scheme 2.1.1. Formation of Ag and Au complexes of NHC-based macrocycles

For instance, metallation of proligand **X78** with silver or gold in the presence of a weakly coordinating anion (Scheme 2.1.1) generates homoleptic bimetallic complexes **X79** and **X80**, respectively.^{9,12} Interestingly, the exocyclic nature of coordination gives rise to a mixture of *syn*- and *anti*-isomers in different ratios depending on the metal ion and the structure of the linker group.¹² The Ag complexes isomerise dynamically in solution, but reflecting their relative M–NHC bond strengths the corresponding Au complexes do not.

Examples of mononuclear complexes are largely limited to small tetradentate macrocycles (Figure 2.1.1), which have marked parallels with porphyrin ligands.^{16–19} Work in this area has been pioneered by the groups of Jenkins, Meyer and Kühn who have reported a range of complexes of this nature.^{20–26} Square planar Fe(II) and square pyramidal Fe(III) compounds of the form **X81** and **X82** are notable examples, and have been used as precursors for the formation of iron(IV) oxo, μ -oxo diiron(III) and iron superoxo complexes by reaction with 2-(*tert*-butylsulfonyl)iodosylbenzene, atmospheric oxygen and KO_2 , respectively.^{24,26–28} Computational studies suggest that these Fe(IV) oxo complexes could be comparable oxidants to cytochrome P450.²⁹ Iron complexes of this nature have correspondingly found application in various catalytic epoxidation and aziridination reactions.^{21,22,30}

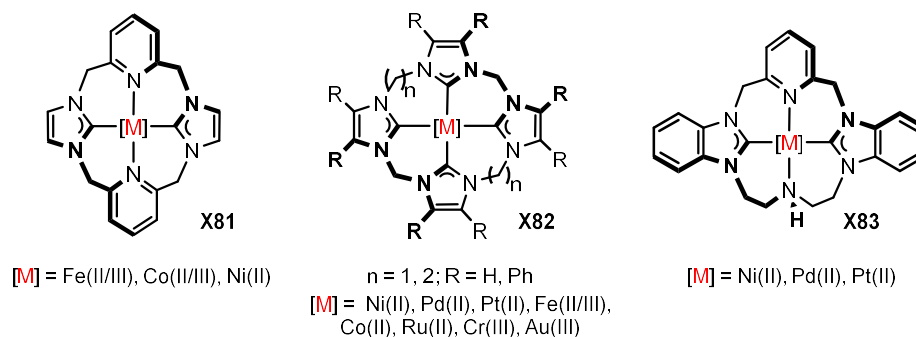


Figure 2.1.1. Previously reported tetradentate NHC-based macrocycles

Complexes **X84** and **X85** bearing 14/15 membered macrocyclic ligands comprise three donors but do not adopt tridentate coordination.^{9,11} The inherent ring strain imposed by the short macrocyclic tethers of **X84** and **X85** hinders the endocyclic coordination of the palladium bromide fragments, enforcing bidentate mutually *cis*-coordination of the carbene donors and no coordination of the central lutidine donor. The expanded cavity of the larger 32-membered macrocyclic ligand of **X87** and 28- and 38-membered macrocycles **X86** described by Saito, however, permit traditional tridentate coordination to the palladium(II) halide fragments.^{31,32}

The activity of these macrocyclic palladium complexes in archetypal C–C coupling reactions has also been evaluated. Whilst **X87** was found to be completely inactive towards Heck couplings, **X84** and **X85** showed reasonable activity in the Sonogashira coupling of aryl halides with phenylacetylene. Likewise, **X86** were found to promote both Mizoroki-Heck reactions and the oxidative homocoupling of phenylacetylene. These reactions, however, required elevated temperatures to reach high turnover numbers and resulted in partial decomposition of the palladium complexes.

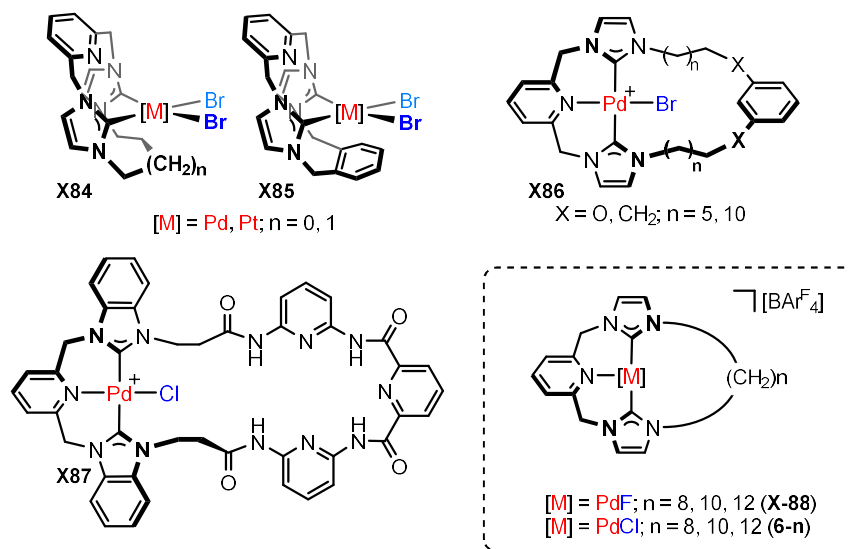


Figure 2.1.2. Previously reported palladium-based pincer macrocycles

As has been observed for the corresponding acyclic analogues, **X86** exhibit atropisomerism on the 1H NMR timescale ($CDCl_3$, 500 MHz), as evidenced by coalescence of the $pyCH_2$ resonances at 373 K.³² The associated barriers are in close agreement with those reported for the related acyclic counterparts ($\Delta G^\ddagger = 57.4 - 59.4$ kJmol $^{-1}$, *cf.* ΔG^\ddagger 52.9 kJmol $^{-1}$) demonstrating that the presence of these long tethers has little impact on the rate of atropisomerism.

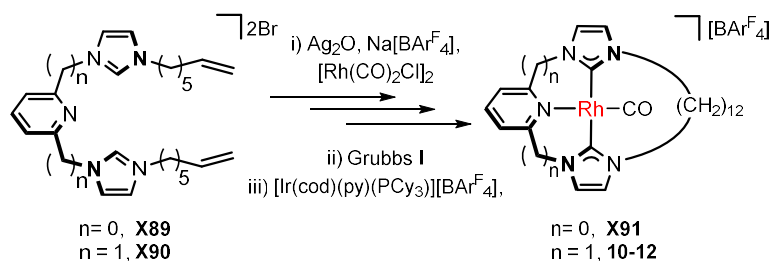
2.1.2 Previous work in the Chaplin group

The synthesis and palladium complexes of a series of NHC-based macrocyclic ligands **3-n** ($n = 8, 10, 12$) have previously been studied in the Chaplin group.³³ Palladium chloride complexes (**6-n**) were prepared using an *in situ* silver transmetallation procedure involving reaction with Ag_2O and $Na[BAr^F_4]$ in CH_2Cl_2 , and their structures probed in solution and the solid-state with a view to evaluating the effect of the macrocyclic aperture size. In contrast to **X87** and acyclic counterparts, the incorporation of the weakly coordinating $[BAr^F_4]^-$ counter anion in place of the outer sphere halide resulted in a considerable energetic barrier to atropisomerism and correspondingly these complexes remain static on the 1H NMR timescale (CD_2Cl_2 , 500 MHz).

Whereas the largest ring ($n = 12$) comfortably accommodates the chloride ligand within the annulus, the smaller rings ($n = 8, 10$) see a loss of symmetry, in

solution and the solid-state, associated with restricted movement of the aliphatic tether over the bound chloride ligand. Using variable low temperature ^1H NMR experiments (185 – 298 K, CD_2Cl_2 , 500 MHz) the activation barriers of this ring flipping were determined ($\Delta G^\ddagger = +43 \text{ kJmol}^{-1}$, **6-8**; $\Delta G^\ddagger = +37 \text{ kJmol}^{-1}$, **6-10**). Replacing the chloride with the less sterically cumbersome fluoride ligand was also shown to significantly reduce the ring flipping barrier ($\Delta G^\ddagger < 34 \text{ kJmol}^{-1}$, **X88**, $n = 10$).³³

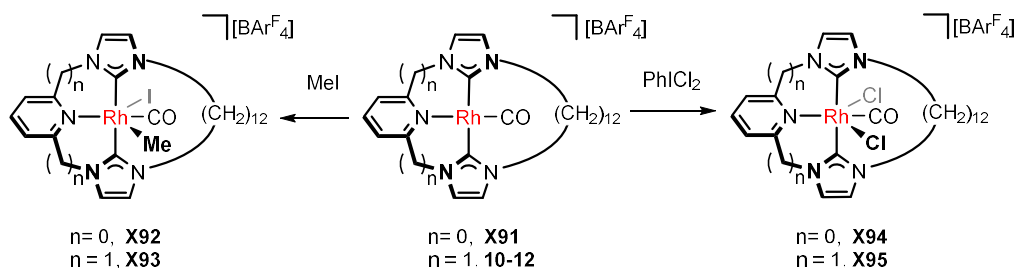
Encouraged by these results, investigations continued into the coordination chemistry of **3-12**, focusing particularly on rhodium derivatives. Preparation of the associated rhodium(I) carbonyl complexes **10-12** and its rigid pyridine centred counterpart **X91** were achieved using metal-templated ring closure (Scheme 2.1.2).^{34,35} Following complexation of the acyclic proligns **X89** and **X90** via Ag-based transmetallation, olefin metathesis and hydrogenation gave complexes **10-12** and **X91** in good yields, over the three steps (45% and 56%, respectively). The contrasting geometry and rigidity of these scaffolds results in marked differences in the structure of these complexes, with the macrocyclic tether being projected to one side of the coordination plane in **X91**, as a consequence of the splayed projection of the NHC donors, whereas, **10-12** sees the ring comfortably accommodate the carbonyl ligand within the macrocyclic cavity.^{34,35}



Scheme 2.1.2. Synthesis of rhodium carbonyl macrocycles **10-12** and **X91**

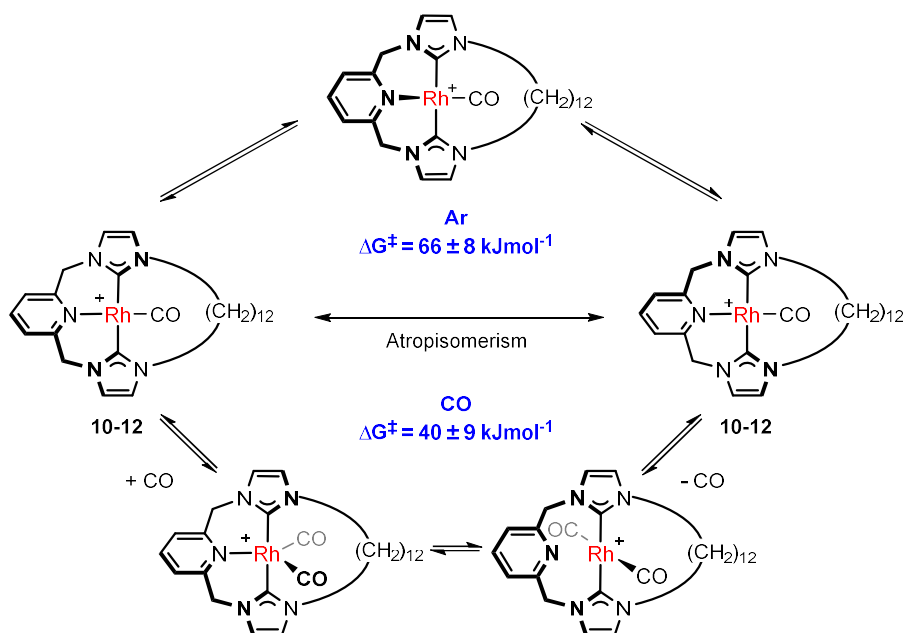
The first instance of divergent reactivity was highlighted during the oxidative addition of MeI to give **X92** and **X93** (Scheme 2.1.3), which proceeded quicker for **X91**. Whilst **X92** was stable, attempts to isolate **X93** showed facile reductive elimination to regenerate **10-12** and therefore was characterised *in situ*. Reactions with PhICl_2 led to the facile formation of both **X94** and **X95**, however,

the adduct bearing the more flexible ligand scaffold was again unstable, again precluding the isolation of **X95**. The oxidation of the rhodium centres during these reactions is evidenced by the higher energy carbonyl IR stretches relative to their rhodium(I) precursors (2067 cm^{-1} **X93**, 2070 cm^{-1} **X92**; 2110 cm^{-1} **X94**, 2111 cm^{-1} **X95**; 1979 cm^{-1} **10-12**, 1986 cm^{-1} **X91**).



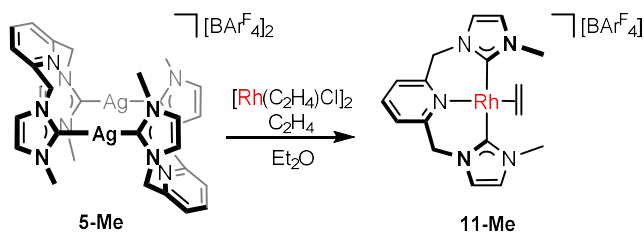
Scheme 2.1.3. Oxidative addition reactions of **X91** and **10-12**

As for its palladium chloride counterpart, isolated **10-12** exhibits C_2 symmetry in solution at room temperature, reflecting high energy atropisomerism and comfortable accommodation of the carbonyl ligand within the ring. However, in the presence of excess carbon monoxide (generated during the synthesis or introduced intentionally) **10-12** becomes significantly more dynamic, exhibiting time-averaged C_{2v} symmetry at room temperature. Substantiated by DFT calculations and VT NMR studies the underlying mechanism was determined (Scheme 2.1.4). Coordination of a second CO ligand forming a 5-coordinate intermediate was shown to facilitate the dissociation of the central pyridine donor ($\Delta G^\ddagger = 40\text{ kJmol}^{-1}$). In the absence of CO this process relies solely on thermally induced atropisomerism, which is associated with a substantially higher barrier to interconversion, $\Delta G^\ddagger = 66\text{ kJmol}^{-1}$.



Scheme 2.1.4. Mechanism of atropisomerism of complex **10-12**

Following these studies, efforts turned to the synthesis of the more reactive rhodium(I) ethylene complexes **11-n** ($n = \text{Me}, 12$). Transmetalation from known **5-Me** to rhodium using $[\text{Rh}(\text{C}_2\text{H}_4)_2\text{Cl}]_2$ under an atmosphere of ethylene afforded **11-Me** in good yield (81%; Scheme 2.1.5),³⁶ however this methodology suffered from persistent difficulties in purification. Despite successive recrystallisations, stubborn silver salts remained, as evidenced by larger than expected Ar^{F} signals in the ^1H NMR spectra (*ca.* 10H vs 8H) and the addition of PPh_3 forming $\text{Ag}(\text{PPh}_3)_2^+$, which was detected by NMR spectroscopy and ESI-MS ($\delta_{31\text{P}} 54.9$, $^1J_{\text{AgP}} = 205 \text{ Hz}$; $631.2 \text{ } m/z$).

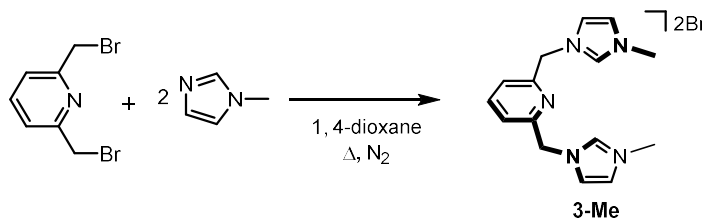


Scheme 2.1.5. Synthesis of **11-Me** from **5-Me**

Similar problems were also observed, albeit to a more substantial extent, during the attempted isolation of **11-12**. In this case the presence of the silver impurities completely precluded isolation of **11-12** and limited its stability when generated *in situ*.

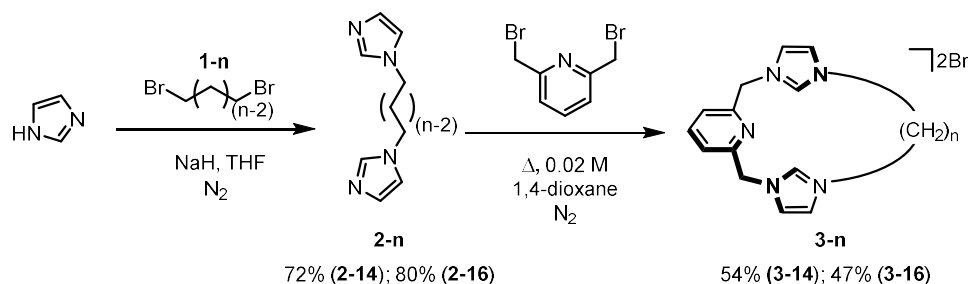
2.2 Proligand synthesis

First reported in 2001, the proligand **3-Me** (Scheme 2.2.1) is a simple methyl flanked acyclic CNC pincer, which was readily prepared using a straightforward literature procedure, involving an S_N2 reaction between the commercially available 2,6-bis(bromomethyl)pyridine and two equivalents of methyl imidazole in refluxing 1,4-dioxane (Scheme 2.2.1).³⁷



Scheme 2.2.1. Synthesis of acyclic proligand **3-Me**

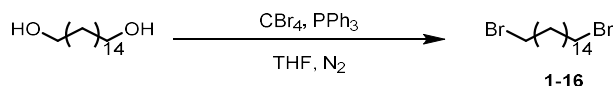
Modification of this procedure, initially by Saito *et al.* and subsequently in the Chaplin group, enabled access to macrocyclic analogues of these pincer proligands; where the imidazolium groups are tethered by a flexible hydrocarbon spacer of varying length ($n = 4, 6, 8, 10, 12$).^{32,33} Extension of this methodology to the larger NHC-based macrocyclic proligands featuring tetradeca- and hexadecamethylene spacers (**3-14** and **3-16**), was successful and the details of the multi-step procedure are discussed in turn below (Scheme 2.2.2).



Scheme 2.2.2. Synthesis of macrocyclic proligands **3-n** ($n = 12, 14, 16$)

The required dibromoalkane starting materials, **1-14** and **1-16**, are both commercially available (Manchester Organics), but required purification on silica (pentane) to remove residual triphenylphosphine oxide (δ_{31p} 29.0, $CDCl_3$). The presence of this impurity strongly suggests these compounds are prepared commercially *via* an Appel-type reaction.^{38,39} Indeed, the synthesis of target

dibromoalkanes can be achieved in this way, for example reaction of hexadecane-1,2,-diol with carbon tetrabromide and triphenylphosphine afforded **1-16** in high purity and yield (84%; Scheme 2.2.3).



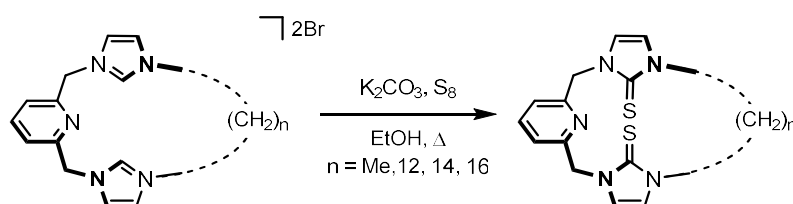
Scheme 2.2.3. Preparation of dibromoalkane **1-16**

With the dibromoalkane starting materials in hand, bis(imidazole)alkane linkers, **2-n**, were readily prepared in high purity and good yield (72 – 80%) from reaction with thoroughly dried imidazole (Scheme 2.2.2). The subsequent macrocyclisation reaction between 2,6-bis(bromomethyl)pyridine and selected linker **2-n**, was carried out under high dilution conditions, involving slow (*ca.* 6 mLh⁻¹) and simultaneous addition of 0.06 M 1,4-dioxane solutions of the two reagents into a large volume of vigorously stirred and refluxing 1,4-dioxane (*ca.* 110 mL per mol of **2-n**). Following recrystallisation, the desired bis(imidazolium) proligands **3-14** and **3-16** were obtained as off-white hygroscopic solids in good isolated yields of 54 and 47% respectively. Notably, reactions conducted under more concentrated conditions, such as those employed for **3-n** (*n* = 8, 10, 12), resulted in considerably lower yields (< 25%), due to extensive oligomerisation.

The structures of **3-14** and **3-16** were confirmed through a combination of NMR spectroscopy and ESI-MS, with the associated data in close agreement with those previously reported for **3-n** (*n* < 14).^{32,33} For instance, the ¹H NMR spectra of **3-14** and **3-16** recorded in CD₂Cl₂ displayed characteristic (pre-carbenic) 2H imidazolium signals, at δ 10.91 and 10.84 for **3-14** and **3-16**, respectively (*cf.* δ 10.81 for **3-12**), and 4H singlet methylene bridge proton (pyCH₂) resonances, at *ca.* δ 5.74 – 5.76. Likewise, the associated ¹³C{¹H} NMR spectra show the corresponding imidazolium carbon signals at δ 138.4 and 138.3 for **3-14** and **3-16**, respectively (*cf.* δ 138.4 for **3-12**). Alternate formulations as higher order oligomers were discounted using high-resolution mass spectrometry, with only [M-Br]⁺ ion peaks with the expected integer isotope pattern observed at 514.2557 (calcd 514.2540) and 542.2848 (calcd 542.2853) *m/z*, for **3-14** and **3-16** respectively.

As further corroboration of their structures, air and moisture stable NHC thione (NHCS) derivatives of **3-n** were prepared, **4-n** (Scheme 2.2.4). These are potentially interesting soft donor ligands in their own right, for the construction of metalloenzyme mimics,⁴⁰⁻⁴³ use in C-C cross coupling reactions^{44,45} and norbornene polymerisations,^{46,47} as well as use as latent carbene precursors. The latter, however, requires the use of molten potassium and elevated temperatures (*viz.* **X97**, Figure 2.2.1).⁴⁸⁻⁵¹

Using a modified literature procedure,⁵² involving the deprotonation of the respective imidazolium salts with K₂CO₃ in the presence of elemental sulfur, the complete series of bis(imidazole-2-thione) functionalised pincers **4-n** were obtained in good isolated yields (59 – 76%) following purification on silica (CH₂Cl₂:MeOH; Scheme 2.2.4).



Scheme 2.2.4. Preparation of bis(imidazole-2-thiones), **4-n** ($n = \text{Me}, 12, 14, 16$)

Compounds **4-n** were characterised both in solution using NMR spectroscopy and ESI mass spectrometry, and in the case of **4-12** in the solid-state using X-ray diffraction (Figure 2.2.1). Their formation is marked by the absence of characteristic imidazolium signals in the ¹H NMR spectra and significantly downfield shifted NCN signals compared to **3-n** (*ca.* 130 to 160 ppm), which are in close agreement with previously reported bis(imidazol-2-thione) compounds (*cf.* δ 161.2, **X96a**; 162.3, **X97b**; 161.5, **X98a**).^{44,47,51,53,54} The structural metrics of **4-12** are also directly comparable to literature precedents, with the C=S bond distance the most pertinent metric (C122–S102 = 1.6801(12) Å; C107–S101 = 1.6843(12) Å; *cf.* 1.685 Å, **X96a**).^{44,51,53,54} The solid-state structure is further notable for the adoption of a ‘box-like’ conformation, with the imidazole-2-thione groups antiparallel, but orthogonal to the pyridine moiety (86.31° and 84.31°). ESI-MS data and satisfactory elemental analysis provided further verification of the structural formulation of **4-n** and by inference proligands **3-n**.

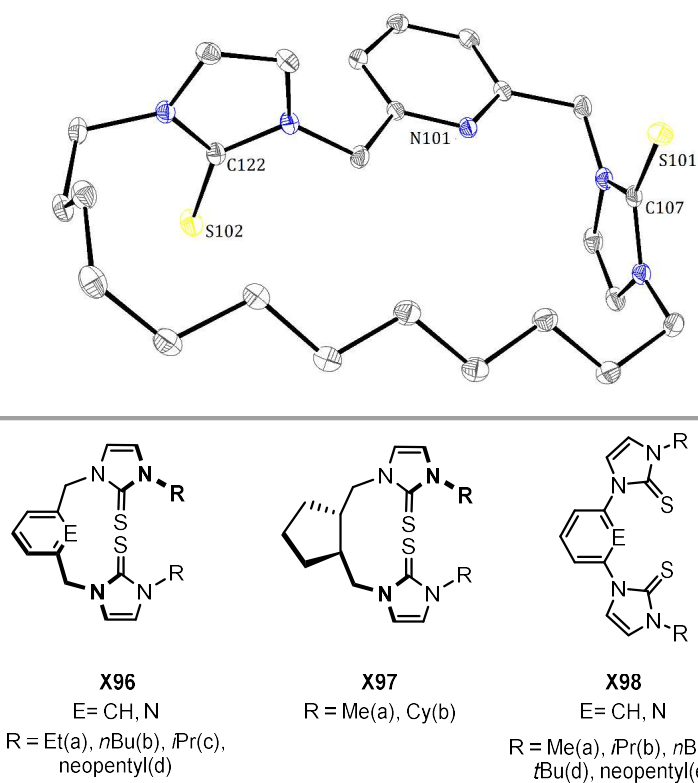
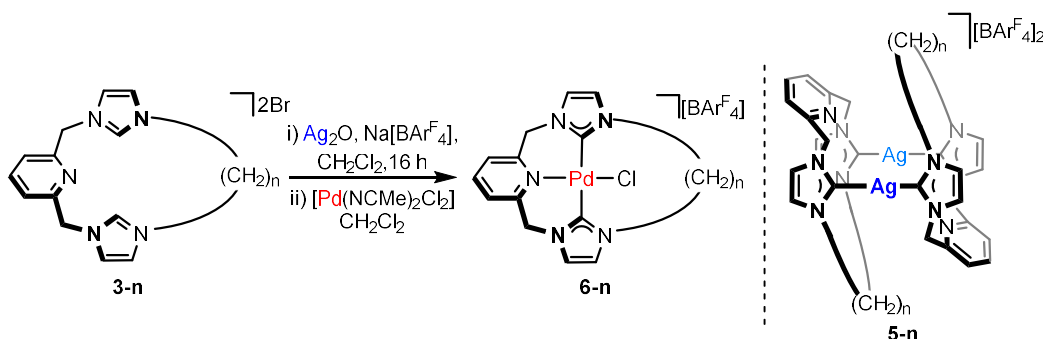


Figure 2.2.1 Solid-state structure of 4-12 and related literature examples. Thermal ellipsoids at 30% probability and hydrogen atoms omitted for clarity

2.3 Synthesis of palladium chloride complexes – 6-n

Palladium(II) chloride complexes of **3-14** and **3-16** were initially targeted to complete a homologous family of complexes, $[\text{Pd}(\text{CNC-}n)\text{Cl}][\text{BAr}^{\text{F}}_4]$ (**6-n**; $n = 8, 10, 12, 14, 16$), first started in the Chaplin group (*vide supra*).³³ The two new complexes were prepared using the established silver transmetallation procedure, involving *in situ* generation of the silver transfer agents, $[\text{Ag}(\text{CNC-}n)]_2[\text{BAr}^{\text{F}}_4]_2$ **5-n**,[†] from reaction between **3-n** and Ag_2O in the presence of $\text{Na}[\text{BAr}^{\text{F}}_4]$. Subsequent transmetallation to palladium results on addition of the palladium(II) precursor $[\text{Pd}(\text{NCMe})_2\text{Cl}_2]$ (Scheme 2.3.1). In this way, **6-14** and **6-16** were isolated as moderately air and moisture stable complexes in reasonable yields (31 – 41%) following purification on silica and fully characterised in solution and the solid-state (*vide infra*).



Scheme 2.3.1. Preparation of palladium chloride complexes **6-n** ($n = 14, 16$)

In the case of **3-16**, direct addition of $[\text{Pd}(\text{NCMe})_2\text{Cl}_2]$ to the reaction mixture containing *in situ* generated **5-16**, led to the isolation of the mixed halide product, $[\text{Pd}(\text{CNC-}16)\text{X}][\text{BAr}^{\text{F}}_4]$ ($\text{X} = \text{Cl}, \text{Br}$). The bromide containing component was first detected by ^1H and $^{13}\text{C}\{^1\text{H}\}$ NMR spectroscopy (Figure 2.3.1) and subsequently identified using high resolution ESI-MS which notably featured the distinctive bromine isotope pattern (*viz.* 646.1730, calcd 646.1737 m/z). Integration of ^1H NMR data indicated that this palladium bromide contaminant accounted for *ca.* 15% of the product mixture. Similar halide scrambling has been described for related platinum(II) bromide complexes in which an analogous *in situ* silver

[†] As conformation **5-14** and **5-16** were independently isolated and characterised as light, air and moisture sensitive solids (see: Chapter 5).

transmetallation procedure from the CNC·2HCl proligand afforded exclusively the [Pt(CNC)Cl]Cl complex on reaction with PtBr₂ as opposed to the anticipated bromide derivative.⁵⁵

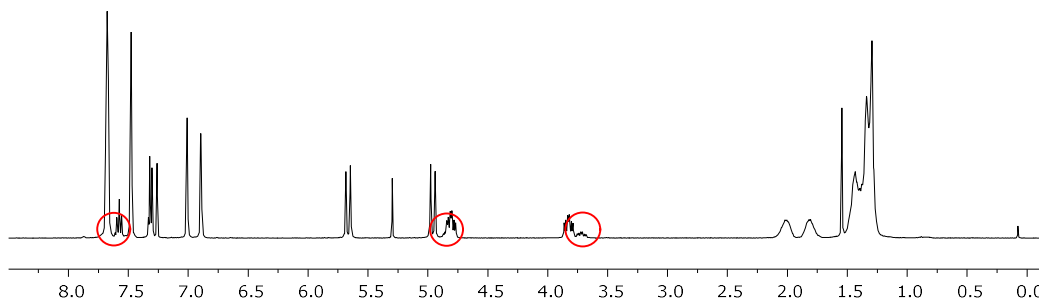


Figure 2.3.1. ¹H NMR spectrum of crude **6-16** (400 MHz, CDCl₃). Signals assigned to bromide containing product are circled.

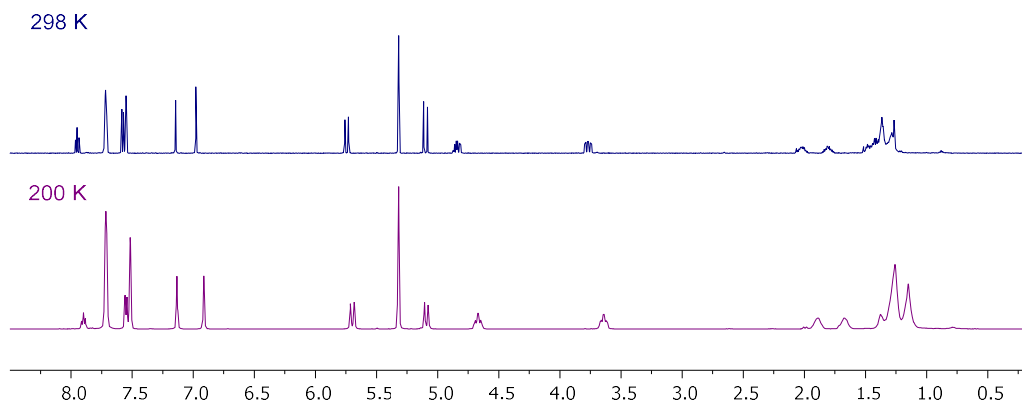
Mixed halide compounds are not observed for the smaller ring systems ($n < 16$), suggesting that it is only with the hexadecamethylene spacer that the larger bromide anion can be comfortably accommodated within the cavity. Despite repeated attempts, separation of the bromide impurity from **6-16** was not possible. Attempted halide exchange reactions using excess of various chloride salts (*e.g.* (nBu)₄NCl) were also met with little success. Gratifyingly, however, slight modification of the existing procedure, involving filtration of *in situ* generated silver complex **5-16** onto [Pd(NCMe)₂Cl₂], avoided incorporation of bromide and enabled isolation of analytically pure **6-16** in moderate yield (41%).

Formation of complexes **6-n** was confirmed by the absence of imidazolium signals in the ¹H NMR spectra (*ca.* 10.8 ppm, CD₂Cl₂) and downfield shifts of the associated ¹³C carbene resonances (*ca.* 138 to 163 ppm, CD₂Cl₂), which interestingly show a positive correlation with the ring size; tending towards that of the acyclic methyl flanked **6-Me** reported in the literature (*cf.* 166.0 ppm, Table 2.3.1).⁵⁶ These complexes also show strong parent cation signals with the predicted isotope pattern in high resolution ESI mass spectra, 574.1926 (calcd 574.1930; **6-14**) and 602.2247 (calcd 602.2244; **6-16**) *m/z*, and their elemental analyses are in good agreement with predicted values.

Table 2.3.1: Selected NMR data for palladium complexes **6-n**^{33,56}

	n	δ_{pyCH_2} /ppm	$^2J_{\text{HH}}$ /Hz	$\delta_{\text{N}_{\text{CN}}}$ /ppm
6-Me	Me	5.76; 5.11	15.1	166.0
6-8	8	5.34; 5.08	15.3	162.4
6-10	10	5.57; 4.98	15.3	163.3
6-12	12	5.63; 4.97	15.0	164.5
6-14	14	5.74; 5.10	15.0	165.6
6-16	16	5.66; 4.95	15.0	165.6

The ^1H NMR spectra of **6-14** and **6-16** are consistent with adoption of C_2 symmetry in solution at 298 K, with distinctly diastereotopic methylene bridge protons ($^2J_{\text{HH}} = 15.0$ Hz). Contrasting the observations reported for the smaller ringed systems ($n < 12$),³³ but consistent with the increased size of the ring cavity, this high symmetry is retained on cooling to 200 K (Figure 2.3.2).


Figure 2.3.2. VT ^1H NMR spectra of **6-14** (500 MHz, CD_2Cl_2)

The difference in solution dynamics can be rationalised further through evaluation of the solid-state structures of **6-14** and **6-16**, which show a marked difference compared with the smaller macrocyclic counterparts. While the smaller macrocyclic complexes ($n < 12$) exhibit C_1 symmetric structures in the solid-state, resulting from steric clashes between the macrocyclic tether and chloride ligand that force the ring to be skewed to one side and cause deviation of the N-Pd-Cl bond angle from linearity, the longer hydrocarbon spacers in **6-12** and these new complexes **6-14** and **6-16** (Figure 2.3.3) enable more ideal C_2 symmetric structures to be adopted.

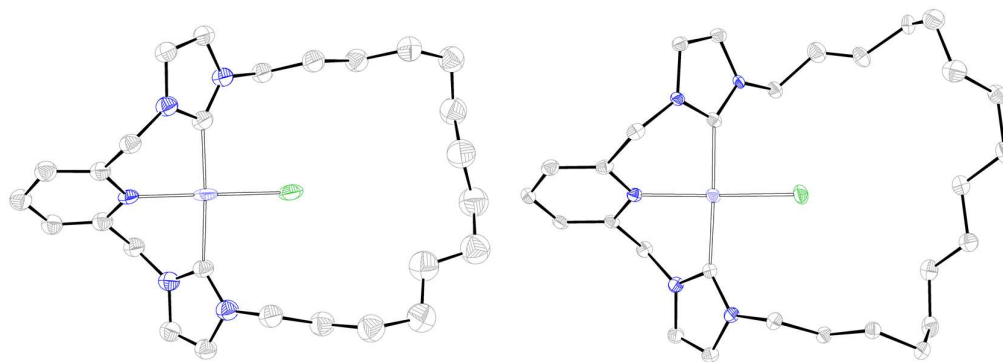
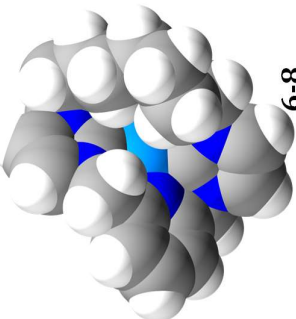
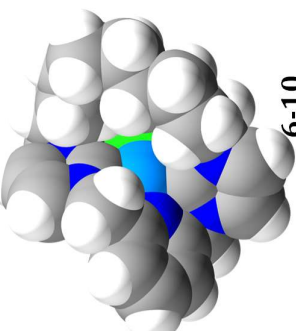
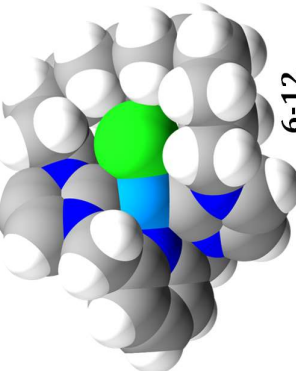
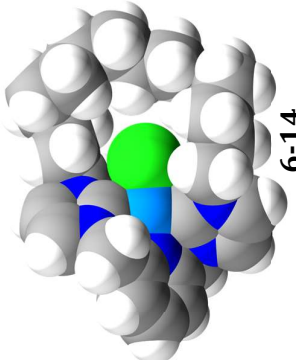
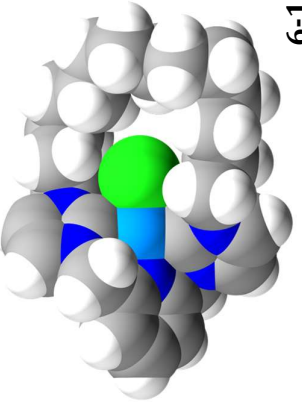
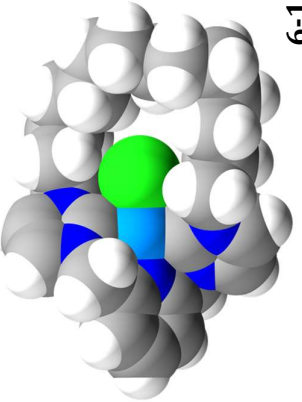
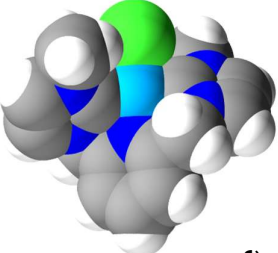


Figure 2.3.3. Solid-state structures of **6-14** and **6-16**. Thermal ellipsoids at 20 and 35% thermal probability, respectively; hydrogen atoms and counter anions omitted for clarity. Structure shown of **6-14** is one of two independent molecules ($Z' = 2$).

The metal coordination geometries of **6-14** and **6-16** are almost ideal square planar arrangements, with N-Pd-Cl bond angles of $179.0(6)^\circ/178.7(6)^\circ$ and $175.77(5)^\circ$, respectively, compared to $163.39(4)^\circ$ in **6-8**. The key parameters for the complete homologous series are summarised in Table 2.3.2 along with spacefill representations of the cationic fragments. Visualising the solid-state structures in this way unambiguously demonstrates the effect of expanding the annulus size, with **6-14** and **6-16** notable for not only accommodating the chloride ligand but leaving additional space.

Combined, the solution and solid-state data convincingly evidence the expected trend towards a larger and more accessible macrocyclic annulus for **6-14** and **6-16**, through which metal-based chemistry can be performed, thus reflecting the notion that they are greater poised to facilitate the formation of supramolecular architectures.

Table 2.3.2: Spacefill representations and selected bond lengths (Å) and angles (°) for **6-n** in the solid-state.

					
6-8	6-10	6-12	6-14		
				6-Me	
6-16	6-16				
	Pd-Cl / Å	Pd-N / Å	Pd-C _{NHC} / Å	N-Pd-Cl / °	C _{NHC} -Pd-C _{NHC} / °
6-Me^a	2.298(5)	2.068(1)	2.026(2); 2.029(2)	178.19(3)	173.60(7)
6-8	2.3051(5)	2.087(2)	1.983(2); 2.073(2)	163.39(4)	168.82(7)
6-10	2.3217(5)	2.080(2)	2.004(2); 2.078(2)	166.29(5)	171.93(8)
6-12	2.287(4)	2.077(10)	2.056(13); 2.036(12)	176.2(3)	172.8(6)
6-14^b	2.286(9); 2.263(9)	2.09(2); 2.03(2)	2.03(3), 2.05(3); 2.05(3), 2.04(2)	179.0(6); 178.7(6)	176(1); 174.6(9)
6-16	2.2910(7)	2.062(2)	2.058(5); 2.033(2)	175.77(5)	171.4(2)
<i>a</i> - Data from 6-Me with the BF ₄ counter anion ⁵⁶ ; <i>b</i> - Z' = 2					

2.4 Effectiveness of Ag(I), Cu(I) and Ni(II) transfer agents

Binding of NHCs to metal centres can be achieved in several ways (Chapter 1.3.3). Transmetalation is a particularly important method for accessing complexes of CNC ligands which feature acidic methylene bridges that can be readily deprotonated under other metallation conditions. Silver is by far the most commonly employed carbene transfer agent; however, its innate redox activity and light sensitivity is such that potential oxidative side reactions hinder its universal applicability. In light of recurrent issues in purification, studies have emerged in the literature targeting alternate transfer agents.^{57,58}

The use of the corresponding silver complexes **5-n**, generated *in situ*, has proven particularly fruitful in the synthesis of the aforementioned palladium complexes **6-n**. However, this method has been ineffective in the formation of rhodium ethylene derivatives **11-n** due to challenges in purification associated with the removal of silver containing by-products (*vide supra*). After surveying the literature, we decided to assay the effectiveness of isolated Ag, Cu, and Ni transfer agents (**5-12**, **9-12** and **7-12**, respectively), using **3-12** as an exemplar ligand. The former two complexes were prepared as part of previous work in the group,³⁶ the latter is novel. Selective transmetalation in high conversion is essential to limit the amount of manipulation and purification required to isolate the extremely reactive target rhodium products.

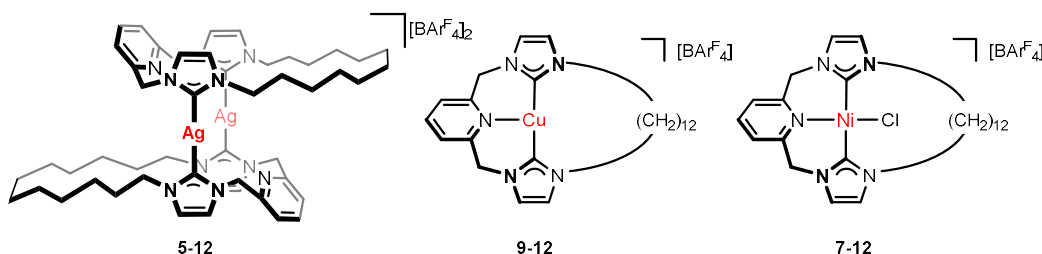
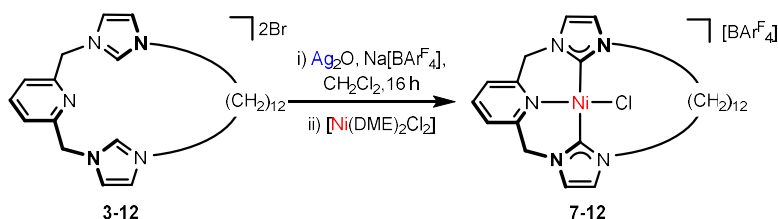


Figure 2.4.1. Transfer agents under investigation

2.4.1 Synthesis of nickel chloride complex - **7-12**

With the view to its use as a carbene transfer agent nickel(II) congener, **7-12** was targeted. Using an analogous procedure to that used in the formation of **6-n** (Scheme 2.4.1); *in situ* formation of **5-12** and subsequent reaction with nickel

precursor $[\text{Ni}(\text{DME})\text{Cl}_2]$, **7-12** was isolated as an air and moisture stable yellow solid following purification on alumina (CH_2Cl_2 ; 29% yield). This poor yield can be attributed to the instability of **7-12** on alumina with the weak Ni–C constituent bonds causing demetallation during purification. This is corroborated by the high yield obtained of the acyclic congener **7-Me** using a modified procedure, which avoided the need for chromatographic purification (79%).[‡]



Scheme 2.4.1. Synthesis of nickel chloride complex **7-12**

Formation of **7-12** was confirmed by NMR spectroscopy, high resolution ESI mass spectrometry and elemental microanalysis. The ESI-MS data gave a peak for the parent cation with the expected integer spacing and anticipated isotope pattern at 498.1929 (calcd 498.1929) m/z (*cf.* 360.0521, calcd 360.0520 m/z , **7-Me**). The NMR spectra (CD_2Cl_2 , 500 MHz) for **7-12** display the expected C_2 symmetric spectroscopic features described previously for **6-n** ($n > 10$), with diastereotopic methylene bridge proton resonances resolved as a pair of doublets at 5.14 and 6.30 ppm ($^2J_{\text{HH}} = 15.0$ Hz; δ 5.16/6.35, $^2J_{\text{HH}} = 15.0$ Hz, **7-Me**) and the carbenic carbon signal is observed at 162.0 ppm (*cf.* δ 163.3, **7-Me**; δ 164.5, **6-12**).

In the solid-state, **7-12** shows the predicted square planar geometry with *mer*-tridentate coordination of the pincer scaffold and the chloride ancillary ligand *trans*-disposed to the pyridine moiety (Figure 2.4.2). The structure also displays an expected contraction of metal-ligand bond lengths in comparison to **6-12** (Ni–Cl, 2.145(2); Ni–N, 1.928(5); Ni–C, 1.898(6), 1.916(6) Å; Pd–Cl, 2.287(4); Pd–N, 2.077(10); Pd–C, 2.036(12), 2.056(13) Å), but otherwise remains isostructural to the palladium-based analogue (Figure 2.3.3). The structural metrics of **7-12** also mirror those of related complex **X99a**; Ni–N (1.929(12) Å;

[‡] *Adaption of this procedure afforded the acyclic analogue 7-Me in excellent yield (See Chapter 5). Characterisation data allows direct comparison to 7-12.*

cf. 1.921(3) Å **X99a**), Ni–Cl (2.145(2) Å; cf. 2.278(8) Å **X99a**); Ni–C_{NHC} (1.918(8)/1.892(8) Å cf. 1.923(5)/ 1.920(5) Å **X99a**). Most notably, the chloride ligand is easily accommodated within the macrocyclic aperture, which is orientated to maintain *pseudo-C*₂ symmetry in the solid-state, with an essentially linear N–Ni–Cl bond angle (179.06(15)°; cf. 176.2(3)°, **6-12**).

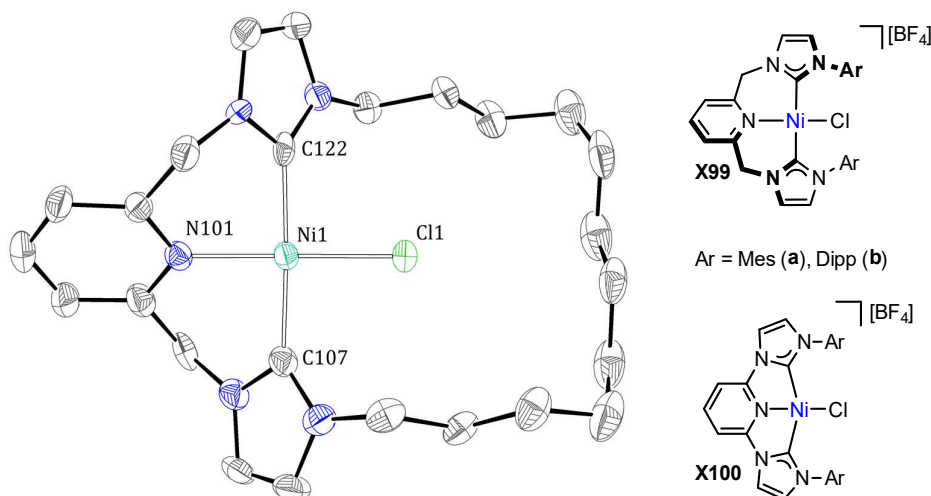


Figure 2.4.2. Solid-state structure of **7-12**. Thermal ellipsoids at 50% probability; hydrogen atoms and anion omitted for clarity. Alongside related literature complexes.^{59–62}

2.4.2 Transmetallation studies

Using the well-defined the silver and copper transfer agents bearing **3-12** (**5-12** and **9-12** respectively) previously reported in the group,⁶³ as well as, the novel nickel compound **7-12**, evaluation of their respective transmetallation capacity towards the formation of d⁸ metal complexes **6-12** (Pd–Cl), **7-12** (Ni–Cl), **10-12** (RhCO) and **11-12** (Rh(C₂H₄)) was conducted. *In situ* reaction monitoring by means of ¹H NMR spectroscopy (CD₂Cl₂, d1 = 5 s), using the [BAr^F₄] resonances (δ 7.72, 8H) as an internal standard, presented insights into the progression of these reactions over time, the results of which are tabulated below (Table 2.4.1).

Table 2.4.1. Transmetalation reactions of **5-12**, **7-12** and **9-12** complexes with late transition metal precursors.

<div style="display: flex; justify-content: space-around; margin-top: 10px;"> <div> <p>[M] = Ag (5-12)</p> <p>[M] = Cu (9-12)</p> <p>[M] = NiCl (7-12)</p> </div> <div> <p>M'' = [Pd(NCMe)₂Cl₂]</p> <p>M'' = [Ni(DME)Cl₂]</p> <p>M'' = [Rh(CO)₂Cl]₂</p> <p>M'' = [Rh(C₂H₄)₂Cl]₂</p> </div> <div> <p>[M'] = PdCl (6-12)</p> <p>[M'] = NiCl (7-12)</p> <p>[M'] = Rh(CO) (10-12)</p> <p>[M'] = Rh(C₂H₄) (11-12)</p> </div> </div>						
M''	M	<i>t</i> /h	T/°C	Product	NMR Yield ^a /%	Isolated yield/%
[Pd(NCMe) ₂ Cl ₂]	Ag	0.5	20	6-12	73	-
[Pd(NCMe) ₂ Cl ₂]	Cu	0.5	20	6-12	23	-
[Pd(NCMe) ₂ Cl ₂]	Ni	48	20	6-12	80 ^b	66
[Rh(CO) ₂ Cl] ₂	Ag	0.5	20	10-12	72	-
[Rh(CO) ₂ Cl] ₂	Cu	0.5	20	10-12	98	82
[Rh(CO) ₂ Cl] ₂	Ni	0.5	20	10-12	98	90
[Ni(DME)Cl ₂]	Ag	20	20	7-12	22 ^b	-
[Ni(DME)Cl ₂]	Ag	20	40	7-12	76	29
[Ni(DME)Cl ₂]	Cu	20	20	7-12	86 ^b	-
[Ni(DME)Cl ₂]	Cu	5	40	7-12	90	27
[Rh(C ₂ H ₄) ₂ Cl] ₂	Ag	0.5	20	11-12	92	-
[Rh(C ₂ H ₄) ₂ Cl] ₂	Cu	0.5	20	11-12	88	-
[Rh(C ₂ H ₄) ₂ Cl] ₂	Ni	1.5	20	11-12	32 ^b	-

a – Calculated from integration of the ¹H NMR data using the Ar^F signals as an internal standard;
b – Incomplete reaction

Suspensions of [Pd(NCMe)₂Cl₂] and the chosen transfer agent required periodic sonication over the course of the reaction to aid solubilisation of the palladium precursor. After 30 minutes the ¹H NMR spectra of the resulting yellow-brown suspensions show no signals pertaining to either **5-12** or **9-12**. Whereas the silver-based transmetalation saw selective formation of **6-12** (73%), the results were less positive when using the less established transfer agents. Whilst **9-12** saw a rapid consumption of starting material the selectivity of this reaction was extremely poor with **6-12** accounting for only 23% of the product mixture. On the other hand, the use of **7-12**, whilst slow,

did see selective conversion and a high isolated yield following a prolonged reaction period (66%).

In comparison, the formation **7-12** was shown to be sluggish under the standard conditions of the experiment for both **5-12** and **9-12** showing only 22% and 86% conversion, respectively after 20 hours of reaction. Again the poor solubility of the metal precursor ([Ni(DME)Cl₂]) being in part responsible. Repeating under more forcing conditions (40 °C) gave significantly higher conversions (76% and 90%, respectively) yet the isolated yields remained poor and in-line with the yield associated with the preparation of **7-12** using the *in situ* methodology (*vide supra*). Curiously, unlike in the formation of **6-12** this reaction proceeded much quicker from **9-12** relative to **5-12**, suggesting the poor rate of conversion is more complex than simply a solubility issue. Ultimately, these results reflect the nuanced nature of transmetallation reactions which makes making predictions about the activity of these transfer agents particularly challenging.

Expanding this study to the target rhodium complexes began with the more synthetically accessible **10-12**, isolated previously in the group (*vide supra*).³⁵ The transmetallation reaction proceeded rapidly and in high fidelity for all three transfer agents (**5-12**, **9-12** and **7-12**), each giving high NMR yields (> 70%). Complete consumption of the transfer precursors was observed within 30 minutes for all examples alongside the formation of **10-12** with high selectivity. Complex **10-12** was subsequently isolated in > 80% yield from both the reactions of **9-12** and **7-12**. Although these yields exceed that of the yield from the *in situ* Ag transmetallation (52%), they require the isolation of the respective transfer agent prior to use as a synthetic precursor and taking this into consideration the respective yields are significantly lower over the numerous steps from **3-12** (38% for **9-12** and 26% for **7-12**).³⁵

The transmetallation studies for the preparation of the more synthetically demanding rhodium(I) ethylene targets **11-n**, presented mixed success. With the high lability of the coordinated ethylene ligand making purification a significant challenge (*vide supra*), the high fidelity of these transformations is of utmost

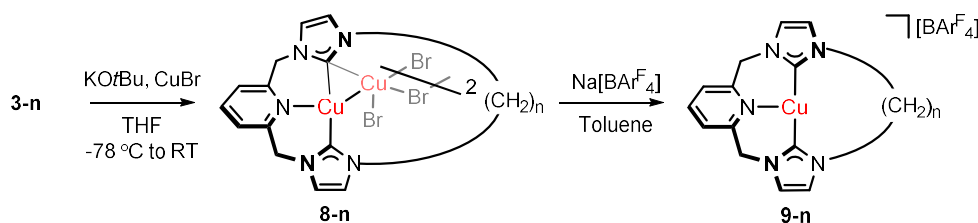
importance. Using the aforementioned procedure with $[\text{Rh}(\text{C}_2\text{H}_4)_2\text{Cl}]_2$, saw rapid consumption of the starting materials (< 30 mins) and selective conversion to **11-12** for both **5-12** and **9-12**. Whereas, the transformation from **7-12** proceeds in a more sluggish fashion with only 32% conversion after 1.5 hours and as such is unlikely to be synthetically useful in the formation of **11-12**. Reflecting on these results and previous purification issues encountered using the *in situ* silver procedure, **9-n** were identified as the most promising in terms of the isolation of analytically pure samples of **11-n** (n = Me, 12, 14, 16).

2.5 Synthesis and characterisation of copper complexes

The well-defined copper transfer agent **9-12** was prepared previously in the group using a two-step procedure from **3-12**, *via* copper bromide intermediate **8-12**, in a good overall yield (46%).⁶³ The synthesis involved deprotonation of **3-12** in the presence of CuBr to generate **8-12**, and the subsequent reaction with excess Na[BAr^F₄] to introduce the weakly coordinating counter anion and form **9-12**. Both **8-12** and **9-12** were isolated and characterised in solution and the solid-state.

2.5.1 Copper(I) bromide adducts – **8-n**

Building on preliminary work in the group using **3-12**,⁶³ Cu(I) complexes **8-n** were first prepared, following low temperature deprotonation of the chosen prolignand (**3-n**) and subsequent reaction with CuBr, and ultimately isolated as pale-yellow solids in moderate to good yields (*n* = Me, 54%; 12, 76%; 14, 83%; 16, 86%; Scheme 2.5.1).



Scheme 2.5.1. Synthesis of copper complexes **8-n** and **9-n** (*n* = Me, 12, 14, 16)

Like other related Cu(I) complexes,⁶⁴ **8-n** proved to be extremely challenging to handle, requiring rigorous application of anaerobic techniques to prevent oxidative decomposition to characteristically green copper(II) derivatives, both in solution and the solid-state. The isolation of **8-Me**, proved especially difficult, exacerbated by extremely poor solubility in most organic solvents (*e.g.* MeCN, THF, Et₂O, CH₂Cl₂) and is reflected in its comparably lower yield.

Characterisation using NMR spectroscopy, ESI-MS and X-ray diffraction (Figure 2.5.1) substantiated the successful formation of **8-n**. The ¹H NMR data collected in CD₂Cl₂ indicates the adoption of C_{2v} symmetry in solution, which can only be reconciled if cation-anion pairing is weak. Similarly, the acquired mass

spectrometric data only demonstrates parent ions for the metal cation $[\text{Cu}(\text{CNC-n})]^+$ viz. 330.0769 (**8-Me**; calcd 330.0774), 496.2492 (**8-14**; calcd 496.2496), 524.2808 (**8-16**; calcd 524.2809) m/z . Attempts to obtain satisfactory elemental microanalyses of **8-n**, however, were frustrated by facile oxidative decomposition.

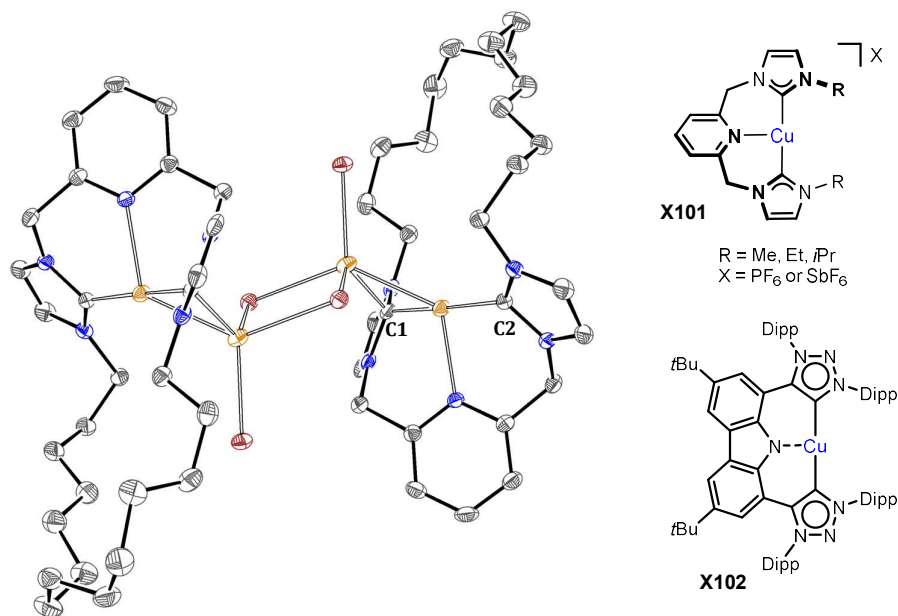
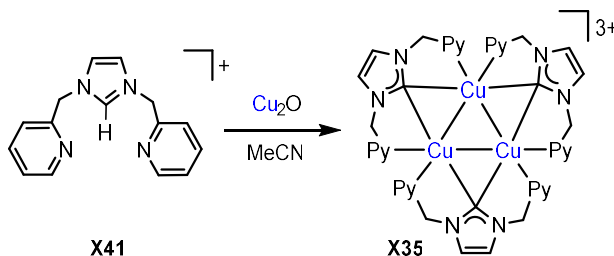


Figure 2.5.1. Solid-state structure of **8-14**. Thermal ellipsoids at 50% probability; hydrogen atoms omitted for clarity. Alongside related literature examples.

Single crystals of **8-14** were obtained from a saturated solution in MeCN and allowed its solid-state structure to be determined using X-ray diffraction. The solid-state structure of **8-12** was also obtained by R. E. Andrew and both are notable for the C_i agglomeration of two $[\text{Cu}(\text{CNC})]^+$ units affixed in an anti-arrangement through coordination to the cuprous bromide dianion $[\text{Cu}_2\text{Br}_4]^{2-}$. The formation of this assembly is marked by adoption of a μ^2 -bridging interaction of one of the NHC donors, which is supported by formation of a short cuprophilic interaction ($\text{Cu}-\text{Cu}$, 2.5182(5) Å, **8-14**; 2.521(5) Å, **8-12**), and leads to distortion of the pincer from an ideal T-shaped coordination geometry ($\text{C1}-\text{Cu1}-\text{C2}$; 171.2(1)°, **8-14**; 167.9(1)°, **8-12**) and an elongation of the Cu-carbene bond (1.977(3) Å, $\text{Cu}-\text{C1}$ vs 1.928(3) Å $\text{Cu}-\text{C2}$; cf. 1.906(1) Å and 1.914(1) Å, **X101** $\text{R} = i\text{Pr}$). This carbene bonding mode is not unprecedented and features in a number of multimetallic Cu complexes,^{65–69} as well as some Ag and Ni complexes.^{70,71}

Trinuclear **35** (Scheme 2.5.2) notably contains three NHCs bound in this way, but unlike **8-n**, this interaction is retained in solution and is associated with considerably lower frequency signals for the carbenic resonances (δ 167 – 169 *cf.* 175.3 – 178.9, **8-n**).^{65,69,72}



Scheme 2.5.2. Synthesis of trinuclear copper complex **X35**

2.5.2 Copper(I) BAr^{F}_4 complexes – **9-n**

Following the successful preparation of **8-n**, salt metathesis using an excess of $\text{Na}[\text{BAr}^{\text{F}}_4]$ in toluene, afforded appreciably more stable and soluble **9-n** in moderate yields (64 – 65%). Formation of these complexes was substantiated using $^{13}\text{C}\{^1\text{H}\}$ NMR spectroscopy, with the carbenic resonances slightly downfield compared with those of the parent **8-n** (δ 179.6 – 180.0 **9-n**, *cf.* 175.3 – 178.9 **8-n**, CD_2Cl_2). The incorporation of the weakly coordinating $[\text{BAr}^{\text{F}}_4]^-$ counter anion is apparent by ^1H NMR spectroscopy by Ar^{F} resonances totalling 12H at 7.72 and 7.56 ppm. These spectra are otherwise notable for sharp resonances and apparent C_{2v} symmetry, with only minor differences in chemical shift compared to **8-n** ($\delta < 0.2$ ppm), consistent with a distinct monocation in solution, for both **9-n** and by inference **8-n**. This is supported by the identification of strong parent cation signals by ESI-MS (330.0781, **9-Me**, calcd 330.0774 m/z ; 496.2492, **9-14**, calcd 496.2496 m/z ; 524.2814, **9-16**, calcd 524.2809 m/z).

Crystals of **9-12** and **9-14** were obtained and permitted characterisation in the solid-state using X-ray diffraction (Figure 2.5.2). Crystals of **9-12** were grown from diffusion of hexane into a CH_2Cl_2 solution at -30°C and the structure is notable for having a single complex in the asymmetric unit ($Z' = 1$),[†] whereas crystals of **9-14**, grown from a THF / hexane layer have a $Z' = 2$.

[†] An alternative polymorph of **9-12** featuring two structurally similar independent complexes ($Z' = 2$) was initially obtained by R. E. Andrew, but for simplicity is not discussed further.⁶³

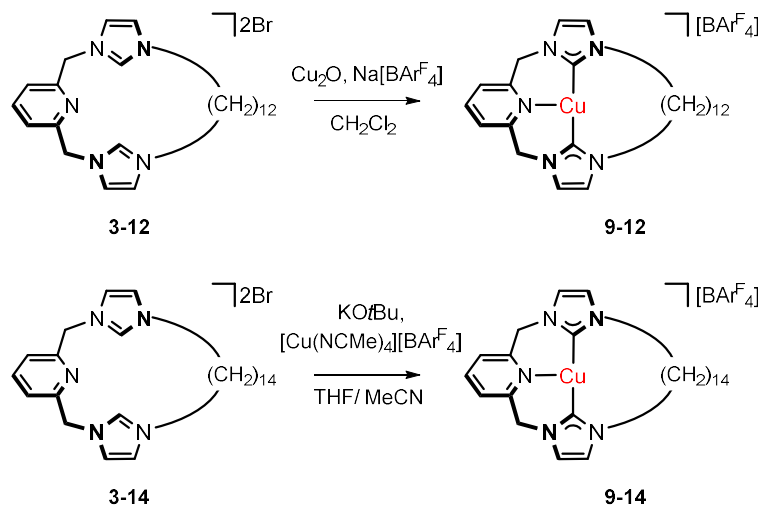


Figure 2.5.2. Solid-state structures of **9-12** and **9-14**. Thermal ellipsoids at 35% probability. Counter anions, hydrogen atoms, solvents and minor disordered components omitted for clarity. Structure shown of **9-14** is one of two independent molecules ($Z' = 2$).

Contrasting the comparable solution characteristics, in the solid-state the nature of the counter anion forces significantly different coordination geometries between **8-n** and **9-n**; with the weakly-coordinating $[\text{BAr}^{\text{F}}_4]^-$ counter anion imposing a chemically discrete cation-anion pair (Figure 2.5.2). The solid-state structures of **9-12** and **9-14** display near C_2 symmetry with the NHC donors orthogonally twisted relative to the coordination plane to enable the metal to adopt a T-shape coordination geometry (C–Cu–N 90.8(1)°, 92.2(1)°, **9-12**; 90.8(1)°, 89.7(1)°, **9-14**). The hydrocarbon tethers are notably skewed to one side of the metal coordination plane and adopt a contorted configuration folding back on themselves towards the copper centre. The Cu–C bond lengths are identical within error (1.898(3) Å, 1.908(4) Å, **9-12**; 1.901(3) Å, 1.900(3) Å, 1.907(3) Å, 1.906(3) Å, **9-14**) reflecting the symmetric binding of the copper centre to the pincer motif. These metrics are consistent with other previously reported copper compounds (1.906(1) Å, 1.914(1) Å, **X101** R = Et).

In an attempt to simplify the synthesis of **9-n**, alternative pathways avoiding the need to isolate highly reactive **8-n** were briefly investigated (Scheme 2.5.3). Motivated by literature precedents, such as the complexation of **X41** to form **X35** (Scheme 2.5.2), the reaction of **3-12** with Cu_2O and $\text{Na}[\text{BAr}^{\text{F}}_4]$ in CH_2Cl_2 was assayed. Although this reaction did generate **9-12**, the reaction proved very

sluggish and separation of the product from unreacted starting material was problematic. A more promising alternative, based on procedures developed by Tahsini *et al.* involving low temperature deprotonation and reaction with $[\text{Cu}(\text{NCMe})_4]^+$,⁶⁴ was also investigated using **3-14**. Whilst **9-14** complex was obtained in a moderate yield (55%), this represented only a modest improvement over our primary method (54% over two steps) and was not considered further.

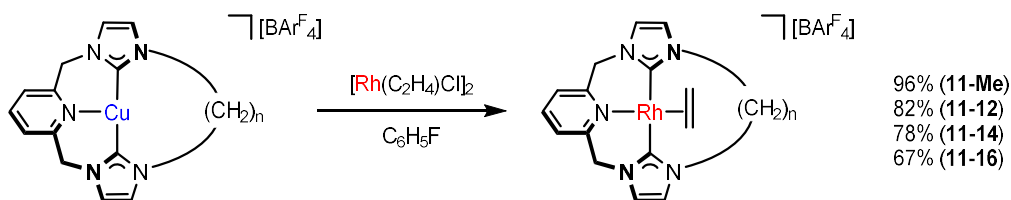


Scheme 2.5.3. Alternate syntheses of **9-n**

2.6 Synthesis of rhodium complexes

2.6.1 Rhodium ethylene complexes – **11-n**

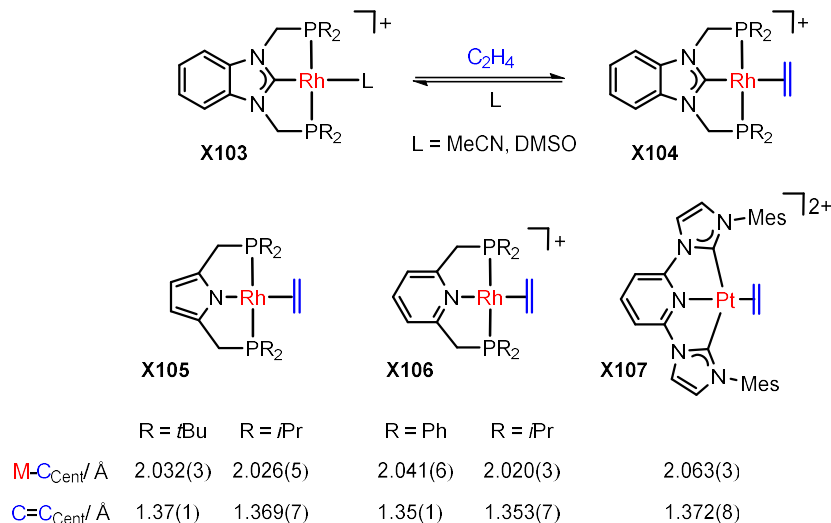
With the complete series of copper transfer agents **9-n** in hand, attention turned to their use in the preparation of rhodium ethylene complexes **11-n** through reaction with $[\text{Rh}(\text{C}_2\text{H}_4)_2\text{Cl}]_2$ (Scheme 2.6.1). In a slight deviation from the procedure used to study this reaction *in situ*, fluorobenzene was chosen as the reaction solvent as it was found to aid precipitation of the copper salt by-products. In this way, **11-n** were isolated in good to excellent yield, following filtration and crystallisation from fluorobenzene/hexane at low temperature ($-30\text{ }^\circ\text{C}$; $n = \text{Me}$, 96%; **12**, 82%; **14**, 78%; **16**, 67%). Due to facile ethylene loss on exposure to reduced pressure, direct crystallisation of **11-n** from the reaction mixture was necessary to obtain samples of high purity. Isolated material can be stored at low temperatures ($-30\text{ }^\circ\text{C}$) under argon without appreciable decomposition but decomposes slowly on dissolution ($t_{1/2}$ ca. 2 weeks for **11-14** in CD_2Cl_2).



Scheme 2.6.1. Preparation of **11-n** ($n = \text{Me}, 12, 14, 16$)

Complexes **11-n** were characterised in solution using ^1H and $^{13}\text{C}\{^1\text{H}\}$ NMR spectroscopy. The carbene resonances of **11-n** are observed as low field doublets as a consequence of coupling to ^{103}Rh ($1J_{\text{RhC}}$ ca. 40 Hz) and, as for their palladium counterparts **6-n**, there is a gradual downfield shift on expansion of the ring (δ 181.9, **11-12**; 183.5, **11-14**; 184.1, **11-16**; 184.8, **11-Me**). This trend is rationalised by subtle changes in the pincer coordination geometry imposed by ring strain of the macrocyclic tether. The bound ethylene ligand gives rise to broad singlets in ^1H NMR spectra which are shifted upfield approximately 2 ppm relative to free ethylene (δ 3.41 – 3.52, CD_2Cl_2 ; cf. δ 3.50 in **X106**, Scheme 2.6.2).⁷³ Although the corresponding signals are not directly observed in the $^{13}\text{C}\{^1\text{H}\}$ NMR

spectra, they can be located at significantly lower frequency than free ethylene (δ ca. 50 ppm **11-n**, cf. 123.2 ppm C₂H₄ in CD₂Cl₂) using correlation experiments. Broadening of the signals could be attributed either to the reversible binding of the ethylene ligand or its low barrier to rotation about the metal-ligand axis.⁷⁴



Scheme 2.6.2. Selected group 9 and 10 ethylene complexes

Broadening is also observed in the ¹H NMR spectra, with the methylene bridge protons observed as broadened singlets in the range 5.75 – 5.03 ppm (CD₂Cl₂, 500 MHz). This indicates that **11-n** are appreciably dynamic on the NMR timescale in contrast to **6-n** and **7-n** (*vide supra*). Typically, atropisomerism in CNC scaffolds is mediated by the coordination of an additional ligand (*viz.* Cl⁻ or CO; Chapter 1). In the absence of a coordinating solvent or anion, the rate enhancement in **11-n** can only be rationalised by coordination of a second ethylene equivalent in an intermolecular ligand exchange reaction, facilitated by the reversible coordination of ethylene. Facile loss of the ethylene ligand was apparent from the ESI mass spectra of these compounds, with [M-C₂H₄]⁺ and/or [M-C₂H₄+O₂]⁺ peaks observed, providing further evidence for the high lability of this ligand: **11-Me**, 402.0424 ([M-C₂H₄+O₂]⁺, calcd 402.0432) *m/z*; **11-12**, 508.1941 ([M-C₂H₄]⁺, calcd 508.1942) and 540.1835 ([M-C₂H₄+O₂]⁺, calcd 540.1840) *m/z*; **11-14**, 568.2162 ([M-C₂H₄+O₂]⁺, calcd 568.2153) *m/z*; **11-16**, 564.2566 ([M-C₂H₄]⁺, calcd 564.2568).

Characterisation in the solid-state using X-ray diffraction was possible for **11-Me** and **11-12** (Figure 2.6.1). The resulting structures are notable for similar metal coordination geometries, with the Rh–C_{NHC} bond lengths of 2.061(3)/2.042(3) Å (**11-Me**) and 2.042(4)/2.036(3) Å (**11-12**), in line with related literature precedents (Scheme 2.6.2).^{73,75,76} Although the ethylene ligands are distorted away from ideal coordination orthogonal to the metal-pincer plane (59.61° **11-Me**; 73.66°, **11-12**; *cf.* 89.31° in **X107**),⁷⁵ the associated metal-centroid (2.0326(15) Å, **11-Me**; 1.9955(19) Å, **11-12**) and C=C (**11-Me**, 1.374(4) Å; **11-12**, 1.362(6) Å, *cf.* 1.3391(13) Å for free ethylene)⁷⁷ bonds are comparable to the most pertinent literature examples (Scheme 2.6.2).

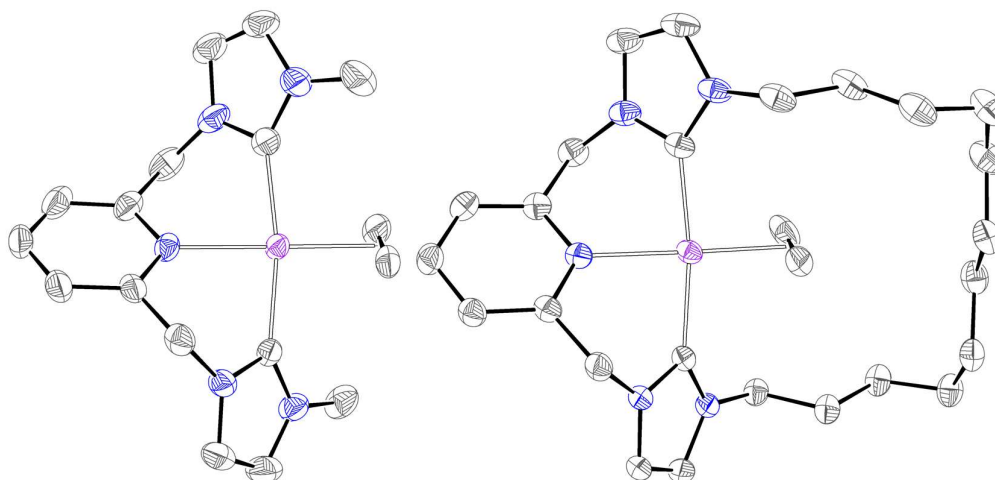


Figure 2.6.1. Solid-state structures of **11-Me** and **11-12**. Thermal ellipsoids at 50% and 35%, respectively; hydrogen atoms and counter anions omitted for clarity.

Compounds **X105**, **X106** and **X107** all display high reactivity associated with facile ligand displacement; a property also reflected in the reversible ethylene binding in **X104**. The comparable spectroscopic and structural properties of complexes **11-n** would suggest similarly weak ethylene coordination, rationalising the observed instability under vacuum and in coordinating solvents.

2.6.2 Rhodium carbonyl complexes – **10-n**

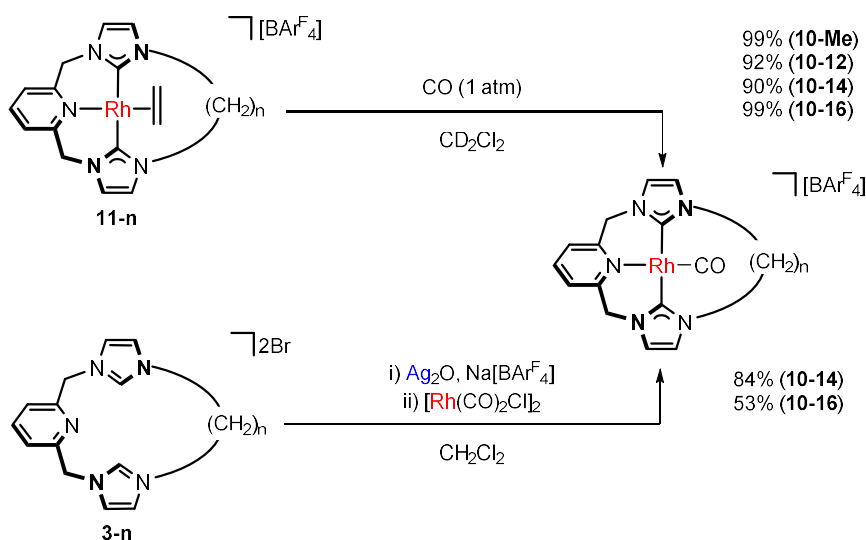
Facile loss of ethylene occurs on reaction of **11-n** with simple monodentate ligands, unsaturated hydrocarbons and moderately coordinating solvents (*vide infra*). Of these reactions, the formation of carbonyl derivatives from reaction with carbon monoxide is of particular interest to quantify the donor ability of the

pincer ligands, exploiting the carbonyl stretching frequency as a reporter group.⁷⁸⁻⁸²

To this end, **11-n** (n = Me, 12, 14, 16) were placed under an atmosphere of carbon monoxide, which resulted in an immediate colour change from bright red to yellow associated with the formation of the corresponding carbonyl derivatives **10-n** (n = Me, 12, 14, 16; Scheme 2.6.3). Following these reactions *in situ* using ¹H NMR spectroscopy, confirmed complete consumption of the ethylene starting materials and presence of free ethylene (δ 5.40, CD₂Cl₂) in all cases within 10 minutes. Under an atmosphere of carbon monoxide the products are observed as C_{2v0} symmetric species, as indicated by a single singlet resonance for the methylene bridge protons (*ca.* δ 5.24, CD₂Cl₂, 400 MHz), as a consequence of rapid atropisomerism of the ligand backbone, promoted by reversible coordination of carbon monoxide as previously described.³⁴ On concentration to dryness and redissolution, static C₂ symmetry is observed on the NMR timescale, as evidenced by diastereotopic methylene bridge protons at *ca.* 5.48/5.02 (²J_{HH} *ca.* 15 Hz). As for the associated group 10 complexes (**6-n** and **7-n**), the high symmetry, maintained down to 185 K, suggests the carbonyl ligands are comfortably accommodated within the rings in **10-n**. Analytically pure samples of **10-n** were obtained in excellent isolated yields (> 90%) in this way, without further purification.

Preparation of **10-Me** and **10-12** have previously been reported *via* an *in situ* silver transmetallation procedure employing the rhodium precursor [Rh(CO)₂Cl]₂, with the latter requiring purification by silica chromatography (*vide supra*). Complexes **10-14** and **10-16** can also be prepared in this way, and were obtained in yields of 84% and 53%, respectively (Scheme 2.6.3).

Successful formation of **10-n** (n = Me, 12, 14, 16) was substantiated by ¹³C{¹H} NMR spectroscopy (CD₂Cl₂, 500 MHz), with the characteristically high frequency carbenic (*ca.* δ 182; ¹J_{RhC} = 42 Hz) and carbonyl resonances (*ca.* δ 194; ¹J_{RhC} = 80 Hz) both observed as doublets due to coupling with ¹⁰³Rh, and ESI-MS, where strong (intact) parent ion peaks were observed: **10-14**, 564.2210 ([M]⁺, calcd 564.2204) *m/z*; **10-16**, 592.2523 ([M]⁺, calcd 592.2517) *m/z*.



Scheme 2.6.3. Formation of complexes **10-n** ($n = \text{Me}, 12, 14, 16$)

The IR spectra of **10-n** each feature a strong characteristic carbonyl stretching band between $1978 - 1980 \text{ cm}^{-1}$, which not only aids in their structural assignment but also acts as a reporter group, probing their respective electronics. In this regard, the negligible change in the carbonyl stretching frequency across the series of **10-n** ($n = \text{Me}, 12, 14, 16$; Table 2.6.1) suggests that the macrocyclic tethers do not significantly augment the donor characteristics of these ligands. As such, it can be inferred that any changes in reactivity are predominantly the result of the unique steric profile of the macrocyclic rings.

Table 2.6.1: Carbonyl stretching frequency of **10-n** (CH_2Cl_2)

n	$\nu(\text{CO}) / \text{cm}^{-1}$
10-Me	1980
10-12	1978
10-14	1978
10-16	1978

Crystals grown of **10-14** and **10-16** allow their structural determination using X-ray diffraction (Figure 2.6.3) which completes the homologous series ($n = \text{Me}, 12, 14, 16$). In the solid-state **10-14** and **10-16** each comprise two independent cationic fragments ($Z' = 2$) stacked in an *anti*-orientation respective to one another, with each adopting the expected *mer*-tridentate coordination and twisted C_2 symmetry of the pincer scaffold. The associated structural metrics are

directly comparable across the series; Rh–N (2.134 – 2.165 Å), Rh–C_{CO} (1.753 – 1.811 Å) and Rh–C_{NHC} (1.999 – 2.079 Å) (Table 2.6.2).

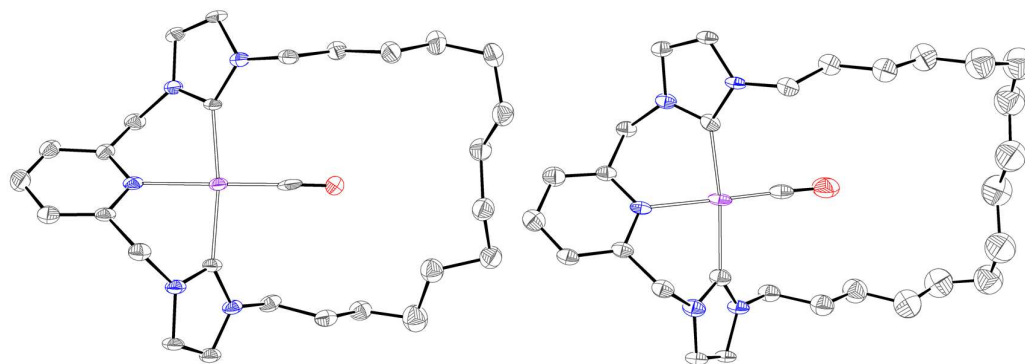
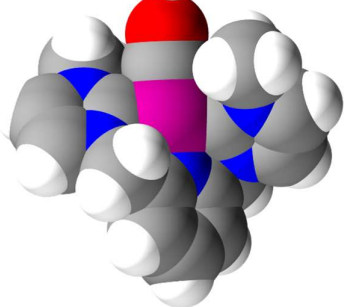
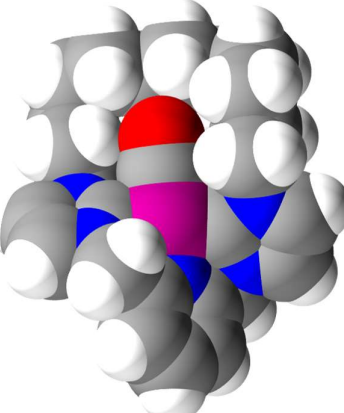
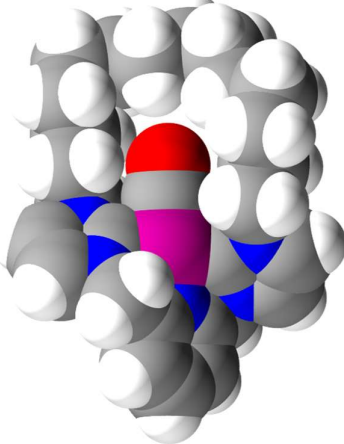
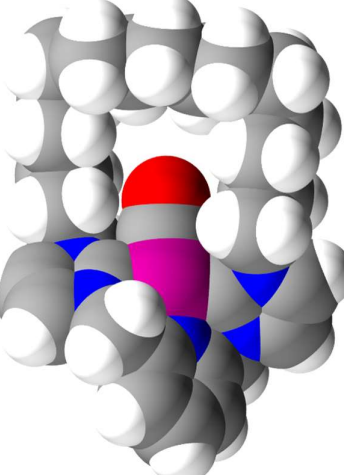


Figure 2.6.3. Solid-state structures of complexes **10-n** ($n = 14$ and 16). Thermal ellipsoids at 35% probability. Hydrogen atoms, counter anions and minor distorted components omitted for clarity. Structures of both are one of two independent molecules ($Z' = 2$).

Contrasting the solid-state structure of **10-12**, which shows minor displacement of the macrocyclic tether,³⁵ the spacefill representations of **10-14** and **10-16** show cavities of sufficient size to encapsulate the CO ligand without distortion. The absence of unfavourable steric clashes between the macrocycle and carbonyl ligand is evidenced by more linear N–Rh–C_{CO} bond angles; **10-12** 175.20(1)°, **10-14** 179.2(5)°, **10-16** 178.8(8)°, **10-Me** 178.99(12)°.

Even more so than for **6-14** and **6-16**, the ease in which the carbonyl ligand can be accommodated within the macrocyclic cavity of **10-14** and **10-16**, with residual unoccupied space, highlights their potential use in the formation of interlocked [2]rotaxanes.

Table 2.6.2: Spacefill representations and selected bond lengths (Å) and angles (°) of **10-n**

	10-Me	10-12	10-14	10-16
				
Rh-N / Å	2.134(2)	2.148(8); 2.134(8)	2.13(1); 2.13(2)	
Rh-C_{NHC} / Å	1.804(3)	1.80(1); 1.80(2)	1.77(2); 1.70(2)	
Rh-C_{NHC} / Å	2.036(3), 2.042(3)	2.046(9), 2.043(8); 2.40(1), 2.05(1)	2.07(2), 2.04(1); 2.04(2), 2.02(2)	
N-Rh-C_{co} / °	175.20(1)	179.2(5); 178.0(5)	178.8(8); 178.7(7)	
C_{NHC}-Rh-C_{NHC} / °	172.77(12)	172.4(4); 171.5(4)	172.4(6); 171.9(8)	
$a - Z' = 2$				

2.7 References

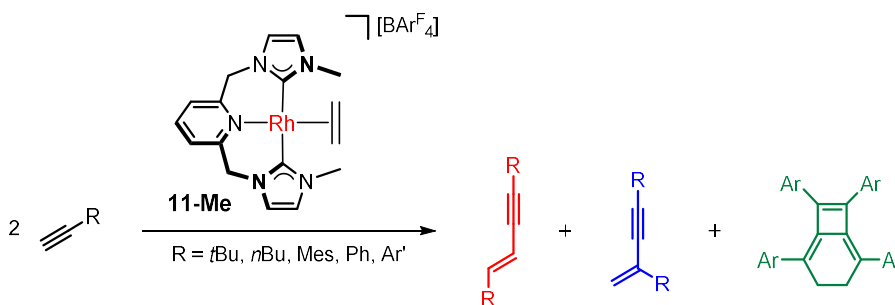
- 1 D. K. Cabbiness and D. W. Margerum, *J. Am. Chem. Soc.*, 1969, **91**, 6540–6541.
- 2 C. Röhlich and K. Köhler, *Adv. Synth. Catal.*, 2010, **352**, 2263–2274.
- 3 M. Ranocchiari and A. Mezzetti, *Organometallics*, 2009, **28**, 1286–1288.
- 4 R. Bigler and A. Mezzetti, *Org. Lett.*, 2014, **16**, 6460–6463.
- 5 C. M. Drain, A. Varotto and I. Radivojevic, *Chem. Rev.*, 2009, **109**, 1630–1658.
- 6 G. de la Torre, P. Vázquez, F. Agulló-López and T. Torres, *Chem. Rev.*, 2004, **104**, 3723–3750.
- 7 F. E. Hahn, V. Langenhahn, T. Lügger, T. Pape and D. Le Van, *Angew. Chem. Int. Ed.*, 2005, **44**, 3759–3763.
- 8 A. Flores-Figueroa, T. Pape, K.-O. Feldmann and F. E. Hahn, *Chem. Commun.*, 2010, **46**, 324–326.
- 9 C. Radloff, H.-Y. Gong, C. Schulte to Brinke, T. Pape, V. M. Lynch, J. L. Sessler and F. E. Hahn, *Chem. Eur. J.*, 2010, **16**, 13077–13081.
- 10 P. G. Edwards and F. E. Hahn, *Dalton Trans.*, 2011, **40**, 10278–10288.
- 11 A. Biffis, M. Cipani, E. Bressan, C. Tubaro, C. Graiff and A. Venzo, *Organometallics*, 2014, **33**, 2182–2188.
- 12 A. Biffis, M. Cipani, C. Tubaro, M. Basato, M. Costante, E. Bressan, A. Venzo and C. Graiff, *New J. Chem.*, 2013, **37**, 4176–4184.
- 13 P. J. Altmann, D. T. Weiss, C. Jandl and F. E. Kühn, *Chem. Asian J.*, 2016, **11**, 1597–1605.
- 14 R. McKie, J. A. Murphy, S. R. Park, M. D. Spicer and S. Zhou, *Angew. Chem. Int. Ed.*, 2007, **46**, 6525–6528.
- 15 T. Lu, C.-F. Yang, C. A. Steren, F. Fei, X.-T. Chen and Z.-L. Xue, *New J. Chem.*, 2018, **42**, 4700–4713.
- 16 M. V. Baker, B. W. Skelton, A. H. White and C. C. Williams, *Organometallics*, 2002, **21**, 2674–2678.
- 17 K. Kawano, K. Yamauchi and K. Sakai, *Chem. Commun.*, 2014, **50**, 9872–9875.
- 18 Z. S. Ghavami, M. R. Anneser, F. Kaiser, P. J. Altmann, B. J. Hofmann, J. F. Schlagintweit, G. Grivani and F. E. Kühn, *Chem. Sci.*, 2018, **9**, 8307–8314.
- 19 M. R. Anneser, S. Haslinger, A. Pöthig, M. Cokoja, J.-M. Basset and F. E. Kühn, *Inorg. Chem.*, 2015, **54**, 3797–3804.
- 20 Z. Lu, S. A. Cramer and D. M. Jenkins, *Chem. Sci.*, 2012, **3**, 3081–3087.
- 21 S. A. Cramer and D. M. Jenkins, *J. Am. Chem. Soc.*, 2011, **133**, 19342–19345.
- 22 P. P. Chandrachud, H. M. Bass and D. M. Jenkins, *Organometallics*, 2016, **35**, 1652–1657.
- 23 I. Klawitter, M. R. Anneser, S. Dechert, S. Meyer, S. Demeshko, S. Haslinger, A. Pöthig, F. E. Kühn and F. Meyer, *Organometallics*, 2015, **34**, 2819–2825.
- 24 S. Meyer, I. Klawitter, S. Demeshko, E. Bill and F. Meyer, *Angew. Chem. Int. Ed.*, 2013, **52**, 901–905.
- 25 C. Kupper, A. Schober, S. Demeshko, M. Bergner and F. Meyer, *Inorg. Chem.*, 2015, **54**, 3096–3098.
- 26 M. R. Anneser, G. R. Elpitiya, X. B. Powers and D. M. Jenkins, *Organometallics*, 2019, **38**, 981–987.
- 27 M. R. Anneser, S. Haslinger, A. Pöthig, M. Cokoja, V. D’Elia, M. P. Högerl, J.-M. Basset and F. E. Kühn, *Dalton Trans.*, 2016, **45**, 6449–6455.
- 28 C. Schremmer, C. Cordes, I. Klawitter, M. Bergner, C. E. Schiewer, S. Dechert, S. Demeshko, M. John and F. Meyer, *Chem. – A Eur. J.*, 2019, **25**, 3918–3929.
- 29 F. G. Cantú Reinhard and S. P. de Visser, *Chem. Eur. J.*, 2017, **23**, 2935–2944.
- 30 J. W. Kück, M. R. Anneser, B. Hofmann, A. Pöthig, M. Cokoja and F. E. Kühn, *ChemSusChem*, 2015, **8**, 4056–4063.
- 31 K. Meyer, A. F. Dalebrook and L. J. Wright, *Dalton Trans.*, 2012, **41**, 14059–14067.

- 32 S. Saito, I. Azumaya, N. Watarai, H. Kawasaki and R. Yamasaki, *Heterocycles*, 2009, **79**, 531–548.
- 33 R. E. Andrew and A. B. Chaplin, *Dalton Trans.*, 2014, **43**, 1413–1423.
- 34 R. E. Andrew, D. W. Ferdani, C. A. Ohlin and A. B. Chaplin, *Organometallics*, 2015, **34**, 913–917.
- 35 R. E. Andrew and A. B. Chaplin, *Inorg. Chem.*, 2015, **54**, 312–322.
- 36 R. E. Andrew, University of Warwick, 2016.
- 37 S. Gründemann, M. Albrecht, J. A. Loch, J. W. Faller and R. H. Crabtree, *Organometallics*, 2001, **20**, 5485–5488.
- 38 R. Appel, *Angew. Chem. Int. Ed.*, 1975, **14**, 801–811.
- 39 T. W. Baughman, J. C. Sworen and K. B. Wagener, *Tetrahedron*, 2004, **60**, 10943–10948.
- 40 J. R. Miecznikowski, M. A. Lynn, J. P. Jasinski, E. Reinheimer, D. W. Bak, M. Pati, E. E. Butrick, A. E. R. Drozdowski, K. A. Archer, C. E. Villa, E. G. Lemons, E. Powers, M. Siu, C. D. Gomes and K. N. Morio, *J. Coord. Chem.*, 2014, **67**, 29–44.
- 41 J. R. Miecznikowski, J. P. Jasinski, M. A. Lynn, S. S. Jain, E. E. Butrick, A. E. R. Drozdowski, K. A. Archer and J. T. Panarra, *Inorg. Chim. Acta*, 2013, **394**, 310–321.
- 42 J. R. Miecznikowski, W. Lo, M. A. Lynn, B. E. O’Loughlin, A. P. DiMarzio, A. M. Martinez, L. Lampe, K. M. Foley, L. C. Keilich, G. P. Lisi, D. J. Kwiecien, C. M. Pires, W. J. Kelly, N. F. Kloczko and K. N. Morio, *Inorg. Chim. Acta*, 2011, **376**, 515–524.
- 43 J. R. Miecznikowski, W. Lo, M. A. Lynn, S. Jain, L. C. Keilich, N. F. Kloczko, B. E. O’Loughlin, A. P. DiMarzio, K. M. Foley, G. P. Lisi, D. J. Kwiecien, E. E. Butrick, E. Powers and R. Al-Abbasee, *Inorg. Chim. Acta*, 2012, **387**, 25–36.
- 44 G. E. Tyson, K. Tokmic, C. S. Oian, D. Rabinovich, H. U. Valle, T. K. Hollis, J. T. Kelly, K. A. Cuellar, L. E. McNamara, N. I. Hammer, C. E. Webster, A. G. Oliver and M. Zhang, *Dalton Trans.*, 2015, **44**, 14475–14482.
- 45 W.-G. Jia, L.-L. Gao, Z.-B. Wang, L.-Y. Sun and Y.-F. Han, *Organometallics*, 2019, **38**, 1946–1954.
- 46 W.-G. Jia, Y.-B. Huang, Y.-J. Lin and G.-X. Jin, *Dalton Trans.*, 2008, 5612–5620.
- 47 W.-G. Jia, Y.-B. Huang and G.-X. Jin, *J. Organomet. Chem.*, 2009, **694**, 4008–4013.
- 48 F. E. Hahn, L. Wittenbecher, D. Le Van and R. Fröhlich, *Angew. Chem. Int. Ed.*, 2000, **39**, 541–544.
- 49 F. E. Hahn, L. Wittenbecher, R. Boese and D. Bläser, *Chem. Eur. J.*, 1999, **5**, 1931–1935.
- 50 N. Kuhn and T. Kratz, *Synthesis*, 1993, **1993**, 561–562.
- 51 C. Marshall, M. F. Ward and W. T. A. Harrison, *J. Organomet. Chem.*, 2005, **690**, 3970–3975.
- 52 R. Patchett, R. C. Knighton, J. D. Mattock, A. Vargas and A. B. Chaplin, *Inorg. Chem.*, 2017, **56**, 14345–14350.
- 53 M. Raynal, C. S. J. Cazin, C. Vallée, H. Olivier-Bourbigou and P. Braunstein, *Dalton Trans.*, 2009, 3824.
- 54 R. M. Silva, M. D. Smith and J. R. Gardinier, *J. Org. Chem.*, 2005, **70**, 8755–8763.
- 55 D. Serra, P. Cao, J. Cabrera, R. Padilla, F. Rominger and M. Limbach, *Organometallics*, 2011, **30**, 1885–1895.
- 56 D. J. Nielsen, K. J. Cavell, B. W. Skelton and A. H. White, *Inorg. Chim. Acta*, 2002, **327**, 116–125.
- 57 J. Ruiz, D. Sol, J. F. Van der Maelen and M. Vivanco, *Organometallics*, 2017, **36**, 1035–1041.
- 58 R. J. Rubio, G. T. S. Andavan, E. B. Bauer, T. K. Hollis, J. Cho, F. S. Tham and B. Donnadieu, *J. Organomet. Chem.*, 2005, **690**, 5353–5364.
- 59 K. Inamoto, J. Kuroda, E. Kwon, K. Hiroya and T. Doi, *J. Organomet. Chem.*, 2009, **694**, 389–396.
- 60 K. Yoshida, S. Horiuchi, T. Takeichi, H. Shida, T. Imamoto and A. Yanagisawa, *Org.*

- Lett.*, 2010, **12**, 1764–1767.
- 61 A. Steffen, M. G. Tay, A. S. Batsanov, J. A. K. Howard, A. Beeby, K. Q. Vuong, X.-Z. Sun, M. W. George and T. B. Marder, *Angew. Chem. Int. Ed.*, 2010, **49**, 2349–2353.
- 62 S. Zhang, X. Li, H. Sun, O. Fuhr and D. Fenske, *J. Organomet. Chem.*, 2016, **820**, 41–45.
- 63 R. E. Andrew, C. M. Storey and A. B. Chaplin, *Dalton Trans.*, 2016, **45**, 8937–8944.
- 64 D. Domyati, S. L. Hope, R. Latifi, M. D. Hearn and L. Tahsini, *Inorg. Chem.*, 2016, **55**, 11685–11693.
- 65 C. Chen, H. Qiu and W. Chen, *J. Organomet. Chem.*, 2012, **696**, 4166–4172.
- 66 X. Liu and P. Braunstein, *Inorg. Chem.*, 2013, **52**, 7367–7379.
- 67 X. Han, L.-L. Koh, Z.-P. Liu, Z. Weng and T. S. A. Hor, *Organometallics*, 2010, **29**, 2403–2405.
- 68 S. Díez-González, E. C. Escudero-Adán, J. Benet-Buchholz, E. D. Stevens, A. M. Z. Slawin and S. P. Nolan, *Dalton Trans.*, 2010, **39**, 7595–7606.
- 69 V. J. Catalano, L. B. Munro, C. E. Strasser and A. F. Samin, *Inorg. Chem.*, 2011, **50**, 8465–8476.
- 70 R. Della Pergola, M. Bruschi, A. Sironi, V. Colombo and A. Sironi, *Organometallics*, 2014, **33**, 5610–5613.
- 71 V. S. Thoi and C. J. Chang, *Chem. Commun.*, 2011, **47**, 6578–6580.
- 72 X. Liu and W. Chen, *Organometallics*, 2012, **31**, 6614–6622.
- 73 M. Feller, Y. Diskin-Posner, L. J. W. Shimon, E. Ben-Ari and D. Milstein, *Organometallics*, 2012, **31**, 4083–4101.
- 74 R. Cramer, *J. Am. Chem. Soc.*, 1964, **86**, 217–222.
- 75 D. Serra, P. Cao, J. Cabrera, R. Padilla, F. Rominger and M. Limbach, *Organometallics*, 2011, **30**, 1885–1895.
- 76 S. Nakayama, S. Morisako and M. Yamashita, *Organometallics*, 2018, **37**, 1304–1313.
- 77 E. Hirota, Y. Endo, S. Saito, K. Yoshida, I. Yamaguchi and K. Machida, *J. Mol. Spectrosc.*, 1981, **89**, 223–231.
- 78 C. A. Tolman, *J. Am. Chem. Soc.*, 1970, **92**, 2953–2956.
- 79 M. Nonnenmacher, D. M. Buck and D. Kunz, *Beilstein J. Org. Chem.*, 2016, **12**, 1884–1896.
- 80 H. V. Huynh, *Chem. Rev.*, 2018, **118**, 9457–9492.
- 81 G. L. Parker, S. Lau, B. Leforestier and A. B. Chaplin, *Eur. J. Inorg. Chem.*, 2019, **2019**, 3791–3798.
- 82 S. R. Muhammad, J. W. Nugent, K. Tokmic, L. Zhu, J. Mahmoud and A. R. Fout, *Organometallics*, 2019, [acs.organomet.9b00337](https://doi.org/10.1021/acs.organomet.9b00337).

Chapter 3 – Catalytic terminal alkyne coupling reactions

Terminal alkyne dimerisation reactions represent a conceptually simple, atom-economical method for the formation of conjugated 1,3-enynes. This chapter describes the evaluation of **11-Me** as a pre-catalyst for these reactions, using a range of aryl and alkyl functionalised alkynes. Kinetic studies have been conducted to help interrogate the underlying mechanism, with an emphasis on elucidating the factors that govern selectivity, leading to coherent proposals. During these investigations unexpected onwards reactivity promoted by **11-Me**, leading to the formation of 2,5,7,8-tetrasubstituted bicyclo[4.2.0]octa-1,5,7-trienes from the *in situ* generated *gem*-1,3-enynes, was discovered. The scope and mechanism of this intriguing auto-tandem catalytic process were also explored, and the results are described herein.

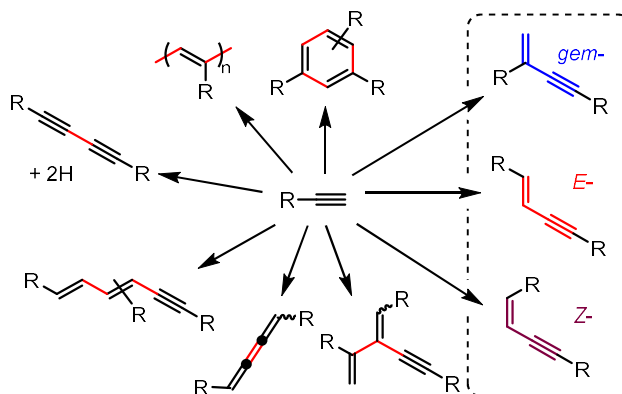


Publications resulting from the work described in this chapter:

- C. M. Storey, M. R. Gyton, R. E. Andrew, A. B. Chaplin, *Angew. Chem. Int. Ed.* 2018, **57**, 12003–12006.
- C. M. Storey, M. R. Gyton, T. Krämer, A. B. Chaplin, *manuscript in preparation*.

3.1 Introduction

As a conceptually straightforward and atom economical method for the preparation of conjugated 1,3-enynes, the transition metal catalysed dimerisation of terminal alkynes is a reaction of growing prominence.^{1–3} These enyne moieties are not only of interest as versatile unsaturated synthons, but also feature in biologically active compounds^{4,5} and functional materials.^{6,7} Given their high utility, investigations have identified a wide-range of species capable of catalysing this process, including, complexes of early and late transition metals,^{8–12} f-elements,^{13,14} rare earth metals,¹⁵ and main group elements.^{16,17} However, the regio- and stereo-selective formation of these 1,3-enyne products remains difficult to both predict and realise. In addition to competing metal-catalysed reactions of terminal alkynes that can lead to a range of alternative unsaturated products (Scheme 3.1.1), the formal addition of the C(sp)–H bond of one alkyne across another is a process that can result in three different enyne products by virtue of competing head-to-head (*E*-/*Z*-) and head-to-tail couplings (*gem*-; Scheme 3.1.1).¹⁸



Scheme 3.1.1. Metal catalysed reactions of terminal alkynes

Though a wide variety of catalysts have been shown to promote these reactions, few can produce a single enyne isomer with high fidelity. Seminal investigations in the 1990s by Trost, showed $[\text{Pd}(\text{OAc})_2]$, in combination with tris(2,6-dimethoxyphenyl)phosphine, catalysed the selective formation of *gem*-1,3-enynes with moderate turnover numbers (TON 12 – 18). In addition, this system was also active in cross-dimerisation reactions of internal alkynes with turnover frequencies exceeding 35 h^{-1} .¹⁹ In contrast, a more modern study using a

palladium complex bearing sterically bulky NHC ligands (IPr) in the presence of the same electron rich phosphine showed high efficacy for the formation of *E*-enynes (51 – 94%).²⁰ Correspondingly, investigations into simple monodentate phosphine-based rhodium complexes by Goldman ([Rh(PMe₃)₃Cl])²¹ and Ishikawa ([Rh(PPh₃)₃Cl])²² revealed high activity in homocouplings but with orthogonal selectivity profiles depending on the substrate employed (*gem*- or *E*-). For instance, Goldman's complex showed quantitative formation of the *E*-enyne from *tert*-butyl acetylene under the standard reaction conditions (2 mol%, 25 – 50 °C, C₆D₆) but exclusively the *gem*-isomer, resulting from head-to-tail dimerisation, when using phenylacetylene.

Building on early landmarks and subsequent developments involving monodentate ligated systems, application of pincer complexes in terminal alkyne coupling reactions is of contemporary interest. For instance, complexes **X108**, **X110** and **X112** have emerged, amongst others, as highly effective catalysts showcasing the ability of this divergent ligand class to enforce high reaction control (Figure 3.1.1).

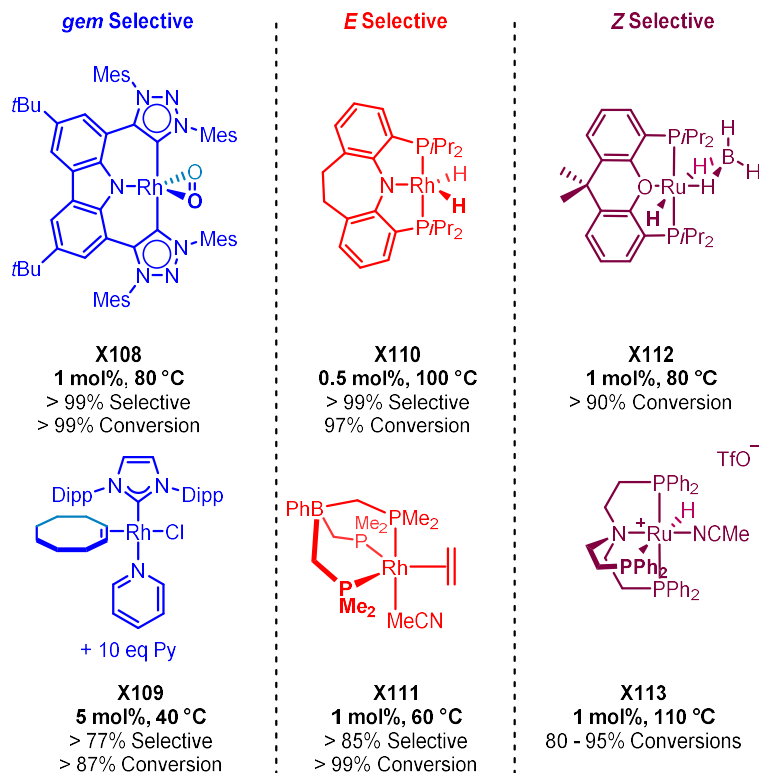


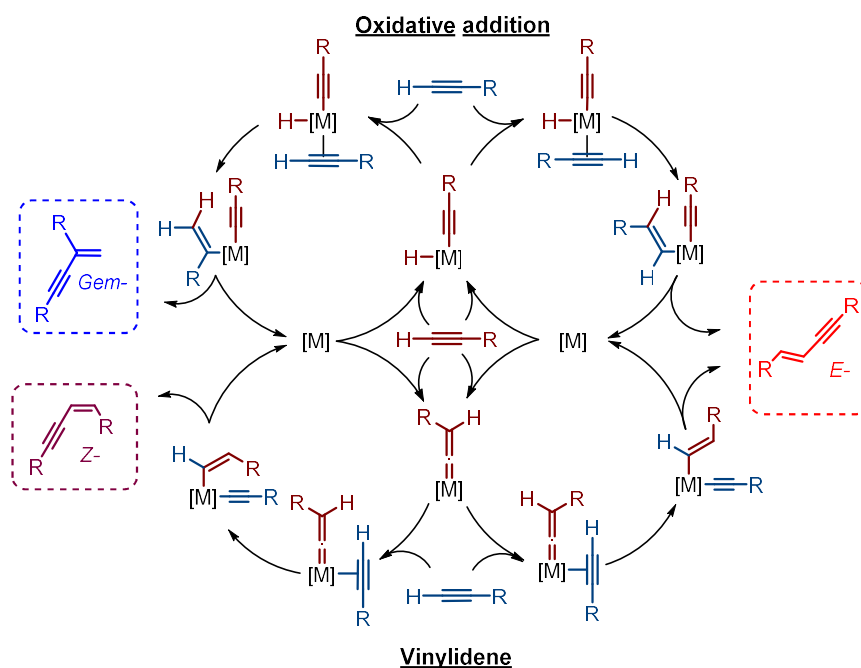
Figure 3.1.1. Examples of selective terminal alkyne coupling catalysts

Mesoionic carbene complex **X108** is noteworthy for the efficient and selective homocoupling of terminal alkynes into *gem*-enynes (1 mol%, 80 °C). For instance, 1-hexyne and a series of heteroatom functionalised alkyl alkynes were converted exclusively to the corresponding *gem*-enynes, while phenylacetylene afforded a mixture of *gem*- and *E*- products (89% and 11%, respectively).²³ Conversely, **X110** principally affords *E*-enynes (> 90%) under similar conditions (0.5 mol%, 100 °C) for a range of alkyl and aryl alkynes.¹⁰ Closely related Rh(PNP) and Rh(PCP) catalysts, reported by Ozerov *et al.*, demonstrate reduced selectivity, but conferred mixtures composed predominately of *gem*- and *E*- products.²⁴ Moreover, a series of rare *pseudotetrahedral* d⁸-metal complexes bearing an unusual tripodal phosphine ligand (**X111**) have recently been found to promote these reactions again to mixtures containing only *gem*- and *E*- isomers (2 mol%, 60 °C, 85 – 95% *E*-; balance *gem*-).⁸ The contrasting selectivity across these systems highlights the nuanced nature of alkyne coupling reactions. Comparing the selectivity of these rhodium complexes bearing chelating ligands with the earlier examples featuring simple monodentate ancillary ligands (*vide supra*), it is clear that rigid nature of the pincer scaffolds imparts higher selectivity irrespective of the chosen substrate.

The exclusive formation of *Z*-enynes has mainly been described for ruthenium complexes (*cf.* **X112** and **X113**). Complex **X112** performs the *Z*-selective dimerisation of alkynes with high TONs and TOFs (TON = 97 and 92; TOF = 215 h⁻¹ and 92 h⁻¹ at 80 °C for Ph and *t*Bu alkynes, respectively) outperforming its heavier group 8 osmium congener (TOF = 100 h⁻¹ and 30 h⁻¹ 110 °C, Ph and *t*Bu, respectively).²⁵ Likewise, the air and moisture stable **X113** was found to dimerise a range of aliphatic and aromatic alkynes to the corresponding *Z*-enynes with high fidelity (1 mol%, 110 °C, > 80% isolated yield).²⁶ Looking to move away from the use of the precious metals, more recent studies have found iron catalysts to be highly efficient in the selective dimerisation of terminal alkynes to the corresponding *Z*-enyne isomers.^{9,27–29} Initially the homodimerisation of aromatic alkynes by iron catalysts (FeCl₃, DMEDA (30 mol%) and KO*t*Bu (3 eq.), 145 °C, toluene, 2 h) was found to generate mixtures of *E*- and *Z*-enynes.²⁸ Despite exhibiting only marginal catalytic activity (TON = 3) this finding inspired work

into the use of structurally similar [Fe(PNP)] complexes, which are highly selective for the coupling of aromatic alkynes to *Z*-enynes under significantly milder conditions (0.2 – 3 mol%, RT, > 93%, *Z*-).^{27,29,30}

Excepting a few niche examples,^{31,32} the dimerisation catalysts reported in the literature show a clear predilection for a singular alkyne activation mechanism. Commonly accepted mechanisms, relevant to the systems described in this thesis, invoke either the oxidative addition of the first equivalent of alkyne to form an alkynyl-hydride species or the formation of a metal vinylidene intermediate (Scheme 3.1.2).^{1,18,33}



Scheme 3.1.2. Divergent mechanistic pathways for the catalytic dimerisation of terminal alkynes

Both the oxidative addition and vinylidene pathways diverge on reaction with the second equivalent of alkyne. For the former, migratory insertion of either the hydride (hydrometallation) or the alkynyl (carbometallation) ligands can occur, leading to either head-to-tail (*gem*-) or head-to-head (*E*-) products, depending on the relative orientation of the π -bound alkyne. Mixtures of these isomers are most prevalent for d^8 -metal complexes (*e.g.* Rh(I), Pd(II), Pt(II)).^{18,20,34–37}

Whilst the head-to-tail coupling of alkynes into geminal enynes can solely be accounted for using the former scenario, the latter vinylidene pathway is the only

plausible means for the formation of *Z*-isomers. Promotion of alkyne dimerisations to *E*- and *Z*-isomers is most prominent for the group 8 metals, indicative of the vinylidene mechanism being in operation.^{9,25,38} Preparation of a metal vinylidene intermediate, followed by nucleophilic attack on the C α of the vinylidene moiety by the second alkyne equivalent generates a familiar metal alkenyl alkynyl intermediate. Again, these intermediates simply undergo a single reductive elimination step to release the homocoupled product. Like the oxidative addition pathways, the stereoselectivity of this mechanistic route is imposed at the insertion step, discriminating between the two head-to-head coupled stereoisomers.

In the context of previously reported dimerisation reactions promoted by rhodium pincer complexes (*viz.* **X108** – **X110**), where reactive three-coordinate Rh(I) 14 valence electron species are most likely the active catalysts, the hydrometallation pathway (Scheme 3.1.2) is most likely operative.^{10,24} This assertion is supported by the observed product distributions, notable for the absence of *Z*-enyne products irrespective of the ligand periphery and thus steric congestion in the metal coordination sphere. Formation of rhodium vinylidene complexes from reaction between rhodium(I) precursors and terminal alkynes is, however, well precedented^{39–44} and as such the existence of a vinylidene mechanism cannot be discounted without supporting evidence.

3.2 Pre-catalyst substitution reactions

Onwards reactivity of the rhodium complexes prepared in Chapter 2 relies on the ability to access reactive three-coordinate and formally 14 valence electron derivatives $\{\text{Rh}(\text{CNC})\}^+$. Having established a facile route to rhodium(I) ethylene complexes **11-n**, the lability of the ethylene ligand and by extension the accessibility of the $\{\text{Rh}(\text{CNC})\}^+$ fragment was probed through ligand substitution reactions. Dissolving **11-Me** in a range of coordinating solvents – viz. d_3 -MeCN, d_6 -DMSO, THF and d_5 -pyridine, or exposing a CH_2Cl_2 solution to an atmosphere of CO, as described previously, resulted in facile displacement of the ethylene ligand. These reactions were monitored *in situ* by ^1H NMR spectroscopy using the relative integrals of the *N*-methyl proton resonances (py for **13-Me**) and emergence of free ethylene (δ ca. 5.4 ppm) as spectroscopic handles. These data are collated in Table 3.2.1.

Table 3.2.1. Ligand substitution reactions of **11-Me**

Product	L	NMR Yield (%) ^a		
		10 Minutes	1 Hour	5 Hours
12-Me	d_3 -MeCN	77.0	84.0	94.0
13-Me	THF ^b	95.5	quant.	-
14-Me	d_5 -Pyridine	65.3	-	quant.
15-Me	d_6 -DMSO	quant.	-	-
10-Me	CO^c	quant.	-	-

^a) Determined from ^1H NMR data, using Ar^F signals as an internal standard. ^b) Analysed using a C_6D_6 capillary. ^c) in CD_2Cl_2 solution (ca. 1 atm CO)

These substitution reactions highlight the need to employ a weakly coordinating solvent to avoid attenuating the catalytic activity of **11-Me** by reversible solvent binding. In the context of identifying reaction intermediates, however, this behaviour can be beneficial and on the basis of the data presented in Table 3.2.1 isolation of **15-Me** was targeted. To this end, reaction of **11-Me** with a stoichiometric amount of DMSO in CH_2Cl_2 afforded the appreciably air and

moisture sensitive product in good yield, following purification by recrystallisation (77%; CH₂Cl₂/hexane), which was subsequently characterised in solution and the solid-state (Figure 3.2.1).

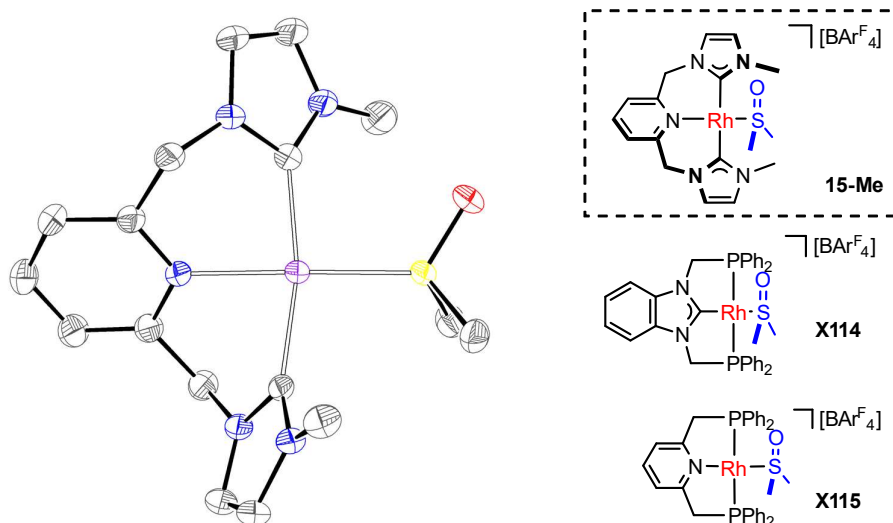


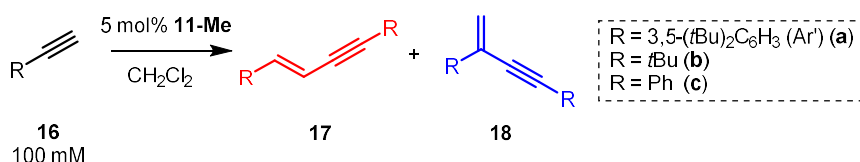
Figure 3.2.1. Solid state structure of **15-Me**. Thermal ellipsoids at 50% probability; hydrogen atoms and anion omitted for clarity. Selected bond lengths (Å) and angles (°): Rh-C_{NHC}, 2.03702(5), 2.03970(5); Rh-N, 2.088(2); C_{NHC}-Rh-C_{NHC}, (167.2221(5)).

The NMR spectra of **15-Me** are largely unchanged compared with the parent ethylene complex **11-Me**, with the complex retaining *C*_{2v} symmetry on DMSO coordination. Notable features associated with the coordinated DMSO include a broad resonance at 3.14 ppm in the ¹H NMR spectrum (CD₂Cl₂, 500 MHz) and a distinct doublet at 52.8 ppm (*J*_{RhC} = 30 Hz) in the ¹³C{¹H} NMR spectrum. Downfield shifts of these resonances relative to free DMSO (δ_H 2.62 and δ_C 40.8)⁴⁵ confirm metal coordination, which is further supported by the presence of ¹⁰³Rh coupling in the ¹³C{¹H} NMR spectrum. The magnitude of *J*_{RhC} coupling constant suggests that the DMSO interacts with the rhodium centre through the soft sulfur donor as opposed to the hard oxygen centre and indeed this connectivity was confirmed by X-ray diffraction (Figure 3.2.1). Bond lengths and angles of the pincer in **15-Me** are in-line with other Rh(I) species described previously (*cf.* **10-Me**/**11-Me**) and the metrics about the DMSO ligand (Rh-S, 2.1774(6) Å; S=O, 1.483(2) Å) mirror those of related complexes *viz.* **X114** (Rh-S, 2.283(1) Å; S=O, 1.480(4) Å) and **X115** (Rh-S, 2.1870(9) Å; S=O, 1.474(3) Å).^{46,47}

3.3 Terminal alkyne dimerisation

3.3.1. Homocoupling in CH₂Cl₂

With previous results highlighting the need for a weakly coordinating solvent, CH₂Cl₂ was initially used as the reaction solvent for assessing the catalytic activity of **11-Me** (Scheme 3.3.1). Under relatively mild conditions (5 mol% **11-Me**, 100 mM CH₂Cl₂, 25 °C) compared with literature precedents **X108** – **X113** (*cf.* 60 – 110 °C), **11-Me** was found to be an efficient pre-catalyst for terminal alkyne homodimerisation of bulky aromatic terminal alkyne **16a** (3,5-di(*tert*-butyl)phenylacetylene; prepared using a literature procedure),⁴⁸ *tert*-butyl alkyne **16b** and phenylacetylene **16c** (Table 3.3.1).



Scheme 3.3.1. Terminal alkyne dimerisation catalysed by **11-Me**

Monitoring the reaction progress using ¹H NMR spectroscopy (CD₂Cl₂), indicated the facile and selective dimerisation of **16a** (*t*_{1/2} = 4.2 h) into *gem*-enyne **18a**, as evidenced by the emergence of signals at δ 5.96 and 5.71 pertaining to the geminal alkene protons (independently verified, *vide infra*). Geminal selectivity was also apparent for **16c**, albeit at a considerably slower rate (*t*_{1/2} = 17.5 h), whereas, **16b** afforded the *E*-product **17b** exclusively. The formation of **17b** and **18c** were confirmed by the appearance of alkene resonances, at δ 6.05/5.39 (³*J*_{HH} = 16.2 Hz) and δ 6.02/5.77 (²*J*_{HH} = 1.0 Hz) respectively, which are in agreement with related literature data.^{20,49,50}

Table 3.3.1. Selectivity of terminal alkyne coupling

R	Alkyne	<i>t</i> _{1/2} /h ^a	Distribution at 50% conversion ^a		Distribution at 100% conversion ^a	
			18	17	18	17
Ar'	16a	4	100	-	88 ^b	-
<i>t</i> Bu	16b	3	-	100	-	89 ^c
Ph	16c	17	100	-	91 ^b	-

^a) Determined from ¹H NMR data, using Ar^F signals as an internal standard. ^b) Balance of material made up with tetrameric species. ^c) Balance of material made up with trimeric species.⁵¹

Examination of the time-course plots for these reactions further, indicates contrasting kinetics for the aromatic and aliphatic substrates (Figure 3.3.1). Both **16a** and **16c** show zero-order substrate dependence, albeit at considerably different rates. Whereas, **16b** sees a complex time-dependence which does not fit with an integer-order reaction. Despite a fast initial rate, the reaction slows considerably at *ca.* 40% conversion. The dramatic reduction in rate gives rise to extended reaction times to reach completion at 25 °C (*ca.* 88 hours). We initially attributed this reduction in rate to product inhibition.

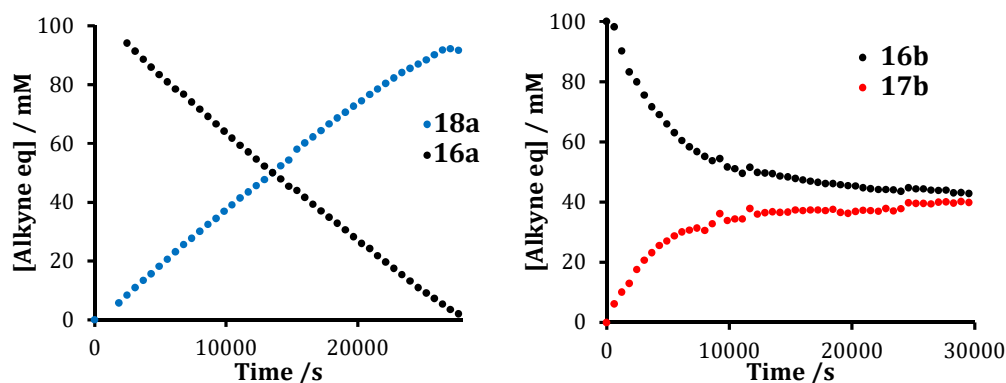
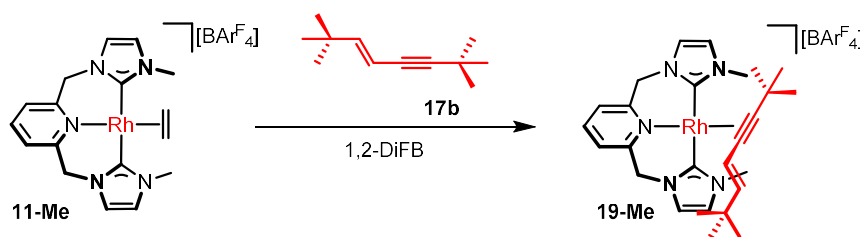


Figure 3.3.1. Time-course plots for the homocoupling of **16a** (left) and **16b** (right)

To test this theory, the reaction of an isolated sample of **17b** (prepared using a literature procedure)⁴⁹ with **11-Me** in 1,2-difluorobenzene (1,2-DiFB) showed quantitative NMR conversion to **19-Me** after 2 hours, which was isolated in excellent yield following washing with pentane (94%, Scheme 3.3.2).[†]



Scheme 3.3.2. Preparation of bound enyne complex **19-Me**

The formation of **19-Me** was confirmed in solution using NMR spectroscopy and in the solid-state by X-ray diffraction (Figure 3.3.2). The ¹H NMR spectrum (CD₂Cl₂) evidenced a new *C*₁ symmetric species with two inequivalent 3H *N*-methyl signals (δ 3.44/3.41), which supports the binding of an asymmetric ligand

[†] The related mesityl congener was also prepared using an analogous procedure (59%) and fully characterised (see Chapter 5)

in solution. Enyne coordination was corroborated by the shift in alkene resonances relative to free **17b** in the ^1H NMR spectrum (**19-Me** δ 6.38/5.97, $^3J_{\text{HH}}$ = 15.3 Hz), which are comparable to similar rhodium bound enyne species.¹⁰ The presence of ^{103}Rh coupling to the alkyne carbons ($^1J_{\text{RhC}}$ = 12/15 Hz), consistent with other π -bound alkynes and enynes (δ 80 – 100 ppm),[‡] further supporting enyne coordination. Unfortunately, the intact parent cation was not observed by ESI-MS ($[\text{M}]^+$ calcd 534.21 m/z), presumably due to facile enyne dissociation under the conditions of analysis, preventing structural verification in this way. Nevertheless, crystals grown from a CH_2Cl_2 /hexane solution allowed the conclusive structural assignment of **19-Me** in the solid-state (Figure 3.3.2).

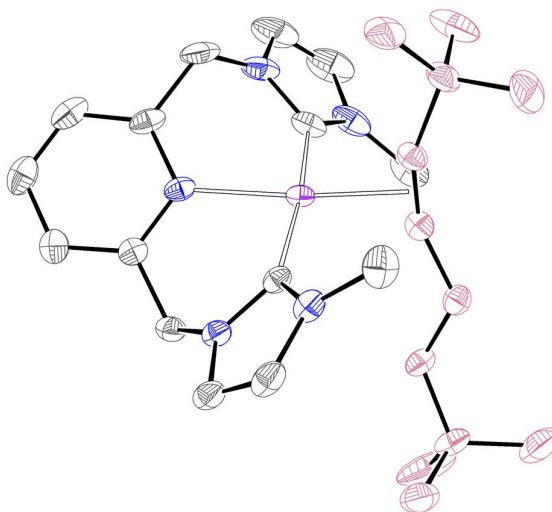


Figure 3.3.2. Solid-state structure of **19-Me** with thermal ellipsoids at 35% probability; hydrogen atoms and counter anion omitted for clarity

The solid-state structure of **19-Me** confirms the predicted π -binding of **17b** evidenced by the close approach of the alkyne carbons to the rhodium centre (Rh-Cent, 2.006(3) Å). The pincer geometry in **19-Me** is unchanged with respect to the parent ethylene species ($\text{C}_{\text{NHC}}\text{-Rh-C}_{\text{NHC}}$ 172.4(2)° vs 169.6(1)° **11-Me**) with structural metrics comparable to other Rh(I) species of CNC-Me (Rh-C_{NHC} 2.048(3), 2.026(5) Å; Rh-N 2.113(4) Å).

With product binding established, efforts turned to examining its effect on the rate of turnover. The catalytic activity of **19-Me** was probed under the standard

[‡] Compared with diphenyl acetylene adduct isolated in 85% yield from reaction of **11-Me** with diphenyl acetylene (see Chapter 5)

reaction conditions and progressed with an almost identical profile to that observed for **11-Me**, with two kinetic regimes in operation (< 40% conversion and > 50% conversion). Repeating the catalytic reaction in the presence of excess **17b** (25 mM) was expected to show a rate of alkyne turnover in-line with that of the latter regime, but this was not the case. Instead, catalysis using **19-Me** progressed with equally complex reaction kinetics, featuring a facile initial reaction rate which plateaus at higher conversions (> 40%), alongside an increased level of trimer formation.[†] Given these results, further *in situ* evaluation of the catalytic intermediates formed during the homodimerisation of **16b** by **11-Me** was conducted. Whilst initially only one broad organometallic species is observed by ¹H NMR spectroscopy, indicated by a single *para*-pyridine resonance at 7.94 ppm, during the latter stages of the reaction (*t* > 1.5 h) at least two major intermediates are present (δ 7.98 and 7.94). The emergence of the second intermediate coincides with the reduced rate of alkyne consumption and acceleration in the rate of trimer formation, indicative of competing reaction pathways, however these were not studied further.

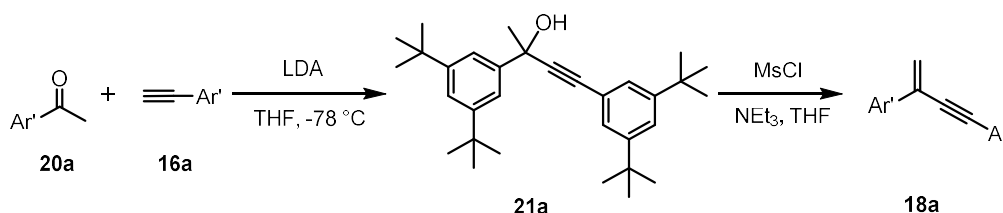
Interrogating the time-course plots associated with the homodimerisation of aromatic enynes **16a** and **16c** more closely, additional metal-based reactivity was observed at conversions > *ca.* 90% (*vide infra*). However, quenching the reactions with carbon monoxide at *ca.* 85% conversion enabled both **18a** and **18c** to be isolated in synthetically practical yields (73% and 80% respectively) by sequestering the catalytically active species as **10-Me**. Compounds **18a** and **18c** were found to have limited stability in the solid-state, presumably oligomerising to insoluble products, but could be stored as alkane solutions (*e.g.* hexane/pentane) at low temperature (-30 °C) for prolonged periods with minimal decomposition.

3.3.2. Organic preparation of *gem*-enyne – **18a**

To confirm the structure of novel enyne **18a** an independent synthetic procedure was devised (Scheme 3.3.3). Ketone **20a** was initially synthesised using a Bouveault substitution reaction between the *in situ* generated 3,5-bis(*tert*-

[†] Identified through comparison with data obtained by Dr Rhiann Andrew⁵¹

butyl)phenyl lithium, prepared through lithium-halogen exchange of 3,5-bis(*tert*-butyl)phenyl bromide, with *n*-BuLi and DMA affording a hemiaminal intermediate.⁵² Following hydrolysis under acidic conditions (HCl, 2 M) and purification on silica, **20a** was isolated in reasonable yield (49%). Nucleophilic attack of the *in situ* generated lithium acetylide, formed through deprotonation of **16a** with LDA, on the carbonyl of ketone **20a** led to the formation of tertiary alcohol **21a**. The separation of this product from unreacted **20a** proved a significant challenge; repeated separation using flash column chromatography followed by preparatory TLC could only achieve an ultimate purity of *ca.* 92% in minor quantities (used for characterisation). Unable to purify **21a** on a synthetically practical scale, the crude material (60%) was used in the dehydration reaction promoted by mesylchloride in THF:NEt₃ without further purification.



Scheme 3.3.3. Rhodium-free synthesis of *gem*-enyne **18a**

Despite quantitative conversion, the propensity of **18a** to undergo oligomerisation on concentration reduced the isolated yield of this reaction (57%) and thus hindered full characterisation using this sample. However, the key enyne signals could be identified in the associated ¹H NMR spectrum (CDCl₃, δ 5.94/ 5.73, ²J_{HH} = 1 Hz) and the parent ion was observable by ESI-MS (451.3341 [M+Na]⁺, calcd 451.3335 *m/z*). Using this sample as a reference the formation of **18a** during the catalytic reaction using **11-Me** was confirmed and full characterisation data could then be obtained using **18a** prepared in that way.

3.3.3. Kinetic investigations into alkyne dimerisation

In order to probe the mechanism of the dimerisation reaction promoted by **11-Me**, kinetic studies using **16a** as the model substrate were conducted. Plotting the consumption of **16a** against time, using the integral of the terminal alkyne proton resonance in the ¹H NMR spectra (δ 3.07, CD₂Cl₂), revealed a distinct

linear dependence over the course of the reaction, indicative of a zero-order dependence in substrate (Figure 3.3.2). This was further substantiated when the reaction was performed at half the concentration of substrate (50 mM **16a**) which proceeded at an identical rate. Repeating the reaction using double the catalyst loading (10 mol% **11-Me**) for the same concentration of **16a** (100 mM) showed a two-fold enhancement in rate relative to the that observed for the standard catalytic conditions ($t_{1/2} = 2$ h vs $t_{1/2} = 4$ h), indicating first-order dependence in catalyst. Based on these results the rate law for this process was determined as shown in Figure 3.3.3.

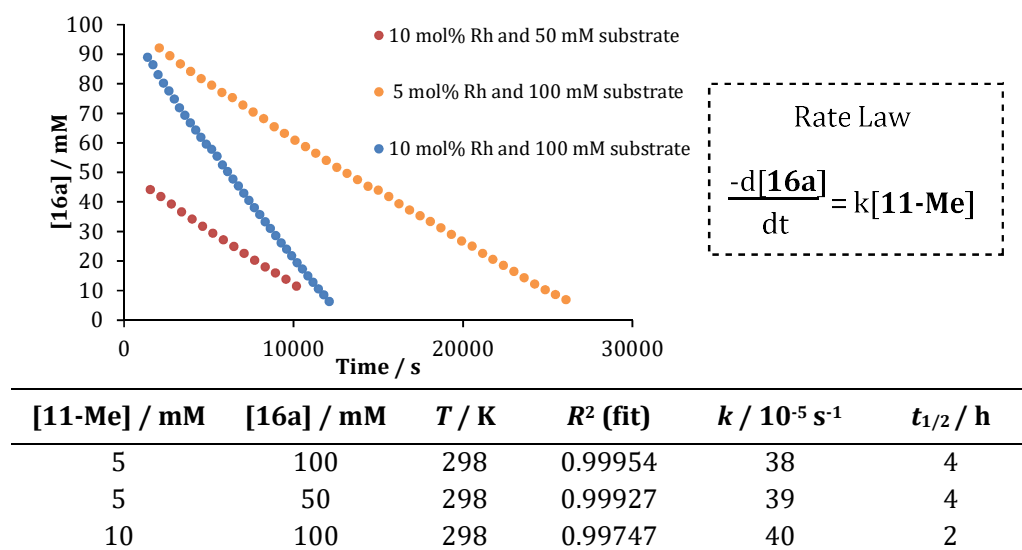
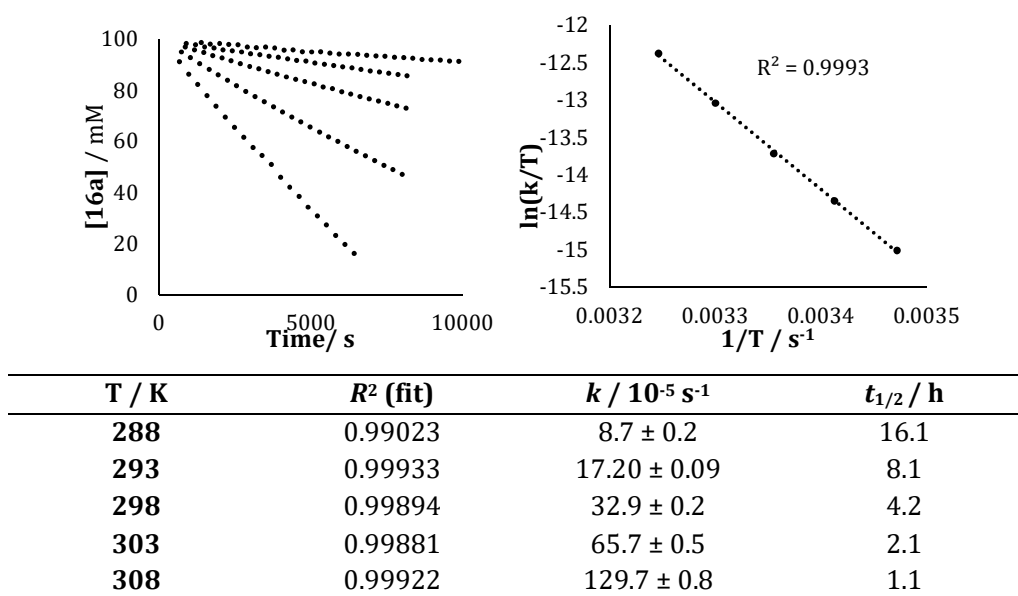


Figure 3.3.3. Catalytic alkyne coupling of **16a** promoted by **11-Me** under different concentration regimes

Using variable temperature ¹H NMR studies (CD₂Cl₂, 600 MHz, 288 – 308 K) an Eyring analysis was conducted (Table 3.3.2), allowing the activation barriers for this process to be determined: $\Delta G^\ddagger(298\text{ K}) = 93 \pm 3\text{ kJmol}^{-1}$, $\Delta H^\ddagger = 97 \pm 1\text{ kJmol}^{-1}$, $\Delta S^\ddagger = 15 \pm 5\text{ JK}^{-1}\text{mol}^{-1}$. These values show a large enthalpic barrier but a favourable positive entropy term which supports a dissociative rate limiting step, *e.g.* reductive elimination.

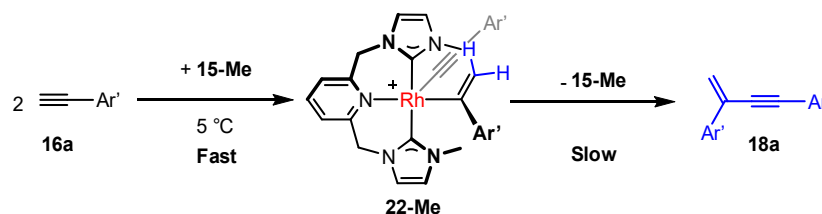
Table 3.3.2. Temperature dependence of the dimerisation of **16a** catalysed by **11-Me**

Alternately, the use of **15-Me** bearing the more coordinating DMSO ligand as the pre-catalyst under the same reaction conditions (5 mol% **15-Me**, 100 mM **16a**, CD_2Cl_2 , 25 °C) exclusively afforded the **18a**, analogously to the reaction catalysed by **11-Me**, but with an order of magnitude rate decrease ($t_{1/2} = 36$ h). The increased rhodium DMSO binding strength clearly has a detrimental impact on the catalytic activity of **15-Me** not only owed to the reduced accessibility of the 14 valence electron $\{\text{Rh}(\text{CNC})\}^+$ species but also due to competitive binding of DMSO throughout the catalytic cycle. Whilst this loss of catalytic activity would typically be viewed as a drawback, the reduced reaction rate facilitated a more detailed investigation of the catalytic intermediates.

3.3.4. Catalytic intermediates

Throughout the course of the catalysis using either **11-Me** or **15-Me** a single persistent organometallic species was observed in solution. The C_1 symmetric species was evidenced by the presence of two *N*-methyl wingtip signals (δ 4.44 and 4.13) and inequivalent methylene bridge protons in the ^1H NMR spectra (CD_2Cl_2). In order to identify this intermediate the sluggish turnover of **15-Me** was exploited. Using a lower temperature (5 °C) and higher concentration regime (33 mol% **15-Me**), which is more amenable to characterisation, the catalytic resting state was identified as the rhodium (III) alkynyl-alkenyl species **22-Me**

(Scheme 3.3.4). This assignment was supported by the ESI-MS of the reaction mixture which contains a strong molecular ion peak containing two alkyne equivalents present at 798.3985 (798.3977 calcd) m/z , corresponding to the cationic fragment of **22-Me**. In this light, the rate reduction can be rationalised by DMSO coordination between *trans*-disposed alkynyl and alkenyl ligands which impedes the C–C bond forming reductive elimination.



Scheme 3.3.4. Generation of intermediate **22-Me** from **15-Me**

Key features of the ^1H NMR spectrum of *in situ* generated **22-Me** collected at 5 °C (Figure 3.3.3) include the distinct asymmetry of the pincer backbone demonstrated most effectively by the four diagnostic methylene bridge resonances (δ 6.22, 5.95, 5.10, 4.88; $^2J_{\text{HH}} = 15.0/15.5$ Hz) as well as two ^1H signals at 4.79 and 3.21 ppm, which show characteristic geminal coupling ($^2J_{\text{HH}} = 2.9/2.1$ Hz). These signals mirror those observed during the reaction conducted under the standard catalytic conditions corroborating its assignment as the reaction intermediate and catalytic resting state.

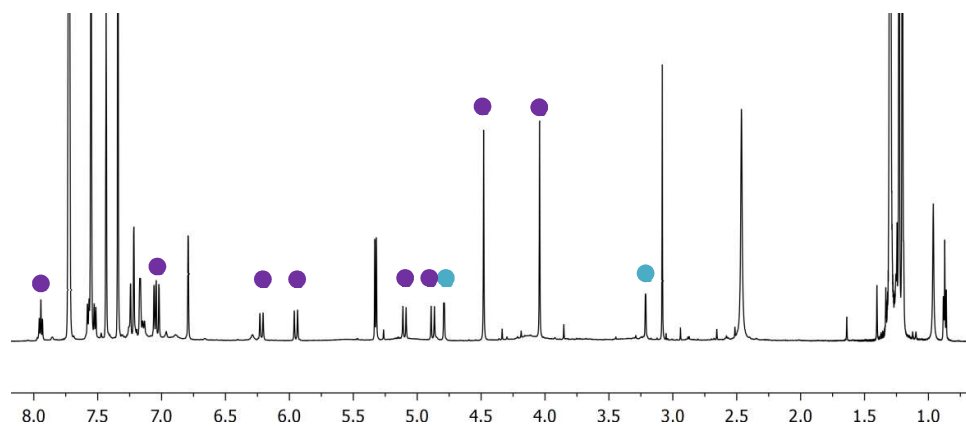


Figure 3.3.3. ^1H NMR spectra of **22-Me** generated *in situ* (600 MHz, CD_2Cl_2 , 278 K).

Purple – asymmetric pincer scaffold; Blue – geminal protons

Substantiating their assignment, a HSQC correlation experiment confirmed the geminal alkene protons reside on the same carbon atom (δ 119.9). The ^1H NMR spectrum of **22-Me** is also notable for the lack of any high field signals ($\delta < 0$),

ruling out a hydride containing resting state and ^{103}Rh coupling in the $^{13}\text{C}\{^1\text{H}\}$ NMR spectrum also helps to substantiate the structure of **22-Me**. For instance, the alkynyl carbons at 111.8 ppm ($^2J_{\text{RhC}} = 11$ Hz) and 101.9 ppm ($^1J_{\text{RhC}} = 55$ Hz) and the α -alkenyl carbon at 153.8 ppm ($^1J_{\text{RhC}} = 36$ Hz) appear as doublets with the magnitude of J_{RhC} reflecting their respective distances from the rhodium nucleus.

To determine the overall configuration of the alkynyl and alkenyl ligands around the rhodium centre, *i.e.* their arrangement in space, a NOESY experiment was conducted (Figure 3.3.4). The NOESY spectrum shows the predicted correlations between adjoining environments on the pincer scaffold alongside exchange peaks between the diastereotopic environments. Diagnostic signals come between the geminal alkene proton at 4.79 ppm, the *ortho*-Ar' protons of the alkenyl ligand (δ 7.22) and the *N*-methyl appendages (δ 4.48/ 4.04).

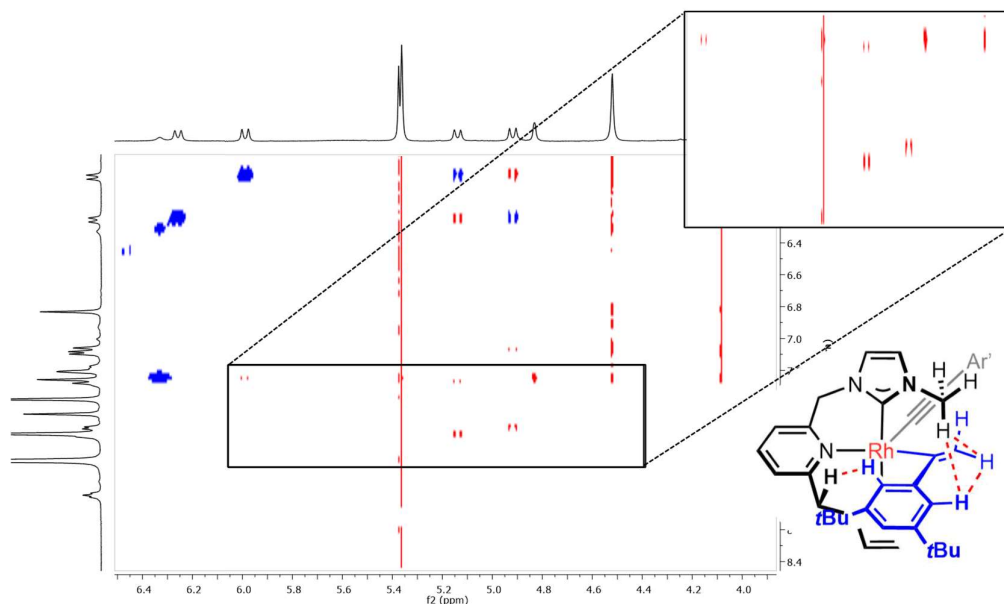
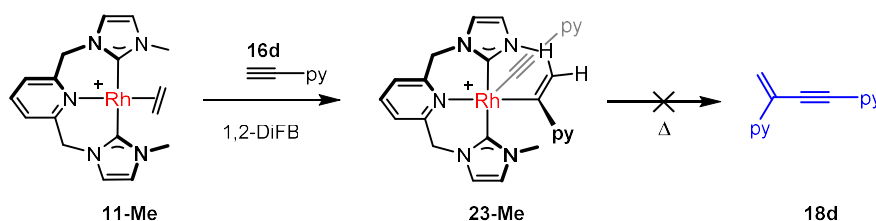


Figure 3.3.4. NOESY NMR spectra of intermediate **22-Me** (CD_2Cl_2 , 600 MHz, 5 °C)

The absence of correlations between the pyCH_2 and alkene resonances in the NOESY spectrum, alongside the lack of pyridine correlations with the corresponding aromatic signals, strongly discredits apical coordination of the alkenyl ligand. As such, the basal coordination of the alkenyl donor and apical coordination of the alkynyl ligand in **22-Me** was tentatively proposed. This assertion is supported by the close approach of the geminal alkenyl protons and

N-methyl groups (Figure 3.3.4) and correlations between the methylene bridge protons and the *ortho*-Ar' protons. Unfortunately, the isolation and therefore unambiguous assignment of **22-Me** via X-ray diffraction was encumbered by facile reductive elimination.

The assignment of intermediate **22-Me** was further substantiated by a trapping experiment using 2-ethynylpyridine (**16d**). Containing an additional nitrogen donor moiety, **16d** was hoped to aid the isolation of the catalytic intermediate by impeding reductive elimination. Monitoring the reaction between **11-Me** and excess **16d** at ambient temperature (Scheme 3.3.5) allowed an initial transient rhodium hydride intermediate to be directly observed by ^1H NMR spectroscopy (δ -17.62, $^1J_{\text{RhH}} = 28.5$ Hz, 1,2-DiFB). This hydride was short-lived and after an hour the spectrum showed one predominant organometallic species (**23-Me**), which underwent no further reaction on prolonged heating at elevated temperature (80 °C, 18 h). Prominent spectral features of **23-Me** include an asymmetric pincer backbone, evidenced by two ^3H resonances for the methyl appendages (δ 4.18/2.87) and at least three doublets pertaining to the protons of the methylene bridges (δ 5.38, 5.05, 4.85; $^2J_{\text{HH}} = 15$ Hz), with the other presumably obscured by the residual solvent peak, and a ^1H signal at 6.05 ppm with characteristic geminal coupling (*viz.* $^2J_{\text{HH}} = 1.6$ Hz). Supported by ESI-MS analysis (576.1373, calcd 576.1377 m/z), **23-Me** was cautiously identified as the Rh(III) *gem*-alkenyl alkynyl complex, where chelation through the pyridine moiety completes the octahedral coordination sphere.



Scheme 3.3.5. Reaction of **11-Me** with 2-ethynylpyridine **16d**

With reductive elimination aptly precluded, **23-Me** was isolated and its structure interrogated further in a solvent more suited to characterisation (*viz.* CD_2Cl_2). The ^1H NMR spectrum revealed a mixture of species comprised predominantly of **23-Me** (*ca.* 72%), which showed similar spectral characteristics to data obtained

in situ. Additional information included the location of the second geminal alkenyl signal (δ 6.47/ 5.96), which correlated to the same carbon resonance (δ 119.8) in an HMBC experiment, confirming their assignment as geminal alkene resonances. In the $^{13}\text{C}\{^1\text{H}\}$ NMR spectrum the α -protons of the alkenyl and alkynyl ligands (δ 137.0, $^1J_{\text{RhC}} = 25$ Hz; δ 98.8, $^1J_{\text{RhC}} = 56$ Hz, respectively) as well as the β -alkynyl carbon (δ 106.4, $^2J_{\text{RhC}} = 12$ Hz) show coupling to ^{103}Rh with magnitudes similar to those observed for **22-Me**, further corroborating the assignment.

Crystals were obtained from this product mixture allowing solid-state structural elucidation of **23-Me** using X-ray diffraction (Figure 3.3.5; 1.2 Å resolution). Complex **23-Me** was confirmed as the Rh(III) alkynyl alkenyl intermediate with the alkynyl group residing in the axial position relative to the pincer coordination plane, the alkenyl group equatorial and the additional pyridine donor completing the coordination sphere, *trans* to the alkynyl ligand. Spectral similarities between **22-Me** and **23-Me** therefore support the catalytic resting state adopting an analogous structure.

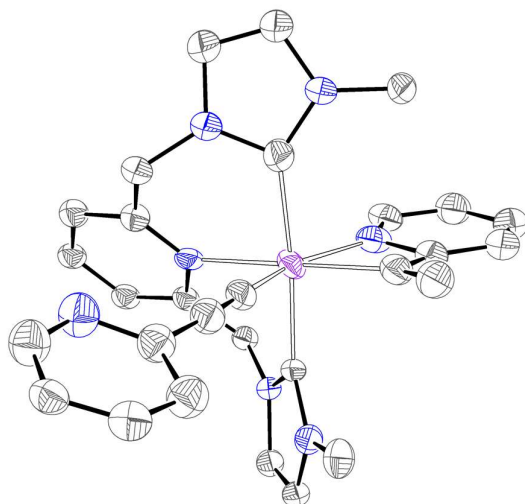
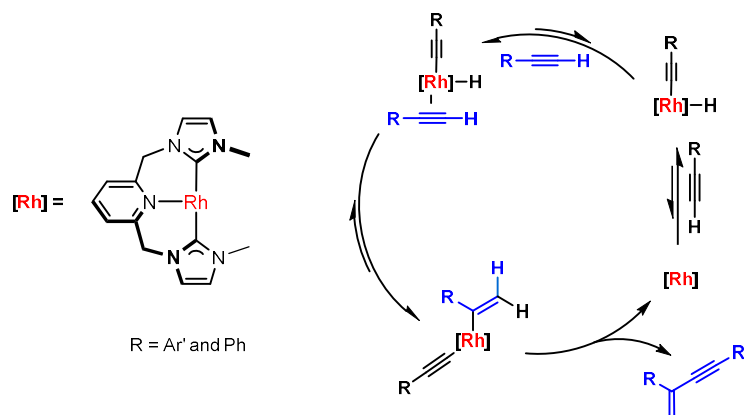


Figure 3.3.5. Solid-state structure of **23-Me**. Thermal ellipsoids at 30% probability; hydrogen atoms and counter anion omitted for clarity. Selected bond lengths (Å): Rh–N 2.25(2), Rh–C_{NHC} 2.01(2)/2.01(2), Rh–C_{alkyne} 1.92(2), C≡C 1.21(3), Rh–C_{alkene} 2.02(2), C=C 1.30(3)

3.3.5. Dimerisation mechanism

Like other rhodium terminal alkyne catalysts reported previously, **11-Me** formed *E*- or *gem*-enyne products, or mixtures thereof.^{23,24,53} The presence of head-to-tail

products and absence of *Z*-enynes implies an operative oxidative addition mechanism. Based on the determined rate equation, thermodynamic parameters and observed intermediates, the catalytic cycle for the dimerisation of **16a** promoted by **11-Me** was proposed as an oxidative addition hydrometallation pathway (Scheme 3.3.6) with turnover limiting reductive elimination. Given the analogous selectivity observed when using the phenyl derivative **16c**, and the formation of **23-Me**, it can be assumed that this reaction and other aromatic substituents are likely to proceed *via* an analogous reaction manifold.



Scheme 3.3.6. Proposed catalytic cycle for the homodimerisation of **16a**

In the case of **16b** however, the selectivity is reversed, and initial investigations indicate a more complex mechanism. For instance, the apparent stronger binding of the *E*-enyne product presumably leads to numerous off-cycle reactions which dampen the reaction rate.⁵¹ In the absence of detailed mechanistic investigations the mechanism behind the homocoupling of **16b** cannot be conclusively determined, but given the pathway outlined for the aromatic alkynes it is also likely to progress *via* an oxidative addition hydrometallation pathway, differing by the orientation of which the second alkyne binds.

3.3.6. Homodimerisation in 1,2-difluorobenzene

Plotting the consumption of **16a** as a function of time across the temperature range (288 – 308 K) showed slight deviation from linearity as the reaction progressed (Figure 3.3.6). This aberration is more pronounced for the lower temperatures where the reaction time is longest and is attributed to catalyst

decomposition in CH_2Cl_2 , an issue that was also noted for the pre-catalyst **11-Me** (Chapter 2).

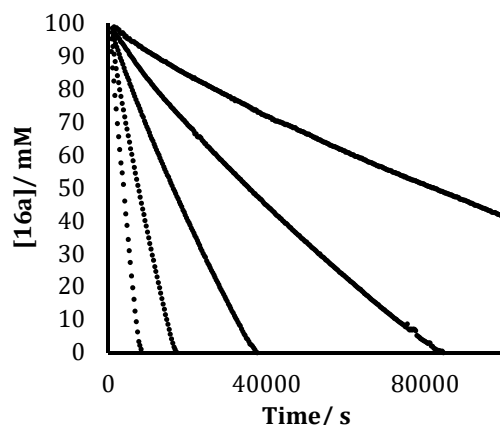


Figure 3.3.6. Variable temperature time-course plots for the dimerisation of **16a** monitored by ^1H NMR spectroscopy (CD_2Cl_2 , 288 – 308 K, 600 MHz)

In light of the catalyst instability in CH_2Cl_2 , the more inert 1,2-DiFB was chosen as the replacement reaction solvent. To ensure that the catalyst remained active and selectivity unchanged, the reaction between **16a** and **11-Me** under identical conditions as those in CH_2Cl_2 , was first assayed in 1,2-DiFB. Switching the solvent in this way led to a significant rate enhancement without loss of selectivity ($\text{TOF} = 2.5 \text{ h}^{-1}$ CH_2Cl_2 vs $\text{TOF} = 30 \text{ h}^{-1}$ 1,2-DiFB). The time-course plot of this reaction shows linear reaction progression indicative of a zero-order substrate dependence, and repeating the reaction using instead 8 mol% **11-Me** showed a *ca.* 1.5 times rate enhancement, consistent with first-order catalyst dependence; both mirroring the outcomes described previously in CD_2Cl_2 .

A distinctly asymmetric catalytic resting state consistent with **22-Me**, was again observed throughout the homocoupling, exhibiting two ^1H *gem* alkenyl signals at δ 3.26 and 4.50 and associated *t*Bu signals at δ 1.30 and 1.33. The concentration of **22-Me** appeared to decrease over the course of the reaction and appears linked to the increasing concentration of **18a**, which notably does not fully correspond to the consumption of **16a**. These observations infer transition from **22-Me** to a new catalytic resting state, featuring coordinated *gem*-enyne, over the course of the reaction. Nevertheless, these results remain consistent with the mechanistic conclusion devised based on earlier data collected in CD_2Cl_2 ,

whereby the reaction proceeds *via* a hydrometallation pathway with rate-limiting reductive elimination (Scheme 3.3.6).

Given these findings, the temperature dependence of this catalytic transformation in 1,2-DiFB was studied using ^1H NMR spectroscopy over the same temperature window as the analogous investigation in CH_2Cl_2 (600 MHz, 288 – 308 K; Figure 3.3.7). In this case, the activation barrier is considerably lowered relative to the barrier in CD_2Cl_2 (ΔG^\ddagger (298K) = 87 ± 5 vs 93 ± 3 kJ mol^{-1}) as a consequence of a noticeably increased entropic contribution (ΔS^\ddagger = $+28 \pm 9$ vs $+15 \pm 5$ $\text{J K}^{-1}\text{mol}^{-1}$), with the enthalpic component remaining the same within error (ΔH^\ddagger = 95 ± 3 vs 97 ± 1 kJ mol^{-1}). The increase in entropy associated with the reductive elimination step in 1,2-DiFB can be qualified by differences in the solvation of the low coordinate Rh(III) intermediate **22-Me**.

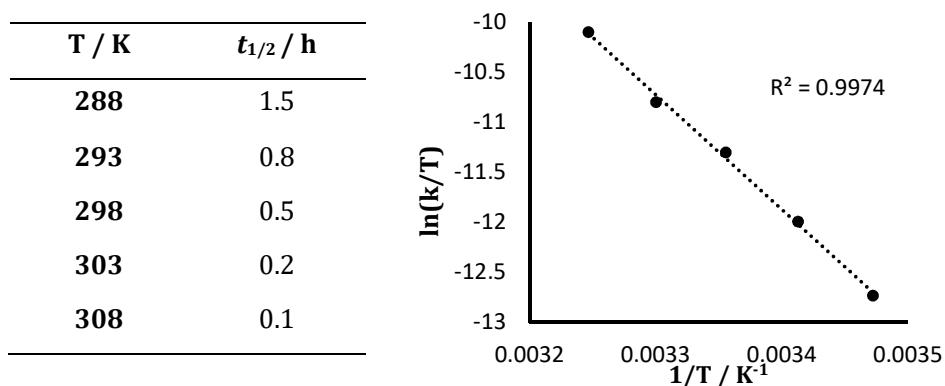
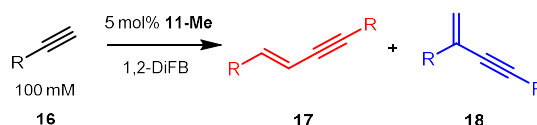


Figure 3.3.7. Eyring analysis of the dimerisation of **16a** by **11-Me** in 1,2-DiFB

A similar rate enhancement was also observed for the homocoupling of **16c** ($t_{1/2}$ = 1.2 h) when switching from CD_2Cl_2 to 1,2-DiFB. With the **11-Me** catalysed dimerisation more efficient in 1,2-DiFB, the scope of this process was extended (Table 3.3.3). For instance, the *n*Bu alkyne (**16e**) was investigated as to mimic the electronics of **16b** but with a distinctly different steric profile and **16f** was explored as to probe the impact sterics have on the reactivity of aryl alkynes.

Table 3.3.3. Catalytic terminal alkyne dimerisation mediated by **11-Me**



Substrate		$t_{1/2}$ /hours	Distribution at 50%		Distribution at 100%	
			18	17	18	17
16a	Ar'	0.5	100	-	92 ^b	-
16b	<i>t</i> Bu	4.5	-	100	-	85 ^c
16c	Ph	1.2	100	-	94 ^b	-
16e	<i>n</i> Bu	5	80	20	83	17
16f	Mes	0.2	40	60	42	58

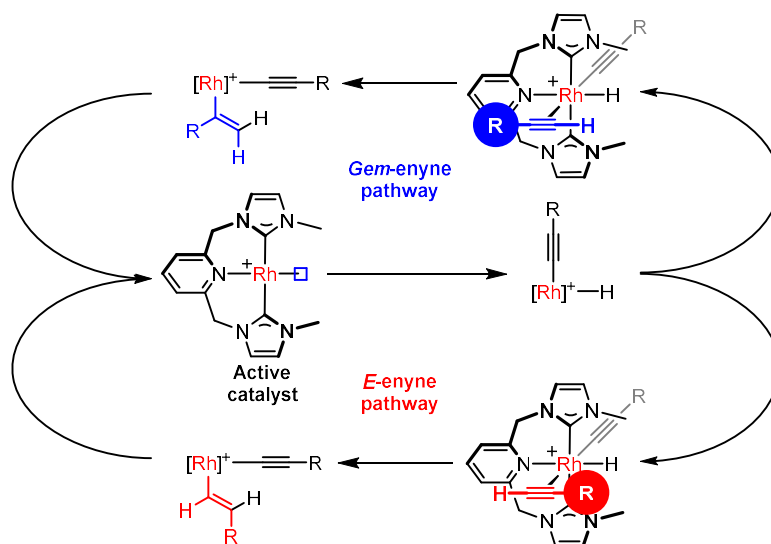
^a) Determined from ¹H NMR data, using Ar^F signals as an internal standard; ^b) balance of material made up with tetrameric species; ^c) balance of material made up with trimeric species

Evaluation of the results summarised in Table 3.3.3 shows increased activity of **11-Me** towards the homocoupling of aromatic alkynes, particularly in the more weakly coordinating solvent, compared with aliphatic substrates ($t < 3$ h vs $t > 10$ h). For instance, the homocoupling of **16e** using **11-Me** proceeded at a similar initial rate to **16b** ($t_{1/2}$ ca. 5 h), which is largely unaffected by the change in solvent. Whereas **16f** shows rapid conversion, reaching completion in under an hour. However, neither the reaction of **16e** nor **16f** proceeded selectively. Notably, the homodimerisation of **16e** shows opposing selectivity to **16b**, giving an 83:17 mixture of **18e** and **17e** and unlike the other aryl substrates, **16f** also gives a mixture of *E*- and *gem*- products. Isolation of all enyne products generated was facilitated by quenching the associated reaction mixture with CO prior to concentration *in vacuo* and extraction of the organic products into hexane. For reactions resulting in multiple enyne products separation of the isomers was achieved by column chromatography (**17/18d** silica, hexane; **17/18e** silica, toluene/hexane) and their identification confirmed through comparison with literature data.^{20,35,49,50,54,55}

3.3.7. Discussion of selectivity

Orthogonal product selectivity driven by the substrate, as is the case for **11-Me**, is not uncommon for terminal alkyne coupling reactions.^{23,56–58} This divergent selectivity is most pronounced for **16b** and **16c**, where the former sees exclusive head-to-head dimerisation (**17b**) and the latter head-to-tail dimerisation (**18c**).

With both processes proposed to proceed *via* a hydrometallation pathway, the selectivity is thought to be determined on coordination of the second alkyne equivalent. Opposing selectivity is also observed between **16a** and **16f** as well as between **16e** and **16b** despite having comparable electronic properties. As such, the contrasting selectivity has been rationalised by unfavourable steric clashes between the terminal *t*Bu group of **16b** and the lutidine moiety on the puckered pincer scaffold, interactions which are largely absent in the case of **16e** and predominantly planar, aromatic variants (Scheme 3.3.7). The exception to this hypothesis is **16f** where the proximity of the *ortho* methyl substituents are thought to destabilise the geminal pathway through unfavourable steric clashes. On the other hand, the steric bulk pertaining to the *meta*-disposed *t*Bu groups on **16a** is far removed from the reactive centre and thus has little impact on the selectivity.



Scheme 3.3.7. Divergent reaction pathways enforced by steric clashes

Seeking to gain deeper understanding of these bifurcating pathways, DFT calculations were conducted, using **16b** and **16c** as representative substrates.[‡] Initial investigations aimed to resolve the underlying mechanistic pathway. These calculations supported an operative hydrometallation pathway for **16c**, with substantial activation barriers associated with the alkynyl migratory insertion in the carbometallation mechanism (*cf.* $\Delta G^\ddagger = 94.1 - 108.0 \text{ kJmol}^{-1}$, **16c**).

[‡] Computational analysis performed by Dr Tobias Krämer. Mechanisms evaluated with structures optimised at the B3PW91-D3 level using a combination of the SDD and 6-31G** basis sets.

In-line with experimental observations (*vide supra*), the calculated reaction profiles for the homodimerisation of **16b** and **16c** indicated selectivity towards **17** and **18**, respectively (Figures 3.3.8 and 3.3.9).

Supporting the hypothesis that this selectivity is driven by steric clashes during the second alkyne coordination event, the energetics associated with the alkyne π -binding to the alkynyl-hydride complex ($\Delta\Delta G = -2.1$ kJmol⁻¹) and subsequent barrier to migratory insertion ($\Delta\Delta G^\ddagger = -8.4$ kJmol⁻¹) are favoured for the geminal pathway relative to the *E*-pathway. Matching the experimental findings, evaluation of the calculated reaction profiles indicated a rate-limiting reductive elimination step ($\Delta G^\ddagger = 90.8$ kJmol⁻¹) and the rhodium(III) alkenyl-alkynyl intermediate as the catalytic resting state. Despite the reductive elimination generating the *E*-isomer being lower in energy ($\Delta G^\ddagger = 76.6$ kJmol⁻¹), it is inaccessible from the Rh(III) alkenyl alkynyl resting state, which is formed irreversibly with respect to product formation ($\Delta G^\ddagger = 124.6$ kJmol⁻¹), *i.e.* the migratory insertion is identified as the selectivity determining step.

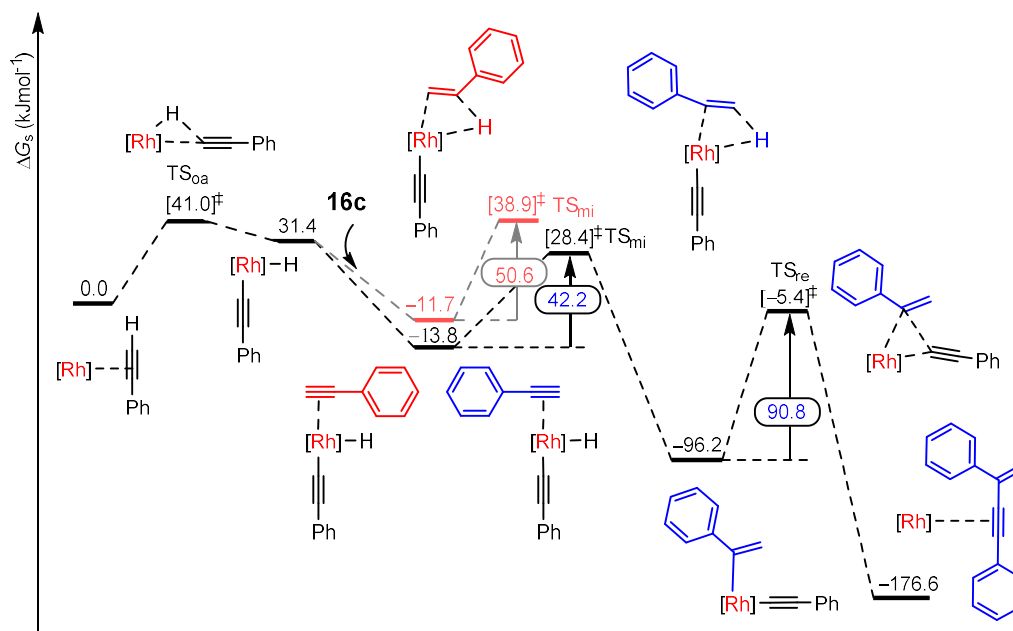


Figure 3.3.8. Reaction profile for the homodimerisation of **16c**

The calculated profile for the dimerisation of **16b** is more complex (Figure 3.3.9). Despite the intermediate with the π -bound alkyne orientated as to give **17b** being favoured by 10.9 kJmol⁻¹ the onwards reactivity is favoured for the *gem*-selective

mechanism (*cf.* 45.2 kJmol⁻¹ vs 49.8 kJmol⁻¹). The geminal pathway continues to be favoured up until the ultimate reductive elimination step, where unlike in the case of **16c**, the reverse reaction, *viz.* β -hydride elimination, is more energetically accessible (*cf.* $\Delta G^\ddagger = 81.2$ kJmol⁻¹) compared with the forward reductive elimination ($\Delta G^\ddagger = 108.8$ kJmol⁻¹) introducing reaction reversibility. Retracing the reaction pathway back to the rhodium(III) alkynyl-hydride species and progression instead *via* the *E* reaction route allows reductive elimination of **17b**, which is markedly energetically favoured ($\Delta G^\ddagger = 67.7$ kJmol⁻¹). Reflecting on the calculated barriers, the geminal alkenyl-alkynyl species is indicated to be the catalytic resting state ($\Delta G = -42.7$ kJmol⁻¹) and the β -hydride elimination the rate determining step of the reaction. As such, the selectivity of this process appears to not be governed simply by the initial alkyne binding event, but rather the substantial energetic barrier associated with reductive elimination to give **18b** and the reversibility of preceding mechanistic steps.

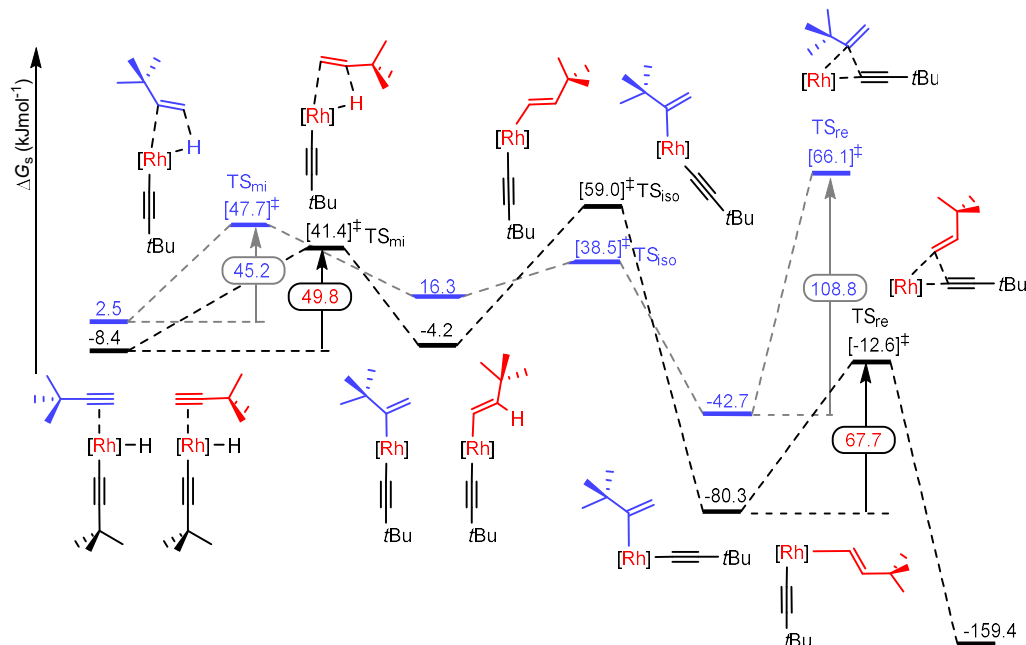
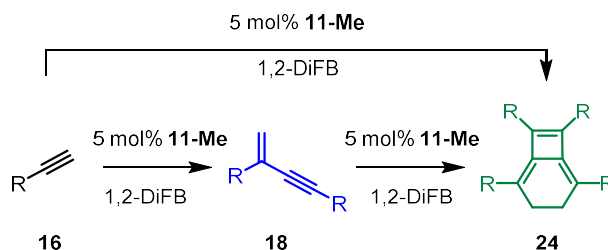


Figure 3.3.9. Reaction profile for the homodimerisation of **16b**

3.4 Catalytic formation of bicyclo[4.2.0]octa-1,5,7-trienes

Whilst studying the homodimerisation of **16a** and **16c** catalysed by **11-Me**, additional onwards reactivity was discovered involving the annulation of **18** into bicyclo[4.2.0]octa-1,5,7-trienes **24** (Scheme 3.4.1).



Scheme 3.4.1. Catalytic formation of **24** via **18**

Following the reaction of **16a** catalysed by **11-Me** beyond the dimerisation step using *in situ* ^1H NMR spectroscopy (1,2-DiFB), showed a clear stepwise reaction progression, with almost exclusive conversion of **16a** into **18a** before onset of the ensuing annulation reaction (Figure 3.4.1). The transformation of **18a** into **24a** proceeded quantitatively within 4 hours at 25 °C, as evidenced by appearance of a characteristic 4H signal at 2.87 ppm and two new 36H *t*Bu resonances at 1.03 and 1.11 ppm. Likewise, reacting isolated **18a** (50 mM) with **11-Me** (10 mol%) also showed quantitative conversion into **24a** with a similar rate to the reaction *via in situ* generated **18a**, confirming that the catalytic annulation is mechanistically independent of the initial alkyne homocoupling reaction.

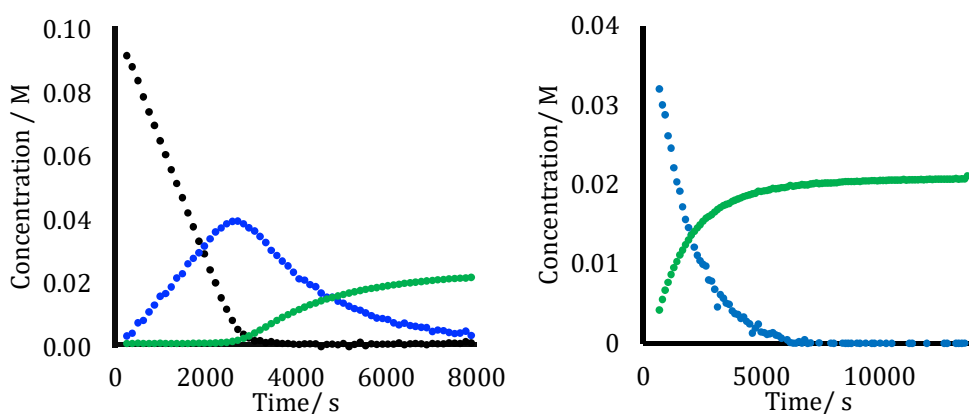


Figure 3.4.1. Time course plots for the annulation reaction to generate **24a**; Left – auto-tandem process from **16a** (1,2-DiFB, 5 mol% **11-Me**, 298 K, left); Right – reaction from isolated **18a** (1,2-DiFB, 10 mol% **11-Me**, 298 K)

The ability of **11-Me** to promote the two mechanistically distinct transformations (*viz.* terminal alkyne dimerisation and enyne annulation) sequentially is reminiscent of tandem catalytic processes. The capacity of **11-Me** to perform these steps with high temporal control, independent of an external trigger, means it can be categorised as an auto-tandem catalyst.⁵⁹⁻⁶¹

After quenching the reaction with CO, **24a** was isolated in excellent yield following extraction into tetramethylsilane (TMS; 94%). Crystals suitable for study by X-ray diffraction were grown by slow evaporation of a TMS solution, facilitating the unambiguous characterisation of **24a** in the solid-state (Figure 3.4.2). Owing to the steric bulk of the arene appendages, these groups are twisted out of the plane of the central bicyclic scaffold. In this way **24a** adopts a helical structure which gives rise to two isomers, both of which are present in the asymmetric unit ($Z' = 2$). The lack of conjugation in the six-membered ring of **24a** is indicated by the puckering of the cyclohexadiene ring out of the plane of the central fused unit (27.5°) and by the longer C3–C4 bond (1.536(6)/ 1.542(5), Å) relative to double bonds C1=C2 and C5=C6 (1.338(4) – 1.340(5) Å).

Isobenzenes of this type have limited literature precedent, with only one example of their preparation *via* metal-catalysed dimerisation of geminal enynes.^{62,63} Saito and Yamamoto *et al.* described the efficient ‘zipper’ annulation of electron deficient perfluorinated enynes using a nickel(0) catalyst (*viz.* Ni(PPh₃)₄), reactivity which was not emulated by the palladium analogue nor similar rhodium (RhCl(PPh₃)₃) systems. This report postulated a mechanism for this transformation, however, no further investigations in support of this were described. As a result, very little is understood about the scope and mechanism of this reaction.

3.4.1. Scope of the reaction

With the auto-tandem catalytic behaviour of **11-Me** established and given the paucity of similar reactions in the literature, investigations continued into this process. Building on the initial discovery when using **16a** and **16c**, the substrate scope was extended to other aromatic substrates **16g** – **16k** (Table 3.4.1). The intermediacy of the corresponding *gem*-enyne (**18**) in these transformations was

confirmed by *in situ* reaction monitoring using ^1H NMR spectroscopy (1,2-DiFB), evidenced particularly by the geminal alkene proton resonances (*cf.* 5.5 – 6.0 ppm; Table 3.4.1). Conducting these reactions at higher temperature (65 °C) enabled **24a**, **24c** and **24g-k** to be successfully isolated in good to excellent yields (64 – 94%).

Table 3.4.1. Scope of the auto-tandem catalysis promoted by **11-Me**

R	Product	t/ h	Yield/ %	δ of intermediate 18
3,5- <i>t</i> Bu ₂ Ph	24a	4.0	94	5.93; 5.67
Ph	24c	4.0	76	5.82; 5.61
3,5-F ₂ Ph	24g	8.0	75	5.81; 5.56
3,5-(OMe) ₂ Ph	24h	7.0	64	5.87; 5.64
4-FPh	24i	6.0	82	5.74; 5.57
4-OMePh	24j	6.5	79	5.73; 5.51
3,5-(CF ₃) ₂ Ph	24k	5.5	79	5.99; 5.89

Compounds **24** were fully characterised in solution using NMR spectroscopy (CD_2Cl_2), which contain a characteristic 4H singlet resonance corresponding to the CH_2 protons (δ 2.90 – 3.11) and associated resonance in the $^{13}\text{C}\{^1\text{H}\}$ NMR spectra (δ 30.0 – 28.5). Other diagnostic signals include those associated with the quaternary carbon atoms of the bicyclic scaffold at 149.0 – 146.8 ppm for C7/C8; 135.6 – 134.9 ppm for C1/C6 and 119.2 – 117.0 ppm for C2/C5. In addition, the solid-state structure of **24g** was obtained and the structural metrics are comparable to those of **24a** as well as related literature compounds (C7=C8 1.341(2) Å; C1=C2 1.381(3) Å; C5=C6 1.339(2) Å C3–C4 1.540(3) Å; *cf.* **X116**, C3–C4 1.49(1) Å; C1=C2/ C5=C6 1.336(9)/ 1.330(9) Å; C7=C8 1.336(8) Å).⁶²

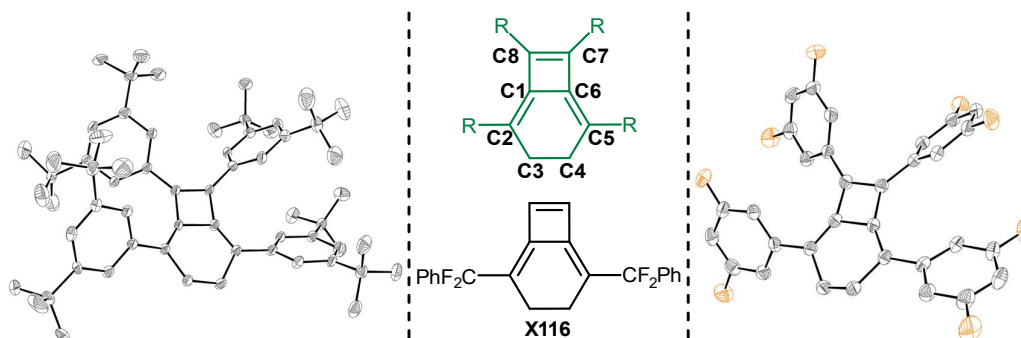
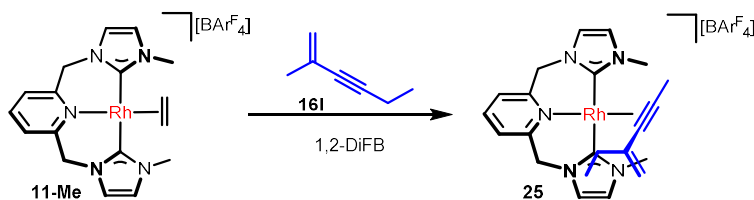


Figure 3.4.2. Solid-state structures of **24a** and **24g**. Thermal ellipsoid at 50% probability; hydrogen atoms and minor disordered components omitted for clarity. The structure shown of **24a** is one of two independent molecules ($Z' = 2$).

From these studies, the applicability of this tandem process towards aromatic substrates was established; showing tolerance to a range of both electron donating and electron withdrawing substituents in both the *para* and *meta* positions of the arene. However, the standard catalytic reaction using the sterically cumbersome mesityl alkyne **16f** did not result in formation of **24f**. Even under the more forcing conditions employed for the one-pot isolation procedure (10 mol% **11-Me**, 50 mM **16**, 65 °C), the reaction of **16f** afforded only a 20:80 mixture of **17** and **18** respectively.

The catalytic dimerisation of aliphatic alkynes **16b** and **16e** described previously (5 mol% **11-Me**, 100 mM **16**, 1,2-DiFB, 25 °C) also showed no evidence of tetramer formation (*vide supra*). Whilst this is unsurprising for **16b** which showed exclusive *E*-selectivity, the inability of **18e** to be transformed into **24e** over prolonged periods suggests that the annulation catalysed by **11-Me** is not applicable for aliphatic enynes. Moreover, under high temperature conditions neither **16b** nor **16e** produced **24**, but instead mixtures of **17b** and related trimeric products, and **17e** and **18e**, respectively, were formed. To confirm that the absence of enyne coupling for **18e** is due to its aliphatic character, rather than competitive binding of **17e**, **11-Me** was reacted with the commercial enyne **18l** (Scheme 3.4.2). Under catalytic conditions **18l** did not generate **24l** and instead one asymmetric organometallic species which showed no evidence of catalytic turnover even at 65 °C, was observed. This compound adopts *C*₁ symmetry in the ¹H NMR spectrum (1,2-DiFB) and was identified as the π -bound enyne species **25** supported by the upfield shift in the associated alkene resonances; δ 4.51 and 4.61 shifted *ca.* 0.5 ppm relative to the free enyne.



Scheme 3.4.2. Attempted annulation of **18l** generating **25**

Overviewing the results of these scoping reactions, it appears that the annulation of *gem*-enyne promoted by **11-Me** is limited to terminal aryl enynes bearing

ortho and *para* substituents. However, these studies are clearly not exhaustive, for example, enynes bearing two different appendages were not investigated.

3.4.2. Kinetic investigations

Probing the mechanism behind the annulation reaction of **18a** further, kinetic analyses were conducted, aided by convenient spectroscopic signatures deriving from the *t*Bu protons of the Ar' group, which enable the concentrations of free **16a**, **18a**, and **24a** to be monitored over time. Evaluating the consumption of **18a** as a function of time indicates a first-order dependence in substrate for the enyne dimerisation catalysed by **11-Me**. Repeating the reaction with varying concentrations of **16a**, and by extension **18a**, provided further confirmation. Increasing the catalyst loading from 5 mol% to 8 mol% saw a 2.6-fold increase in the rate of **24a** formation reflecting a second-order dependence in **11-Me**. As a result, the rate law was derived for this reaction (Figure 3.4.3).

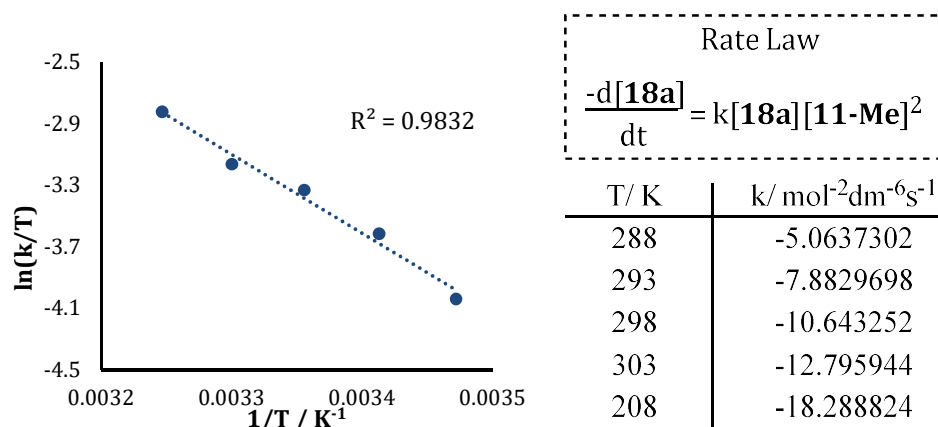


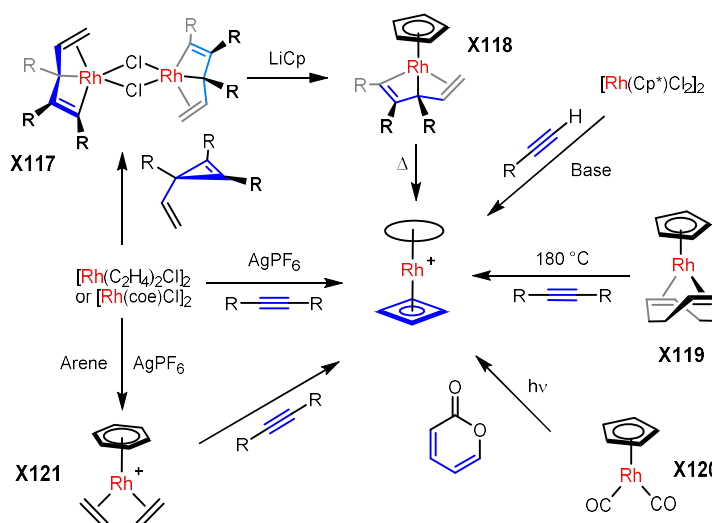
Figure 3.4.3. Eyring analysis of the catalytic formation of **24a** (288 – 308 K)

From the temperature dependence investigations, the activation parameters for the annulation reaction were determined; $\Delta G^\ddagger(298 \text{ K}) = 67 \pm 6 \text{ kJmol}^{-1}$, $\Delta H^\ddagger = 43 \pm 3 \text{ kJmol}^{-1}$, $\Delta S^\ddagger = -83 \pm 11 \text{ JK}^{-1}\text{mol}^{-1}$. The magnitude of the energy barrier is significantly smaller than that of the initial dimerisation step and ordinarily you would expect these reactions to run concurrently. However, the asynchronicity of these pathways can be explained by the necessity for two rhodium centres and an equivalent of **18a** in the rate determining step, a requirement that is unlikely up until high alkyne consumption. Unlike the initial alkyne dimerisation, the

enyne dimerisation has a large negative entropy term indicating an associative rate limiting step.

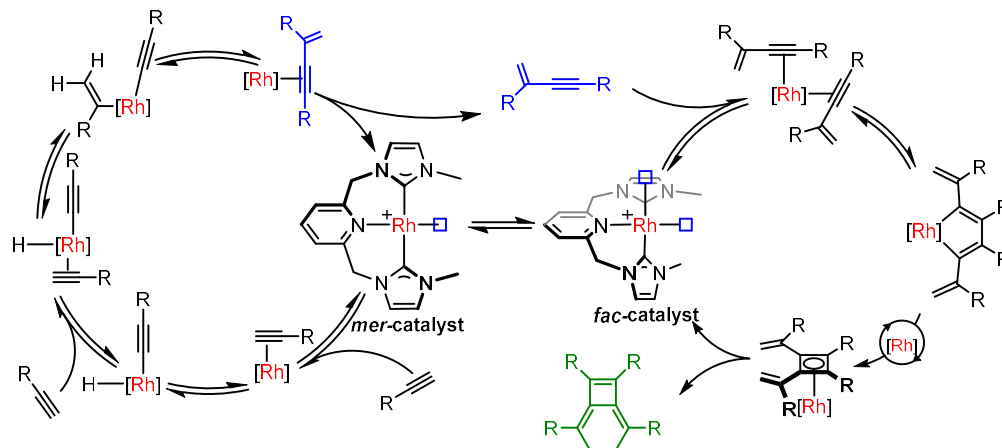
3.4.3. Mechanistic proposal

Given the absence of an observable intermediate during the annulation reaction, focus turned to the literature for mechanistic inspiration. Reports of reactions between rhodium and alkynes are comprehensive, with notable examples including [2+2+2] cycloadditions and inter- and intramolecular reductive couplings.^{64–70} Rhodium-based metallacyclopentadienes are important compounds which feature as reactive intermediates in the former and are the products of the latter,^{68,71} as well as possessing interesting luminescent properties in their own right.^{72–74} Another species that features in the literature as a product of the reaction between rhodium and alkynes are cyclobutadienes (Scheme 3.4.3). Most notably, complex **X121** has been reported to promote the dimerisation of internal alkynes into their corresponding cyclobutadiene adducts.^{75,76} Employing instead the commercially available rhodium alkene dimers $[\text{Rh}(\text{C}_2\text{H}_4)_2\text{Cl}]_2$ and $[\text{Rh}(\text{coe})\text{Cl}]_2$ as the rhodium precursor, the [2+2+2] cyclotrimerisation of three equivalents of alkyne was observed alongside the aforementioned [2+2] cycloaddition forming the related sandwich complex in good yields using a one-pot procedure ($\text{R} = \text{Et}$, 70%).^{75,77}



Scheme 3.4.3. Examples of rhodium cyclobutadiene complexes in the literature

Building on these literature precedents, Yamamoto and co-workers' mechanistic proposal for their Ni(0) catalysed annulation,⁶² and the observed rate law, the formation of bicyclo[4.2.0]octa-1,5,7-trienes is suggested to occur *via* the mechanism outlined in Scheme 3.4.4.



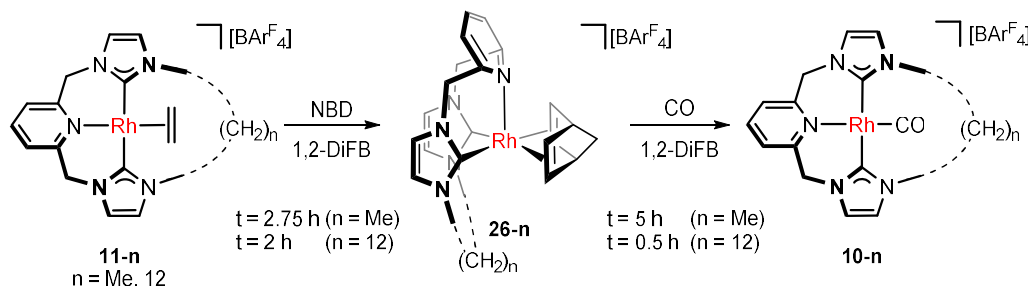
Scheme 3.4.4. Proposed mechanism of the tandem catalytic process

The hypothesised mechanism involves the initial formation of *gem*-enynes *via* the hydrometallation mechanism as described above, which is in operation until **16** is consumed. The second cycle commences when the concentrations of enyne and active catalyst are both large, in line with an autonomous tandem process.

The postulated annulation mechanism invokes a *mer* to *fac* pincer ligand isomerisation, which widens the accessible face of the metal coordination sphere and enables the π -coordination of two geminal alkynes. Oxidative coupling then affords a rhodacyclopentadiene intermediate, in which the CNC pincer could in principle adopt either coordination geometry. There is potential for either step of these steps to proceed *via* a bimetallic transition state, however, we advocate a mechanism whereby the second catalyst equivalent aids the transformation of the metallacyclopentadiene into the corresponding cyclobutadiene complex. Following a pericyclic rearrangement of the cyclobutadiene intermediate, metal catalysed or otherwise, **24** would be released from the catalytic cycle. With the evidence available at this stage of the investigations, *viz.* the determined rate law (*vide supra*), the rate determining step of the proposed catalytic cycle is suggested to be the formation of the rhodium cyclobutadiene complex.

3.4.4. Supporting evidence: *fac-mer* ligand isomerisation

Ligand exchange reactions were carried out to probe the flexibility of the pincer scaffold and its propensity to adopt a facial coordination at rhodium, (Scheme 3.4.5). By reacting **11-Me** with the conformationally rigid NBD in 1,2-DiFB it was hoped that the chelating nature of the diene would not only displace the labile ethylene ligand but also enforce isomerism of the pincer backbone to accommodate the favoured coordination mode of the diene co-ligand. Indeed, monitoring the reaction between **11-Me** and one equivalent of NBD using ^1H NMR spectroscopy showed facile and exclusive conversion of **11-Me** to a new C_s symmetric species **26-Me** ($t = 2.75$ h) with the signals attributed to bound NBD present at δ 3.19, 2.78 and 0.88, shifted upfield relative to free NBD (*cf.* δ 6.56, 3.35 and 1.83).



Scheme 3.4.5. Ligand exchange reactions of **11-n** and **26-n**

The same reaction sequence was applied to **11-12** to examine if the unusual macrocyclic ligand topology has an impact on the isomerisation of the resulting complexes. The reaction between **11-12** and NBD progressed as the acyclic congener, showing full conversion to **26-12** within 2 hours. Scaling up these procedures to facilitate the isolation of **26-n**, the products were afforded as pale-yellow solids in good yields after washing with pentane (76%, **26-Me**; 69%, **26-12**).

Crystals of **26-n** ($n = \text{Me}, 12$) were grown from a CH_2Cl_2 /pentane layer and 1,2-DiFB/ hexane layer, respectively and allowed the structural assignment of these complexes to be determined using X-ray diffraction (Figure 3.4.4). In the solid-state **26-n** adopt the predicted facial coordination geometry of the pincer scaffold evidenced by the narrow angle between the carbene donors ($\text{C}_{\text{NHC}}\text{-Rh-C}_{\text{NHC}}$ $103.6(1)^\circ$ **26-Me**; $102.5(2)^\circ$ **26-12**). The complexes also assume distorted

trigonal bipyramidal metal coordination geometries, with an extended rhodium-pyridine bond length relative to their square planar, meridional ligated analogues (Rh–N 2.327(2) Å **26-Me**, 2.334(3) Å **26-12**; *cf.* 2.1159(18) Å **11-Me**). The structures are also notable for the differing rhodium carbene bond lengths between the axial and equatorial NHC positions (*cf.* 2.026(2) Å **26-Me**, 2.042(4) Å **26-12**, axial; 2.118(3) Å **26-Me**, 2.115(4) Å **26-12**, equatorial) and the asymmetric binding of the NBD to the metal centre, with the alkene functionality twisted relative to the C_{NHC}–Rh–C_{NHC} coordination plane (66.61° and 61.34°). Nevertheless, the structural metrics of **26-n** are in-line with related compounds described in the literature (Rh–C_{ent} 2.1435(19)/1.964(2) Å **26-Me**, 1.965(2)/2.135(3) Å **26-12** *cf.* 2.096(2)/2.103(3) Å **X122**; Rh–C_{NHC} 2.118(3)/2.026(2) Å **26-Me**, 2.042(4)/2.115(4) Å **26-12** *cf.* 2.050(3)/2.027(3) Å **X122**).

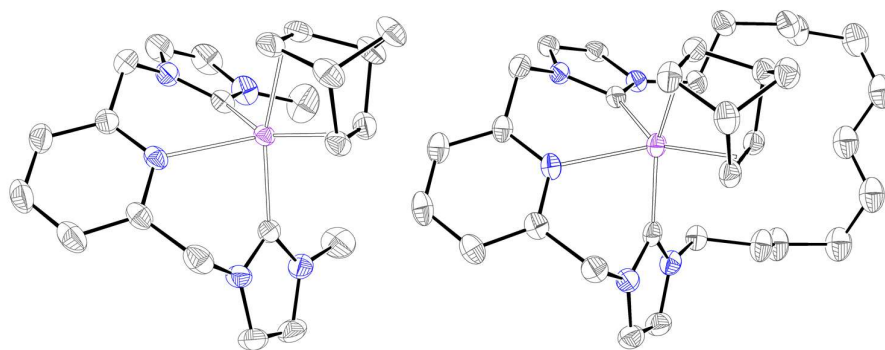


Figure 3.4.4. Solid-state structures of **26-Me** and **26-12**. Thermal ellipsoids at 50% and 35% probability, respectively; hydrogen atoms, counter anions and minor disordered components omitted for clarity.

The formation of **26-n** was substantiated using NMR spectroscopy (CD₂Cl₂) and ESI-MS. The ¹H NMR spectra of these isolated complexes mirror those collected *in situ* and confirm the preservation of C_s symmetry with the methylene bridges giving rise to a pair of sharp doublets at 4.97 and 5.13 ppm (²J_{HH} = 14 Hz) for **26-Me** and 4.99 and 5.19 ppm (²J_{HH} = 14 Hz) for **26-12**. The retention of NBD coordination in solution was evidenced by ESI-MS, which contains the strong parent cation peaks: **26-Me** 462.1159 (462.1160 calcd *m/z*) and **26-12** 600.2563 (600.2568 calcd *m/z*) and using ¹H NMR spectroscopy where NBD coordination is reflected in the upfield shift in the associated signals (δ 3.51/3.13/1.16, **26-Me**; δ 3.49/3.10/1.17, **26-12**) relative to those of free NBD (δ 6.75/3.57/1.97). The appearance of the NBD resonances as three sharp singlets indicates free

rotation on the NMR timescale (500 MHz). The retention of facial coordination of the pincer in solution is corroborated by the increased magnitude of the $^{103}\text{Rh}-\text{C}$ coupling observed for the carbenic resonances in the $^{13}\text{C}\{^1\text{H}\}$ NMR spectra relative to the coupling observed for related meridional complexes ($^1J_{\text{RhC}} = 51 \text{ Hz}$ *cf.* 40 – 43 Hz, **11-n** and **10-n**). This coupling value is more in-line with the coupling observed for **X122** ($^1J_{\text{RhC}} = 52.6 \text{ Hz}$, d_6 -DMSO; Figure 3.4.5), which adopts mutually *cis*-bidentate coordination of the carbene moieties which are directly *trans*-disposed to the coordinated diene.⁷⁸

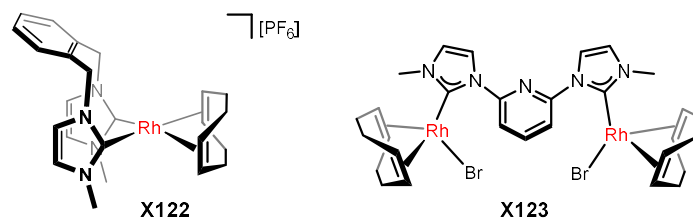


Figure 3.4.5. Related literature examples of rhodium NHC diene complexes

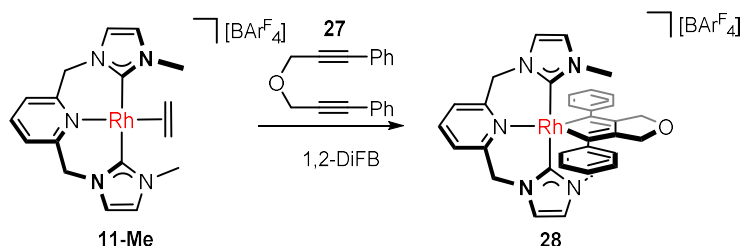
With the facial coordination in **26-n** ($n = \text{Me}, 12$) confirmed, the reversal of this isomerism back to *mer*-pincer ligation was subsequently targeted. Promoted by the displacement of NBD with the strongly coordinating CO ligand, **10-n** were formed quantitatively alongside free NBD when **26-n** were exposed to an atmosphere of CO ($t = 5 \text{ hours}$ for **26-Me** and $t = 0.5 \text{ hours}$ for **26-12**).

3.4.5. Supporting evidence: Intermediacy of metallacyclopentadienes

Another feature of the proposed catalytic mechanism for the annulation reaction that needs evidencing is the ability of the $\{\text{Rh}(\text{CNC})\}^+$ fragment to promote the formation of a metallacyclopentadiene. To test this theory, pre-catalyst **11-Me** was reacted with several internal alkynes and diynes in the hope that these would act as enyne mimics and trap out intermediates formed during the dimerisation of **18** to **24**.

The reaction of **11-Me** with diyne **27** (prepared using a modified literature procedure)⁷⁹ in 1,2-DiFB saw a gradual colour change from red to green over an hour at ambient temperature. *In situ* ^1H NMR analysis showed a steady loss of signals attributed to **11-Me** and the quantitative conversion to a new C_2 symmetric complex **28** (Scheme 3.4.6). Concentrating the solution to dryness and

washing with hexane to remove residual **27** afforded **28** as an air and moisture sensitive green solid in excellent yield (97%).



Scheme 3.4.6. Preparation of metallacyclopentadiene **28**

The structural assignment of **28** is strongly supported by ^1H NMR spectroscopy (CD_2Cl_2 , 500 MHz), which shows four 2H doublets related to the two independent methylene environments, pyCH_2 and OCH_2 (δ 5.17/4.98, $^2J_{\text{HH}} = 15.7$ Hz and δ 4.73/4.54, $^2J_{\text{HH}} = 12.7$ Hz, respectively) as well as a single 6H singlet pertaining to the *N*-methyl wingtips (δ 3.53). The formation of a metallacyclopentadiene complex was confirmed by the characteristic chemical shift and ^{103}Rh coupling observed for the α -carbon of the rhodacycle in the $^{13}\text{C}\{^1\text{H}\}$ NMR spectrum (δ 150.8, $^1J_{\text{RhC}} = 41$ Hz). The coordinative unsaturation of **28** gives rise to C_2 symmetry in solution on the NMR timescale due to the rapid interconversion between two C_1 conformations mediated by the *pseudorotation* of the metallacyclopentadiene ligand about the pincer coordination plane; a phenomena that has recently been investigated for structurally similar biphenyl complexes.⁸⁰

The five-coordinate complex **28** is particularly susceptible to binding additional ligands in the vacant coordination site, including adventitious water, which is evidenced by an abrupt colour change from green to yellow. This subdued colour was also observed when the reaction was conducted in d_3 -MeCN indicating solvent coordination. This was supported by ^1H NMR spectroscopy (d_3 -MeCN, 300 MHz) which shows significant peak broadening and partial decoalescence of the *N*-methyl and methylene signals. The reduction in the rate of fluxionality can be reconciled by solvent coordination in the sixth coordination site, which perturbs the interconversion between the two C_1 symmetric species thus reducing the rate of *pseudorotation*. Whilst initial crystals grown from the reaction mixture were of the water adduct, the solid-state structure of the

coordinatively unsaturated species was obtained when repeating the process under scrupulously anhydrous conditions (Figure 3.4.6).

The solid-state structure of **28** shows two structurally distinct cations in the asymmetric unit ($Z' = 2$) each displaying C_1 symmetry and a distorted square pyramidal geometry at rhodium (C_{NHC}-Rh-C_{NHC} 171.92(9)°/174.51(9)°; N-Rh-C1 171.69(8)°/174.75(8)°; C1-Rh-C2 81.11(9)°/82.20(8)°). The structural metrics of the metallacyclopentadiene moiety in **28** are in line with related literature examples; Rh-C1 2.022(2)/2.029(2) Å, Rh-C2 2.012(2)/2.024(2) Å; **X126** 2.035(6)/2.048(6) Å; **X126** 2.05(1)/2.03(2) Å.⁸¹

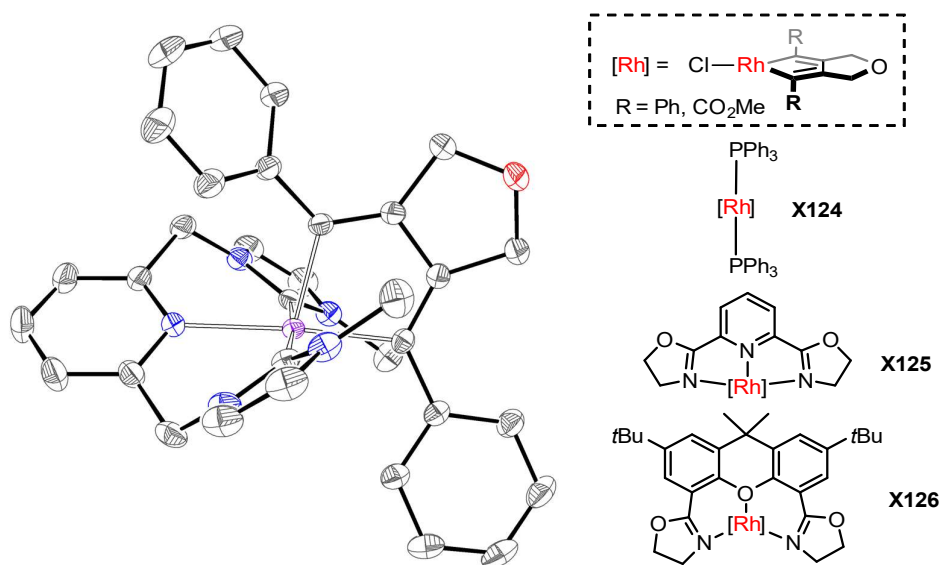
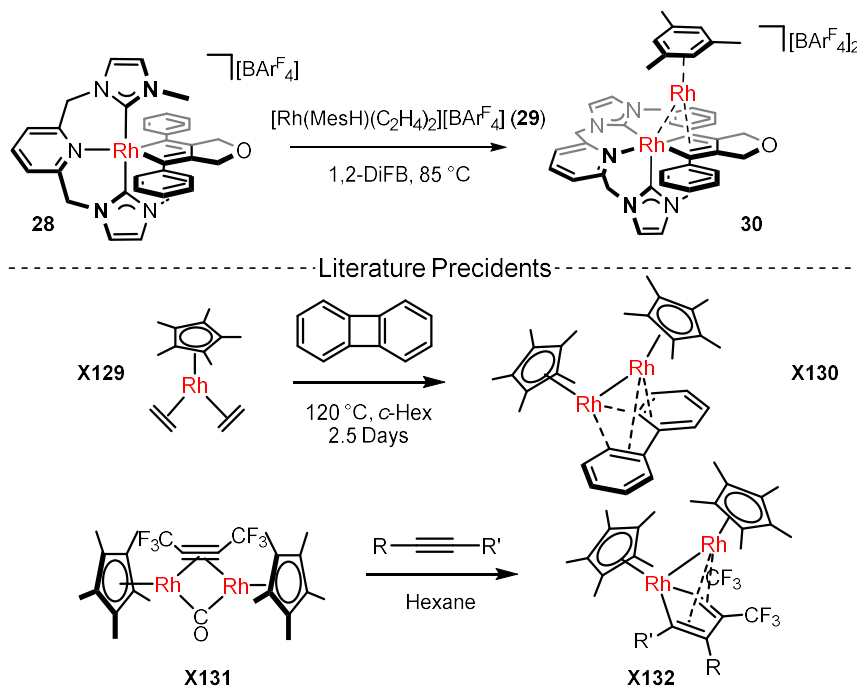


Figure 3.4.6. A solid-state structure of **28** and related literature precedents. Thermal ellipsoids at 50% probability; hydrogen atoms and counter anion omitted for clarity. Structure shown is one of two independent molecules ($Z' = 2$).

3.4.6. Supporting evidence: Bimetallic intermediates

As the rate law for this transformation shows a second-order dependence in catalyst, two steps in the proposed mechanistic cycle were identified that could invoke a bimetallic transition state; the oxidative coupling to form the proposed metallacyclopentadiene or the transformation of the metallacyclopentadiene into a cyclobutadiene species. Unable to replicate the former without considerable synthetic venture, investigations focused on probing whether the latter is plausible for the systems under investigation.

Prolonged heating of **28** in the presence of $[\text{Rh}(\text{MesH})(\text{C}_2\text{H}_4)_2][\text{BAR}^{\text{F}}_4]$ (**29**), kindly donated by Dr Matthew Gyton, saw a gradual colour change from green to fuchsia over 5 days at 85 °C (Scheme 3.4.7). The *in situ* ^1H NMR spectrum showed loss of signals associated with both parent compounds alongside the emergence of a new C_1 symmetric complex and free ethylene.



Scheme 3.4.7. Synthesis of **30** and related bimetallic complexes

Coordinated mesitylene was observed at 5.94 and 1.83 ppm ($\Delta\delta$ 0.07 and 0.22, relative to **29**) and compared with **28** the methylene resonances of both the pincer and the rhodacyclopentadiene were split out into 8 inequivalent environments. The bimetallic nature of **30** was corroborated by $^{13}\text{C}\{^1\text{H}\}$ NMR spectroscopy, in which the metallacyclopentadiene protons appear as doublets of doublets due to coupling to two different ^{103}Rh centres. Curiously, the carbenic carbon resonances are markedly different, whilst one remains reasonably conventional for rhodium(III) carbenes (δ 182.9, $1J_{\text{RhC}} = 39$ Hz),^{51,82,83} the other is dramatically shifted upfield (δ 161.1) and couples to two rhodium centres with vastly different magnitudes ($J_{\text{RhC}} = 71/5$ Hz). Based on these observations the structure of **30** was proposed, whereby the second rhodium centre interacts through the π -system of the metallacyclopentadiene. Comparable rhodium

bimetallics based on rhodium-Cp scaffolds have previously been reported (*viz.* **X130** and **X132**).^{84,85}

The absence of a solid-state structure prevented the unambiguous assignment of **30**, however, evidence corroborating the proposed structure was obtained using a NOESY experiment (Figure 3.4.7). Correlations between the two *N*-methyl appendages are indicative of close approach which can only be reconciled by the pincer adopting a facial coordination geometry. Interactions between the mesityl methyl groups and two methylene protons of the oxolane ring and one from the pincer scaffold supports a structure where the second rhodium centre resides above the cyclopentadiene ring. To aid the visualisation of these results the geometry of **30** was optimised using DFT calculations (Figure 3.4.7).

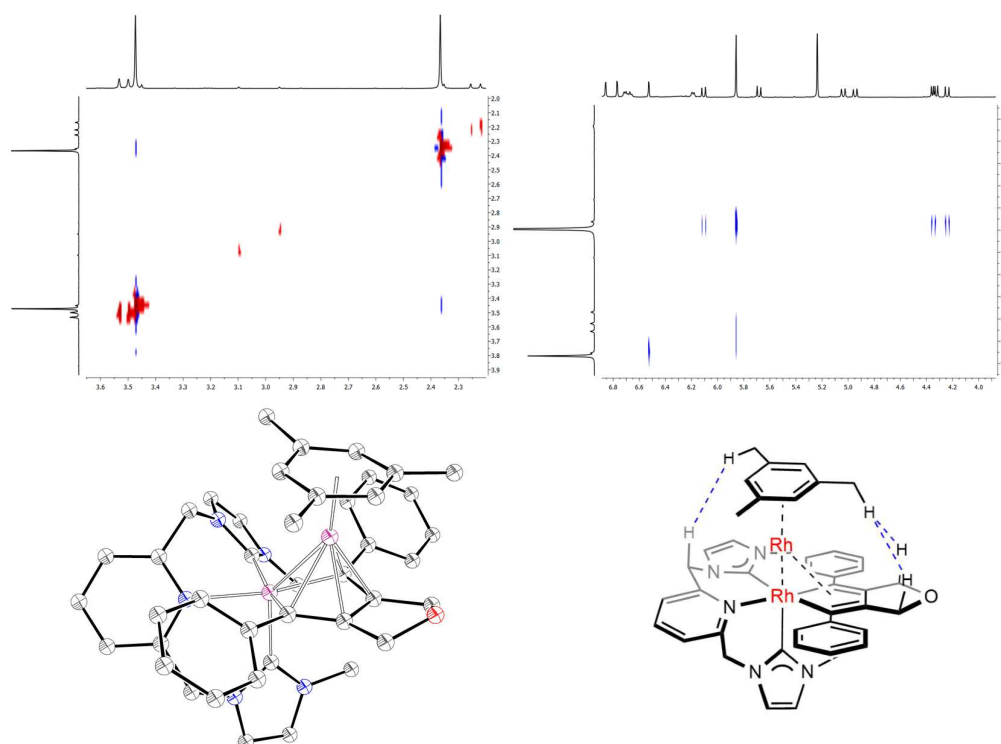
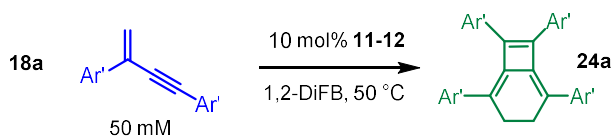


Figure 3.4.7. Key correlations in the NOESY experiment (CD₂Cl₂, 500 MHz) and the optimised geometry calculated of complex **30**[‡]

[‡] Geometry optimisation conducted by Dr Tobias Krämer at the B3PW91-D3 level using a combination of the SDD and 6-31G** basis sets.

3.4.7. Comparison with macrocyclic analogue

Reaction of the macrocyclic congener **11-12** with isolated **18a** under the standard catalytic conditions (Scheme 3.4.8) was conducted to evaluate the impact ligand topology has on the enyne coupling. In this regard complex **11-12** was found to promote the formation of **24a**, albeit with significantly slower rate of turnover compared with **11-Me**, even at elevated temperatures (46% conversion, 45 days, 50 °C). Higher temperatures were not targeted due to the thermal instability of **18a**. Despite the sluggish conversion, the catalytic activity of **11-12** strongly corroborates an annulation reaction which invokes facial pincer coordination as the Ar' group is too sterically cumbersome to fit through the macrocyclic annulus required for meridional coordination (see Chapter 4).



Scheme 3.4.8. Catalytic annulation reaction using complex **11-12**

With the rate determining step of this reaction shown to require the interaction of at least three components each with significant steric bulk it is unsurprising that the rate of this reaction is markedly reduced when using **11-12**. The additional steric bulk of the dodecamethylene tether limits the close approach of other species due to unfavourable clashes

3.4.8. Summary of findings

In conclusion, the mechanism behind this unusual tandem process is yet to be conclusively determined. However, the results of the kinetic studies helped to construct a plausible reaction mechanism (Scheme 3.4.4), which has been supported by probing reactions using model substrates. For instance, the ability of the pincer backbone to move between *mer* and *fac* coordination modes promoted by the varying demands of the co-ligands was confirmed using ligand exchange reactions. In addition, the isolation of the *fac*-pincer supported dirhodium metallacyclopentadiene complex **30** provided strong support of the proposed enyne dimerisation pathway. Investigations into this transformation remain ongoing within the group.

3.5 References

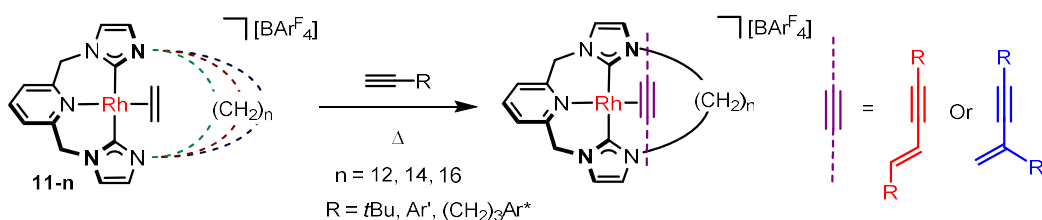
- 1 B. M. Trost and J. T. Masters, *Chem. Soc. Rev.*, 2016, **45**, 2212–2238.
- 2 Y. Zhou, Y. Zhang and J. Wang, *Org. Biomol. Chem.*, 2016, **14**, 6638–6650.
- 3 B. M. Trost, *Science*, 1983, **219**, 245–250.
- 4 S. L. Iverson and J. P. Uetrecht, *Chem. Res. Toxicol.*, 2001, **14**, 175–181.
- 5 N. Zein, A. M. Sinha, W. J. McGahren and G. A. Ellestad, *Science*, 1988, **240**, 1198–1201.
- 6 C.-P. Liu, J. J. Newby, C. W. Müller, H. D. Lee and T. S. Zwier, *J. Phys. Chem. A*, 2008, **112**, 9454–9466.
- 7 G. Chen, L. Wang, D. W. Thompson and Y. Zhao, *Org. Lett.*, 2008, **10**, 657–660.
- 8 A. M. Geer, A. Julián, J. A. López, M. A. Ciriano and C. Tejel, *Chem. Eur. J.*, 2018, **24**, 17545–17556.
- 9 F. Xue, X. Song, T. T. Lin, K. Munkrup, S. F. Albawardi, K.-W. Huang, T. S. A. Hor and J. Zhao, *ACS Omega*, 2018, **3**, 5071–5077.
- 10 W. Weng, C. Guo, R. Çelenligil-Çetin, B. M. Foxman and O. V. Ozerov, *Chem. Commun.*, 2006, 197–199.
- 11 R. H. Platel and L. L. Schafer, *Chem. Commun.*, 2012, **48**, 10609–10611.
- 12 G. V. Oshovsky, B. Hessen, J. N. H. Reek and B. de Bruin, *Organometallics*, 2011, **30**, 6067–6070.
- 13 M. Nishiura, Z. Hou, Y. Wakatsuki, T. Yamaki and T. Miyamoto, *J. Am. Chem. Soc.*, 2003, **125**, 1184–1185.
- 14 S. Ge, V. F. Q. Norambuena and B. Hessen, *Organometallics*, 2007, **26**, 6508–6510.
- 15 K. Komeyama, T. Kawabata, K. Takehira and K. Takaki, *J. Org. Chem.*, 2005, **70**, 7260–7266.
- 16 A. K. Dash and M. S. Eisen, *Org. Lett.*, 2000, **2**, 737–740.
- 17 M. Hasenbeck, T. Müller and U. Gellrich, *Catal. Sci. Technol.*, 2019, **9**, 2438–2444.
- 18 L. Rubio-Pérez, R. Azpíroz, A. Di Giuseppe, V. Polo, R. Castarlenas, J. J. Pérez-Torrente and L. A. Oro, *Chem. Eur. J.*, 2013, **19**, 15304–15314.
- 19 B. M. Trost, C. Chan and G. Ruhter, *J. Am. Chem. Soc.*, 1987, **109**, 3486–3487.
- 20 C. Jahier, O. V. Zatolochnaya, N. V. Zvyagintsev, V. P. Ananikov and V. Gevorgyan, *Org. Lett.*, 2012, **14**, 2846–2849.
- 21 W. T. Boese and A. S. Goldman, *Organometallics*, 1991, **10**, 782–786.
- 22 J. Ohshita, K. Furumori, A. Matsuguchi and M. Ishikawa, *J. Org. Chem.*, 1990, **55**, 3277–3280.
- 23 G. Kleinhans, G. Guisado-Barrios, D. C. Liles, G. Bertrand and D. I. Bezuidenhout, *Chem. Commun.*, 2016, **52**, 3504–3507.
- 24 C. J. Pell and O. V. Ozerov, *ACS Catal.*, 2014, **4**, 3470–3480.
- 25 J. Alós, T. Bolaño, M. A. Esteruelas, M. Oliván, E. Oñate and M. Valencia, *Inorg. Chem.*, 2014, **53**, 1195–1209.
- 26 X. Chen, P. Xue, H. H. Y. Sung, I. D. Williams, M. Peruzzini, C. Bianchini and G. Jia, *Organometallics*, 2005, **24**, 4330–4332.
- 27 O. Rivada-Wheelaghan, S. Chakraborty, L. J. W. Shimon, Y. Ben-David and D. Milstein, *Angew. Chem. Int. Ed.*, 2016, **55**, 6942–6945.
- 28 G. C. Midya, S. Paladhi, K. Dhara and J. Dash, *Chem. Commun.*, 2011, **47**, 6698–6700.
- 29 N. Gorgas, L. G. Alves, B. Stöger, A. M. Martins, L. F. Veiros and K. Kirchner, *J. Am. Chem. Soc.*, 2017, **139**, 8130–8133.
- 30 N. Gorgas, B. Stöger, L. F. Veiros and K. Kirchner, *ACS Catal.*, 2018, **8**, 7973–7982.
- 31 Q. Liang, K. M. Osten and D. Song, *Angew. Chem.*, 2017, **129**, 6414–6417.
- 32 Q. Liang, K. Sheng, A. Salmon, V. Y. Zhou and D. Song, *ACS Catal.*, 2019, **9**, 810–818.
- 33 S. Kiyota, H. Soeta, N. Komine, S. Komiya and M. Hirano, *J. Mol. Catal. A Chem.*, 2017, **426**, 419–428.
- 34 P. Žak, M. Bołt, J. Lorkowski, M. Kubicki and C. Pietraszuk, *ChemCatChem*, 2017, **9**, 3627–3631.

- 35 C. Xu, W. Du, Y. Zeng, B. Dai and H. Guo, *Org. Lett.*, 2014, **16**, 948–951.
- 36 A. M. Geer, A. Julián, J. A. López, M. A. Ciriano and C. Tejel, *Chem. Eur. J.*, 2014, **20**, 2732–2736.
- 37 K. Mochizuki, K. Sakai, T. Kochi and F. Kakiuchi, *Synthesis*, 2013, **45**, 2088–2092.
- 38 M. A. Esteruelas, L. A. Oro and N. Ruiz, *Organometallics*, 1994, **13**, 1507–1509.
- 39 O. Nürnberg and H. Werner, *J. Organomet. Chem.*, 1993, **460**, 163–175.
- 40 B. Windmüller, O. Nürnberg, J. Wolf and H. Werner, *Eur. J. Inorg. Chem.*, 1999, **1999**, 613–619.
- 41 M. R. Gyton, T. M. Hood and A. B. Chaplin, *Dalton Trans.*, 2019, **48**, 2877–2880.
- 42 M. J. Cowley, J. M. Lynam and A. C. Whitwood, *J. Organomet. Chem.*, 2010, **695**, 18–25.
- 43 H. Kim and C. Lee, *J. Am. Chem. Soc.*, 2005, **127**, 10180–10181.
- 44 I. Kovacic and H. Werner, *New J. Chem.*, 2011, **35**, 2018–2021.
- 45 H. E. Gottlieb, V. Kotlyar and A. Nudelman, *J. Org. Chem.*, 1997, **62**, 7512–7515.
- 46 A. Plikhta, A. Pöthig, E. Herdtweck and B. Rieger, *Inorg. Chem.*, 2015, **54**, 9517–9528.
- 47 C. Hahn, J. Sieler and R. Taube, *Polyhedron*, 1998, **17**, 1183–1193.
- 48 R. Zhang, X. Hao, X. Li, Z. Zhou, J. Sun and R. Cao, *Cryst. Growth Des.*, 2015, **15**, 2505–2513.
- 49 C. Yang and S. P. Nolan, *J. Org. Chem.*, 2002, **67**, 591–593.
- 50 R. E. Islas, J. Cárdenas, R. Gaviño, E. García-Ríos, L. Lomas-Romero and J. A. Morales-Serna, *RSC Adv.*, 2017, **7**, 9780–9789.
- 51 R. E. Andrew, University of Warwick, 2016.
- 52 In *Comprehensive Organic Name Reactions and Reagents*, John Wiley & Sons, Inc., Hoboken, NJ, USA, 2010, pp. 490–492.
- 53 C.-C. Lee, Y.-C. Lin, Y.-H. Liu and Y. Wang, *Organometallics*, 2005, **24**, 136–143.
- 54 S. Ventre, E. Derat, M. Amatore, C. Aubert and M. Petit, *Adv. Synth. Catal.*, 2013, **355**, 2584–2590.
- 55 M. J. Dabdoub, V. B. Dabdoub and J. V. Comasseto, *Tetrahedron Lett.*, 1992, **33**, 2261–2264.
- 56 W. T. Boese and A. S. Goldman, *Organometallics*, 1991, **10**, 782–786.
- 57 J. Ohshita, K. Furumori, A. Matsuguchi and M. Ishikawa, *J. Org. Chem.*, 1990, **55**, 3277–3280.
- 58 I. P. Kovalev, K. V. Yevdakov, Y. A. Strelenko, M. G. Vinogradov and G. I. Nikishin, *J. Organomet. Chem.*, 1990, **386**, 139–146.
- 59 D. E. Fogg and E. N. dos Santos, *Coord. Chem. Rev.*, 2004, **248**, 2365–2379.
- 60 J. E. Camp, *Eur. J. Org. Chem.*, 2017, **2017**, 425–433.
- 61 N. Shindoh, Y. Takemoto and K. Takasu, *Chem. Eur. J.*, 2009, **15**, 12168–12179.
- 62 S. Saito, T. Tanaka, T. Koizumi, N. Tsuboya, H. Itagaki, T. Kawasaki, S. Endo and Y. Yamamoto, *J. Am. Chem. Soc.*, 2000, **122**, 1810–1811.
- 63 H. Hopf, H. Berger, G. Zimmermann, U. Nüchter, P. G. Jones and I. Dix, *Angew. Chem. Int. Ed.*, 1997, **36**, 1187–1190.
- 64 C. Sieck, M. G. Tay, M.-H. Thibault, R. M. Edkins, K. Costuas, J.-F. Halet, A. S. Batsanov, M. Haehnel, K. Edkins, A. Lorbach, A. Steffen and T. B. Marder, *Chem. Eur. J.*, 2016, **22**, 10523–10532.
- 65 J. P. Rourke, A. S. Batsanov, J. A. K. Howard and T. B. Marder, *Chem. Commun.*, 2001, 2626–2627.
- 66 C. Sieck, D. Sieh, M. Sapotta, M. Haehnel, K. Edkins, A. Lorbach, A. Steffen and T. B. Marder, *J. Organomet. Chem.*, 2017, **847**, 184–192.
- 67 P. W. Kletnieks, A. J. Liang, R. Craciun, J. O. Ehresmann, D. M. Marcus, V. A. Bhirud, M. M. Klaric, M. J. Hayman, D. R. Guenther, O. P. Bagatchenko, D. A. Dixon, B. C. Gates and J. F. Haw, *Chem. Eur. J.*, 2007, **13**, 7267–7267.
- 68 A. Dachs, S. Osuna, A. Roglans and M. Solà, *Organometallics*, 2010, **29**, 562–569.
- 69 K. Yoshida, I. Morimoto, K. Mitsudo and H. Tanaka, *Tetrahedron*, 2008, **64**, 5800–

- 5807.
- 70 G. Domínguez and J. Pérez-Castells, *Chem. Soc. Rev.*, 2011, **40**, 3430–3444.
- 71 J. P. Collman, J. W. Kang, W. F. Little and M. F. Sullivan, *Inorg. Chem.*, 1968, **7**, 1298–1303.
- 72 A. Steffen, R. M. Ward, M. G. Tay, R. M. Edkins, F. Seeler, M. van Leeuwen, L.-O. Pålsson, A. Beeby, A. S. Batsanov, J. A. K. Howard and T. B. Marder, *Chem. Eur. J.*, 2014, **20**, 3652–3666.
- 73 A. Steffen, K. Costuas, A. Boucekkine, M.-H. Thibault, A. Beeby, A. S. Batsanov, A. Charaf-Eddin, D. Jacquemin, J.-F. Halet and T. B. Marder, *Inorg. Chem.*, 2014, **53**, 7055–7069.
- 74 A. Steffen, M. G. Tay, A. S. Batsanov, J. A. K. Howard, A. Beeby, K. Q. Vuong, X.-Z. Sun, M. W. George and T. B. Marder, *Angew. Chem. Int. Ed.*, 2010, **49**, 2349–2353.
- 75 N. V. Shvydkiy, E. A. Trifonova, A. M. Shved, Y. V. Nelyubina, D. Chusov, D. S. Perekalin and A. R. Kudinov, *Organometallics*, 2016, **35**, 3025–3031.
- 76 D. S. Perekalin, N. V. Shvydkiy, Y. V. Nelyubina and A. R. Kudinov, *Chem. Eur. J.*, 2015, **21**, 16344–16348.
- 77 O. I. Afanasyev, A. A. Tsygankov, D. L. Usanov, D. S. Perekalin, N. V. Shvydkiy, V. I. Maleev, A. R. Kudinov and D. Chusov, *ACS Catal.*, 2016, **6**, 2043–2046.
- 78 M. Poyatos, E. Mas-Marzá, J. A. A. Mata, M. Sanaú and E. Peris, *Eur. J. Inorg. Chem.*, 2003, **2003**, 1215–1221.
- 79 S. Moulin, H. Dentel, A. Pagnoux-Ozherelyeva, S. Gaillard, A. Poater, L. Cavallo, J.-F. Lohier and J.-L. Renaud, *Chem. Eur. J.*, 2013, **19**, 17881–17890.
- 80 T. M. Hood, B. Leforestier, M. R. Gyton and A. B. Chaplin, *Inorg. Chem.*, 2019, **58**, 7593–7601.
- 81 H. Nishiyama, E. Niwa, T. Inoue, Y. Ishima and K. Aoki, *Organometallics*, 2002, **21**, 2572–2574.
- 82 R. E. Andrew and A. B. Chaplin, *Inorg. Chem.*, 2015, **54**, 312–322.
- 83 C. M. Storey, M. R. Gyton, R. E. Andrew and A. B. Chaplin, *Angew. Chem. Int. Ed.*, 2018, **57**, 12003–12006.
- 84 C. Baimbridge, R. Dickson, G. Fallon, I. Grayson, R. Nesbit and J. Weigold, *Aust. J. Chem.*, 1986, **39**, 1187–1203.
- 85 C. Perthuisot, B. L. Edelbach, D. L. Zubris and W. D. Jones, *Organometallics*, 1997, **16**, 2016–2023.

Chapter 4 – Terminal alkyne coupling reactions through a ring

Building on results described in the preceding chapter and preliminary work in the group, this chapter describes the study of terminal alkyne homocoupling reactions promoted by macrocyclic rhodium(I) pincer complexes **11-n** ($n = 12, 14, 16$). With the acyclic analogue **11-Me** displaying orthogonal product selectivity for alkynes bearing *t*Bu and 3,5-di-*tert*-butylphenyl (Ar') substituents, particular attention is given to assessing the impact of the unique ligand topology, conferred by the polymethylene tethers, has on reactions of these alkynes. These are presented in turn, including determination of the related activation parameters across the homologous series **11-n** ($n = 12, 14, 16, \text{Me}$). Aiming to exploit this methodology as an active metal template approach for the synthesis of [2]rotaxanes, the synthesis and reactivity of an extremely sterically bulky trityl-terminated alkyne (Ar*) was also evaluated.



Publications resulting from the work described in this chapter:

- C. M. Storey, M. R. Gyton, R. E. Andrew and A. B. Chaplin; *Angew. Chem. Int. Ed.*, **2018**, 57, 12003-12006
- C. M. Storey, M. R. Gyton, R. E. Andrew and A. B. Chaplin; *manuscript in preparation*.

4.1 Introduction

4.1.1 Overview of interlocked architectures

Mechanically interlocked molecules (MIMs) are compounds not connected *via* chemical bonds but instead held together by physical constraints which prevent covalent bonds intersecting one another.^{1–3} Therefore mechanical bonds between the entangled units of an interlocked structure are such that the individual components generally cannot be separated from each other without the breakage of at least one covalent bond. The archetypal and simplest examples of these architectures are rotaxanes and catenanes (Figure 4.1.1).

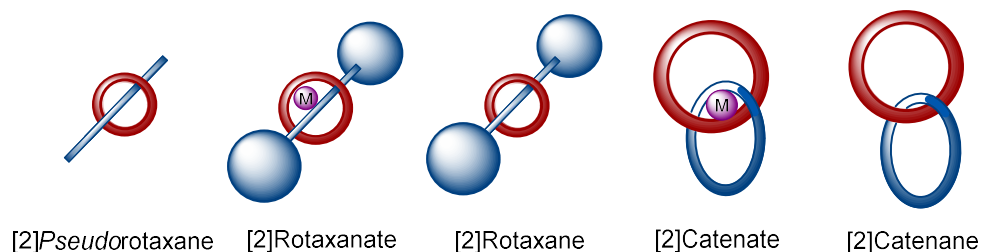


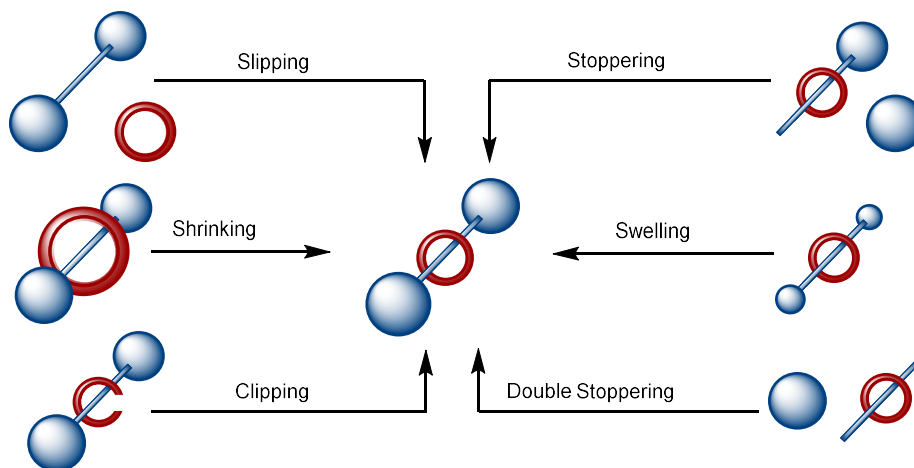
Figure 4.1.1. Interpenetrated compounds

Rotaxanes, from the Latin '*rota*' (wheel) and '*axis*' (axle), comprise a macrocyclic component penetrated by a linear axle terminated or 'stoppered' by a sterically bulky end functionality. On the other hand, catenanes, derived from the Latin '*catena*' meaning chain, feature interlocking ring components. Traditionally, both rotaxanes and catenanes are prepared *via pseudorotaxane* 'template' intermediates, where a rod-like linear molecule is held through a macrocyclic annulus by favorable intermolecular interactions prior to stoppering for the former or clipping for the latter (Scheme 4.1.1).

The first reported [2]catenane was prepared in 1960 by Wasserman, using a non-template approach in which acyloin condensation of a diester in the presence of a large hydrocarbon macrocycle gave a 1% yield of the interlocked product.⁴ The first example of a rotaxane was reported a few years later and, whilst this again relied on a statistical slippage approach, repeated recycling of the axle component improved the yield to 6%.⁵ Nevertheless, both these syntheses rely on statistical methods, which is reflected in extremely poor yields that are impractical for large scale preparations of MIMs.

4.1.2 Methods of synthesising rotaxanes and catenanes

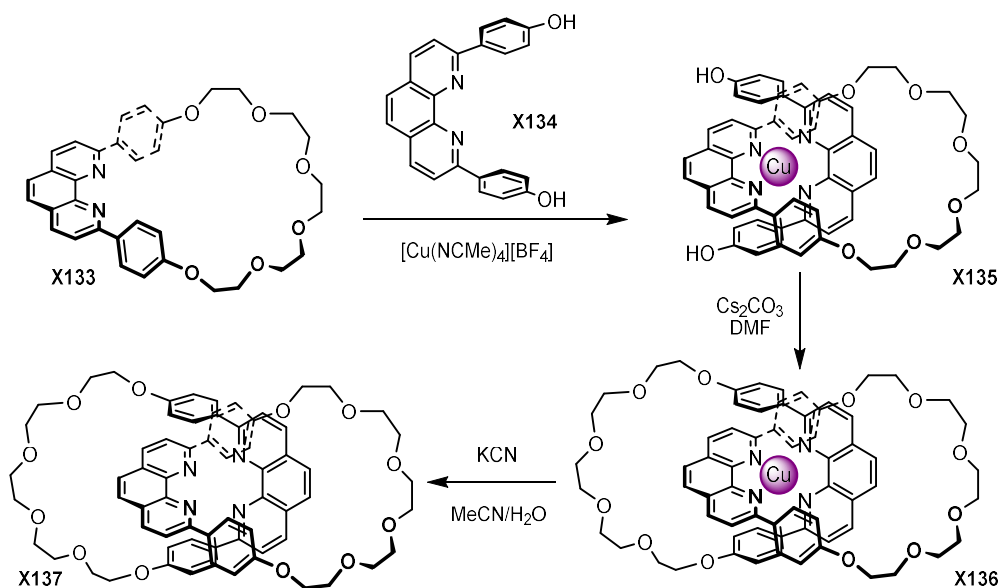
Research in this field has developed significantly from these early studies (Scheme 4.1.1),⁶ with the formation of *pseudorotaxanes* enabled by supramolecular interactions, including: hydrogen and halogen bonding, ion-ion, dipole-dipole, π - π and ion- π interactions in addition to leveraging solvophobic effects.



Scheme 4.1.1. Methods for forming [2]rotaxanes

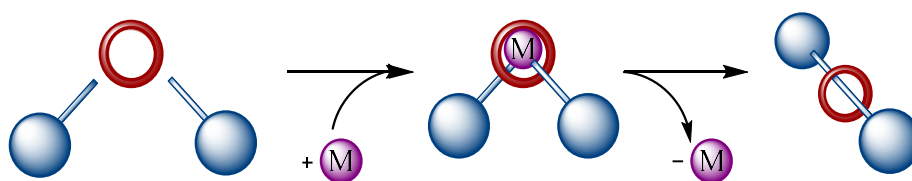
Rotaxanes can be accessed *via* a range of methodologies (Scheme 4.1.1) but the most commonly employed are clipping, where the macrocyclic component is ‘clipped’ around the preformed axle, and stoppering, whereby the end of a *pseudorotaxane* is capped with a bulky stoppering unit.

In 1983 Jean-Pierre Sauvage revolutionised the formation of MIMs by developing a synthetic strategy termed passive metal templation.⁷ By exploiting the rigid and predictable coordination geometry of a metal centre, this seminal work described how binding supramolecular building blocks in a suitably preorganised fashion could promote the formation of interlocking geometries upon employment of ring closing reactions. This report described two approaches; a double clipping reaction pathway which afforded the catenate product **X136** in 27% yield and a reaction involving one preformed macrocycle **X133** in a single threading and clipping event which gave a marked improvement in yield (42%, Scheme 4.1.2).



Scheme 4.1.2. Sauvage's seminal metal template catenane synthesis

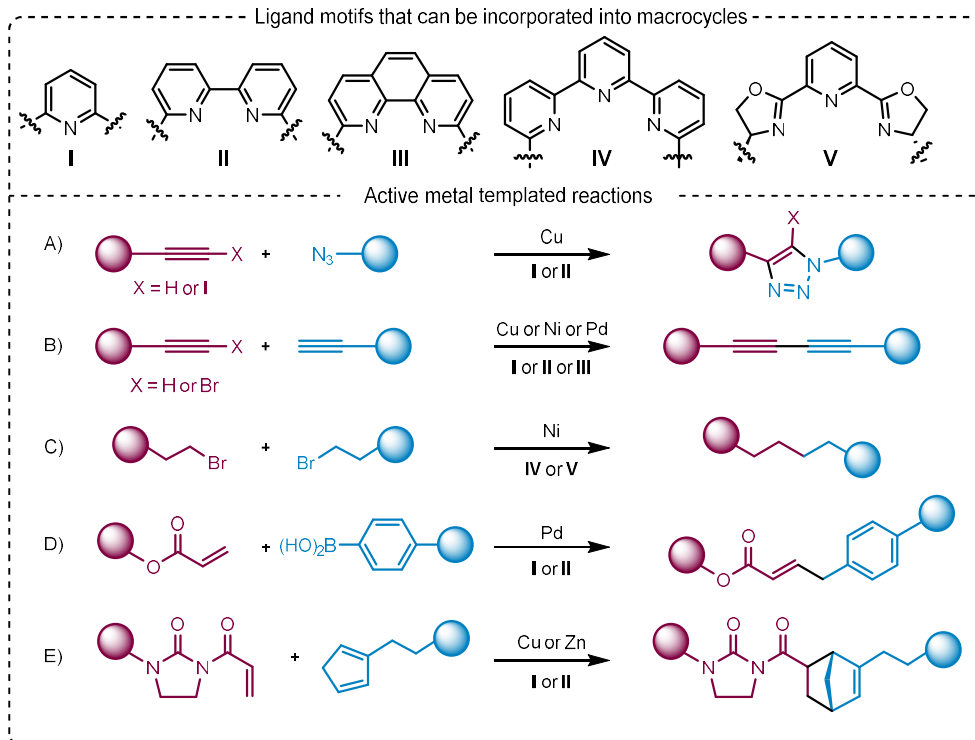
Passive metal template approaches undoubtedly paved the way for the synthesis of increasingly complex mechanically interlocked structures,⁹ but it could be argued that the full potential of the metal-ion was not being exploited. In this light, 2006 saw the development of a new approach for the formation of interlocked molecules by Leigh and co-workers, in which the chemistry of the metal-atom template takes an active role in mediating the covalent bond forming reaction between two half-axes through the macrocyclic annulus, which results in the generation of a new mechanical bond (Scheme 4.1.3).^{10–12}



Scheme 4.1.3. Active metal template strategy

The first example of an active metal templated synthesis employed the copper(I) catalysed alkyne azide 1,3-cycloaddition 'click' reaction (CuAAC) to mediate the formation of a triazole linkage through the aperture of the macrocycle (A, Scheme 4.1.4). Reaction of equimolar quantities of a pyridine-based macrocycle, terminal alkyne and azide with $[\text{Cu}(\text{NCMe})_4][\text{PF}_6]$ gave the desired [2]rotaxane product in 57% yield following KCN demetallation, alongside balance 'free' axle (43%). Optimisation of these reaction conditions saw an improvement in yield (97% wrt

macrocycle) and the reaction could be made catalytic in the presence of a pyridine cocatalyst that helps to mediate decomplexation and thus turnover.



Scheme 4.1.4. Reactions and ligand scaffolds used in the active-metal template synthesis of rotaxanes.

Since Leigh's initial report, the active metal template CuAAC methodology has been successfully expanded to a range of monodentate and bidentate pyridine-based macrocycles (Scheme 4.1.4).¹³ Tridentate analogues, on the other hand, were found to be inactive, presumably due to the lack of vacant coordination sites available to bind half-axle components. Goldup *et al.* have also expanded the synthetic utility of this approach to include much smaller macrocycles.^{14,15} Interestingly they found that the increased steric constraints do not diminish the efficacy of the threading event, but rather promote the interlocking reaction giving up to quantitative yields if the [2]rotaxane products.

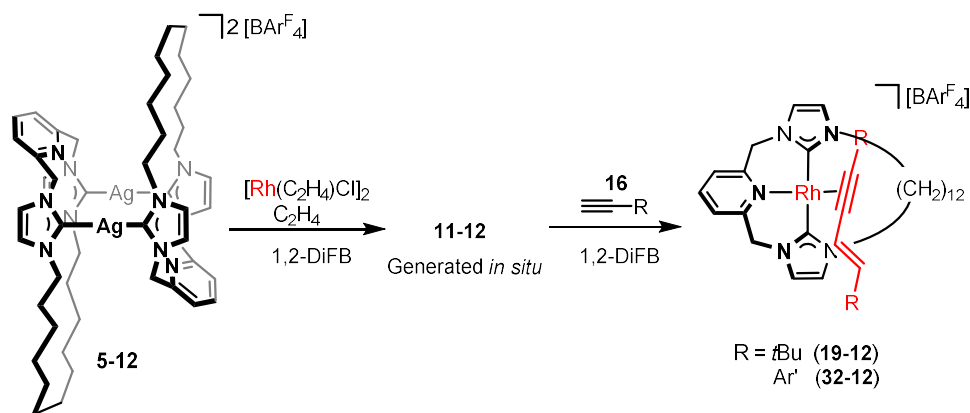
The CuAAC reaction is well-suited to the active metal template approach due to its synthetic simplicity, fast reaction rates, high yields and the chemical robustness of the 1,2,3-triazole linkage formed. As such, it is the most commonly used reaction for the formation of rotaxanes. Nevertheless, the scope of reactions used in active metal templated syntheses continues to expand.^{16,17} For instance,

Saito *et al.* detailed the active metal synthesis of a family of rotaxanes formed from a single Cu(I) phenanthroline-based macrocyclic complex. This well-defined species was used to access rotaxanes *via* both Glaser-Hay alkyne homocoupling reactions (B) as well as Ulmann-type couplings.¹⁸ The former was built upon by the Leigh group to include the heterocoupling of different half-axes in a Cadiot-Chodkiewicz reaction affording rotaxanes in 85% isolated yield.¹⁹

Moving away from the traditional copper catalysed reactions, reports have also emerged using palladium cross-coupling reactions in active metal templation.^{20,21} Recognising the issues associated with the loss of endotopic metal binding on reduction to Pd(0) these reactions focused on catalytic reactions based around Pd(II), including, alkyne homocoupling (B) and oxidative Heck coupling (D).²¹ Other reactions employed in the active metal template synthesis of rotaxanes include nickel catalysed sp^3 - sp^3 couplings (C)²²⁻²⁴ and Diels-Alder reactions (E).²⁵

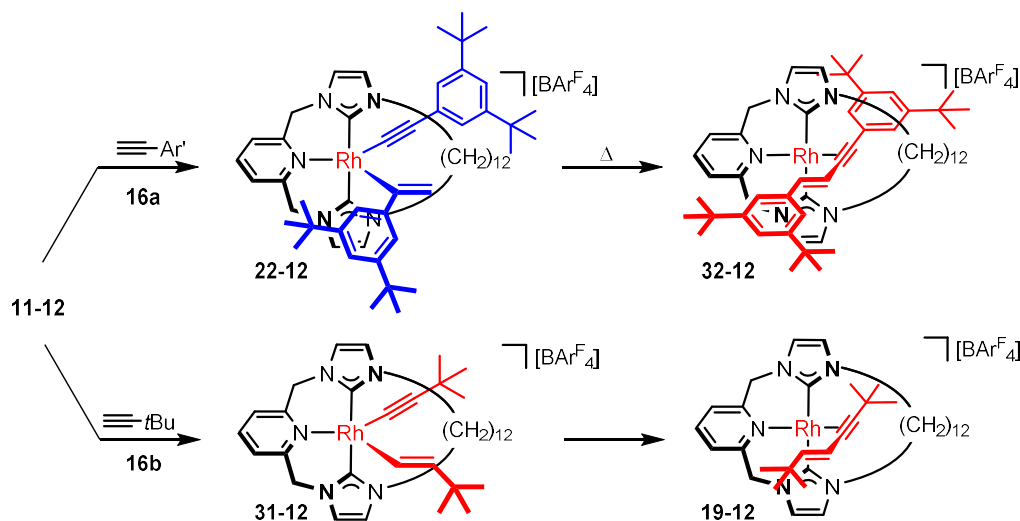
4.1.5 Previous work in the Chaplin group

Coordination of a rhodium(I) center within the cavity of the macrocyclic NHC-based ligands, CNC-n, provides a method for exploiting the rich organometallic chemistry of rhodium pincer complexes for active metal template reactions and research within the group has been working towards this goal. In particular, terminal alkyne homocoupling reactions employing **11-12**, generated *in situ* from the silver complex **5-12**, have proved fruitful, enabling the isolation of [2]rotaxanate complexes **19-12** and **32-12** in 66% and 39% yield, respectively (R. E. Andrew; Scheme 4.1.5).²⁶ These results demonstrate the potential of terminal alkyne dimerisation reactions for the formation of interlocked complexes, however, progression was encumbered by persistent silver-based impurities and the absence of a well-defined rhodium(I) starting material.



Scheme 4.1.5. Preparation of interlocked *E*-enynes via *in situ* generated **11-12**

With the method for accessing analytically pure samples of **11-12** established (Chapter 2), the mechanism underlying these reactions could be examined (M. R. Gyton). Notably, the introduction of the macrocyclic tether imparts additional kinetic control, facilitating the isolation of rhodium(III) intermediates, which is not possible using the acyclic counterpart (**11-Me**, Chapter 3). Reaction of *tert*-butyl alkyne (**16b**) with **11-12** afforded rhodium(III) alkenyl-alkynyl **31-12** exclusively, which upon heating gave **19-12**: both consistent with a hydrometallation mechanism (Scheme 4.1.6).



Scheme 4.1.6. Reaction of isolated **11-12** with terminal alkynes

Reflecting the reactivity of **11-Me**, reaction of **11-12** with 2.1 equivalents of **16a** led to exclusive formation of the rhodium(III) alkenyl alkynyl species **22-12** (Scheme 4.1.6).²⁷ However, the onwards reactivity of this intermediate did not reflect the expected one-step transformation generating an interlocked *gem*-

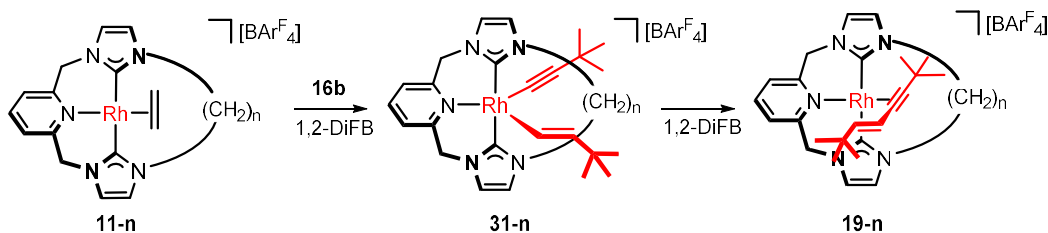
enyne, but instead the *E*-isomer **32-12** was formed. This switch in selectivity necessitates a reversible reaction sequence initiated by an unusual β -hydride elimination and terminated by an alternate C–C bond forming reductive elimination step. This was supported by a deuterium labelling study using $\text{Ar}'\text{-C}\equiv\text{C-D}$ in which deuterium became incorporated into both positions of the interpenetrated enyne by both ESI-MS and ^1H NMR spectroscopy.

Probing the divergent selectivity of **11-Me** and **11-12**, where the C–C bond forming reductive elimination is assigned as the rate-determining step in both cases, an Eyring analysis enabled the associated barrier to be determined ($\Delta G^\ddagger(298\text{ K}) = 106 \pm 3\text{ kJmol}^{-1}$). Comparison to that determined for **11-Me** (Chapter 3), indicates that an additional energetic penalty of at least 13 kJmol^{-1} when conducting the reaction through the annulus of the macrocycle, a destabilisation that facilitates the change in product selectivity.

4.2 Homocoupling of *tert*-butyl alkyne

4.2.1 Synthesis and characterisation of enyne complexes – **19-n**

Expanding on the work conducted within the Chaplin group using **11-12** (*vide supra*), the larger ringed **11-14** and **11-16** were employed in terminal alkyne coupling reactions. In this way the impact of the ring size on the rate and selectivity of these transformations can be systematically investigated. Using well-defined samples of **11-n** ($n = 14, 16$) in the reaction with 2.2 equivalents of *tert*-butyl alkyne **16b** in 1,2-difluorobenzene (1,2-DiFB) showed the complete consumption of **11-n** in < 2 hours alongside the formation of a new C_1 symmetric species, as indicated by *in situ* reaction monitoring using ^1H NMR spectroscopy. The formation of the desired interlocked species **19-n** was corroborated by integral ^1H doublets at 6.03 ppm (**19-14**) and 5.97 ppm (**19-16**) associated with one of the alkene protons ($^3J_{\text{HH}} = 15.2$ Hz) and four doublets at δ 5.77/ 5.32/ 4.94/ 4.84 ($^2J_{\text{HH}} = 14.6$ Hz; **19-14**) and δ 5.77/ 5.39/ 4.94/ 4.86 ($^2J_{\text{HH}} = 14.5$ Hz; **19-16**) attributed to the methylene bridge protons, paralleling obtained data for **19-Me** (Chapter 3) and **19-12**.²⁶



Scheme 4.2.1. Synthesis of **19-14** and **19-16**

In addition to **19-n**, trace quantities of unthreaded axle **17b** were also generated over the course of this reaction, which was identified through comparison of the data with a reference sample prepared using a literature procedure (δ 5.95/ 5.29 $^3J_{\text{HH}} = 16.2$ Hz, 1,2-DiFB).²⁸ The formation of free **17b** is presumably attributed to a minor component of the homocoupling occurring adjacent, as opposed to through, the macrocyclic aperture based on the associated difference in rate. Following removal of the free axle by washing the reaction residues with neohexane or TMS, **19-14** and **19-16** were isolated as bright red solids in excellent yields (81% and 91%, respectively).

Compounds **19-14** and **19-16** were characterised using NMR spectroscopy, ESI-MS and X-ray diffraction (*vide infra*), with notable spectroscopic features and structural metrics summarised in Tables 4.2.1 and 4.2.2. The ESI-MS of **19-n** ($n = 14, 16$) feature strong molecular ion peaks at 700.3822 (calcd 700.3820) and 728.4135 (calcd 728.4133) m/z , respectively. Retention of the enyne component under the conditions of analysis suggests that, compared with **19-Me**, the macrocyclic tethers encourage stronger binding of the axle, presumably due to mechanical entrapment. Like the *in situ* ^1H NMR spectra, the spectra collected in CD_2Cl_2 show the adoption of C_1 symmetry in solution. In the $^{13}\text{C}\{^1\text{H}\}$ NMR spectra the inequivalent methylene bridge carbons (δ 56.0 – 56.3) and carbenic carbons (δ 181.9 – 185.0) appear as pairs of doublets due to coupling with ^{103}Rh . The minor variation in chemical shifts ($\Delta\delta$ 0.2 and $\Delta\delta$ 2.6, respectively) and almost identical coupling constants ($^3J_{\text{RhC}} = 0 - 3$ Hz, $^1J_{\text{RhC}} = 41 - 43$ Hz) for these signals across the series suggests that the ring size has little impact on the bonding of the pincer scaffold in **19-n**.

Table 4.2.1 Selected NMR data for **19-n** (CD_2Cl_2)

	19-12^a	19-14	19-16	19-Me
$\delta_{\text{H}} \text{pyCH}_2$	5.87; 5.45; 5.11; 5.05	5.92; 5.54; 5.11; 5.05	5.92; 5.59; 5.11; 5.05	5.84; 5.60; 5.11; 5.06
$^2J_{\text{HH}}$	14.8; 14.7	14.6; 14.5	14.6; 14.5	14.6; 14.4
$\delta_{\text{C}} \text{pyCH}_2$	56.3; 56.2	56.3; 56.0	56.3; 56.0	56.3; 56.0
$^3J_{\text{RhC}}$	-	3	2	2
$\delta_{\text{C}} \text{NHC}$	184.4; 181.9	184.6; 182.2	185.0; 182.8	184.9; 184.5
$^1J_{\text{RhC}}$	43	41	41	41
$\delta_{\text{H}} \text{CH}=\text{CH}$	7.44; 6.05	6.91; 6.07	6.60; 6.00	6.38; 5.97
$^3J_{\text{HH}}$	15.3	15.3	15.2	15.3
$\delta_{\text{C}} \text{CH}=\text{CH}$	114.7; 158.0	112.2; 156.2	111.3; 154.5	110.8; 153.5
$\delta_{\text{C}} \text{C}\equiv\text{C}$	89.5; 72.8	93.2; 74.3	95.4; 75.6	97.2; 75.1
$^1J_{\text{RhC}}$	14; 10	15; 11	16; 12	15; 12

^a – Collected by Dr Rhiann Andrew

On the other hand, there is a clear trend between the chemical shifts of the enyne resonances and the ring size in both the ^1H and ^{13}C NMR data. The pronounced downfield shift in the ^1H alkene resonances from those of the free enyne (*cf.* 6.09 and 5.41 ppm, **17b**) on binding that was noted for **19-Me** is further exacerbated as the ring size is reduced, with **19-12** showing the biggest disparity ($\Delta\delta$ 1.35 ppm). Paralleling this observation, the chemical shifts of the corresponding

carbon signals also trend downfield with ring contraction (δ 114.0/158.0, **19-12** to δ 110.8/153.5, **19-Me**), whilst the associated alkynyl carbon signals follow the opposite trajectory (δ 89.7/72.8, **19-12** vs 97.2/75.1, **19-Me**). The variation in chemical shift can be reconciled by evaluation of the environment in which the alkene moiety resides. For instance, the solid-state structures of **19-n** (Figure 4.2.1) show that in the smaller rings ($n = 12, 14$) the alkene functionality is held significantly closer to the rhodium centre (Rh-C4, 3.298(3) Å, **19-12**; 3.49(2) Å **19-14**; 3.483(3) Å **19-16**; 3.583(4) Å, **19-Me**), which may explain the downfield shift of alkene resonances for the smaller rings.

The anticipated interpenetrated nature of these complexes was confirmed by X-ray diffraction (Figure 4.2.2), in which coordination of the alkyne moiety to the rhodium centre is verified by the close interaction of the alkynyl carbons with the metal centre (Table 4.2.2). The structural metrics for these complexes are consistent across the series, as well as with corresponding rhodium(I) complexes **10-n** and **11-n** (Chapter 2).

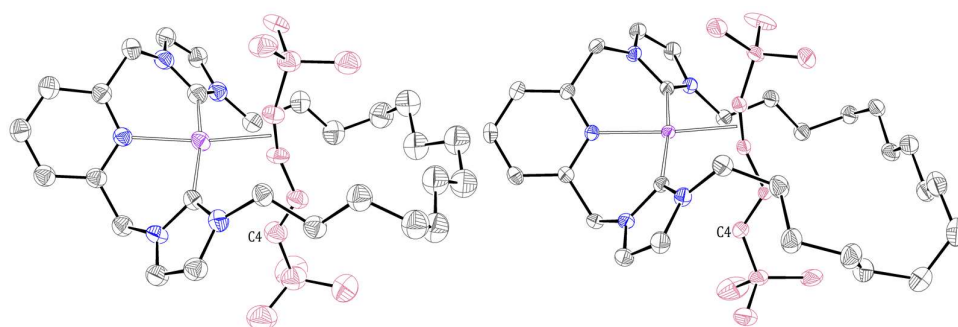


Figure 4.2.1. Solid-state structures of **19-14** and **19-16**. Thermal ellipsoids at 35% probability; anions, residual solvent molecules and hydrogen atoms omitted for clarity.

Emulating **19-Me**, the rhodium alkyne binding in **19-14** and **19-16** causes the bound enyne to be tilted approximately 70° relative to the metal pincer coordination plane, with no substantial perturbations from this geometry caused by disparities in macrocycle size. Skewing of the enyne coordination in this way can be rationalised when considering the steric profile imposed by the wingtip substituents, which form a discrete diagonal channel in which the enyne can bind. In addition, the alkyne functionality itself (C–C≡C–C) sees significant distortions from linearity (158(2)° and 162(2)° **19-14**; 157.4(2)° and 160.4(2)° **19-16**). The magnitude of this distortion increases with ring expansion tending towards those

observed for **19-Me**, a feature which would ordinarily be indicative of a significant component of metal backbonding into the alkyne π^* antibonding orbitals. However, there is little variance of the $\text{C}\equiv\text{C}$ bond lengths and $^1J_{\text{RhC}}$ coupling constants, and instead crystal packing effects are implicated.

Table 4.2.2 Selected structural metrics for **19-n**

	19-12^a	19-14	19-16	19-Me
$\text{C}\equiv\text{C}/\text{\AA}$	1.244(6)	1.22(3)	1.245(3)	1.246(5)
$\text{C}=\text{C}/\text{\AA}$	1.333(5)	1.31(3)	1.323(3)	1.328(6)
$\text{Rh}-\text{C}\equiv\text{C}_{\text{cent}}/\text{\AA}$	2.019(3)	2.040(14)	2.019(2)	2.006(3)
$\text{Rh}-\text{C}_{\text{NHC}}/\text{\AA}$	2.071(3); 2.038(3)	2.07(2); 2.01(2)	2.060(2); 2.016(2)	2.048(3); 2.026(5)
$\text{Rh}-\text{N}/\text{\AA}$	2.103(3)	2.12(2)	2.107(2)	2.113(4)
$\text{Rh}\cdots\text{C4}/\text{\AA}$	3.298(3)	3.49(2)	3.483(3)	3.583(4)
$\angle\text{C}-\text{C}\equiv\text{C}/^\circ$	160.3(4); 164.9(4)	158(2); 162(2)	157.4(2); 160.4(2)	154.0(4); 156.7(4)

a - Crystals grown by Dr Rhiann Andrew

4.2.2 Kinetic investigations

Unlike during the formation **19-12**, described previously, intermediate formation of **31-16** could not be detected at ambient temperature despite *in situ* reaction monitoring during the formation of **19-16**. The equivalent intermediate **31-14** can be observed during the synthesis of **19-14** but is short-lived ($t < 30$ mins) precluding its isolation. Nevertheless, the *in situ* characterisation of both intermediates was achieved using low temperature ^1H NMR spectroscopy (1,2-DiFB, 288 K). Diagnostic signals attributed to the β -alkenyl proton were observed at δ 3.89 ($^3J_{\text{HH}} = 12.4$ Hz, $^4J_{\text{HH}} = 1.5$ Hz) and δ 3.63 ($^3J_{\text{HH}} = 14.6$ Hz) for **31-14** and **31-16** respectively, in-line with the corresponding data collected for **31-12** (*cf.* δ 3.65, $^3J_{\text{HH}} = 12.6$ Hz, $^4J_{\text{HH}} = 3.2$ Hz). The presence of **31-n** in these reactions substantiates the hypothesis that the dimerisation reaction proceeds *via* an oxidative addition hydrometallation mechanism with rate limiting C-C bond reductive elimination irrespective of ring size.

Looking in more detail at the relative rates of reductive elimination using variable temperature ^1H NMR spectroscopy (1,2-DiFB), the impact of the steric constraints imposed by the macrocyclic tether was interrogated. For the smallest ring, these kinetic studies could be conducted from the isolated intermediate

31-12, whereas, for the larger rings ($n = 14, 16$) the enhanced rate of onward reactivity frustrated the isolation of **31-n** and as a result, these investigations were conducted from variants generated *in situ* from reaction of the respective ethylene compounds, **11-n** ($n = 14, 16$) and 2.05 equivalents of **16b**. Monitoring the reaction progression using the distinct *t*Bu resonances as a spectroscopic handle to follow the consumption of **31-n** and by inference generation of **19-n** the relative reaction rates could be elucidated.

The formation of **19-n** ($n = 12, 14, 16$) follows first-order reaction kinetics unanimously across all ring sizes, consistent with a single rate-limiting reductive elimination step (Figure 4.2.2). Preliminary evaluation of the relative reaction kinetics across the series shows an increase in rate with ring expansion. For instance, **31-12** requires heating (313 K) to promote the reductive elimination step whereas, the reaction using **11-14** and **11-16** proceed at ambient temperature. Comparing the kinetics for the formation of **19-14** and **19-16** at 288 K indicates more facile reductive elimination for the larger analogue demonstrated by the marked reduction in reaction time ($t_{1/2}$ *ca.* 1.3 h; $t_{1/2} < 10$ mins, respectively).

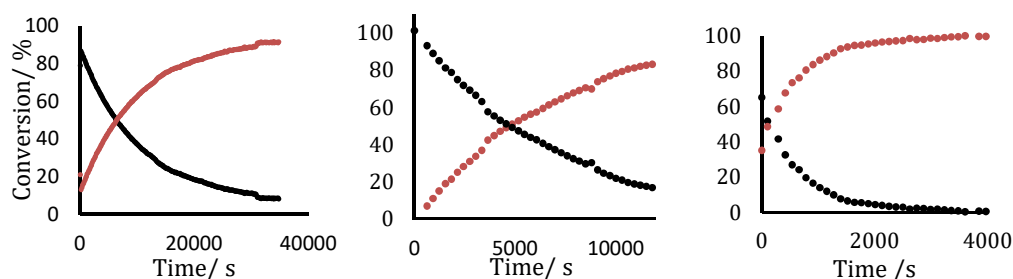


Figure 4.2.2. Reaction progression plots of for the formation of **19-12** (313 K; left), **19-14** (288 K; centre) and **19-16** (288 K; right)

The first-order reaction kinetics were maintained across a wide-temperature range (313 – 333 K, $n = 12$; 278 – 293 K, $n = 16$) and looking at the temperature dependence of these reactions in more detail allows the associated activation barriers for **31-12** and **31-16** to be determined (Table 4.2.1).

Table 4.2.1. Thermodynamic parameters for the formation of **19-n**

	Solvent	$\Delta G^\ddagger(298\text{ K}) / \text{kJmol}^{-1}$	$\Delta H^\ddagger / \text{kJmol}^{-1}$	$\Delta S^\ddagger / \text{JK}^{-1}\text{mol}^{-1}$
19-12	C ₂ D ₄ Cl ₂	109 ± 2	125 ± 1	54 ± 3
19-12	1,2-DiFB	101 ± 3	88 ± 1	-44 ± 4
19-16	1,2-DiFB	86 ± 6	75 ± 3	-38 ± 11

Reflecting on these results, a marked reduction in activation energy is observed as the ring size is increased from $n = 12$ to $n = 16$ ($\Delta\Delta G^\ddagger = 15 \text{ kJmol}^{-1}$) suggesting the spatial constraints imposed by the hydrocarbon tether hinder C–C bond formation. The larger activation energy for **19-12** is associated with a substantial increase in the enthalpic contribution, and the negative entropy values step can be rationalised by the ordered transition state invoked during this transformation; where the alkenyl and alkynyl ligands are forced to adopt a rigid three-centred configuration and the conformational flexibility of the macrocyclic tether is restricted. Although the kinetic analysis is yet to be conducted for **19-14**, extrapolation of these trends and preliminary data at 288 K would suggest that the energetic barrier lies between those of **19-12** and **19-16**.

Comparison of the thermodynamic parameters calculated for the formation of **19-12** in both 1,2-DiFB and the less weakly coordinating solvent, C₂D₄Cl₂,[†] shows a slight energetic preference for the reaction conducted in the former ($\Delta\Delta G^\ddagger = 8 \text{ kJmol}^{-1}$). In this case, the reduced energetic barrier is a consequence of the substantial decrease in enthalpic penalty ($\Delta H^\ddagger = 88 \text{ kJmol}^{-1}$ vs 125 kJmol^{-1}). However, unlike the reactions in 1,2-DiFB, the reductive elimination in C₂D₄Cl₂ is characterised by a positive entropic term ($\Delta S^\ddagger = +54 \text{ JK}^{-1}\text{mol}^{-1}$) due to dissociation of CH₂Cl₂/C₂D₄Cl₂, coordination which has been evidenced by a crystal structure of **31-12** obtained in the group (M. R. Gyton).

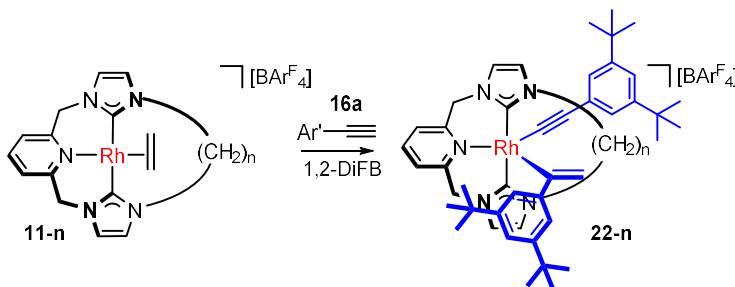
The reactivity and subtle trends in spectral data both show a clear trend across the series, with the behavior tending towards that of the acyclic congener with increasing tether length. As such, it can be concluded that the reduction in steric congestion surrounding the metal centre encourages reactivity and as such showcases how the reactivity of these systems can be finely tuned through modifications in topology introduced by changes in ring size.

[†] Determined by Dr Matthew Gyton

4.3 Homocoupling of 3,5-di(*tert*-butyl)phenyl alkyne

4.3.1 Synthesis and characterisation of Rh(III) intermediates – **22-n**

Given the orthogonal selectivity observed for the homodimerisation of **16a** using **11-12** and the catalytic reaction using **11-Me**, investigations turned to examining the impact the larger ring analogues have on the reactivity and, more pertinently, the selectivity of this process. Monitoring the reaction of **11-n** ($n = 14, 16$) with 2.0 equivalents of **16a** in 1,2-DiFB by ^1H NMR spectroscopy showed quantitative formation of new species within an hour (Scheme 4.3.1). Repeating this procedure on a scale more amenable to isolation, **22-14** and **22-16** were isolated as air and moisture sensitive yellow solids in excellent yields (73% and 90%, respectively).



Scheme 4.3.1. Synthesis of Rh(III) complexes **22-n**

The composition of these novel complexes was determined using ESI-MS, which exhibit strong parent ion signals consistent with the formulation $[\text{Rh}(\text{CNC-}n)(\mathbf{16a})_2]^+$ (964.5699, calcd 964.5698 m/z , **22-14**; 992.6016, calcd 992.6011 m/z , **22-16**), and supported by satisfactory microanalyses. Presumably as a consequence of the confined metal coordination sphere, these complexes are appreciably dynamic in solution at ambient temperature on the NMR timescale, showing significant peak broadening in both the ^1H and $^{13}\text{C}\{^1\text{H}\}$ NMR spectra (500 MHz, CD_2Cl_2). Limited structural assignment was possible from these spectra alone, however, combined with low temperature ^1H NMR spectra (185 – 298 K; Figure 4.3.1) and data collected in the more weakly coordinating 1,2-DiFB solvent, which are significantly sharper, **22-n** were assigned as rhodium(III) *gem* alkenyl-alkynyl complexes.

Key signals in the ^1H NMR spectra (1,2-DiFB, 400 MHz) which corroborate this structural assignment include geminal alkene protons (δ 5.74/5.71, **22-14**; δ 5.79/5.77, **22-16**) and a pair of low frequency ^1H *t*Bu signals indicating two chemically distinct stopper environments (1.19/1.16 ppm **22-14**; 1.18/0.98 **22-16**). The signals attributed to the methylene bridge protons of the ligand scaffold, of which three can be directly observed with the other presumably obscured by the solvent peak, appear as distinct doublets (δ 4.93/4.33/2.97, $^2J_{\text{HH}}$ = 14.1, 15.3, 14.8 Hz, **22-14**; δ 4.94/4.34/3.04, $^2J_{\text{HH}}$ = 15.4, 15.2, 15.5 Hz, **22-16**) demonstrating C_1 symmetry. Considerable broadening of the pyridyl and methylene bridge proton resonances in CD_2Cl_2 relative to 1,2-DiFB suggests that coordination induced dynamics are operational, potentially in the form of atropisomerism of the pincer ligand backbone. Conversely, the increased dynamic behavior in CH_2Cl_2 could be associated with positional isomerism of the alkenyl and alkynyl ligands between apical and basal coordination sites, fluxionality that could be promoted by reversible solvent coordination disrupting the low hapticity arene π interaction (*vide infra*). Variable temperature ^1H NMR studies of **22-n** (CD_2Cl_2 , 500 MHz) see this dynamic process frozen out on cooling to 250 K, with the broad signals resolved into a sharp C_1 symmetric species. This is particularly evidenced by the resonances attributed to the diastereotopic pyCH_2 protons resolved as a set of four doublets each with geminal coupling ($^2J_{\text{HH}}$ = *ca.* 15 Hz) and the pyridyl resonances resolved into two sharp doublets (δ 7.57/7.30, $^3J_{\text{HH}}$ = 8.5 Hz, **22-14**; δ 7.58/7.31, $^3J_{\text{HH}}$ = 7.7 Hz, **22-16**).

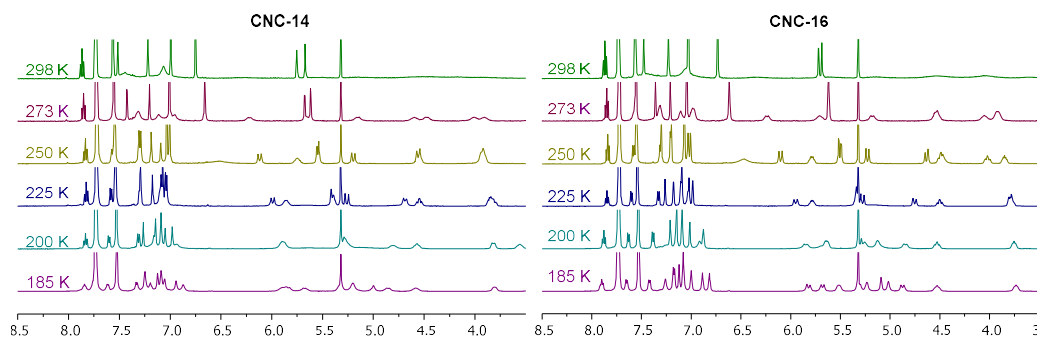


Figure 4.3.1. VT ^1H NMR spectra of **22-14** and **22-16** (500 MHz, CD_2Cl_2 , 185 – 298 K)

Cooling further to 185 K resulted in decoalescence of the lower frequency ^1H *t*Bu resonances (δ 1.02, **22-14**; δ 1.03, **22-16**) into two inequivalent ^1H signals (δ 1.13/0.59, **22-14**; δ 1.13/0.96, **22-16**) suggesting that rotation of one the

aromatic rings in these systems is significantly perturbed. This can be rationalised when looking at the solid-state structure of **22-12** (Figure 4.3.2).[‡] Whereas, the alkynyl ligand is free to rotate around the Rh-C≡C-Ar' axis due to the steric bulk being sufficiently retracted from the pincer coordination plane, the aryl ring of the alkenyl ligand experiences restricted rotation due to the π interaction between the Ar' moiety and the rhodium centre which also results in steric clashes between the *t*Bu appendages and the puckered methylene bridges of the pincer backbone (cf. Figure 4.3.2).

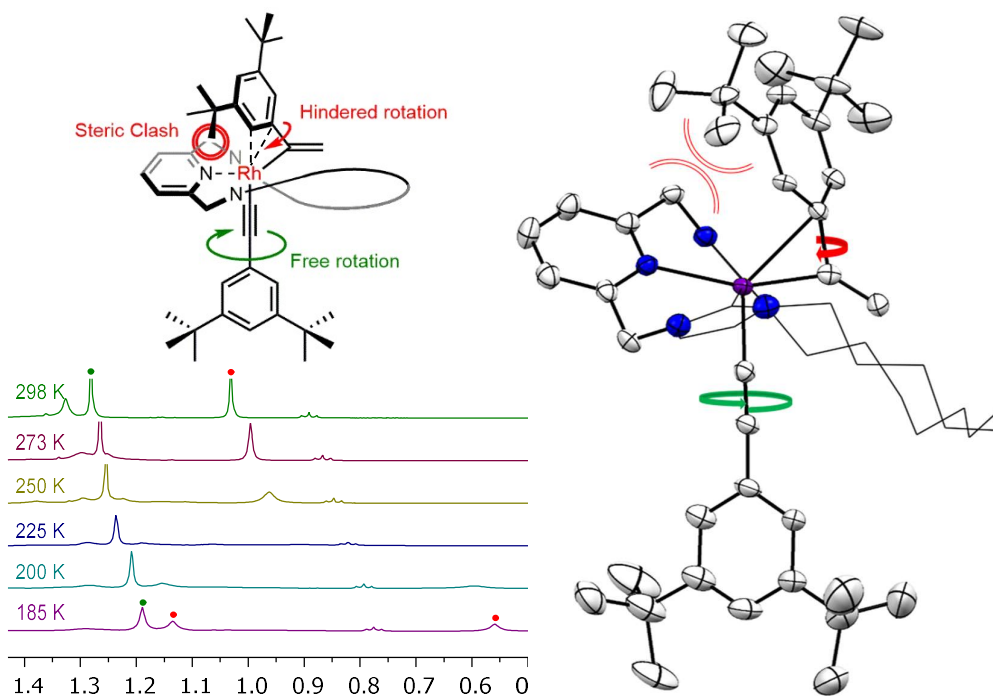


Figure 4.3.2. VT ^1H NMR data of complex **22-14** (500 MHz, CD_2Cl_2 , 185 – 298 K); skeletal representations of **22-n** demonstrating steric clashes.

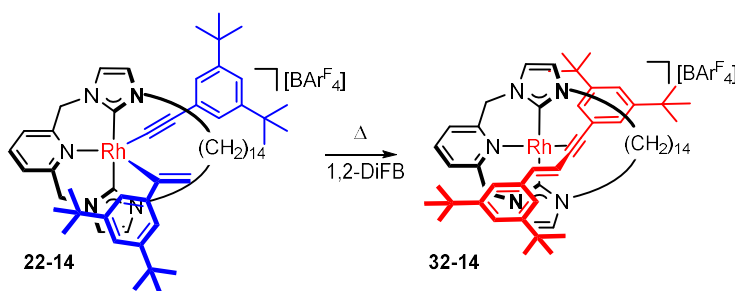
The geminal alkenyl protons are some of the only environments observed as sharp signals at 298 K (δ 5.75, $^2J_{\text{HH}} = 2.8$ Hz, δ 5.67, **22-14**; δ 5.72, $^2J_{\text{HH}} = 2.8$ Hz, δ 5.66, $^2J_{\text{HH}} = 1.1$ Hz, **22-16**), which are comparable with those previously reported for **22-12** (δ 5.76, $^2J_{\text{HH}} = 2$ Hz, δ 5.57), corroborating the assignment of **22-n**.²⁷ Correlation experiments confirm that these protons reside on the same carbon atom (δ 114.5, **22-14**; δ 115.3, **22-16**) and the HMBC experiment locates the adjacent α -alkenyl carbon resonance which shows considerable ^{103}Rh coupling reflecting direct coordination and thus the structure of **22-n** ($^1J_{\text{RhC}} = 25.1$ Hz).

[‡] Crystals grown by Dr Matthew Gyton

Cross-peaks associated with the four-bond correlation between the geminal alkenyl signals and the α -alkynyl carbon resonances in the HMBC experiment facilitates the location of these signals (δ 85.7, **22-14**; δ 86.6, **22-16**). Again, the magnitude of the J_{RhC} couplings indicate alkynyl ligation as opposed to coordination in a π -capacity, which would be the case for the reductive elimination product.

4.3.2 Synthesis and characterisation of interlocked enyne complexes

Mirroring the catalytic dimerisation of **16a** by **11-Me** (Chapter 3), the formation of **22-n** ($n = 12, 14, 16$) supports an operative hydrometallation pathway, with the additional kinetic stabilisation introduced by the hydrocarbon tethers precluding onward reductive elimination at ambient temperature. The additional energetic encumbrment for the macrocyclic analogues is likely owed to steric constraints in the ligand topology. Inspection of the structure of **22-n**, with the two half axle components projected to opposing sides of the ring, the subsequent C–C bond formation would be anticipated to occur through the macrocyclic aperture in a transformation reminiscent of active-metal template approaches for the construction of MIMs. Indeed, heating a solution of **22-14** in 1,2-DiFB promotes the onwards reaction and results in the exclusive formation of **32-14** (Scheme 4.3.2). Interestingly, emulating the reactivity of the dodecamethylene congener previously investigated in the group (**32-12**), this complex is not the envisaged interlocked geminal product formed *via* single C–C bond forming reductive elimination step, but instead the interlocked *E*-isomer.

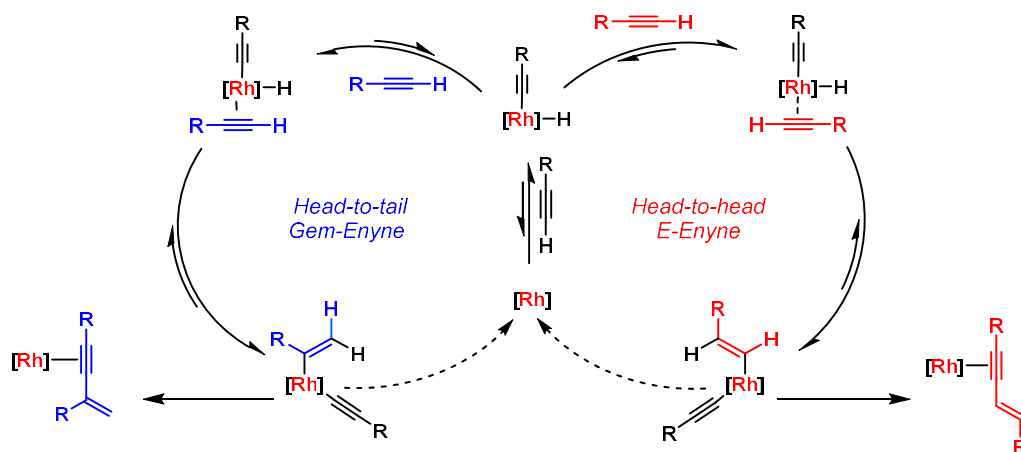


Scheme 4.3.2 C–C bond forming reductive elimination to generate **32-14**

Following purification by washing with cold hexane ($-78\text{ }^\circ\text{C}$), **32-14** was isolated in a good yield (84%) and fully characterised in solution using NMR spectroscopy (CD_2Cl_2) and ESI-MS (964.5702, calcd 964.5698 m/z). The occurrence of

reductive elimination was corroborated by $^{13}\text{C}\{^1\text{H}\}$ NMR spectroscopy with two carbenic carbon signals (δ 182.4/182.0, $^1J_{\text{RhC}} = 42$ Hz) consistent with those of analogous Rh(I) enyne species, **32-12** (δ 182.0/181.4, $^1J_{\text{RhC}} = 42$ Hz) and **19-n** (*vide supra*).^{26,27} The regiochemistry of the resulting enyne was established most readily from the ^1H NMR spectrum, where the alkene resonances display distinctive *trans*-coupling (δ 7.29/7.00, $^3J_{\text{HH}} = 15.2$ Hz) in-line with the corresponding data reported for **32-12** (δ 8.05/7.01, $^3J_{\text{HH}} = 15.2$ Hz).

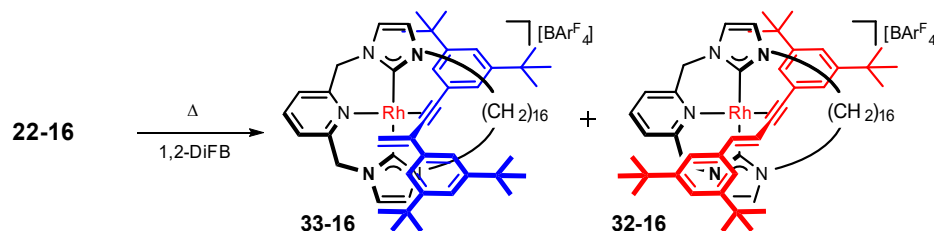
The switch in selectivity between **22-14** and **32-14** highlights the requirement for the migratory insertion step of mechanism to be reversible. Evaluation of the hydrometallation pathway behind the terminal alkyne dimerisation promoted by **11-n** (Scheme 4.3.3), the multistep transformation of **22-14** to generate **32-14** requires: an initial β -hydride elimination to regenerate the alkynyl hydride species followed by a series of rearrangement and migratory insertion steps to afford the opposing Rh(III) alkenyl alkynyl complex, and completed with reductive elimination to afford the observed isomer **32-14**. For this pathway to be exclusively operational the energetic barrier associated with the reverse reaction must be surmountable and the competing barrier to direct reductive elimination to afford the interlocked *gem*-isomer considerably more substantial, presumably due to the spatial restrictions imposed by the macrocyclic ring.



Scheme 4.3.3. Hydrometallation mechanism for terminal alkyne coupling

By extension it can be envisioned that as the ring size is increased the spatial and energetic constrictions associated with direct reductive elimination will be reduced and therefore the selectivity should tend towards that of the acyclic

congener **11-Me**. Indeed, heating complex **22-16** at 85 °C for 18 hours resulted in the formation of two distinct C_1 symmetric species by *in situ* ^1H NMR spectroscopy (1,2-DiFB), which were elucidated by the presence of 8 distinct doublets between 4.0 – 6.5 ppm, each with characteristic geminal coupling ($^2J_{\text{HH}} = \text{ca. } 14.5 \text{ Hz}$). Following concentration and washing with TMS the mixture of complexes could be obtained in a combined yield of 83% (43% **32-16** and 57% **33-16**; Scheme 4.3.4).



Scheme 4.3.4. Reductive elimination of **22-16** to give a mixture of **32-16** and **33-16**

Gratifyingly, separation of the two regioisomers could be achieved through successive recrystallisations and subsequently isolated in moderate yields (40% **33-16**; 25% **32-16**). Initially, **33-16** was crystallised from a diethyl ether solution layered with excess hexane and following this, crystals of **32-16** were grown from a saturated hexane solution cooled to 4 °C. The crystals obtained of both **32-16** and **33-16** in this way were of sufficient quality to allow their solid-state structures to be determined using X-ray diffraction (Figure 4.3.3).

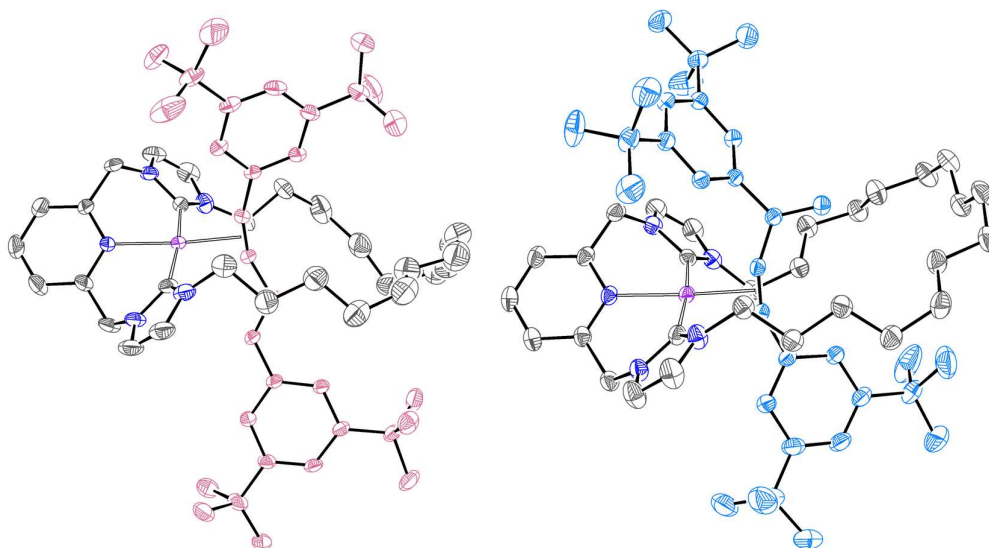


Figure 4.3.3. Solid-state structures of **32-16** and **33-16**. Thermal ellipsoids at 35% probability and anions, hydrogen atoms, minor distorted components and residual solvent molecules omitted for clarity.

The solid-state structures of **32-16** and **33-16** unambiguously confirmed their assignment as the interpenetrated *E*- and *gem*- enynes respectively. Both complexes display C_1 symmetry in the solid-state and their pincer metrics are comparable with those of **32-12** (Table 4.3.1) as well as with the other rhodium(I) complexes bearing these NHC-based pincer macrocycles described previously, and throughout this thesis.^{26,27,29}

Table 4.3.1. Solid-state metrics for interlocked complexes **32-12**, **32-16** and **33-16**

	32-12	32-16	33-16
Rh-N/ Å	2.105(3)	2.117(2)	2.121(2)
Rh-C_{NHC}/ Å	2.052(3); 2.042(3)	2.053(5); 2.036(3)	2.061(3); 2.060(3)
∠ C_{NHC}-Rh-C_{NHC} /°	173.9(1)	173.2(1)	173.8(1)
Rh-C≡C_{cent}/ Å	1.981(2)	1.996(2)	1.990(2)
C≡C/ Å	1.255(4)	1.265(6)	1.255(3)
C=C/ Å	1.338(4)	1.339(6)	1.334(4)

Despite the divergent regiochemistry of the threaded enyne, the solid-state structures show minimal variation in structural metrics associated with the different axes, including sharing similar bond lengths for the component C≡C and C=C bonds of the enyne motifs. In addition, the bond length between the rhodium centre and the centroid of the alkyne moiety is the same, within error, for both isomers (*viz.* 1.99 Å) as well as with the smaller ringed congener **32-12** (*cf.* 1.98 Å), indicating comparable metal binding strengths for the two isomers.

Further examination of the solid-state structure of **33-16** highlights the close approach of the terminal methylene group and the hydrocarbon tether (*cf.* Figure 4.3.4), which demonstrates the tight fit of the axle within the macrocyclic aperture. This emphasises the increased lateral steric demand of the geminal alkene moiety relative to the *E*-isomer which may explain the absence of the formation of this isomer with the smaller ringed congeners, where the annulus size is significantly reduced making the close approach more pronounced and clashes more likely.

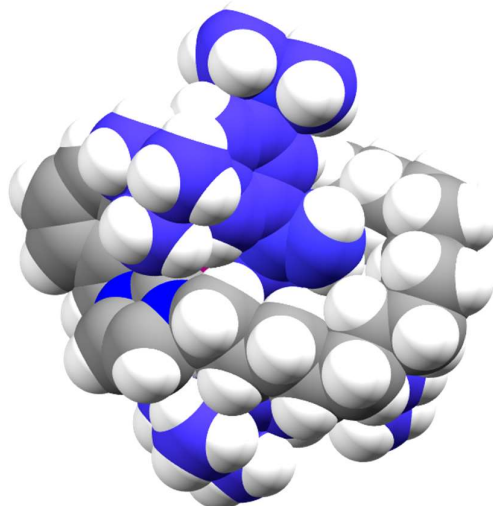


Figure 4.3.4. Spacefill representation of **33-16**

In solution the retention of the interpenetrated structure of **32-16** was confirmed through a combination of NMR spectroscopy (CD_2Cl_2) and ESI-MS (992.6007, calcd 992.6011, m/z), with the associated data in close agreement with those previously described for **32-12** and **32-14** (Table 4.3.2).²⁷ For instance, the characteristic alkene resonances appear at 7.81 and 6.95 ppm ($^3J_{\text{HH}} = ca. 15 \text{ Hz}$) in the ^1H NMR spectrum and the corresponding carbon signals are located at 142.3 and 114.3 ppm (*cf.* δ 143.0/114.5, **32-14**; δ 142.8/117.2, **32-12**). The NMR spectra of **33-16** display comparable signals associated with the pincer ligand environments. In particular, the methylene bridge protons give rise to four doublets at 5.83, 5.16, 4.26 and 3.94 ppm each with distinctive geminal coupling $^2J_{\text{HH}} = 14.7 \text{ Hz}$ (*cf.* δ 5.97, 5.97, 5.22, 5.18, $^2J_{\text{HH}} = 14.6/15.6 \text{ Hz}$, **32-16**). Two of these resonances are shifted upfield relative to **32-n** likely due to additional shielding experienced by proximity to the ring current of the Ar' group, *cf.* Figure 4.3.3. Also implied by the solid-state structures the magnitude of the ^{103}Rh coupling to the alkyne carbons (*cf.* $^1J_{\text{RhC}} = 14 \text{ Hz}$) is comparable, suggesting similar degrees of metal interaction.

Table 4.3.2. Selected NMR data for **32-n** and **33-16** (CD₂Cl₂)

	32-12	32-14	32-16	33-16
$\delta_{\text{H}} \text{CH=CH}$	8.05; 7.01	7.29; 7.00	7.81; 6.95	-
$^3J_{\text{HH}}$	15.3; 15.3	15.2; 15.1	15.8; 15.3	-
$\delta_{\text{H}} \text{C=CH}_2$	-	-	-	6.13; 5.73
$\delta_{\text{C}} \text{C=C}$	142.8; 117.2	143.0; 114.5	142.3; 114.3	138.7; 122.0
$\delta_{\text{C}} \text{C}\equiv\text{C}$	88.9; 83.6	91.0; 83.4	92.3; 84.0	89.4; 84.6
$^1J_{\text{RhC}}$	14; 13	14; 13	14; 14	14; 14
$\delta_{\text{C}} \text{C}_{\text{NHC}}$	182.0; 181.3	182.4; 182.0	182.8; 182.5	181.8; 181.0
$^1J_{\text{RhC}}$	42	42	41	42

4.3.3 Kinetics studies and mechanistic implications

Given the change in selectivity observed across the series of **22-n** (n = 12, 14, 16, Me), variable temperature ¹H NMR studies were conducted in order to gain a deeper insight into the differences in energetic barriers of these reactions that give rise to this divergence. Like the homocoupling reaction of *t*Bu alkyne by **11-n** (n = 12, 14, 16) the conversion of **22-n** into interlocked species **32-n** and **33-16** shows consistent first-order dependence over the examined temperature window (328 – 358 K).

Eyring analysis for the formation of **32-12** in C₂D₄Cl₂ (328 – 348 K) has been conducted previously in the group and comparison with the catalytic transformation mediated by **11-Me** highlighted a significant energetic perturbation when the homocoupling is conducted through the aperture of the ring (*vide supra*). Since these initial studies, the coordinating ability of the reaction solvent has been shown to influence the energetics of these processes. Repeating the reductive coupling from **22-12** in 1,2-DiFB allowed the solvent dependence of this transformation to be probed (333 – 348 K; Table 4.3.3). Curiously, the activation barrier determined for the reaction in 1,2-DiFB remains consistent, within error to that previously determined in C₂D₄Cl₂ (104 kJmol⁻¹ vs 106 kJmol⁻¹). However, the component enthalpic and entropic barriers differ considerably; with a substantially lower enthalpic penalty (93 kJmol⁻¹ vs 119 kJmol⁻¹) for the reaction conducted in the more weakly coordinating solvent, which is offset by a negative entropy term (-37 JK⁻¹mol⁻¹ vs 44 JK⁻¹mol⁻¹). Examining these results from a fundamental perspective, the differences can be rationalised by solvent coordination to the Rh(III) intermediate similarly to that

described for the formation of **19-n** (*vide supra*) and inferred by the fluxional behavior of these intermediates in CH₂Cl₂. The dissociative process in C₂D₄Cl₂ comprises a higher enthalpic contribution but benefits from a disordered transition state.

Table 4.3.3. Thermodynamic parameters for the reductive elimination of **22-n**

	32-12	32-12	32-14	32-16	33-16
Solvent	C ₂ D ₄ Cl ₂	1,2-DiFB	1,2-DiFB	1,2-DiFB	1,2-DiFB
ΔG[‡](298 K)/ kJmol⁻¹	106 ± 3	104 ± 6	116 ± 7	114 ± 7	112 ± 2
ΔH[‡] / kJmol⁻¹	119 ± 1	93 ± 3	133 ± 4	102 ± 3	102 ± 1
ΔS[‡] / JK⁻¹mol⁻¹	44 ± 4	-37 ± 10	59 ± 11	-41 ± 10	-34 ± 2

Measuring the temperature dependence of the overall transformation of **22-16** allowed the overall rate constant *k*_{obs} to be determined and coupled with the resultant product distribution the rate constants for the component pathways could be extracted (*k*_E and *k*_G for **32-16** and **33-16** respectively). Using independent Eyring analyses almost identical activation barriers were determined for the formation of **32-16** and **33-16** which explains the almost equal product distribution for this reaction. Moreover, comparable enthalpic and entropic terms advocate the occurrence of similar transitions, consistent with both relating to the alternate reductive elimination steps. This is corroborated when comparing with related data determined for the reaction of **31-n** to generate **19-n** (*vide supra*), which also comprise negative entropy values associated with the single reductive elimination step.

Comparing the energetic parameters between ring sizes (n = 12, 14, 16) shows a less clear trend across the series. Rather unexpectedly an increase in the activation barrier is observed as the macrocycle is extended from n = 12 to n = 14 (104 kJmol⁻¹ and 116 kJmol⁻¹, respectively) and then negligible change occurs as the ring is expanded further (114 kJmol⁻¹, n = 16). These results contradict those of **19-n** and suggest that the factors influencing the thermodynamics of these transformations are decidedly more complex. For instance, the parameters associated with the formation of **32-14** are markedly different to those of **32-12** and **32-16**; featuring a more substantial enthalpic penalty and a positive entropic term, which suggests a different rate determining step is operative for this ring

size. The positive value of ΔS^\ddagger suggests an increase in disorder in the transition state usually attributed to dissociative processes. The rationale behind the change in rate determining step across the series of ring sizes, however, is yet to be fully understood. Additional investigations are therefore required in order to understand these distinctions in behaviour fully.

4.4 Homocoupling of a terminal alkyne with a trityl stoppering group

Whilst encouraging with respect to onwards reactivity of the interlocked targets, the expansion of the macrocyclic annulus increases the risk of axle dethreading, particularly in the case where the size disparity between stopper and macrocycle is at its highest (*viz.* **19-16**). Evaluating the spatial demands of the axle termini (Figure 4.4.1) it could be envisaged that the relatively small steric profile of the *t*Bu appendage may not be sufficient to retain mechanical entrapment even within the smaller macrocycles ($n = 12, 14$). To circumvent these issues, a much bulkier trityl-based stoppering group Ar^* was targeted.³⁰⁻³⁶

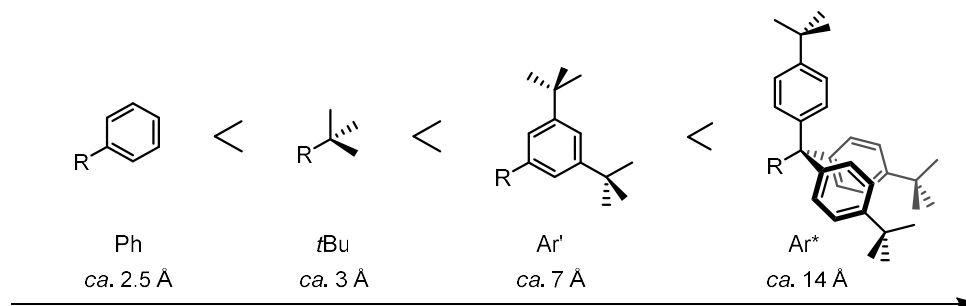


Figure 4.4.1. Comparison of the steric bulk of various stopper groups - approximate diameter size calculated from crystallographic data

Alongside the increased spatial demand of Ar^* , the introduction of a propylene spacer between the terminal alkyne motif and the stoppering group was hoped to withdraw the steric bulk away from the reactive centre. Retraction of the steric bulk in this way was anticipated to encourage further reactivity of the resulting interlocked complexes by allowing more ready access to the metal centre. As such, **16m** ($\text{HC}\equiv\text{C}(\text{CH}_2)_3\text{Ar}^*$) combines electronic properties that resemble *t*Bu alkyne **16b** with a steric profile more akin to that of **16a**.

4.4.1 Preparation of trityl-based alkyne - **16m**

Following an existing literature procedure, tris(*tert*-butyl)methane (**36**) was prepared in a reasonable yield (67%) over two steps (Scheme 4.4.1).³⁷ Synthesis of the alkyl bromide terphenyl stopper **39**, was initially targeted through low temperature deprotonation ($-78\text{ }^\circ\text{C}$) of **36** to using *n*BuLi the presence of the deaggregating agent HMPA to generate the tris(*tert*-butylphenyl)methanide-carbanion *in situ*. Subsequent reaction with 2-(3-chloro-



Originally, the direct reaction of the trityl carbanion with 1,3-dibromopropane to obtain **39** was avoided amongst fears of disubstitution and elimination side reactions. Pleasingly, strict stoichiometric addition of *n*BuLi and excess dibromopropane afforded compound **39** in one step in a 36% yield. However, difficulties in purification followed, with the separation from the unwanted alkene terminated by-product particularly laborious and therefore the previous pathway was employed for subsequent preparations.

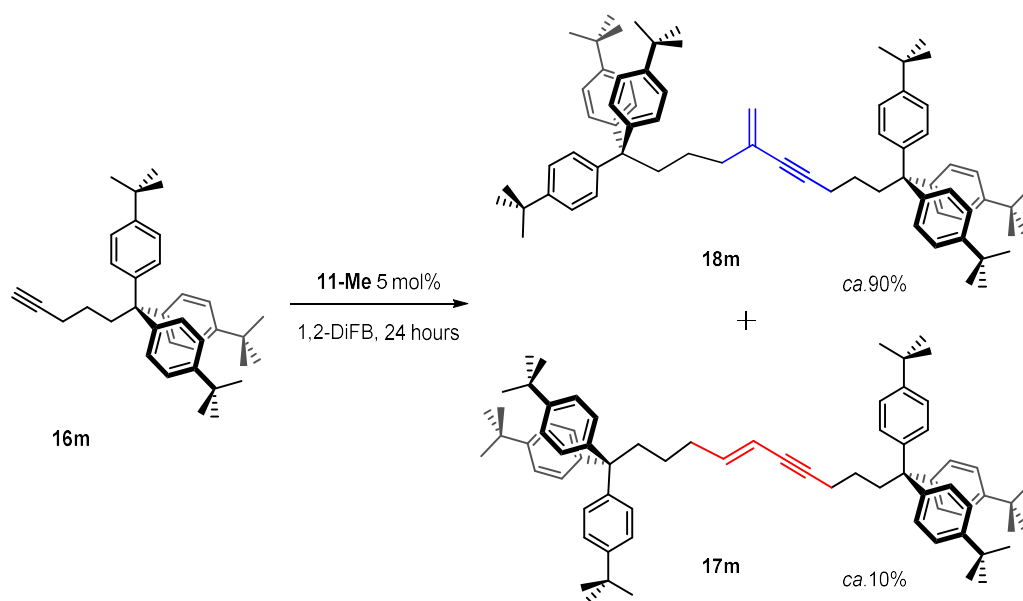
With **39** in hand the installation of the terminal alkyne moiety was achieved *via* a substitution reaction using lithium acetylide in THF:HMPA to give **16m** as a white solid in reasonable yield (51%). This novel half axle was characterised using NMR spectroscopy (CDCl₃) and elemental microanalysis. In particular, the identification of the terminal alkyne proton in the ¹H NMR spectrum (δ 1.99, $^4J_{\text{HH}} = 2.6$ Hz) confirmed the installation of the alkyne motif and the presence of a distinct 27H signal at 1.30 ppm associated with the *t*Bu protons provides an important spectroscopic handle for reaction monitoring of later reactivity studies.

4.4.2 Homocoupling catalysed by **11-Me**

The homodimerisation of **16m** catalysed by **11-Me** using the standard conditions (5 mol%, 100 mM, 1,2-DiFB) afforded a 9:1 mixture of *gem*- and *E*- isomers (**18m** and **17m** respectively) after quenching with carbon monoxide (Scheme 4.4.2). The resulting product distribution was determined for the crude reaction mixture by integration of alkene ¹H resonances, δ 5.99/5.41 for **17m** and δ 5.25/5.09 for **18m**, relative to the Ar^F signals (1,2-DiFB).

Following purification on silica (hexane/CH₂Cl₂) the major *gem*-isomer **18m** was isolated in good yield (87%) and characterised using NMR spectroscopy (CDCl₃), which shows a pair of doublets associated with the terminal alkene protons at 5.26 and 5.09 ppm ($^2J_{\text{HH}} = 2.0$ Hz, $^2J_{\text{HH}} = 1.6$ Hz). A COSY experiment indicates correlations between these signals and a HSQC experiment showed that they reside on the same carbon atom (*viz.* δ 120.1) corroborating the structural assignment. Unfortunately, the limited quantity of **17m** prevented its full characterisation, nevertheless the typical doublet of triplets and a corresponding

doublet in the crude ^1H NMR spectrum (CDCl_3) evidenced the presence of an alkene with *E*-configuration (δ 5.92, $^3J_{\text{HH}} = 15.3$, 7.5 Hz; δ 5.33, $^3J_{\text{HH}} = 15.3$ Hz) supporting the assignment as **17m**. The characterisation of these enyne axes represents important reference data for use during latter reactions.



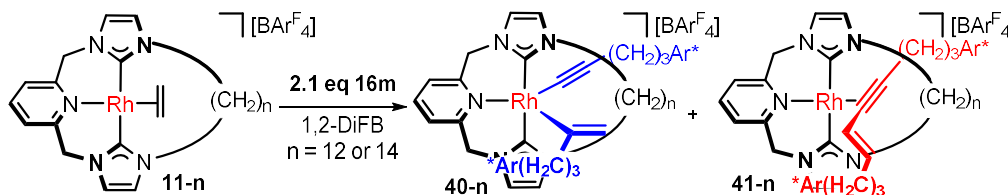
Scheme 4.4.2. Catalytic preparation of **17m** and **18m** using **11-Me**

Curiously, the selectivity of this reaction mirrors that observed when using 1-hexyne, **16e** (Chapter 3), which can be rationalised when considering the relative steric profiles of the two substrates. Whilst at first glance the associated spatial demands of these substrates are markedly different, the steric bulk of **16m** is in fact far removed from the reactive alkyne moiety and coupled with its increased flexibility unlikely to incur steric clashes with the pincer scaffold. As such, **16m** behaves as the simple linear alkyne equivalent **16e** giving a mixture of products with a preference for the geminal isomer.

4.4.3 Homocoupling through rings

With the reactivity and selectivity of the catalytic dimerisation of **16m** by **11-Me** established and having demonstrated the propensity of **11-n** ($n = 12, 14, 16$) to promote terminal alkyne coupling reactions through their macrocyclic annuli in a process resembling active-metal templated syntheses (*vide supra*), the reaction manifold was expanded to include trityl functionalised **16m**. Particular emphasis was placed on the selectivity of this reaction when using the macrocyclic

congeners **11-n** ($n = 12, 14, 16$). Using the established methodology described for the preparation of **19-n** and **32-n**, the progress of the reaction between **11-n** ($n = 12, 14$) and 2.1 equivalents of **16m** alkyne was evaluated using *in situ* ^1H NMR spectroscopy (1,2-DiFB). The reaction showed complete consumption of **11-n** within 30 minutes at ambient temperature alongside the emergence of broad signals indicative of the predominant formation of a new asymmetric species alongside a minor amount of a second C_1 symmetric species.



Scheme 4.4.3. Synthesis of **40-n**

Comparison with the observations noted during the synthesis of **19-n** and **22-n**, the major species were tentatively assigned as Rh(III) alkenyl alkynyl intermediates **40-n**. Indeed, the *in situ* ^1H NMR data corroborates this assignment, with key signals attributed to the geminal alkene protons (δ 4.65/3.81, **40-12**; δ 4.62/4.04, **40-14**) and two intense low frequency signals associated with the *t*Bu groups (δ 1.18/1.12, **40-12**; δ 1.14/1.11, **40-14**). The ESI-MS of the reaction mixture supports this assignment with the expected signal for the cationic rhodium fragment bearing two alkyne equivalents present at 1464.9148 (calcd 1464.9141) m/z for **40-12** and 1493.9513 (calcd 1493.9487) m/z for **40-14**.

Compound **40-14** was subsequently isolated in good yield following removal of excess **16m** though washing with HMDSO (67%) and the spectrum collected in a more accommodating characterisation solvent (CD_2Cl_2). The ^1H NMR spectrum of **40-14** shows the key pyCH_2 resonances as a series of doublets each with the expected geminal coupling (δ 4.84/5.12/5.61/5.66, $^2J_{\text{HH}} = 15.4 - 15.9$ Hz). Signals associated with the *t*Bu groups (δ 1.29/1.28) and geminal alkenyl protons (δ 3.70/2.62) further supported the structural assignment of **40-14** as the geminal alkenyl alkynyl species. Yet the most conclusive evidence comes from the $^{13}\text{C}\{^1\text{H}\}$ NMR spectrum where the carbenic carbon resonances are significantly lower in

frequency compared with those of **19-n** and **32-n** (δ 176.7/175.5, $^1J_{\text{RhC}} = 40/41$ Hz; cf. δ 185.0 – 182.0, $^1J_{\text{RhC}} = 41\text{--}42$ Hz, **19-n/32-n**) and the alkenyl and alkynyl resonances show definitive ^{103}Rh coupling to the α -carbons (δ 157.2, $^1J_{\text{RhC}} = 36$ Hz, $\underline{\text{C}}(\text{CH}_2)$; δ 87.5, $^1J_{\text{RhC}} = 57$ Hz, $\underline{\text{C}}\equiv\text{C}(\text{CH}_2)_3\text{Ar}^*$), which is absent for the β carbons (δ 113.0, $\text{C}(\underline{\text{C}}\text{H}_2)$; δ 68.9, $\text{C}\equiv\underline{\text{C}}(\text{CH}_2)_3\text{Ar}^*$). The magnitude of this coupling is significantly higher than the associated reductive eliminated products (cf. $^1J_{\text{RhC}} = 14$ Hz, **19-n**), attributed to a greater σ -bonding character between the alkyne and the ^{103}Rh centre, corroborating the assignment of **40-14** and by inference **40-12**.

The increased spectral visibility also exposed the presence of a second minor organometallic species signifying that this reaction does not proceed selectively, but instead affords a mixture of products (85:15, **40-n:41-n**). The other product features an *E*-alkene motif evidenced by the alkene protons, which give rise to two signals in the ^1H NMR spectrum; a doublet of triplets at 6.41 ppm ($^3J_{\text{HH}} = 6.9$, 15.1 Hz) and an obscured doublet at 5.85 ppm ($^3J_{\text{HH}} = 13.5$ Hz). Through comparison with later data obtained for **41-16** this has been tentatively assigned as the interlocked Rh(I) *E*-enyne species (*vide infra*). In the absence of the constraints imposed by the macrocycle, **11-Me** successfully promoted the dimerisation of **16m** to a mixture of *E*- and *gem*- regioisomers (*vide supra*) suggesting the activation barriers for each process are roughly comparable. By extension, it is unsurprising that the reaction using the macrocyclic analogues gives a similar distribution of isomers for the associated reaction intermediate. However, as shown for the onwards reactivity of **22-n**, the presence of the macrocyclic tether can have a substantial impact on the activation barriers associated with the final reductive elimination steps which can enforce switches in selectivity.

Corresponding 1,2-DiFB solutions were heated at 80 °C to explore the onwards reactivity of **40-n** ($n = 12, 14$) but after 18 hours no appreciable change in the ^1H NMR spectra for either ring size was observed. The failure of **40-n** ($n = 12, 14$) to undergo reductive elimination can be attributed to the incumbent thermodynamic instability of the forward C–C bond forming reaction, presumably due to spatial constriction of the nearby macrocyclic tether (cf. **32-n**

$n > 16$). This is in direct contrast to reductive elimination *via* the *E*-mechanism which is thought to progress unhindered by the rings. Moreover, the fixed ratio of isomers and lack of growth in the signals pertaining to **41-14** suggests that the reverse β -hydride elimination is also significantly energetically disfavoured in these systems. These observations can be reconciled when considering that the formation of interlocked geminal enynes has been shown to be energetically disfavoured for **16a** and the smaller ringed congeners ($n < 16$, *vide supra*) attributed to their increased spatial demand. The high energetic penalty of β -elimination from an sp^2 centre to generate an alkyne is unsurprising given its relative paucity in the literature.^{38–41}

In contrast to the smaller ring systems, the reaction between **11-16** and **16m** at 65 °C in 1,2-DiFB resulted in a much darker red solution after 18 hours and a notably sharper ^1H NMR spectrum compared with that of **40-n**, signifying further reaction progression. The new complex shows C_1 symmetry in solution, with the diastereotopic methylene bridges giving rise to four doublets in the ^1H NMR spectrum (δ 5.42/5.34/4.61/4.60, $^2J_{\text{HH}} = 14.6$ Hz) alongside two characteristic ^1H geminal alkene protons signals (δ 5.82/5.23). Following concentration to dryness and washing with TMS the ^1H NMR spectrum (CD_2Cl_2) of the isolated reaction mixture showed a mixture of two C_1 symmetric species in a rough 92:8 ratio in a combined yield of 84%. These species were assigned as complexes **42-16** and **41-16**, respectively (Figure 4.4.2).

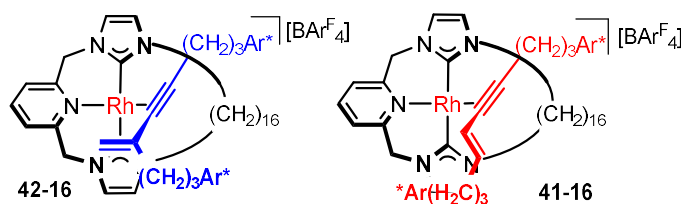


Figure 4.4.2. Mixture of products formed from the reaction of **11-16** and **16m**

Data associated with the major species **42-16** is consistent with a geminal alkene containing species ($\delta_{\text{H}} 5.62/5.03$) with the minor species again comprising an *E*-alkene moiety ($\delta 6.31$, $^3J_{\text{HH}} = 14.5$, 7.2 Hz, $\delta 5.95$, $^3J_{\text{HH}} = 14.9$ Hz). The $^{13}\text{C}\{^1\text{H}\}$ NMR data for **42-16** confirms that the reductive elimination has occurred, with ^{103}Rh coupling to the alkyne carbons ($\delta 89.6/77.3$, $^1J_{\text{RhC}} = 14$ Hz) in-line with expected

values for a π -bound alkyne complex (*cf.* 11 – 16 Hz, **19-n** and **32-n**). In addition, coupling between the rhodium centre and the alkene resonances (δ 136.1/118.6) was not observed and the carbenic carbon signals at 183.8 and 183.4 ppm ($^1J_{\text{RhC}}$ = 41 Hz) are shifted downfield relative to **40-n** ($\Delta\delta$ *ca.* 8 ppm) corroborating the structural assignment.

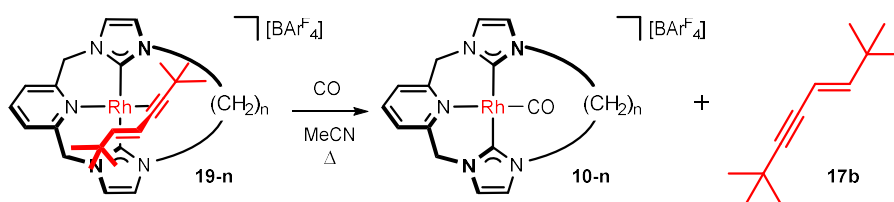
Similarities between the data for **42-16**, the minor *E*-containing product (**41-16**) and other Rh(I) enyne species (**19-n**, **32-n** and **33-16**) contributed to its assignment as the reductively eliminated product. However, being formed in such trace quantities made attaining $^{13}\text{C}\{^1\text{H}\}$ NMR data for **41-n** and thus confirmation of its assignment particularly challenging. Satisfactory microanalysis obtained for this mixture confirms a composition comprising only dimeric alkyne complexes, which was further supported by ESI-MS which showed the parent cation signal (1520.9798, calcd 1520.9767 *m/z*) and no signals for higher order oligomers. Unfortunately, separation of **42-16** and **41-16** was hindered by their instability towards chromatographic conditions and the comparably high solubility of both isomers in a wide range of organic solvents (MeOH – TMS) meant that repeated crystallisation attempts were unsuccessful. Unable to separate the two isomers, further reactivity studies were not conducted using these species.

The presence of only *E*- and *gem*-products in the dimerisation reactions of **16m** by **11-n** supports an operative oxidative addition hydrometallation mechanism. However, the selectivity of this process is less well defined compared with **16a** and **16b**, which can be attributed to the energy differences between the competing pathways being less pronounced. Unlike the *t*Bu and Ar' stoppering groups, the alkyl chains in **16m** are effectively too long and flexible to evoke large differences in the energetics of the divergent mechanisms based on steric demands of the stoppering unit. Nevertheless, favourability towards the geminal isomer suggests a common preference for head-to-tail dimerisation of **16m** using **11-n** (*n* = Me, 12, 14, 16).

4.5 Reactivity of interlocked compounds

4.5.1 Dethreading studies

The effectiveness of the bulky groups to mechanically entrap the enynes within the macrocyclic complexes was evaluated through reactions using the strongly coordinating carbon monoxide ligand (Scheme 4.5.1). This is particularly important for **19-16** where the size complementarity between the stopper and cavity is at its lowest. Deslipping of [2]rotaxanes using flash vacuum pyrolysis, conventional heating, or microwave irradiation has been reported in the literature.^{42–44}



Scheme 4.5.1. Dethreading studies of **19-n** ($n = 12, 14, 16$)

The reaction of **19-n** ($n = 12, 14, 16$) with CO results in the initial formation of a new C_s symmetric species (**43-n**) observed by ^1H NMR spectroscopy (d_3 -MeCN, 300 MHz, Figure 4.5.1). Spectral data obtained for this species does not match that of the starting complexes, nor the expected product formed following a successful dethreading event **10-n**. The chemical shifts attributed to the alkene resonances of the axle are shifted $\Delta\delta$ 1.37 – 0.68 relative to free **17b** and *ca.* 0.4 ppm relative to **19-n**. Removing the atmosphere of CO, either through repeated degasses (> 8 freeze-pump-thaw cycles) or concentration to dryness *in vacuo* and redissolution, returns the sample back to **19-n**.

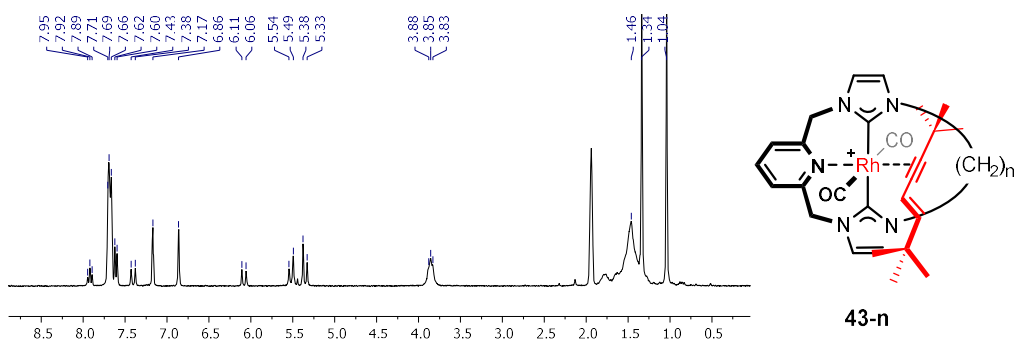


Figure 4.5.1. ^1H NMR spectrum of **43-12** and proposed structure of **43-n** under CO (1 atm; d_3 -MeCN, 300 MHz)

Whilst the identity of **43-n** is yet to be unambiguously assigned, the reversible nature of CO binding indicates weak coordination of the carbonyl ligands and the high symmetry of this species could to be attributed to coordination assisted atropisomerism of the pincer backbone. Facile interconversion between the two C_1 symmetric species mediated by reversible CO coordination and the partial dissociation of either, or both, the enyne axle and central pyridine donor could give rise to the time-averaged C_s symmetry observed (Figure 4.5.1) in a similar fashion to that described previously for **10-12**.⁴⁵

Following the immediate quantitative transformation from **19-n** to **43-n** on exposure to a CO atmosphere ([A] to [B]; Figure 4.5.2), the progress of onwards reactivity was monitored periodically using ^1H NMR spectroscopy (300 MHz). Heating d_3 -MeCN solutions of **43-n** under CO (1 atm) at 85 °C resulted in the slow formation of a new C_{2v} symmetric species, identified as **10-n** alongside the growth of signals associated with free **17b**, both determined through comparison with reference samples (Figures 4.5.2 and 4.5.3). The exclusive generation of **10-n** and **17b** from this reaction confirms the slow displacement of the axle from within the macrocyclic annulus proceeding *via* a deslipping mechanism.

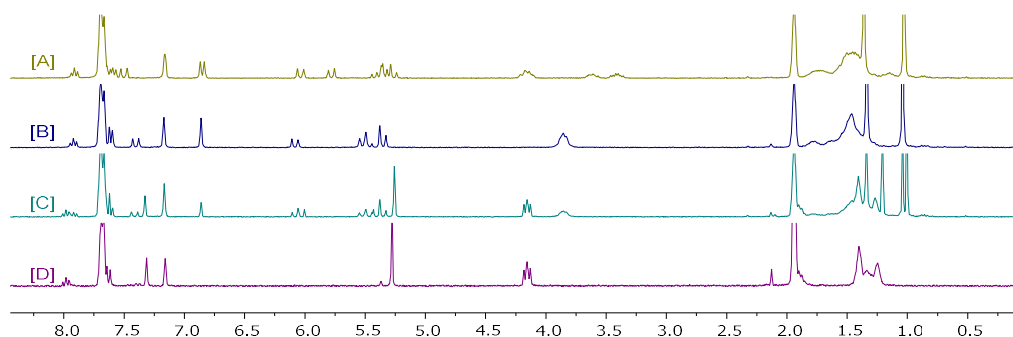
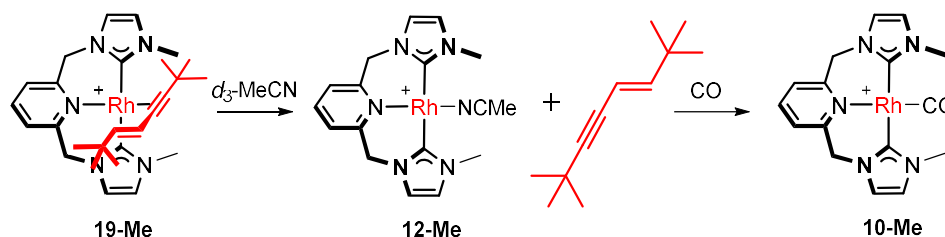


Figure 4.5.2. Reaction progression of the dethreading of **19-12** monitored by ^1H NMR spectroscopy (d_3 -MeCN, 298 K, 300 MHz): [A] Isolated **19-12**; [B] Reaction at 85 °C after $t = 15$ mins; [C] Reaction at 85 °C after $t = 90$ hours; [D] Isolated **10-12** under CO

The relative rate of axle displacement across the series reflects the reduction in mechanical entrapment and thus strength of the mechanical bond as the ring is expanded. For instance, whilst **19-12** and **19-14** were sluggish, exhibiting extended half-lives and requiring prolonged forcing conditions to drive the reaction to completion (**19-12** $t_{1/2} = 70$ h, **19-14** $t_{1/2} = 162$ h), the dethreading reaction of **19-16** proceeded rapidly, generating **10-16** and **17b** in < 1 hour.

Although the energetic barriers of these reaction have not been determined, qualitative analysis of the relative rate of dethreading across the series suggests that axle extrusion from **19-16** has a considerably lower activation barrier than for **19-12** and **19-14**, which indicates a significant weakening of the mechanical bond as the ring is expanded. The additional kinetic stability introduced by the macrocyclic tethers is further highlighted through comparison to acyclic **19-Me** (Scheme 4.5.2). In this case the bound enyne is readily displaced on addition of the mildly coordinating d_3 -MeCN solvent at ambient temperature, affording a mixture of the MeCN adduct **12-Me** (Chapter 3) and free **17b** (Figure 4.5.3). Subsequent introduction of CO (1 atm) saw immediate quantitative conversion of **12-Me** to **10-Me**, reflecting the increased binding affinity of CO.



Scheme 4.5.2. Reaction of **19-Me** under standard dethreading conditions

The facile reactivity of **19-Me** illustrates the weak coordination of the enyne to the rhodium centre in the absence of the macrocyclic tether. Therefore, despite the *t*Bu group not being sufficient to afford true mechanical entrapment, the interpenetration of the enyne moiety through the macrocyclic annuli clearly introduces a component of kinetic stabilisation to the systems.

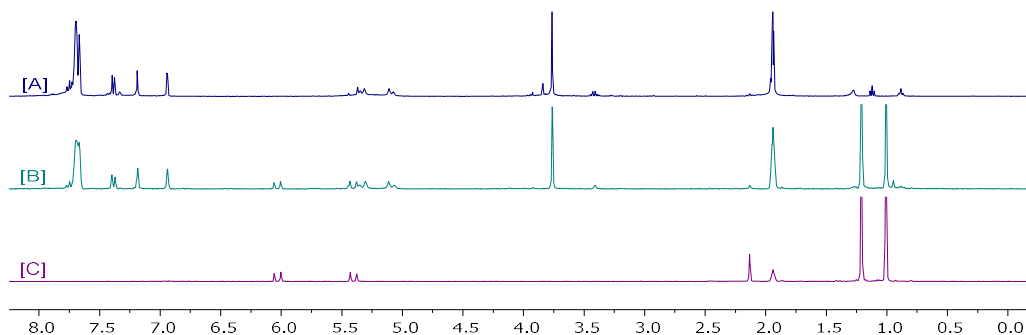
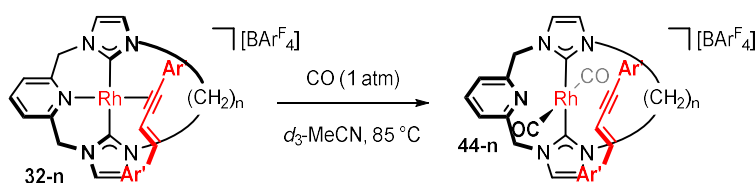


Figure 4.5.3. Reaction progress of the enyne displacement from **19-Me** using ^1H NMR spectroscopy (d_3 -MeCN, 298 K, 300 MHz): **[A]** Isolated **12-Me** (400 MHz); **[B]** Reaction at $t < 15$ mins; **[C]** Isolated **17b**

In contrast to the dethreading reactions of **19-n** ($n = 12, 14, 16$), the Ar' moiety is suitably sterically cumbersome such that even under equivalent dethreading reaction conditions no apparent loss of the axle was observed for **32-n** ($n = 12, 14, 16$) and **33-16** by ^1H NMR spectroscopy or ESI-MS. The sole change during this reaction comes from the growth of signals pertaining to a bis(carbonyl) complex **44-n**, the composition of which was supported by LR ESI-MS (992.5, **44-12**; 1020.5, **44-14**; 1048.6, **44-16** m/z). Like previously described for **43-n**, the ^1H NMR spectra of **44-n** show high symmetry (C_s) despite the asymmetric nature of the interpenetrated enyne, which again advocates highly dynamic behaviour on the NMR timescale facilitated by CO coordination. These carbonyl ligands are relatively weakly bound in comparison to those in **10-n** and can be removed by exposing these complexes to high vacuum (10^{-3} mbar). Prolonged heating of **44-12** at 100°C under vacuum allowed the regeneration of interlocked compound **32-12**.

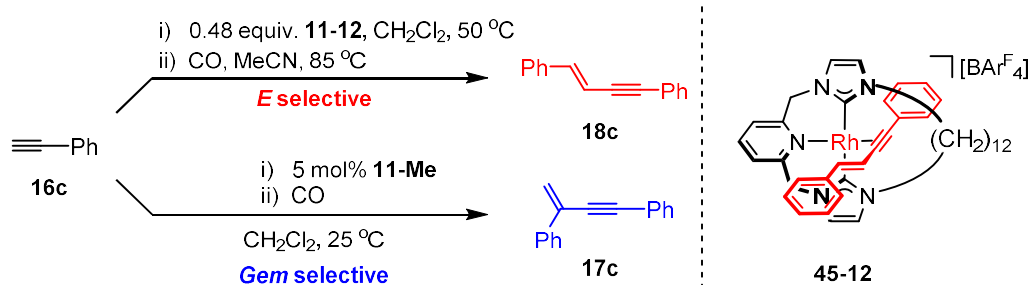


Scheme 4.5.3. Reactions of **32-n** with CO

The axle retention in these complexes is indicative of a robust mechanical bond between the axle and NHC-based macrocycle owed to the sufficient spatial demand of the Ar' stopper.

4.5.2 Exploiting the selectivity switch

With the phenyl moiety less sterically demanding than *t*Bu (Figure 4.4.1), it was thought that the ability to dethread the axle from the ring and the propensity of the macrocyclic tether to switch the selectivity of the dimerisation of aromatic alkynes could be exploited in order to develop the synthetic utility of these complexes. As a proof-of concept the orthogonal selectivity of the acyclic complex, **11-Me**, (Chapter 3) and isolated macrocyclic complex **11-12** was exploited to prepare both the *gem*-enyne **18c** (catalytically) and the *E*-isomer **17c** (stoichiometrically) from the common starting material, **16c** (Scheme 4.5.4).



Scheme 4.5.4. Exploiting the contrasting selectivity of **11-Me** and **11-12** to prepare **17c** and **18c**

Isolation of **18c** was achieved through employing standard catalytic conditions described throughout chapter 3 using **11-Me** (5 mol%, 100 mM **16c**, 25 °C). The progress of the reaction was monitored using ^1H NMR spectroscopy and the reaction quenched using carbon monoxide when the reaction reached 75% conversion (24 hours). Quenching with CO was necessary to preclude the formation of the tetrameric product (**24c**), by sequestering the active Rh(I) fragment as the catalytically inert **10-Me**, therefore facilitating the isolation of the **18c** in a moderate yield (65%).

In contrast, more forcing conditions were required in the case of the macrocyclic analogue **11-12**. Reaction of a slight excess of **16c** (2.1 eq) with **11-12** in CH_2Cl_2 at 50 °C for 5 hours gave the interpenetrated *E*-enyne product, **45-12**,[†] along with trace amounts of the undesired *gem*-isomer. The formation of small quantities of free **18c** can be attributed to a minor amount of coupling occurring outside of the macrocyclic cavity, facilitated by the flexibility of the hydrocarbon tether. Fortunately, this unwanted isomer could be removed through washing with cold hexane (0 °C) prior to the dethreading of **17c**. Displacement of **17c** from the macrocyclic aperture was achieved through reaction with CO in refluxing MeCN (85 °C) and the product isolated in a good yield (84% wrt **11-12**, 80% wrt **16c**) following purification on alumina (hexane). The characterisation data for **17c** prepared in this way was consistent with data reported in the literature.⁴⁶ Despite requiring relatively forcing conditions compared with that of the acyclic counterpart, this reaction demonstrates the impact that a conceptually simple

[†] The interwoven complex was also isolated and characterised as a mildly air and moisture sensitive red solid in good yield (84%) (see Chapter 5).

modification in ligand topology has on the selectivity of this reaction. Moreover, this highlights the potential such the ligand design principles could have in terms of developing synthetically viable catalysts.

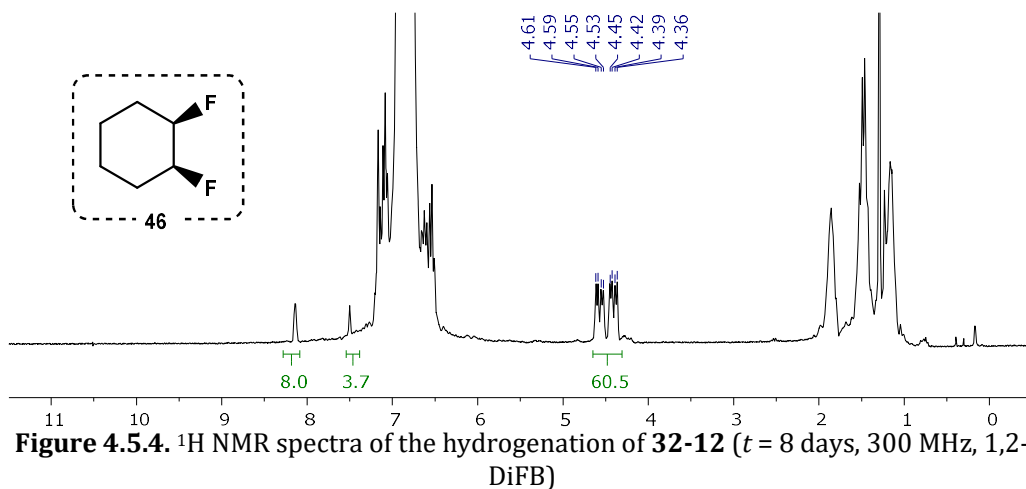
Disappointingly, repeated attempts to make the macrocyclic reaction catalytic were met with little success. This is due, in part, to the sluggish nature of the isomerisation and subsequent reductive elimination steps. Under catalytic conditions (5 mol% **11-12**, 100 mM **16c**) the slow reaction progression provides the opportunity for the insertion of a third equivalent of alkyne into the Rh(III) alkenyl-alkynyl intermediate, which in turn promotes the formation of unwanted trimeric products, identified using LR-ESI MS (814.5, calcd 814.3 m/z). Moreover, the partial mechanical entrapment introduced by the macrocyclic ring means this complex requires reaction with the strongly coordinating CO ligand under forcing conditions in order to dethread **17c**. However, these conditions lead to the formation of the chemically robust rhodium carbonyl complex **10-12**, which renders the rhodium center catalytically inactive.

4.5.3 Reactions with hydrogen

With the Ar' stoppering functionality confirmed as sufficient to prevent ring slippage, efforts were turned to exploring the reactivity of **32-n** ($n = 12, 14, 16$) and **33-16**. In particular, reactions with hydrogen were explored with the aim of saturating the enyne moiety. In the absence of functionality, rhodium-axle interactions would be limited allowing the axle to shuttle freely in the resulting metal-based rotaxane.

Initially, probing the hydrogenation of **32-12** in 1,2-DiFB on a small scale in a J. Young's valve NMR tube saw no reactivity under mild conditions (1 atm H₂, RT), in fact, extremely forcing conditions (4 atm, 95 °C) were required before any reaction was observed. After 8 days of heating, the red solution began to fade and demetallation was evidenced visually by the formation of rhodium metal. The *in situ* ¹H NMR spectrum taken at this point (1,2-DiFB) was devoid of signals attributed to **32-12** but instead showed the emergence of a new 60H doublet of doublets of doublets at 4.47 ppm ($^2J_{FH} = 49.5$ Hz, $^3J_{FH} = 17.9$ Hz, $^3J_{HH} = 7.7$ Hz) alongside three substantial low frequency signals between 0.8 – 2.3 ppm (Figure

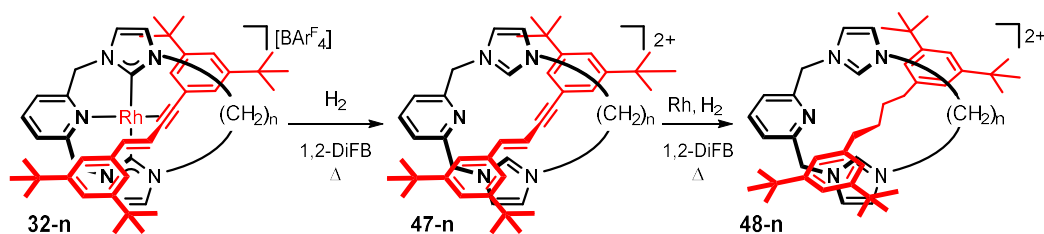
4.5.4). The intensity of these signals relative to the Ar^F signals indicate that these cannot be attributed to **32-12** and must instead be associated with solvent reduction.



Indeed, hydrogenation of fluoroarenes catalysed by rhodium complexes has been reported in the literature,⁴⁷ and whilst homogeneous catalysts are favoured for the hydrogenation of alkenes, the hydrogenation of aromatic systems is typically achieved using heterogeneous systems.⁴⁸ Unable to isolate the hydrogenation product due to its high volatility, the *in situ* ¹H NMR data was used to identify **46** as the fully saturated product. The likely *cis*-selectivity of the hydrogenation was determined by the magnitude of the ¹⁹F coupling, which suggests that the hydrogenation of 1,2-DiFB in these reactions is promoted by adventitiously formed nanoparticulate rhodium rather than homogeneously, by intact **32-n**,^{47,49} which is supported by the formation of **46** only occurring following visual complex decomposition.

Seeking to avoid this issue, other non-reactive solvents *e.g.* 1,4-dioxane were tested in this reaction, however, the limited solubility of both **32-n** and the products formed hindered reactivity. With the view that the competing solvent hydrogenation did not interfere with the complex reaction, other than to consume H₂, further investigations continued in 1,2-DiFB, periodically replenishing the hydrogen atmosphere in order to maintain an acceptable rate of reaction.

Alternately, conducting the hydrogenation of **32-12** under analogous conditions but instead in a J. Young's valve ampule saw a significant rate enhancement, with decolouration and colloidal rhodium visible within 8 hours at 95 °C, without the necessity to supplement the hydrogen atmosphere. The increased head space and agitation were credited for this improved reactivity and after 48 hours at reflux complete consumption of **32-12** was evidenced by LR ESI-MS. Growth of a peak of half integer spacing attributed to the interlocked imidazolium salt **47-12** ($[M]^{2+}$ 418.1, calcd 417.8, m/z) and an integer spaced signal attributed to $[M+BAr^F_4]^+$ (1698.6, calcd 1698.7, m/z) were also observed.*



Scheme 4.5.5. Reactions of complexes **32-n** with H_2 to generate **48-n**

The decomposition of **32-n** was rationalised by the initial formation of the Rh(I) dihydrogen complex by ligand displacement of the π -bound enyne, followed by oxidative addition to give the Rh(III) dihydride species which is proposed to be unstable under the reaction conditions, with the isolation of the related non-interlocked RhCNC-12 dihydride, prepared in the group, precluded by its limited stability.⁵⁰ In addition, reductive decomposition of CNC complexes has been described previously for palladium methyl complexes (Chapter 1.3.4)^{51,52} and a similar reductive elimination process may be responsible for the decomplexation of the NHC pincer to give the bis(imidazolium) salts **47-n**. However, this decomposition process does not account for the identity of the second counter anion required to maintain charge balance in the system. Furthermore, the full distribution of decomposition products remains ambiguous.

Despite hydrogenation of free enyne (**17c**) proceeding under relatively mild conditions (Pd/C, 4 atm H_2 , 25 °C, $CDCl_3$),²⁶ under comparable conditions **32-12** showed no reaction (Pd/C, 4 atm H_2 , 25 °C, 1,2-DiFB). This disparity can be

* Hydrogenation of **19-n** ($n = 12, 14, 16$) under these conditions resulted in similar decomposition and as a consequence axle dethreading affording the associated bis(imidazolium) prolignands **3-n**

reconciled by the kinetic stabilisation provided by the macrocyclic tethers as aptly illustrated by the solid-state structure of **32-12**, where the hydrocarbon tether resides tightly around the enyne axle and the stopper groups cap the cavity encasing the reactive moieties inside. Surrounding the unsaturated enyne functionality in this way shields it from interaction with even small reactants such as H₂. Similar kinetic stabilisation of unsaturated bonds within [2]rotaxane structures have been described by Vögtle *et al.* (Figure 4.5.5).^{53,54} In their systems the hydrogenation of internal alkene moieties of the axle components using Pd/C (3 atm H₂, RT) proceeds within 18 and 64 hours, for the unthreaded variants, whereas the [2]rotaxane species took considerably longer (64 and 120 h, respectively). Reflecting on these reports, it was concluded that significantly more forcing conditions would likely be required to promote the hydrogenation of the enyne axles of **32-n**.

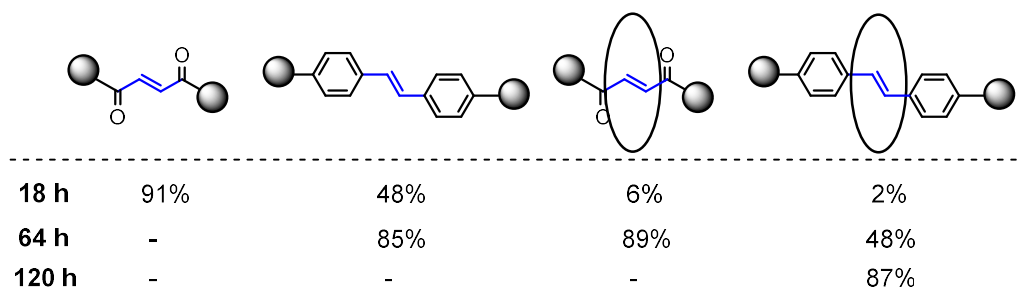


Figure 4.5.5. Example of hydrogenative stability provided by a ring

After 48 hours of reaction, despite quantitative decomplexation, the hydrogenation of the enyne to generate **48-n** failed to reach completion, evidenced by complex overlapping ESI-MS signals. The slow conversion suggests that hydrogenation of the axle catalysed heterogeneously is not particularly fruitful, reconciled by the limited accessibility to the unsaturated centres. Therefore, to encourage the hydrogenation an external homogeneous hydrogenation catalyst was added to the reaction mixture. However, even after addition of 10 mol% of [Rh(PPh₃)₃Cl] the hydrogenation remained sluggish and after 3 days traceable quantities of **47-12** still persisted.

Under comparable conditions (4 atm H₂, 1,2-DiFB, 95 °C), solutions of **32-14**, **32-16** and **33-16** displayed demetallation decomposition at a considerably faster rate. Evaluation of the product mixture after 8 hours using ESI-MS showed

complete loss of **32-n** ($n = 14, 16$) and the emergence of peaks associated with **47-n** ($[M]^{2+}$ 431.9, calcd 431.84, **47-14**; 446.2, calcd 445.86, **47-16** m/z) as well as evidence for **48-n** ($[M]^{2+}$ 434.9, calcd 434.86, **48-14**; 449.2, calcd 448.88, **48-16**, m/z) and intermediate species. Reflecting the expanded cavity and thus accessibility the use of an external catalyst was not necessitated for the larger rings which saw complete hydrogenation of the enyne moiety to generate **48-n** ($n = 14, 16$) in 72 and 60 hours, respectively, promoted solely by colloidal rhodium.

Unfortunately, the high affinity of bis(imidazolium) salts for both alumina and silica precluded purification of **47-n** and **48-n** by chromatography and the high hygroscopicity of the unprotected imidazolium moiety alongside the complexity of the resulting reaction mixture made the use of other purification techniques operationally ambitious. As such, despite numerous purification attempts, including methods involving sulfur protection, the isolation and unambiguous characterisation of **48-12** was futile and therefore not trialed for **32-n** ($n > 12$) or **33-16**.

4.6 References

- 1 J. F. Stoddart, *Angew. Chem. Int. Ed.*, 2017, **56**, 11094–11125.
- 2 F. M. Raymo and J. F. Stoddart, *Chem. Rev.*, 1999, **99**, 1643–1664.
- 3 In *The Nature of the Mechanical Bond*, John Wiley & Sons, Inc., Hoboken, NJ, USA, 2016, pp. 1–54.
- 4 E. Wasserman, *J. Am. Chem. Soc.*, 1960, **82**, 4433–4434.
- 5 I. T. Harrison and S. Harrison, *J. Am. Chem. Soc.*, 1967, **89**, 5723–5724.
- 6 I. T. Harrison, *J. Chem. Soc., Chem. Commun.*, 1972, 231–232.
- 7 C. O. Dietrich-Buchecker, J. P. Sauvage and J. P. Kintzinger, *Tetrahedron Lett.*, 1983, **24**, 5095–5098.
- 8 P. R. Ashton, T. T. Goodnow, A. E. Kaifer, M. V. Reddington, A. M. Z. Slawin, N. Spencer, J. F. Stoddart, C. Vicent and D. J. Williams, *Angew. Chem. Int. Ed.*, 1989, **28**, 1396–1399.
- 9 D. B. Amabilino and J. F. Stoddart, *Chem. Rev.*, 1995, **95**, 2725–2828.
- 10 V. Aucagne, K. D. Hänni, D. A. Leigh, P. J. Lusby and D. B. Walker, *J. Am. Chem. Soc.*, 2006, **128**, 2186–2187.
- 11 M. Denis and S. M. Goldup, *Nat. Rev. Chem.*, 2017, **1**, 0061.
- 12 J. D. Crowley, S. M. Goldup, A.-L. Lee, D. A. Leigh and R. T. McBurney, *Chem. Soc. Rev.*, 2009, **38**, 1530–1541.
- 13 V. Aucagne, J. Berná, J. D. Crowley, S. M. Goldup, K. D. Hänni, D. A. Leigh, P. J. Lusby, V. E. Ronaldson, A. M. Z. Slawin, A. Viterisi and D. B. Walker, *J. Am. Chem. Soc.*, 2007, **129**, 11950–11963.
- 14 H. Lahlali, K. Jobe, M. Watkinson and S. M. Goldup, *Angew. Chem. Int. Ed.*, 2011, **50**, 4151–4155.
- 15 E. A. Neal and S. M. Goldup, *Chem. Sci.*, 2015, **6**, 2398–2404.
- 16 L. D. Movsisyan, M. Franz, F. Hampel, A. L. Thompson, R. R. Tykwinski and H. L. Anderson, *J. Am. Chem. Soc.*, 2016, **138**, 1366–1376.
- 17 M. Franz, J. A. Januszewski, F. Hampel and R. R. Tykwinski, *Eur. J. Org. Chem.*, 2019, **2019**, 3503–3512.
- 18 S. Saito, E. Takahashi and K. Nakazono, *Org. Lett.*, 2006, **8**, 5133–5136.
- 19 J. Berná, S. M. Goldup, A.-L. Lee, D. A. Leigh, M. D. Symes, G. Teobaldi and F. Zerbetto, *Angew. Chem. Int. Ed.*, 2008, **47**, 4392–4396.
- 20 J. Berná, J. D. Crowley, S. M. Goldup, K. D. Hänni, A.-L. Lee and D. A. Leigh, *Angew. Chem. Int. Ed.*, 2007, **46**, 5709–5713.
- 21 J. D. Crowley, K. D. Hänni, A.-L. Lee and D. A. Leigh, *J. Am. Chem. Soc.*, 2007, **129**, 12092–12093.
- 22 S. M. Goldup, D. A. Leigh, R. T. McBurney, P. R. McGonigal and A. Plant, *Chem. Sci.*, 2010, **1**, 383–386.
- 23 J. J. Danon, D. A. Leigh, P. R. McGonigal, J. W. Ward and J. Wu, *J. Am. Chem. Soc.*, 2016, **138**, 12643–12647.
- 24 J. Echavarren, M. A. Y. Gall, A. Haertsch, D. A. Leigh, V. Marcos and D. J. Tetlow, *Chem. Sci.*, DOI:10.1039/C9SC02457C.
- 25 J. D. Crowley, K. D. Hänni, D. A. Leigh and A. M. Z. Slawin, *J. Am. Chem. Soc.*, 2010, **132**, 5309–5314.
- 26 R. E. Andrew, University of Warwick, 2016.
- 27 C. M. Storey, M. R. Gyton, R. E. Andrew and A. B. Chaplin, *Angew. Chem. Int. Ed.*, 2018, **57**, 12003–12006.
- 28 C. Yang and S. P. Nolan, *J. Org. Chem.*, 2002, **67**, 591–593.
- 29 R. E. Andrew and A. B. Chaplin, *Inorg. Chem.*, 2015, **54**, 312–322.
- 30 J. M. Mercurio, R. C. Knighton, J. Cookson and P. D. Beer, *Chem. Eur. J.*, 2014, **20**, 11740–11749.
- 31 A. N. Basuray, H.-P. Jacquot de Rouville, K. J. Hartlieb, T. Kikuchi, N. L. Strutt, C. J. Bruns, M. W. Ambrogio, A.-J. Avestro, S. T. Schneebeli, A. C. Fahrenbach and J. F.

- Stoddart, *Angew. Chem. Int. Ed.*, 2012, **51**, 11872–11877.
- 32 J. J. Danon, D. A. Leigh, P. R. McGonigal, J. W. Ward and J. Wu, *J. Am. Chem. Soc.*, 2016, **138**, 12643–12647.
- 33 D. A. Leigh, L. Pirvu, F. Schaufelberger, D. J. Tetlow and L. Zhang, *Angew. Chem. Int. Ed.*, 2018, **57**, 10484–10488.
- 34 J. M. Van Raden, B. M. White, L. N. Zakharov and R. Jasti, *Angew. Chem. Int. Ed.*, 2019, **58**, 7341–7345.
- 35 A. Joosten, Y. Trolez, V. Heitz and J.-P. Sauvage, *Chem. Eur. J.*, 2013, **19**, 12815–12823.
- 36 M. Xue, Y. Yang, X. Chi, X. Yan and F. Huang, *Chem. Rev.*, 2015, **115**, 7398–7501.
- 37 H. W. Gibson, S. H. Lee, P. T. Engen, P. Lecavalier, J. Sze, Y. X. Shen and M. Bheda, *J. Org. Chem.*, 1993, **58**, 3748–3756.
- 38 M. E. O'Reilly, S. Dutta and A. S. Veige, *Chem. Rev.*, 2016, **116**, 8105–8145.
- 39 P. Espinet and A. C. Albéniz, *Curr. Methods Inorg. Chem.*, 2003, **3**, 293–371.
- 40 M. Etienne, R. Mathieu and B. Donnadieu, *J. Am. Chem. Soc.*, 1997, **119**, 3218–3228.
- 41 C. McDade and J. E. Bercaw, *J. Organomet. Chem.*, 1985, **279**, 281–315.
- 42 G. M. Hübner, G. Nachtsheim, Q. Y. Li, C. Seel and F. Vögtle, *Angew. Chem. Int. Ed.*, 2000, **39**, 1269–1272.
- 43 C. Heim, A. Affeld, M. Nieger and F. Vögtle, *Helv. Chim. Acta*, 1999, **82**, 746–759.
- 44 A. Martinez-Cuezva, L. V. Rodrigues, C. Navarro, F. Carro-Guillen, L. Buriol, C. P. Frizzo, M. A. P. Martins, M. Alajarin and J. Bernal, *J. Org. Chem.*, 2015, **80**, 10049–10059.
- 45 R. E. Andrew, D. W. Ferdani, C. A. Ohlin and A. B. Chaplin, *Organometallics*, 2015, **34**, 913–917.
- 46 M. J. Dabdoub, V. B. Dabdoub and J. V. Comasseto, *Tetrahedron Lett.*, 1992, **33**, 2261–2264.
- 47 M. P. Wiesenfeldt, Z. Nairoukh, W. Li and F. Glorius, *Science*, 2017, **357**, 908–912.
- 48 P. J. Dyson, *Dalton Trans.*, 2003, 2964–2974.
- 49 W. R. Dolbier, *Guide to fluorine NMR for organic chemists*, Wiley, 2009.
- 50 M. R. Gyton, B. Leforestier and A. B. Chaplin, *Organometallics*, 2018, **37**, 3963–3971.
- 51 D. J. Nielsen, K. J. Cavell, B. W. Skelton and A. H. White, *Inorg. Chim. Acta*, 2006, **359**, 1855–1869.
- 52 D. J. Nielsen, A. M. Magill, B. F. Yates, K. J. Cavell, B. W. Skelton and A. H. White, *Chem. Commun.*, 2002, 2500–2501.
- 53 C. Reuter and F. Vögtle, *Org. Lett.*, 2000, **2**, 593–595.
- 54 A. H. Parham, B. Windisch and F. Vögtle, *Eur. J. Org. Chem.*, 1999, **1999**, 1233–1238.

Chapter 5 - Experimental procedures

5.1 General Considerations

Air sensitive manipulations were carried out under an inert atmosphere using standard schlenk and glovebox techniques. Glassware was oven-dried (150 °C) and flame-dried under vacuum prior to use. d_3 -MeCN and d_5 -pyridine and CD_2Cl_2 were dried over activated molecular sieves (3 Å) and stored under an argon atmosphere. DMSO and d_6 -DMSO were dried over four successive batches of 3 Å molecular sieves before storage over fresh sieves under an argon atmosphere. d_8 -THF and d_6 -benzene were dried over Na before being vacuum distilled and stored over thoroughly dried 3 Å molecular sieves under an argon atmosphere. Fluorobenzene and 1,2-difluorobenzene were stirred over alumina, distilled from CaH_2 and subsequently stored over successive batches of molecular sieves (3 Å) under an atmosphere of argon. EtOH was sparged with argon for 8 hours before drying over two successive batches of molecular sieves and storage under an argon atmosphere. THF was dried over Na/benzophenone before vacuum distillation and storage under an argon atmosphere over activated molecular sieves (3 Å) and hexane was stored over a potassium mirror under argon. Tetramethylsilane (TMS), and hexamethyldisiloxane (HMDSO) were dried over Na/K₂ alloy before being vacuum distilled and stored over activated molecular sieves (3 Å) under an argon atmosphere. All other anhydrous solvents (< 0.005% H₂O) were purchased from Aldrich, Alfa or Acros, freeze-pump-thaw degassed and stored over 3 Å molecular sieves. Solvents stored and used under a nitrogen atmosphere were transferred from sealed anhydrous solvent bottles into catchpots with no further purification. Na[BAr^F₄],¹ [Rh(C₂H₄)₂Cl]₂,² [Rh(CO)₂Cl]₂,³ CNC-Me·2HBr (**3-Me**),⁴ 3,5-Bis(*tert*-butyl)phenylacetylene (**16a**),⁵ and tris-(4-*tert*-butylphenyl)methane (**36**)⁶ were prepared following literature procedures. Complex [Rh(Mes)(C₂H₄)₂][BAr^F₄] (**29**) was prepared by Dr Matthew Gyton using an adapted literature procedure.⁷ 1,14-bis(bromo)tetradecane was purified prior to use by dissolving in pentane and running through a short plug (silica; pentane). CuBr was purified by subsequent washes with acetic acid and H₂O under nitrogen before being rigorously dried *in vacuo*. Phenylacetylene was purified by distillation prior to storage over

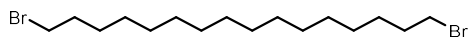
molecular sieves (3 Å) under argon. All other reagents are commercially available and were used without further purification. NMR spectra were recorded on Bruker Avance 300 and 500, Bruker Avance III 400 and 600, Bruker Avance III HD 300, 400 and 500 MHz spectrometers at 298 K. Chemical shifts are quoted in ppm with coupling constants and full width half maxima quoted in Hz. HR ESI-MS were recorded on a Bruker MaXis mass spectrometer, LR ESI-MS were collected using an Agilent 6130B single Quad mass spectrometer and IR spectra were recorded on a PerkinElmer Spectrum 100 FT-IR spectrometer at 298 K using a KBr transmission cell in CH₂Cl₂. Microanalyses performed at the London Metropolitan University by Stephen Boyer.

5.2 Compounds discussed in Chapter 2

5.2.1. Preparation of dibromoalkanes – 1-*n*

Triphenyl phosphine (2.6 eq) was added to a stirring solution of the chosen diol (1.0 eq) and carbon tetrabromide (2.6 eq) in THF under a nitrogen atmosphere and the resulting green suspension stirred for 6 hours. H₂O was added to the resulting cream suspension and the product extracted with ethyl acetate. The combined organic layers were washed with H₂O and brine before being dried over MgSO₄ and the crude product was obtained on removal of volatiles *in vacuo*. Purification *via* flash column chromatography (silica; hexane) afforded the products as white microcrystalline solids.

1,16-dibromohexadecane – 1-16



1,16-hexadecanediol (2.5 g, 9.7 mmol) and carbon tetrabromide (8.3 g, 25 mmol) were reacted with triphenylphosphine (6.6 g, 25 mmol) in THF (40 mL) according to the general procedure to give the product as a microcrystalline white solid. Yield = 3.71 g (84%).

¹H NMR (400 MHz, CDCl₃): δ 3.41 (t, ³J_{HH} = 6.9, 4H, BrCH₂), 1.85 (app. pent., *J* = 7, 4H, BrCH₂CH₂), 1.42 (app. pent., *J* = 7, 4H, CH₂), 1.30-1.22 (m, 20H, CH₂).

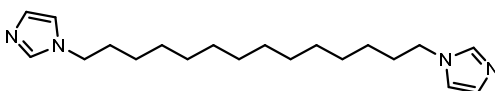
*Data consistent with literature values.*⁸

5.2.2. Preparation of bis(imidazole)alkanes – 2-n

General procedure⁹

NaH (60% w/w in mineral oil) was added portion-wise over 5 minutes to a stirring solution of dried imidazole in THF at 0 °C under a nitrogen atmosphere. The cloudy suspension was allowed to warm to room temperature before the addition of a solution of di(bromo)alkane, **1-n**, in THF. The resulting solution was heated at reflux for 16 hours to give a peach suspension. Once cooled to room temperature the reaction was quenched by the addition of H₂O. The product was then extracted with ethyl acetate and the combined organic extracts were washed with H₂O before being dried over MgSO₄. The crude product was obtained by removing volatiles *in vacuo*.

1,14-Bis(imidazole)tetradecane – 2-14



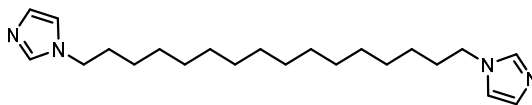
1-14 (1.00 g, 2.81 mmol), imidazole (420 mg, 6.81 mmol) and NaH (60% w/w, 280 mg, 7.02 mmol) in THF (75 mL) were reacted according to the general procedure to obtain the crude product as an off-white solid. Purification *via* recrystallisation from a mixture of ethyl acetate/diethyl ether (1:9) cooled to -20 °C afforded the product as a white microcrystalline solid. Yield = 680 mg (72%).

¹H NMR (500 MHz, CDCl₃): δ 7.46 (s, 2H, NCHN), 7.05 (s, 2H, NCH), 6.90 (s, 2H, NCH), 3.92 (t, ³J_{HH} = 7.1, 4H, NCH₂), 1.84 – 1.71 (m, 4H, CH₂), 1.37 – 1.17 (m, 20H, CH₂).

¹³C{¹H} NMR (126 MHz, CDCl₃): δ 137.2 (s, NCN), 129.5 (s, NCH), 118.9 (s, NCH), 47.2 (s, NCH₂), 31.2 (s, CH₂), 29.7 (s, CH₂), 29.6 (s, CH₂), 29.6 (s, CH₂), 29.2 (s, CH₂), 26.7 (s, CH₂).

HR ESI-MS (positive ion, 4 kV): 331.2857 [M]⁺ (calcd 331.2856) *m/z*.

1,16-Bis(imidazole)hexadecane – 2-16



1-16 (400 mg, 1.04 mmol), imidazole (180 mg, 2.60 mmol) and NaH (60% w/w, 130 mg, 3.12 mmol) in THF (125 mL) were reacted according to the general

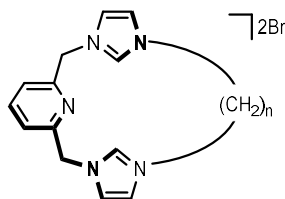
procedure affording the crude product as an off-white solid. Purification *via* recrystallisation from hot diethyl ether slowly cooled to -20 °C afforded the desired product as a white microcrystalline powder. Yield = 330 mg (80%).

¹H NMR (500 MHz, CDCl₃): δ 7.45 (s, 2H, NCHN), 7.05 (s, 2H, NCH), 6.89 (s, 2H, NCH), 4.01 – 3.82 (m, 4H, NCH₂), 1.96 – 1.61 (m, 8H, CH₂), 1.37 – 1.08 (m, 20H, CH₂).

¹³C{¹H} NMR (126 MHz, CDCl₃): δ 137.2 (s, NCN), 129.5 (s, NCH), 118.9 (s, NCH), 47.2 (s, NCH₂), 31.2 (s, CH₂), 29.8 (s, CH₂), 29.7 (s, CH₂), 29.7 (s, CH₂), 29.6 (s, CH₂), 29.2 (s, CH₂), 26.7 (s, CH₂).

HR ESI-MS (positive ion, 4 kV): 359.3170 [M]⁺ (calcd 359.3169) *m/z*.

5.2.3. Preparation of proligands, [CNC-*n*].2HBr – 3-*n*



General Procedure

To refluxing 1,4-dioxane under nitrogen, equimolar solutions of 2,6-bis(bromomethyl)pyridine and chosen bis(imidazole), **2-n**, in 1,4-dioxane (*ca.* 0.06 M, dried over 3 Å molecular sieves) were added simultaneously, dropwise, over 12 hours. The reaction mixture was heated at reflux for a further 6 hours, cooled and the solvent removed *in vacuo*. The product was extracted from the resulting residue using MeCN and vigorous stirring. The suspension was filtered, concentrated and the product obtained through precipitation on addition of excess diethyl ether.

[CNC-12].2HBr – 3-12

Compound prepared using a literature procedure.⁹

¹H NMR (400 MHz, CD₂Cl₂): δ 10.81 (s, 2H, NCHN), 8.19 (s, 2H, NCH), 7.82 – 7.67 (m, 3H, py), 7.39 (s, 2H, NCH), 5.78 (s, 4H, pyCH₂), 4.41 (t, ³J_{HH} = 7.1, 4H, NCH₂), 1.92 (app. t, *J* = 7, 4H, CH₂), 1.50 – 1.17 (m, 16H, CH₂).

*Data consistent with literature values.*⁹

[CNC-14]·2HBr – 3-14

2-14 (1.5 g, 5.4 mmol) was reacted with 2,6-bis(bromomethyl)pyridine (1.2 g, 5.4 mmol) in 1,4-dioxane (600 mL) according to the general procedure and on addition of excess diethyl ether the product was obtained as a pale-yellow oil which slowly crystallised on standing to an off-white microcrystalline solid. Yield = 1.764 g (54%).

¹H NMR (500 MHz, CD₂Cl₂): δ 10.91 (s, 2H, NCHN), 8.12 (s, 2H, NCH), 7.82 – 7.68 (m, 3H, py), 7.32 (s, 2H, NCH), 5.76 (s, 4H, pyCH₂), 4.41 (t, ³J_{HH} = 7.1, 4H, NCH₂), 2.00 – 1.82 (m, 4H, CH₂), 1.44 – 1.02 (m, 20H, CH₂).

¹³C{¹H} NMR (126 MHz, CD₂Cl₂): δ 153.8 (s, py), 139.5 (s, py), 138.4 (s, NCN), 124.3 (s, py), 123.9 (s, NCH), 121.9 (s, NCH), 53.9 (s, pyCH₂), 50.4 (s, NCH₂), 30.3 (s, CH₂), 28.6 (s, CH₂), 28.5 (s, CH₂), 28.5 (s, CH₂), 28.3 (s, CH₂), 25.8 (s, CH₂).

HR ESI-MS (positive ion, 4 kV): 514.2557 [M-Br]⁺ (calcd 514.2540) *m/z*.

[CNC-16]·2HBr – 3-16

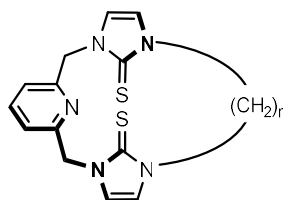
2-16 (2.3 g, 6.4 mmol) was reacted with 2,6-bis(bromomethyl)pyridine (1.7 g, 6.4 mmol) according to the general procedure and the product obtained as an off-white powder. Yield = 1.866 g (47%).

¹H NMR (500 MHz, CD₂Cl₂): δ 10.84 (s, 2H, NCHN), 8.13 (t, ³J_{HH} = 1.6, 2H, NCH), 7.91 – 7.67 (m, 3H, py), 7.34 (t, ³J_{HH} = 1.6, 2H, NCH), 5.76 (s, 4H, pyCH₂), 4.41 (t, ³J_{HH} = 7.3, 4H, NCH₂), 2.04 – 1.83 (m, 8H, CH₂), 1.56 – 0.86 (m, 20H, CH₂).

¹³C{¹H} NMR (126 MHz, CD₂Cl₂): δ 153.8 (s, py), 139.4 (s, py), 138.3 (s, NCN), 124.3 (s, py), 123.9 (s, NCH), 121.8 (s, NCH), 53.9 (s, pyCH₂), 50.4 (s, NCH₂), 30.5 (s, CH₂), 28.9 (s, CH₂), 28.8 (s, CH₂), 28.7 (s, CH₂), 28.6 (s, CH₂), 28.6 (s, CH₂), 26.2 (s, CH₂).

HR ESI-MS (positive ion, 4 kV): 542.2848, [M-Br]⁺ (calcd 542.2853) *m/z*.

5.2.4. Preparation of thione-based macrocycles – 4-n



General procedure¹⁰

The chosen proligand **3-n**, K₂CO₃ and S₈ were suspended in degassed EtOH and refluxed at 85 °C for 18 hours. The resulting suspension was concentrated to dryness and the crude product extracted into CH₂Cl₂. Purification by column chromatography (silica; CH₂Cl₂/MeOH) afforded the desired compounds as pale yellow solids.

CNCS₂-Me – 4-Me

3-Me (50 mg, 0.11 mmol) was reacted with K₂CO₃ (40 mg, 0.29 mmol) and S₈ (75 mg, 0.29 mmol) in EtOH (4 mL) according to the general procedure. The product was afforded as a pale-yellow solid following purification by column chromatography (silica; CH₂Cl₂ to CH₂Cl₂/ MeOH 49:1). Yield = 26.4 mg (73%).

¹H NMR (500 MHz, CDCl₃): δ 7.61 (t, ³J_{HH} = 7.7, 1H, py), 7.23 (d, ³J_{HH} = 7.8, 2H, py), 6.82 (d, ³J_{HH} = 2.4, 2H, NCH), 6.68 (d, ³J_{HH} = 2.4, 2H, NCH), 5.35 (s, 4H, pyCH₂), 3.64 (s, 6H, CH₃).

¹³C{¹H} NMR (126 MHz, CDCl₃): δ 163.2 (s, CS), 155.4 (s, py), 138.1 (py), 122.0 (s, py), 118.0 (s, NCH), 117.3 (s, NCH), 52.8 (s, pyCH₂), 35.5 (s, CH₃).

HR ESI-MS (positive ion, 4 kV): 332.0992 [M+H]⁺ (calcd 332.0998) *m/z*.

Elemental Anal. Calcd for (331.46 g·mol⁻¹): C, 54.36; H, 5.17; N, 21.13. Found: C, 54.18; H, 5.04; N, 21.05.

CNCS₂-12 – 4-12

3-12 (250 mg, 0.44 mmol) was reacted with K₂CO₃ (152 mg, 1.10 mmol) and S₈ (283 mg, 1.10 mmol) in EtOH (12 mL) according to the general procedure. The product was afforded as a pale-yellow solid following purification by column chromatography (silica; CH₂Cl₂ to CH₂Cl₂/MeOH 49:1). Yield = 123 mg (59%). Crystals suitable for X-ray diffraction were grown from a CHCl₃/hexane layer at RT.

^1H NMR (500 MHz, CDCl_3): δ 7.66 (t, $^3J_{\text{HH}} = 7.7$, 1H, py), 7.41 (d, $^3J_{\text{HH}} = 7.6$, 2H, py), 6.88 (d, $^3J_{\text{HH}} = 2.4$, 2H, NCH), 6.59 (d, $^3J_{\text{HH}} = 2.4$, 2H, NCH), 5.32 (s, 4H, pyCH₂), 4.04 (t, $^3J_{\text{HH}} = 6.8$, 4H, NCH₂), 1.75 (app. pent., $J = 7$, 4H, CH₂), 1.41 – 1.14 (m, 16H, CH₂).
 $^{13}\text{C}\{^1\text{H}\}$ NMR (126 MHz, CDCl_3): δ 162.3 (s, CS), 154.9 (s, py), 138.1 (py), 122.8 (s, py), 117.7 (s, NCH), 116.6 (s, NCH), 52.2 (s, pyCH₂), 47.8 (s, NCH₂), 28.3 (s, CH₂), 28.0 (s, CH₂), 27.7 (s, CH₂), 27.7 (s, CH₂), 25.6 (s, CH₂).

HR ESI-MS (positive ion, 4 kV): 492.2230 $[\text{M}+\text{Na}]^+$ (calcd 492.2226) m/z .

Elemental Anal. Calcd for $\text{C}_{25}\text{H}_{35}\text{N}_5\text{S}_2$ (469.71 $\text{g}\cdot\text{mol}^{-1}$): C, 63.93; H, 7.51; N, 14.91. Found: C, 63.86; H, 7.35; N, 14.92.

CNCS₂-14 – 4-14

3-14 (40 mg, 0.067 mmol) was reacted with K_2CO_3 (23 mg, 0.17 mmol) and S_8 (43 mg, 0.17 mmol) in EtOH (3 mL) according to the general procedure. The product was afforded as a pale-yellow solid following purification by column chromatography (silica; CH_2Cl_2 to CH_2Cl_2 :MeOH 19:1). Yield = 24 mg (73%).

^1H NMR (500 MHz, CDCl_3): δ 7.56 (t, $^3J_{\text{HH}} = 7.7$, 1H, py), 7.24 (d, $^3J_{\text{HH}} = 7.7$, 2H, py), 6.75 (d, $^3J_{\text{HH}} = 2.4$, 2H, NCH), 6.55 (d, $^3J_{\text{HH}} = 2.4$, 2H, NCH), 5.27 (s, 4H, pyCH₂), 3.99 (t, $^3J_{\text{HH}} = 6.8$, 4H, NCH₂), 1.77 (app. pent., $J = 7$, 4H, CH₂), 1.33 – 1.02 (m, 20H, CH₂).
 $^{13}\text{C}\{^1\text{H}\}$ NMR (126 MHz, CDCl_3): δ 162.6 (s, CS), 155.2 (s, py), 138.0 (s, py), 122.3 (s, py), 117.7 (s, NCH), 116.7 (s, NCH), 52.3 (s, pyCH₂), 48.0 (s, NCH₂), 28.6 (s, CH₂), 28.5 (s, CH₂), 28.5 (s, CH₂), 28.4 (s, CH₂), 28.4 (s, CH₂), 26.0 (s, CH₂).

HR ESI-MS (positive ion, 4 kV): 520.2537 $[\text{M}+\text{Na}]^+$ (calcd 520.2539) m/z .

Elemental Anal. Calcd for $\text{C}_{27}\text{H}_{39}\text{N}_5\text{S}_2$ (497.76 $\text{g}\cdot\text{mol}^{-1}$): C, 65.15; H, 7.90; N, 14.07. Found: C, 65.04; H, 7.90; N, 13.94.

CNCS₂-16 – 4-16

3-16 (40 mg, 0.064 mmol) was reacted with K_2CO_3 (22 mg, 0.16 mmol) and S_8 (41 mg, 0.16 mmol) in EtOH (3 mL) according to the general procedure. The product was afforded as a pale-yellow solid following purification by column chromatography (silica; CH_2Cl_2 to CH_2Cl_2 :MeOH 49:1). Yield = 26 mg (76%).

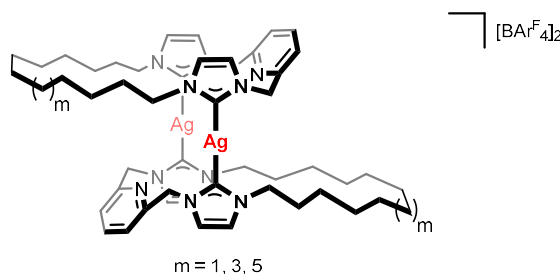
^1H NMR (500 MHz, CDCl_3): δ 7.59 (t, $^3J_{\text{HH}} = 7.8$, 1H, py), 7.20 (d, $^3J_{\text{HH}} = 7.7$, 2H, py), 6.81 (d, $^3J_{\text{HH}} = 2.4$, 2H, NCH), 6.65 (d, $^3J_{\text{HH}} = 2.4$, 2H, NCH), 5.37 (s, 4H, pyCH₂), 4.09 (t, $^3J_{\text{HH}} = 6.7$, 4H, NCH₂), 1.84 – 1.65 (m, 4H, CH₂), 1.38 – 1.07 (m, 24H, CH₂).

$^{13}\text{C}\{^1\text{H}\}$ NMR (126 MHz, CDCl_3): δ 162.8 (s, CS), 155.5 (s, py), 138.0 (s, py), 121.8 (s, py), 117.5 (s, NCH), 116.9 (s, NCH), 52.4 (s, pyCH₂), 48.1 (s, NCH₂), 29.1 (s, CH₂), 29.0 (s, CH₂), 28.8 (s, CH₂), 28.8 (s, CH₂), 28.7 (s, CH₂), 28.7 (s, CH₂), 26.2 (s, CH₂).

HR ESI-MS (positive ion, 4 kV): 548.2852 $[\text{M}+\text{Na}]^+$ (calcd 548.2852) m/z .

Elemental Anal. Calcd for $\text{C}_{29}\text{H}_{43}\text{N}_5\text{S}_2$ (525.82 $\text{g}\cdot\text{mol}^{-1}$): C, 66.24; H, 8.24; N, 13.32. Found: C, 66.35; H, 8.31; N, 13.13.

5.2.5. Preparation of silver complexes, $[\text{Ag}(\text{CNC-}n)]_2[\text{BAR}^{\text{F}}_4]_2 - 5\text{-}n$



General procedure¹¹

A suspension of chosen proligand **3-n** (1.0 eq), $\text{Na}[\text{BAR}^{\text{F}}_4]$ (1.1 eq) and Ag_2O (1.05 eq) in diethyl ether was stirred under nitrogen in the absence of light for 18 hours. The resulting grey suspension was filtered and concentrated *in vacuo*. Subsequent extraction into hot CHCl_3 , filtration and concentration *in vacuo* afforded the products as white powders.

$[\text{Ag}(\text{CNC-12})]_2[\text{BAR}^{\text{F}}_4]_2 - 5\text{-12}$

Compound prepared according to literature procedure.¹¹

^1H NMR (400 MHz, CD_2Cl_2): δ 7.71 (t, $^3J_{\text{HH}} = 8.0$, 1H, py), 7.76 – 7.68 (m, 8H, Ar^{F}), 7.47 (s, 4H, Ar^{F}), 7.28 (d, $^3J_{\text{HH}} = 7.8$, 2H, py), 7.07 (s, 2H, NCH), 6.96 (s, 2H, NCH), 5.19 (s, 4H, pyCH₂), 3.99 (t, $^3J_{\text{HH}} = 7.3$, 4H, NCH₂), 1.82 – 1.63 (m, 4H, CH₂), 1.35 – 1.01 (m, 16H, CH₂).

*Data consistent with literature values.*¹¹

$[\text{Ag}(\text{CNC-14})]_2[\text{BAR}^{\text{F}}_4]_2 - 5\text{-14}$

3-14 (50 mg, 0.084 mmol), $\text{Na}[\text{BAR}^{\text{F}}_4]$ (80 mg, 0.090 mmol) and Ag_2O (20 mg, 0.086 mmol) were reacted according to the general procedure to afford the desired product as a white powder. Yield = 52 mg (46%).

^1H NMR (500 MHz, CD_2Cl_2): δ 7.91 - 7.78 (m, 1H, py), 7.76 - 7.68 (m, 8H, Ar^{F}), 7.55 (s, 4H, Ar^{F}), 7.43 (d, $^3J_{\text{HH}} = 5.3$, 2H, py), 7.18 (br s, 2H, NCH), 7.06 (br s, 2H, NCH), 5.26 (br s, 4H, pyCH_2), 4.04 (t, $^3J_{\text{HH}} = 6.7$, 4H, NCH_2), 1.95 - 1.66 (m, 4H, CH_2), 1.29 (br s, 20H, CH_2).

$^{13}\text{C}\{^1\text{H}\}$ NMR (126 MHz, CD_2Cl_2): δ 181.3 (d, $^2J_{\text{AgC}} = 213$, NCN), 162.3 (q, $^1J_{\text{CB}} = 50$, Ar^{F}), 155.1 (s, py), 140.5 (s, py), 135.3 (s, Ar^{F}), 129.4 (qq, $^2J_{\text{FC}} = 32$, $^3J_{\text{CB}} = 3$, Ar^{F}), 125.1 (q, $^1J_{\text{FC}} = 272$, Ar^{F}), 125.1 (s, py), 123.9 (s, NCH), 120.4 (s, NCH), 118.0 (sept., $^3J_{\text{FC}} = 4$, Ar^{F}), 57.2 (s, pyCH_2), 54.3 (s, NCH_2), 31.8 (s, CH_2), 28.4 (s, CH_2), 27.9 (s, CH_2), 27.2 (s, CH_2), 27.0 (s, CH_2), 26.7 (s, CH_2).

HR ESI-MS (positive ion, 4 kV): 540.2260 [$\text{C}_{27}\text{H}_{39}\text{AgN}_5$] $^+$ (calcd 540.2251) m/z .

[Ag(CNC-16)] $_2$ [BAr $^{\text{F}}$ $_4$] $_2$ – 5-16

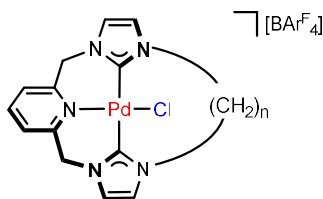
3-16 (50 mg, 0.080 mmol), Na[BAr $^{\text{F}}$ $_4$] (80 mg, 0.090 mmol) and Ag $_2$ O (20 mg, 0.086 mmol) were reacted according to the general procedure to afford the desired product as a white powder. Yield = 38 mg (34%).

^1H NMR (500 MHz, CD_2Cl_2): δ 7.78 - 7.56 (m, 9H, Ar^{F} + py), 7.47 (s, 4H, Ar^{F}), 7.33 (br s, 2H), 7.05 (br s, 2H), 6.97 (d, $^3J_{\text{HH}} = 1.8$, 2H, NCH), 5.16 (s, 4H, pyCH_2), 4.09 - 3.79 (m, 4H, NCH_2), 2.01 - 1.56 (m, 4H, CH_2), 1.34 - 1.05 (m, 24H, CH_2).

$^{13}\text{C}\{^1\text{H}\}$ NMR data for this complex could not be obtained at 298 K due to the dynamic behaviour of the complex in solution.

HR ESI-MS (positive ion, 4 kV): 568.2559 [$\text{C}_{29}\text{H}_{43}\text{AgN}_5$] $^+$ (calcd 568.2564) m/z .

5.2.6. Preparation of palladium chloride complexes, [Pd(CNC- n)Cl][BAr $^{\text{F}}$ $_4$] – 6- n



General Procedure

A suspension of **3- n** (1 eq), Ag $_2$ O (1.1 eq) and Na[BAr $^{\text{F}}$ $_4$] (1.2 eq) in CH_2Cl_2 was stirred under nitrogen in the absence of light for 20 hours. The resulting grey suspension was allowed to settle and filtered into a flask charged with solid [Pd(NCMe) $_2$ Cl $_2$] (1.1 eq). After stirring the resulting suspension for 6 hours, the

solution was passed through a short plug (silica; CH₂Cl₂) to give the crude products.

[Pd(CNC-12)Cl][BAr^F₄] – 6-12

Prepared as described in the literature.⁹

¹H NMR (400 MHz, CDCl₃): δ 7.76 – 7.68 (m, 8H, Ar^F), 7.55 (t, ³J_{HH} = 7.7, 1H, py), 7.48 (s, 4H, Ar^F), 7.32 (d, ³J_{HH} = 7.9, 2H, py), 7.04 (s, 2H, NCH), 6.90 (s, 2H, NCH), 5.62 (d, ²J_{HH} = 15.1, 2H, pyCH₂), 5.00 (d, ²J_{HH} = 15.4, 2H, pyCH₂), 4.78 – 4.58 (m, 2H, NCH₂), 3.85 – 3.61 (m, 2H, NCH₂), 2.25 – 1.99 (m, 2H, CH₂), 1.81 – 1.63 (m, 2H, CH₂), 1.41 (s, 16H, CH₂).

*Data consistent with literature values.*⁹

[Pd(CNC-14)Cl][BAr^F₄] – 6-14

3-14 (45 mg, 0.076 mmol), Ag₂O (21 mg, 0.091 mmol) and Na[BAr^F₄] (89 mg, 0.10 mmol) were reacted according to the general procedure with [Pd(NCMe)₂Cl₂] (23 mg, 0.089 mmol) and the product purified by column chromatography (silica; CH₂Cl₂/hexane 7:3). Removal of the solvent *in vacuo* resulted in isolation of the product as a white solid. Yield = 35 mg (31%). Crystals suitable for X-ray diffraction were grown from a mixture of THF/ hexane at 20 °C.

¹H NMR (500 MHz, CD₂Cl₂): δ 7.95 (t, ³J_{HH} = 7.7, 1H, py), 7.76 – 7.68 (m, 8H, Ar^F), 7.58 (d, ³J_{HH} = 7.7, 2H, py), 7.55 (s, 4H, Ar^F), 7.15 (d, ³J_{HH} = 1.9, 2H, NCH), 6.98 (d, ³J_{HH} = 1.9, 2H, NCH), 5.74 (d, ²J_{HH} = 15.0, 2H, pyCH₂), 5.10 (d, ²J_{HH} = 15.0, 2H, pyCH₂), 4.84 (td, ²J_{HH} = 12.3, ³J_{HH} = 4.8, 2H, NCH₂), 3.77 (td, ²J_{HH} = 12.1, ³J_{HH} = 5.3, 2H, NCH₂), 2.08 – 1.92 (m, 2H, CH₂), 1.89 – 1.72 (m, 2H, CH₂), 1.46 – 1.19 (m, 20H, CH₂).

¹³C{¹H} NMR (126 MHz, CD₂Cl₂): δ 165.6 (s, NCN), 162.3 (q, ¹J_{CB} = 50, Ar^F), 155.7 (s, py), 142.0 (s, py), 135.3 (s, Ar^F), 129.4 (qq, ²J_{FC} = 32, ³J_{CB} = 3, Ar^F), 125.9 (s, py), 125.1 (q, ¹J_{FC} = 272, Ar^F), 122.3 (s, NCH), 121.7 (s, NCH), 118.0 (sept., ³J_{FC} = 4, Ar^F), 56.3 (s, pyCH₂), 51.2 (s, NCH₂), 31.7 (s, CH₂), 29.1 (s, CH₂), 28.5 (s, CH₂), 28.0 (s, CH₂), 27.9 (s, CH₂), 25.1 (s, CH₂).

HR ESI-MS (positive ion, 4 kV): 574.1926 [M]⁺ (calcd 574.1930) *m/z*.

Elemental Anal. Calcd for $C_{59}H_{51}BClF_{24}N_5Pd$ ($1438.73 \text{ g}\cdot\text{mol}^{-1}$): C, 49.26; H, 3.57; N, 4.87. Found: C, 49.17; H, 3.69; N, 4.82.

[Pd(CNC-16)Cl][BAr^F₄] – 6-16

3-16 (55 mg, 0.088 mmol), Ag₂O (25 mg, 0.10 mmol) and Na[BAr^F₄] (96 mg, 0.11 mmol) were reacted according to the general procedure with [Pd(NCMe)₂Cl₂] (26 mg, 0.10 mmol). The product was purified by column chromatography (silica; CH₂Cl₂/hexane 4:1) to give a white solid. Yield = 54 mg (41%). Crystals suitable for X-ray diffraction were grown from a mixture of diethyl ether/pentane at 20 °C.

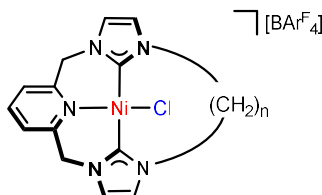
¹H NMR (500 MHz, CD₂Cl₂): δ 7.76 – 7.68 (m, 8H, Ar^F), 7.54 (t, ³J_{HH} = 7.7, 1H, py), 7.48 (s, 4H, Ar^F), 7.29 (d, ³J_{HH} = 7.7, 2H, py), 7.01 (d, ³J_{HH} = 1.8, 2H, NCH), 6.90 (d, ³J_{HH} = 1.8, 2H, NCH), 5.66 (d, ²J_{HH} = 15.0, 2H, pyCH₂), 4.95 (d, ²J_{HH} = 15.0, 2H, pyCH₂), 4.83 (td, ²J_{HH} = 12.3, ³J_{HH} = 5.1, 2H, NCH₂), 3.85 (td, ²J_{HH} = 12.5, ³J_{HH} = 5.1, 2H, NCH₂), 2.08 – 1.94 (m, 2H, CH₂), 1.89 – 1.73 (m, 2H, CH₂), 1.50 – 1.13 (m, 24H, CH₂).

¹³C{¹H} NMR (126 MHz, CD₂Cl₂): δ 165.6 (s, NCN), 162.3 (q, ¹J_{CB} = 50, Ar^F), 155.77 (s, py), 142.0 (s, py), 135.3 (s, Ar^F), 129.4 (qq, ²J_{FC} = 32, ³J_{CB} = 3, Ar^F), 125.9 (s, py), 125.1 (q, ¹J_{FC} = 272, Ar^F), 122.2 (s, NCH), 121.7 (s, NCH), 118.0 (sept., ³J_{FC} = 4, Ar^F), 56.3 (s, pyCH₂), 51.1 (s, NCH₂), 31.7 (s, CH₂), 28.8 (s, CH₂), 28.8 (s, CH₂), 28.5 (s, CH₂), 28.5 (s, CH₂), 28.4 (s, CH₂), 26.0 (s, CH₂).

HR ESI-MS (positive ion, 4 kV): 602.2247 [M]⁺ (calcd 602.2244) *m/z*.

Elemental Anal. Calcd for $C_{61}H_{55}BClF_{24}N_5Pd$ ($1466.79 \text{ g}\cdot\text{mol}^{-1}$): C, 49.95; H, 3.78; N, 4.77. Found: C, 50.18; H, 3.83; N, 4.75.

5.2.7. Preparation of nickel chloride complexes, [Ni(CNC-*n*)Cl][BAr^F₄] – 7-*n*



[Ni(CNC-Me)Cl][BAr^F₄] – 7-Me

A suspension of **3-Me** (100 mg, 0.233 mmol), Na[BAr^F₄] (230 mg, 0.260 mmol) and Ag₂O (57 mg, 0.25 mmol) in diethyl ether (5 mL) was stirred in the absence

of light under nitrogen for 18 hours before being allowed to settle and filtered onto [Ni(DME)Cl₂] (56 mg, 0.26 mmol). The resulting green suspension was stirred in the absence of light for a further 20 hours before being filtered to give a yellow solution. The product was obtained as a yellow powder following the removal of solvents *in vacuo*. Yield = 226 mg (79%).

¹H NMR (500 MHz, CD₂Cl₂): δ 7.80 (t, ³J_{HH} = 7.7, 1H, py), 7.76 – 7.68 (m, 8H, Ar^F), 7.55 (s, 4H, Ar^F), 7.44 (d, ³J_{HH} = 7.7, 2H, py), 7.11 (d, ³J_{HH} = 1.7, 2H, NCH), 6.83 (d, ³J_{HH} = 1.7, 2H, NCH), 6.35 (d, ²J_{HH} = 15.0, 2H, pyCH₂), 5.16 (d, ²J_{HH} = 15.0, 2H, pyCH₂), 3.96 (s, 6H, CH₃).

¹³C{¹H} NMR (126 MHz, CD₂Cl₂): δ 163.3 (s, NCN), 162.3 (q, ¹J_{CB} = 50, Ar^F), 156.5 (s, py), 140.9 (s, py), 135.3 (s, Ar^F), 129.5 (qq, ²J_{FC} = 32, ³J_{CB} = 3, Ar^F), 125.1 (q, ¹J_{FC} = 271, Ar^F), 125.1 (s, py), 124.7 (s, NCH), 121.3 (s, NCH), 118.0 (sept., ³J_{FC} = 4, Ar^F), 55.1 (s, pyCH₂), 38.3 (s, CH₃).

HR ESI-MS (positive ion, 4 kV): 360.0521, [M]⁺ (calcd 360.0520) *m/z*.

Elemental Anal. Calcd for C₄₇H₂₉BClF₂₄N₅Ni (1224.70 g·mol⁻¹): C, 46.09; H, 2.39; N, 5.72. Found: C, 46.04; H, 2.55; N, 5.71.

[Ni(CNC-12)Cl][BAr^F₄] – 7-12

A mixture of **3-12** (100 mg, 0.176 mmol), Ag₂O (45 mg, 0.19 mmol) and Na[BAr^F₄] (172 mg, 0.194 mmol) was suspended in CH₂Cl₂ (3 mL) and stirred under nitrogen in the absence of light for 20 hours. The resulting grey suspension was allowed to settle and the solution filtered into a flask charged with solid [Ni(DME)Cl₂] (40 mg, 0.18 mmol). After stirring the resulting suspension for 6 hours, the solution was passed through a short plug (alumina; CH₂Cl₂) and the product obtained as a yellow powder on removal of volatiles *in vacuo*. Yield = 70 mg (29%). Crystals suitable for X-ray diffraction were grown from a mixture of toluene, diethyl ether, cyclohexane and pentane at 20°C.

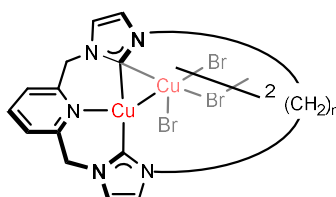
¹H NMR (500 MHz, CD₂Cl₂): δ 7.82 (t, ³J_{HH} = 7.7, 1H, py), 7.76 – 7.68 (m, 8H, Ar^F), 7.55 (s, 4H, Ar^F), 7.45 (d, ³J_{HH} = 7.7, 2H, py), 7.11 (d, ³J_{HH} = 1.7, 2H, NCH), 6.87 (d, ³J_{HH} = 1.7, 2H, NCH), 6.30 (d, ²J_{HH} = 15.0, 2H, pyCH₂), 5.14 (d, ²J_{HH} = 15.0, 2H, pyCH₂), 4.73 (app. t, *J* = 12, 2H, NCH₂), 3.78 – 3.68 (m, 2H, NCH₂), 1.94 (br s, 2H, CH₂), 1.66 (br s, 2H, CH₂), 1.18 – 1.50 (m, 14H, CH₂), 1.09 (br s, 2H, CH₂).

$^{13}\text{C}\{^1\text{H}\}$ NMR (126 MHz, CD_2Cl_2): δ 162.3 (q, $^1J_{\text{CB}} = 50$, Ar^{F}), 162.0 (s, NCN), 156.5 (s, py), 140.9 (s, py), 135.3 (s, Ar^{F}), 129.4 (qq, $^2J_{\text{FC}} = 32$, $^3J_{\text{CB}} = 3$, Ar^{F}), 125.2 (q, $^1J_{\text{FC}} = 271$, Ar^{F}), 125.1 (s, py), 123.0 (s, NCH), 121.4 (s, NCH), 118.0 (sept., $^3J_{\text{FC}} = 4$, Ar^{F}), 55.0 (s, pyCH_2), 51.3 (s, NCH_2), 30.8 (s, CH_2), 28.7 (s, CH_2), 27.5 (s, CH_2), 23.7 (s, CH_2).

HR ESI-MS (positive ion, 4 kV): 498.1929, $[\text{M}]^+$ (calcd 498.1929) m/z .

Elemental Anal. Calcd for $\text{C}_{57}\text{H}_{47}\text{BClF}_{24}\text{N}_5\text{Ni}$ ($1362.95 \text{ g}\cdot\text{mol}^{-1}$): C, 50.23; H, 3.48; N, 5.14. Found: C, 50.62; H, 3.74; N, 5.05.

5.2.8. Preparation of copper bromide complexes, $[\text{Cu}(\text{CNC-}n)]_2[\text{Cu}_2\text{Br}_4] - 8\text{-}n$



General Procedure¹¹

A solution of $\text{KO}t\text{Bu}$ (2.5 eq) in THF was slowly added to a suspension of chosen proligand **3-n** (1.0 eq) and CuBr (3.0 eq) in THF at -78°C to result an orange suspension, which was left stirring for an hour at -78°C before warming to room temperature. After reacting for a further 16 hours the resulting yellow suspension was filtered and extracted with MeCN. The desired products were obtained on removal of volatiles *in vacuo*.

$[\text{Cu}(\text{CNC-Me})]_2[\text{Cu}_2\text{Br}_4] - 8\text{-Me}$

3-Me (100 mg, 0.233 mmol), $\text{KO}t\text{Bu}$ (65 mg, 0.58 mmol) and CuBr (100 mg, 0.697 mmol) were reacted according to the general procedure to give the product as a yellow powder. Yield = 69 mg (54%).

^1H NMR (500 MHz, CD_2Cl_2): δ 7.75 (t, $^3J_{\text{HH}} = 7.7$, 1H, py), 7.29 (d, $^3J_{\text{HH}} = 7.7$, 2H, py), 7.18 (d, $^3J_{\text{HH}} = 1.8$, 2H, NCH), 6.95 (d, $^3J_{\text{HH}} = 1.8$, 2H, NCH), 5.39 (s, 4H, pyCH_2), 3.85 (s, 6H, CH_3).

$^{13}\text{C}\{^1\text{H}\}$ NMR (126 MHz, CD_2Cl_2): δ 178.9 (s, NCN), 156.1 (s, py), 139.2 (s, py), 122.8 (s, py), 122.4 (s, NCH), 122.2 (s, NCH), 56.5 (s, pyCH_2), 38.9 (s, CH_3).

HR ESI-MS (positive ion, 4 kV): 330.0769, $[\text{M}]^+$ (calcd 330.0774) m/z .

[Cu(CNC-12)]₂[Cu₂Br₄] – 8-12

Compound was prepared using a modified literature procedure.¹¹

¹H NMR (300 MHz, CD₂Cl₂): δ 7.80 (t, ³J_{HH} = 7.7, 1H, py), 7.42 (d, ³J_{HH} = 7.7, 2H, py), 7.21 (d, ³J_{HH} = 1.9, 2H, NCH), 6.98 (s, 2H, NCH), 5.37 (s, 4H, pyCH₂), 4.18 (t, ³J_{HH} = 6.9, 4H, NCH₂), 1.86 (pent., ³J_{HH} = 7.1, 4H, CH₂), 1.43 – 1.06 (m, 16H, CH₂).

*Data consistent with literature values.*¹¹

[Cu(CNC-14)]₂[Cu₂Br₄] – 8-14

3-14 (500 mg, 0.840 mmol) was reacted with KO^tBu (236 mg, 2.10 mmol) and CuBr (362 mg, 2.52 mmol) according to the general procedure to give the product as a yellow powder. Yield = 523 mg (83%). Crystals suitable for X-ray diffraction were grown from a saturated solution in MeCN at 18 °C.

¹H NMR (400 MHz, d₃-MeCN): δ 7.85 (t, ³J_{HH} = 7.7, 1H, py), 7.42 (d, ³J_{HH} = 7.7, 2H, py), 7.25 (d, ³J_{HH} = 1.8, 2H, NCH), 7.14 (d, ³J_{HH} = 1.8, 2H, NCH), 5.32 (s, 4H, pyCH₂), 4.18 (t, ³J_{HH} = 7.0, 4H, NCH₂), 1.85 (pent., ³J_{HH} = 7.2, 4H, CH₂), 1.43 – 1.21 (m, 20H, CH₂).

¹H NMR (500 MHz, CD₂Cl₂): δ 7.81 (t, ³J_{HH} = 7.7, 1H, py), 7.36 (d, ³J_{HH} = 7.7, 2H, py), 7.16 (d, ³J_{HH} = 1.8, 2H, NCH), 7.00 (d, ³J_{HH} = 1.8, 2H, NCH), 5.47 (s, 4H, pyCH₂), 4.23 (t, ³J_{HH} = 7.1, 4H, NCH₂), 1.88 (pent., ³J_{HH} = 6.9, 4H, CH₂), 1.50 – 1.09 (m, 20H, CH₂).

¹³C{¹H} NMR (126 MHz, CD₂Cl₂): δ 175.3 (s, NCN), 155.6 (s, py), 139.8 (s, py), 123.5 (s, py), 122.8 (s, NCH), 121.4 (s, NCH), 56.1 (s, pyCH₂), 52.3 (s, NCH₂), 31.5 (s, CH₂), 28.7 (s, CH₂), 28.7 (s, CH₂), 28.4 (s, CH₂), 28.4 (s, CH₂), 26.5 (s, CH₂).

HR ESI-MS (positive ion, 4 kV): 496.2492, [M]⁺ (calcd 496.2496) *m/z*.

[Cu(CNC-16)]₂[Cu₂Br₄] – 8-16

3-16 (200 mg, 0.321 mmol), KO^tBu (100 mg, 0.891 mmol) and CuBr (138 mg, 0.962 mmol) were reacted according to the general procedure to give the product as a yellow powder. Yield = 206 mg (86%).

¹H NMR (500 MHz, CD₂Cl₂): δ 7.82 (t, ³J_{HH} = 7.7, 1H, py), 7.36 (d, ³J_{HH} = 7.7, 2H, py), 7.13 (d, ³J_{HH} = 1.8, 2H, NCH), 7.00 (d, ³J_{HH} = 1.8, 2H, NCH), 5.50 (s, 4H, pyCH₂),

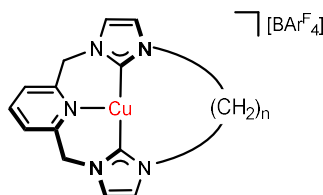
4.23 (t, $^3J_{\text{HH}} = 7.1$, 4H, NCH₂), 1.87 (pent., $^3J_{\text{HH}} = 7.1$, 4H, CH₂), 1.40 – 1.10 (m, 20H, CH₂).

$^{13}\text{C}\{^1\text{H}\}$ NMR (126 MHz, CD₂Cl₂): δ 175.5 (s, NCN),* 155.8 (s, py), 139.8 (s, py), 123.6 (s, py), 122.5 (s, NCH), 121.4 (s, NCH), 56.1 (s, pyCH₂), 52.2 (s, NCH₂), 31.5 (s, CH₂), 29.3 (s, CH₂), 29.1 (s, CH₂), 29.1 (s, CH₂), 28.9 (s, CH₂), 28.8 (s, CH₂), 26.5 (s, CH₂).

HR ESI-MS (positive ion, 4 kV): 524.2808, [M]⁺ (calcd 524.2809) *m/z*.

* Located using a correlation experiment.

5.2.9. Preparation of copper [BAr^F₄] complexes, [Cu(CNC-*n*)] [BAr^F₄]- **9-n**



General Procedure¹¹

A suspension of the chosen copper bromide complex, **8-n** (1.0 eq) and Na[BAr^F₄] (2.5 eq) in toluene was stirred vigorously for 48 hours. After filtration and washing the precipitate with excess CH₂Cl₂ the desired products were obtained *via* removal of volatiles *in vacuo*.

[Cu(CNC-Me)] [BAr^F₄] – **9-Me**

8-Me (50 mg, 0.045 mmol) was reacted with Na[BAr^F₄] (100 mg, 0.113 mmol) in toluene (2 mL) according to the general procedure to afford the product as a yellow powder. Yield = 69 mg (64%).

^1H NMR (500 MHz, CD₂Cl₂): δ 7.86 (t, $^3J_{\text{HH}} = 7.6$, 1H, py), 7.66 – 7.78 (m, 8H, Ar^F), 7.55 (s, 4H, Ar^F), 7.46 (d, $^3J_{\text{HH}} = 7.8$, 2H, py), 7.11 (s, 2H, NCH), 7.02 (s, 2H, NCH), 5.21 (s, 4H, pyCH₂), 3.88 (s, 6H, CH₃).

$^{13}\text{C}\{^1\text{H}\}$ NMR (126 MHz, CD₂Cl₂): δ 180.0 (s, NCN),* 162.2 (q, $^1J_{\text{CB}} = 50$, Ar^F), 154.5 (s, py), 140.4 (s, py), 135.3 (s, Ar^F), 129.4 (qq, $^2J_{\text{FC}} = 32$, $^3J_{\text{CB}} = 3$, Ar^F), 125.2 (q, $^1J_{\text{FC}} = 271$, Ar^F), 124.6 (s, py), 123.0 (s, NCH), 121.5 (s, NCH), 118.0 (sept., $^3J_{\text{FC}} = 4$, Ar^F), 55.3 (s, pyCH₂), 39.4 (s, CH₃).

* Located using a correlation experiment.

HR ESI-MS (positive ion, 4 kV): 330.0781 ([M]⁺, calcd 330.0774) *m/z*.

Elemental Anal. Calcd for $C_{47}H_{29}BCuF_{24}N_5$ ($1360.41 \text{ g}\cdot\text{mol}^{-1}$): C, 47.28; H, 2.45; N, 5.87. Found: C, 47.37; H, 2.39; N, 5.81.

[Cu(CNC-12)][BAr^F₄] – 9-12

Compound prepared using a modified literature procedure.¹¹ Samples suitable for X-ray diffraction were grown from a CH_2Cl_2 /hexane layer at $-30^\circ C$.

¹H NMR (400 MHz, CD_2Cl_2): δ 7.87 (t, $^3J_{HH} = 7.7$, 1H, py), 7.78 – 7.68 (m, 8H, Ar^F), 7.55 (s, 4H, Ar^F), 7.45 (d, $^3J_{HH} = 7.7$, 2H, py), 7.12 (d, $^3J_{HH} = 1.9$, 2H, NCH), 7.04 (s, 2H, NCH), 5.20 (s, 4H, pyCH₂), 4.43 – 4.01 (m, 4H, NCH₂), 2.09 – 1.71 (m, 4H, CH₂), 1.52 – 1.22 (m, 16H, CH₂).

*Data consistent with literature values.*¹¹

[Cu(CNC-14)][BAr^F₄] – 9-14

8-14 (520 mg, 0.361 mmol) was reacted with Na[BAr^F₄] (800 mg, 0.903 mmol) in toluene (15 mL) according to the general procedure to afford the product as a yellow powder. Yield = 641 mg (65%). Crystals suitable for X-ray diffraction were grown from slow diffusion of hexane into a saturated solution in THF at $0^\circ C$.

¹H NMR (500 MHz, CD_2Cl_2): δ 7.85 (t, $^3J_{HH} = 7.7$, 1H, py), 7.77 – 7.68 (m, 8H, Ar^F), 7.55 (s, 4H, Ar^F), 7.44 (d, $^3J_{HH} = 7.8$, 2H, py), 7.11 (d, $^3J_{HH} = 1.7$, 2H, NCH), 7.03 (d, $^3J_{HH} = 1.7$, 2H, NCH), 5.20 (s, 4H, pyCH₂), 4.18 (t, $^3J_{HH} = 7.4$, 4H, NCH₂), 1.87 (app. pent., $J = 7.2$, 4H, CH₂), 1.42 – 1.26 (m, 20H, CH₂).

¹³C{¹H} NMR (126 MHz, CD_2Cl_2): δ 179.9 (s, NCN), 162.3 (q, $^1J_{CB} = 50$, Ar^F), 154.0 (s, py), 140.3 (s, py), 135.4 (s, Ar^F), 129.5 (qq, $^2J_{FC} = 32$, $^3J_{CB} = 3$, Ar^F), 125.2 (q, $^1J_{FC} = 271$, Ar^F), 124.1 (s, py), 123.0 (s, NCH), 120.0 (s, NCH), 118.0 (sept., $^3J_{FC} = 4$, Ar^F), 55.0 (s, pyCH₂), 53.1 (s, NCH₂), 31.8 (s, CH₂), 28.2 (s, CH₂), 27.7 (s, CH₂), 26.8 (s, CH₂), 26.7 (s, CH₂), 26.5 (s, CH₂).

HR ESI-MS (positive ion, 4 kV): 496.24.92, [M]⁺ (calcd 496.2496) *m/z*.

Elemental Anal. Calcd for $C_{59}H_{51}BCuF_{24}N_5$ ($1360.41 \text{ g}\cdot\text{mol}^{-1}$): C, 52.09; H, 3.78; N, 5.15. Found: C, 51.95; H, 3.90; N, 5.07.

[Cu(CNC-16)][BAr^F₄] – 9-16

8-16 (200 mg, 0.134 mmol) was reacted with Na[BAr^F₄] (296 mg, 0.334 mmol) in toluene (12 mL) according to the general procedure to afford the product as a yellow powder. Yield = 126 mg (68%).

¹H NMR (500 MHz, CD₂Cl₂): δ 7.84 (t, ³J_{HH} = 7.7, 1H, py), 7.78 – 7.65 (m, 8H, Ar^F), 7.56 (s, 4H, Ar^F), 7.44 (d, ³J_{HH} = 7.8, 2H, py), 7.09 (s, 2H, NCH), 7.03 (d, ³J_{HH} = 1.7, 2H, NCH), 5.19 (s, 4H, pyCH₂), 4.16 (t, ³J_{HH} = 7.4, 4H, NCH₂), 1.92 – 1.80 (m, 4H, CH₂), 1.44 – 1.21 (m, 24H, CH₂).

¹³C{¹H} NMR (126 MHz, CD₂Cl₂): δ 179.6 (s, NCN), 162.3 (q, ¹J_{CB} = 50, Ar^F), 154.2 (s, py), 140.3 (s, py), 135.4 (s, Ar^F), 129.5 (qq, ²J_{FC} = 32, ³J_{CB} = 3, Ar^F), 125.2 (q, ¹J_{FC} = 271, Ar^F), 124.4 (s, py), 122.9 (s, NCH), 120.1 (s, NCH), 118.0 (sept., ³J_{FC} = 4, Ar^F), 55.1 (s, pyCH₂), 53.1 (s, NCH₂), 32.1 (s, CH₂), 29.3 (s, CH₂), 28.5 (s, CH₂), 27.7 (s, CH₂), 27.5 (s, CH₂), 27.2 (s, CH₂), 26.6 (s, CH₂).

HR ESI-MS (positive ion, 4 kV): 524.2814, [M]⁺ (calcd 524.2809) *m/z*.

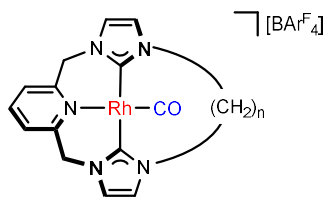
Elemental Anal. Calcd for C₆₁H₅₅BCuF₂₄N₅ (1388.46 g·mol⁻¹): C, 52.77; H, 3.99; N, 5.04. Found: C, 50.22; H, 3.91; N, 4.68.*

*Despite multiple attempts satisfactory microanalyses for this compound could not be obtained.

5.2.10. Transmetalation reactions

A J. Young's valve NMR tube was charged with 0.004/0.008 mmol of **5-12/7-12/9-12** and 1.1 equivalent (per metal) of [Pd(NCMe)₂Cl₂]/[Rh(CO)₂Cl]₂/[Ni(DME)Cl₂]/ [Rh(C₂H₂)₂Cl]₂. CD₂Cl₂ (0.5 mL) was added and the reaction monitored by ¹H NMR spectroscopy (400 MHz) until completion consumption of the Ag/Ni/Cu starting materials. The samples were periodically placed in an ultrasound bath during the course of the reaction.

5.2.11. Preparation of rhodium carbonyl complexes, $[Rh(CNC-n)(CO)][BAR^F_4]$ – 10-n



General procedure from the rhodium ethylene complexes

A solution of chosen rhodium ethylene complex, **11-n**, in 1,2-difluorobenzene was freeze-pump-thaw degassed and placed under an atmosphere of CO (1 atm) resulting in an immediate colour change from red to yellow. The desired products were obtained as yellow solids after removal of volatiles *in vacuo*.

General procedure using silver transfer agent

A suspension of **3-n** (1 eq), Ag₂O (1.1 eq) and Na[BAr^F₄] (1.2 eq) in CH₂Cl₂ (3 mL) was stirred under nitrogen in the absence of light for 20 hours. This was filtered onto [Rh(CO)₂Cl]₂ (1.1 eq) and the resulting orange suspension stirred for a further 8 hours. After this the suspension was filtered and the mildly air and moisture sensitive products obtained through purification by passing through a short plug (silica; CH₂Cl₂).

$[Rh(CNC-Me)(CO)][BAR^F_4]$ – 10-Me

Compound prepared from reaction of **11-Me** (13 mg, 0.010 mmol) with CO (1 atm) according to the general procedure to obtain the product as a bright yellow powder. Yield = 13 mg (99%).

¹H NMR (400 MHz, CD₂Cl₂): δ 7.87 (t, ³J_{HH} = 7.7, 1H, py), 7.67 – 7.77 (m, 8H, Ar^F), 7.55 (s, 4H, Ar^F), 7.50 (d, ³J_{HH} = 7.7, 2H, py), 7.13 (d, ³J_{HH} = 1.9, 2H, NCH), 6.97 (d, ³J_{HH} = 1.8, 2H, NCH), 5.46 (br, 2H, pyCH₂), 5.05 (br, 2H, pyCH₂), 3.83 (s, 6H, NCH₃).
¹³C{¹H} NMR (101 MHz, CD₂Cl₂): δ 193.6 (d, ¹J_{RhC} = 80, CO), 182.9 (d, ¹J_{RhC} = 42, NCN), 162.3 (q, ¹J_{CB} = 50, Ar^F), 158.0 (s, py), 141.5 (s, py), 135.4 (s, Ar^F), 129.5 (qq, ²J_{FC} = 32, ³J_{CB} = 3, Ar^F), 125.2 (q, ¹J_{FC} = 271, Ar^F), 124.9 (s, py), 122.7 (s, NCH), 121.7 (s, NCH), 118.0 (sept., ³J_{FC} = 4, Ar^F), 55.8 (d, ³J_{RhC} = 2, pyCH₂), 38.4 (d, ³J_{RhC} = 1, NCH₃).

^1H NMR (300 MHz, d_3 -MeCN, CO): δ 7.97 (t, $^3J_{\text{HH}} = 7.8$, 1H, py), 7.67 – 7.77 (m, 12H, Ar^F), 7.62 (d, $^3J_{\text{HH}} = 7.8$, 2H, py), 7.30 (d, $^3J_{\text{HH}} = 1.8$, 2H, NCH), 7.11 (d, $^3J_{\text{HH}} = 1.7$, 2H, NCH), 5.31 (s, 4H, pyCH₂), 3.81 (s, 6H, NCH₃).

HR ESI-MS (positive ion, 4 kV): 398.0485, [M]⁺ (calcd 398.0483) m/z .

Elemental Anal. Calcd for C₄₈H₂₉BF₂₄N₅ORh (1261.47 g·mol⁻¹): C, 45.70; H, 2.32; N, 5.55. Found: C, 45.59; H, 2.37; N, 5.67.

IR (CH₂Cl₂): $\nu(\text{CO})$ 1980 cm⁻¹

[Rh(CNC-12)CO][BAr^F₄] – 10-12

Compound prepared from reaction of **11-12** (14 mg, 0.010 mmol) with CO (1 atm) according to the general procedure to give the desired product as a bright yellow powder. Yield = 13 mg (92%).

^1H NMR (400 MHz, CD₂Cl₂): δ 7.89 (t, $^3J_{\text{HH}} = 7.7$, 1H, py), 7.77 – 7.67 (m, 8H, Ar^F), 7.55 (s, 4H, Ar^F), 7.51 (d, $^3J_{\text{HH}} = 7.7$, 2H, py), 7.14 (d, $^3J_{\text{HH}} = 1.9$, 2H, NCH), 7.01 (d, $^3J_{\text{HH}} = 1.9$, 2H, NCH), 5.45 (d, $^2J_{\text{HH}} = 14.9$, 2H, pyCH₂), 5.03 (d, $^2J_{\text{HH}} = 14.9$, 2H, pyCH₂), 4.30 (s, 2H, NCH₂), 3.99 (s, 2H, CH₂), 1.93 (s, 4H, CH₂), 1.84 (s, 4H, CH₂), 1.56 – 1.08 (m, 8H, CH₂).

^1H NMR (300 MHz, d_3 -MeCN (Ar)): δ 7.98 (t, $^3J_{\text{HH}} = 7.9$, 1H, py), 7.73 – 7.65 (m, 12H, Ar^F), 7.62 (d, $^3J_{\text{HH}} = 7.6$, 2H, py), 7.30 (s, 2H, NCH), 7.15 (s, 2H, NCH), 5.29 (s, 4H, pyCH₂), 4.15 (br s, fwhm = 42, 4H, NCH₂), 1.51 – 0.93 (m, 20H, CH₂).

^1H NMR (300 MHz, d_3 -MeCN (CO)): δ 7.98 (t, $^3J_{\text{HH}} = 8.0$, 1H, py), 7.73 – 7.65 (m, 12H, Ar^F), 7.63 (d, $^3J_{\text{HH}} = 8.4$, 2H, py), 7.32 (s, 2H, NCH), 7.16 (s, 2H, NCH), 5.27 (s, 4H, pyCH₂), 4.16 (t, $^3J_{\text{HH}} = 7.8$, 4H, NCH₂), 1.64 – 1.00 (m, 20H, CH₂).

LR ESI-MS (positive ion, 4 kV): 536.2, [M]⁺ (calcd 536.19) m/z .

IR (CH₂Cl₂): $\nu(\text{CO})$ 1978 cm⁻¹

*Data consistent with literature values.*¹²

[Rh(CNC-14)CO][BAr^F₄] – 10-14

3-14 (50 mg, 0.084 mmol), Na[BAr^F₄] (89 mg, 0.10 mmol) and Ag₂O (21 mg, 0.091 mmol) were reacted with [Rh(CO)₂Cl]₂ (18 mg, 0.046 mmol) according to the general procedure to yield the desired product as fine yellow crystals. Yield = 96

mg (84%). Crystals suitable for X-ray diffraction were grown from a mixture of CH₂Cl₂/heptane at 20 °C.

Compound prepared from reaction of **11-14** (14 mg, 0.010 mmol), with CO (1 atm) in CD₂Cl₂ according to the general procedure to afford the product as a yellow powder. Yield = 9 mg (90%).

¹H NMR (500 MHz, CD₂Cl₂): δ 7.88 (t, ³J_{HH} = 7.7, 1H, py), 7.74 – 7.70 (m, 8H, Ar^F), 7.55 (s, 4H, Ar^F), 7.50 (d, ³J_{HH} = 7.7, 2H, py), 7.15 (d, ³J_{HH} = 1.8, 2H, NCH), 7.01 (d, ³J_{HH} = 1.8, 2H, NCH), 5.48 (d, ²J_{HH} = 14.8, 2H, pyCH₂), 5.02 (d, ²J_{HH} = 14.8, 2H, pyCH₂), 4.44 – 4.28 (m, 2H, NCH₂), 3.99 – 3.83 (m, 2H, CH₂), 1.96 – 1.76 (m, 4H, CH₂), 1.54 – 1.11 (m, 20H, CH₂).

¹H NMR (300 MHz, d₃-MeCN (CO)): δ 7.97 (t, ³J_{HH} = 7.8, 1H, py), 7.73 – 7.65 (m, 12H, Ar^F), 7.61 (d, ³J_{HH} = 7.7, 2H, py), 7.31 (s, 2H, NCH), 7.16 (s, 2H, NCH), 5.29 (s, 4H, pyCH₂), 4.14 (t, ³J_{HH} = 8.1, 4H, NCH₂), 1.92 – 1.76 (m, 4H, CH₂), 1.50 – 1.00 (m, 20H, CH₂).

¹H NMR (300 MHz, d₃-MeCN (Ar)): δ 7.95 (t, ³J_{HH} = 7.7, 1H, py), 7.73 – 7.65 (m, 12H, Ar^F), 7.61 (d, ³J_{HH} = 7.8, 2H, py), 7.31 (s, 2H, NCH), 7.15 (s, 2H, NCH), 5.30 (s, 2H, pyCH₂), 5.29 (s, 2H, pyCH₂), 4.27 (br s, fwhm = 32, 2H, NCH₂), 4.00 (br s, fwhm = 32, 2H, NCH₂), 1.77 (br s, fwhm = 42, 4H, CH₂), 1.51 – 1.11 (m, 20H, CH₂).

¹³C{¹H} NMR (126 MHz, CD₂Cl₂): δ 193.7 (d, ¹J_{RhC} = 80, CO), 181.8 (d, ¹J_{RhC} = 42, NCN), 162.3 (q, ¹J_{CB} = 50, Ar^F), 156.1 (s, py), 141.5 (s, py), 135.4 (s, Ar^F), 129.3 (qq, ²J_{FC} = 32, ³J_{CB} = 3, Ar^F), 125.2 (q, ¹J_{FC} = 271, Ar^F), 124.8 (s, py), 122.0 (s, NCH), 121.2 (s, NCH), 118.0 (sept, ³J_{FC} = 4, Ar^F), 55.8 (s, NCH₂), 51.6 (s, CH₂), 32.1 (s, CH₂), 28.5 (s, CH₂), 28.4 (s, CH₂), 28.1 (s, CH₂), 28.1 (s, CH₂), 25.7 (s, CH₂).

HR ESI-MS (positive ion, 4 kV): 564.2210, [M]⁺ (calcd 564.2204) *m/z*.

Elemental Anal. Calcd for C₆₀H₅₁BF₂₄N₅ORh (1427.29 g·mol⁻¹): C, 50.47; H, 3.60; N, 4.91. Found: C, 50.37; H, 3.50; N, 5.01.

IR (CH₂Cl₂): ν(CO) 1978 cm⁻¹

[Rh(CNC-16)CO][BAr^F₄] – 10-16

3-16 (50 mg, 0.080 mmol), Na[BAr^F₄] (80 mg, 0.090 mmol) and Ag₂O (19 mg, 0.084 mmol) were reacted with [Rh(CO)₂Cl]₂ (15 mg, 0.039 mmol) according to the general procedure to yield the desired product as fine yellow crystals. Yield

= 47 mg (53%). Crystals suitable for X-ray diffraction were grown from a mixture of diethyl ether/heptane at 20 °C.

Compound prepared from reaction of **11-16** (14.5 mg, 0.01 mmol) with CO (1 atm) in CD₂Cl₂ (0.5 mL) according to the general procedure to afford the product as a yellow powder. Yield = 14.5 mg (100%).

¹H NMR (500 MHz, CD₂Cl₂): δ 7.87 (t, ³J_{HH} = 7.7, 1H, py), 7.74 – 7.70 (m, 8H, Ar^F), 7.55 (s, 4H, Ar^F), 7.49 (d, ³J_{HH} = 7.7, 2H, py), 7.15 (d, ³J_{HH} = 1.8, 2H, NCH), 7.01 (d, ³J_{HH} = 1.7, 2H, NCH), 5.49 (d, ²J_{HH} = 14.7, 2H, pyCH₂), 5.02 (d, ²J_{HH} = 14.8, 2H, pyCH₂), 4.44 – 4.26 (m, 2H, NCH₂), 3.97 – 3.68 (m, 2H, CH₂), 1.98 – 1.76 (m, 4H, CH₂), 1.51 – 1.16 (m, 24H, CH₂).

¹H NMR (300 MHz, d₃-MeCN (CO)): δ 7.96 (t, ³J_{HH} = 7.7, 1H, py), 7.73 – 7.65 (m, 12H, Ar^F), 7.60 (d, ³J_{HH} = 7.8, 2H, py), 7.31 (s, 2H, NCH), 7.15 (s, 2H, NCH), 5.29 (s, 4H, pyCH₂), 4.13 (t, ³J_{HH} = 7.6, 4H, NCH₂), 1.93 – 1.77 (m, 4H, CH₂), 1.55 – 1.10 (m, 24H, CH₂).

¹H NMR (300 MHz, d₃-MeCN (Ar)): δ 7.96 (t, ³J_{HH} = 7.7, 1H, py), 7.73 – 7.65 (m, 12H, Ar^F), 7.60 (d, ³J_{HH} = 7.8, 2H, py), 7.31 (s, 2H, NCH), 7.15 (s, 2H, NCH), 5.30 (s, 2H, pyCH₂), 5.28 (s, 2H, pyCH₂), 4.27 (br s, fwhm = 28, 2H, NCH₂), 4.00 (br s, fwhm = 30, 2H, NCH₂), 1.92 – 1.70 (m, 4H, CH₂), 1.52 – 1.14 (m, 24H, CH₂).

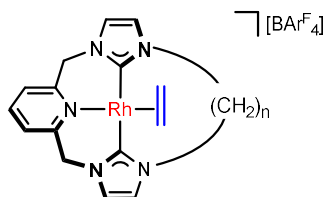
¹³C{¹H} NMR (126 MHz, CD₂Cl₂): δ 193.7 (d, ¹J_{RhC} = 80, CO), 182.0 (d, ¹J_{RhC} = 42, NCN), 162.3 (q, ¹J_{CB} = 50, Ar^F), 156.1 (s, py), 141.5 (s, py), 135.3 (s, Ar^F), 129.4 (qq, ²J_{FC} = 32, ³J_{CB} = 3, Ar^F), 125.2 (q, ¹J_{FC} = 271, Ar^F), 124.7 (s, py), 122.0 (s, NCH), 121.0 (s, NCH), 118.0 (sept., ³J_{FC} = 4, Ar^F), 55.8 (s, pyCH₂), 51.6 (s, NCH₂), 31.9 (s, CH₂), 28.7 (s, CH₂), 28.5 (s, CH₂), 28.5 (s, CH₂), 28.4 (s, CH₂), 28.3 (s, CH₂), 26.4 (s, CH₂).

HR ESI-MS (positive ion, 4 kV): 592.2523, [M]⁺ (calcd 592.2517) *m/z*.

Elemental Anal. Calcd for C₆₂H₅₅BF₂₄N₅ORh (1455.83 g·mol⁻¹): C, 51.15; H, 3.81; N, 4.81. Found: C, 51.26; H, 3.63; N, 4.91.

IR (CH₂Cl₂): ν(CO) 1978 cm⁻¹

5.2.12. Preparation of rhodium ethylene complexes, $[Rh(CNC-n)(C_2H_4)][BAr^F_4] - 11-n$



General Procedure

In an argon filled glovebox, a solution of $[Rh(C_2H_4)_2Cl]_2$ (0.6 eq) in fluorobenzene was added to a stirring solution of the chosen copper transfer agent **9-n** (1.0 eq) in fluorobenzene. The resulting red suspension was stirred for 1 hour before being filtered and layered with hexane. Storage at $-30\text{ }^{\circ}\text{C}$ afforded the title compounds as red crystalline solids, which were isolated on decantation of the supernatant and subsequent washing with hexane.

$[Rh(CNC-Me)(C_2H_4)][BAr^F_4] - 11-Me$

$[Rh(C_2H_4)_2Cl]_2$ (14 mg, 0.035 mmol) was reacted with **9-Me** (70 mg, 0.059 mmol) in fluorobenzene (2 mL) according to the general procedure to obtain the product as a red crystalline solid. Yield = 75 mg (96%). Crystals suitable for X-ray diffraction were grown from a CH_2Cl_2 /pentane layer.

1H NMR (400 MHz, CD_2Cl_2): δ 7.79 (t, $^3J_{HH} = 7.7$, 1H, py), 7.74 – 7.70 (m, 8H, Ar^F), 7.55 (s, 4H, Ar^F), 7.44 (d, $^3J_{HH} = 7.7$, 2H, py), 7.04 (d, $^3J_{HH} = 1.8$, 2H, NCH), 6.73 (d, $^3J_{HH} = 1.8$, 2H, NCH), 5.74 (br s, 2H, $pyCH_2$), 5.03 (br s, 2H, $pyCH_2$), 3.50 (br s, 4H, C_2H_4), 3.46 (s, 6H, NCH_3).

1H NMR (500 MHz, DiFB): δ 8.14 – 8.11 (m, 8H, Ar^F), 7.49 (br s, 4H, Ar^F), 7.45 (t, $^3J_{HH} = 7.6$, 1H, py), 7.14 (d, $^3J_{HH} = 7.7$, 2H, py), 6.45 (s, 2H, NCH), 5.42 (br s, fwhm = 45, 2H, $pyCH_2$), 4.80 (br s, fwhm = 47, 2H, $pyCH_2$), 3.38 (s, 4H, C_2H_4), 3.23 (s, 6H, NCH_3). *Selected data only.*

$^{13}C\{^1H\}$ NMR (101 MHz, CD_2Cl_2): δ 184.8 (d, $^1J_{RhC} = 40$, NCN), 162.3 (q, $^1J_{CB} = 50$, Ar^F), 155.9 (s, py), 139.5 (s, py), 135.4 (s, Ar^F), 129.5 (qq, $^2J_{FC} = 32$, $^3J_{CB} = 3$, Ar^F), 125.2 (q, $^1J_{FC} = 271$, Ar^F), 124.0 (s, py), 123.0 (s, NCH), 120.8 (s, NCH), 118.0 (sept., $^3J_{FC} = 4$, Ar^F), 56.2 (d, $^3J_{RhC} = 2$, $pyCH_2$), 36.5 (s, NCH_3).

HR ESI-MS (positive ion, 4 kV): 402.0424, $[M-C_2H_4]+[O_2]^+$ (calcd 402.0432) m/z .

Elemental Anal. Calcd for $C_{49}H_{33}BF_{24}N_5Rh$ ($1261.52 \text{ g}\cdot\text{mol}^{-1}$): C, 46.65; H, 2.64; N, 5.61. Found: C, 46.72; H, 2.69; N, 5.61.

$[Rh(CNC-12)(C_2H_4)][BAr^F_4] - 11-12$

$[Rh(C_2H_4)_2Cl]_2$ (46 mg, 0.12 mmol) was reacted with **9-12** (260 mg, 0.20 mmol) in fluorobenzene (12 mL) according to the general procedure to afford the product as a red crystalline material. Yield = 238 mg (82%). Crystals suitable for X-ray diffraction were grown from a CH_2Cl_2 /hexane layer at -30°C .

1H NMR (500 MHz, CD_2Cl_2): δ 7.84 (t, $^3J_{HH} = 7.7$, 1H, py), 7.77 – 7.67 (m, 8H, Ar^F), 7.56 (s, 4H, Ar^F), 7.48 (d, $^3J_{HH} = 7.7$, 2H, py), 7.06 (d, $^3J_{HH} = 2.0$, 2H, NCH), 6.78 (d, $^3J_{HH} = 2.0$, 2H, NCH), 5.32 (br s, 4H, $pyCH_2$), 3.77 (dd, $^3J_{HH} = 8.8$, 7.6, 4H, NCH_2), 3.41 (s, 4H, C_2H_4), 1.79 (br s, 4H, CH_2), 1.56 – 1.19 (m, 16H, CH_2).

$^{13}C\{^1H\}$ NMR (126 MHz, CD_2Cl_2): δ 181.9 (d, $^1J_{RhC} = 41$, NCN), 162.3 (q, $^1J_{CB} = 50$, Ar^F), 155.8 (s, py), 139.8 (s, py), 135.4 (s, Ar^F), 129.5 (qq, $^2J_{FC} = 32$, $^3J_{CB} = 3$, Ar^F), 125.2 (q, $^1J_{FC} = 271$, Ar^F), 124.2 (s, py), 121.7 (s, NCH), 121.4 (s, NCH), 118.0 (sept., $^3J_{FC} = 4$, Ar^F), 56.3 (s, $pyCH_2$), 49.9 (s, CH_2), 47.0 (s, C_2H_4), 31.5 (s, CH_2), 28.9 (s, CH_2), 27.6 (s, CH_2), 27.5 (s, CH_2), 24.4 (s, CH_2).

1H NMR (300 MHz, DiFB): δ 8.22 – 7.98 (m, 8H, Ar^F), 7.53 (t, $^3J_{HH} = 8.4$, 1H, Ar^F), 7.50 (s, 4H, Ar^F), 5.32 (br s, fwhm = 31, 4H, $pyCH_2$), 3.55 (t, $^3J_{HH} = 8.2$, 4H, NCH_2), 3.23 (s, 4H, C_2H_4), 1.54 (br s, fwhm = 30, 4H, CH_2), 1.36 – 1.02 (m, 16H, CH_2).

Selected data only.

HR ESI-MS (positive ion, 4 kV): 508.1941, $[M-C_2H_4]^+$ (calcd 508.1942) m/z , 540.1835 $[M-C_2H_4]^+ + [O_2]$, (calcd 540.1840) m/z .

Despite multiple attempts, satisfactory microanalysis data could not be obtained for this compound. Data is consistent with partial loss/substitution of ethylene during the analysis.

Elemental Anal. Calcd for $C_{59}H_{51}BF_{24}N_5Rh$ ($1399.77 \text{ g}\cdot\text{mol}^{-1}$): C, 50.63; H, 3.67; N, 5.00. Calcd for $C_{59}H_{51}BF_{24}N_5Rh-C_2H_4$ ($1371.72 \text{ g}\cdot\text{mol}^{-1}$): C, 49.91; H, 3.45; N, 5.11. Calcd for $C_{59}H_{51}BF_{24}N_5Rh-C_2H_4 + O_2$ ($1403.71 \text{ g}\cdot\text{mol}^{-1}$): C, 48.77; H, 3.38; N, 4.99. Found: C, 50.15; H, 3.62; N, 4.88.

[Rh(CNC-14)(C₂H₄)] [BAr^F₄] – 11-14

[Rh(C₂H₄)₂Cl]₂ (10 mg, 0.026 mmol) was reacted with **9-14** (58 mg, 0.043 mmol) in fluorobenzene (3 mL) according to the general procedure to afford the product as a red crystalline material. Yield = 51 mg (78%).

¹H NMR (500 MHz, CD₂Cl₂): δ 7.79 (t, ³J_{HH} = 7.7, 1H, py), 7.74 – 7.63 (m, 8H, Ar^F), 7.55 (s, 4H, Ar^F), 7.44 (d, ³J_{HH} = 7.7, 2H, py), 7.06 (d, ³J_{HH} = 1.9, 2H, NCH), 6.79 (d, ³J_{HH} = 1.8, 2H, NCH), 5.75 (br s, 2H, pyCH₂), 5.10 (br s, 2H, pyCH₂), 3.66 (br s, 4H, NCH₂), 3.50 (br s, 4H, C₂H₄), 1.73 (br s, 4H, CH₂), 1.50 – 1.20 (m, 20H, CH₂).

¹³C{¹H} NMR (126 MHz, CD₂Cl₂): δ 183.5 (d, ¹J_{RhC} = 41, NCN), 162.3 (q, ¹J_{CB} = 50, Ar^F), 155.9 (s, py), 139.6 (s, py), 135.4 (s, Ar^F), 129.5 (qq, ²J_{FC} = 32, ³J_{CB} = 3, Ar^F), 125.2 (q, ¹J_{FC} = 271, Ar^F), 123.9 (s, py), 121.3 (s, NCH), 121.2 (s, NCH), 118.0 (sept., ³J_{FC} = 4, Ar^F), 56.2 (s, pyCH₂), 49.8 (s, NCH₂), 31.7 (s, CH₂), 29.8 (s, CH₂), 29.0 (s, CH₂), 28.3 (s, CH₂), 28.0 (s, CH₂), 25.4 (s, CH₂).

HR ESI-MS (positive ion, 4 kV): 568.2162, [M-C₂H₄]⁺+ [O₂] (calcd 568.2153) *m/z*, 609.2429, [M-C₂H₄]⁺ + [CH₃CN+O₂] (calcd 609.2419) *m/z*.

Elemental Anal. Calcd for C₆₁H₅₅BF₂₄N₅Rh (1427.82 g·mol⁻¹): C, 51.31; H, 3.88; N, 4.91. Found: C, 51.27; H, 3.74; N, 4.84.

[Rh(CNC-16)(C₂H₄)] [BAr^F₄] – 11-16

[Rh(C₂H₄)₂Cl]₂ (50.4 mg, 0.130 mmol) was reacted with **9-16** (300 mg, 0.216 mmol) in fluorobenzene (8 mL) according to the general procedure to afford the product as red crystals. Yield = 210 mg (67%).

¹H NMR (500 MHz, CD₂Cl₂): δ 7.77 (t, ³J_{HH} = 7.7, 1H, py), 7.74 – 7.63 (m, 8H, Ar^F), 7.55 (s, 4H, Ar^F), 7.42 (d, ³J_{HH} = 7.7, 2H, py), 7.06 (d, ³J_{HH} = 1.8, 2H, NCH), 6.79 (d, ³J_{HH} = 1.8, 2H, NCH), 5.68 (br s, 2H, pyCH₂), 5.07 (br s, 2H, pyCH₂), 3.66 (br s, 4H, NCH₂), 3.52 (br s, 4H, C₂H₄), 1.73 (br s, 4H, CH₂), 1.57 – 1.17 (m, 20H, CH₂).

¹³C{¹H} NMR (126 MHz, CD₂Cl₂): δ 184.1 (d, ¹J_{RhC} = 41, NCN), 162.3 (q, ¹J_{CB} = 50, Ar^F), 156.0 (s, py), 139.5 (s, py), 135.4 (s, Ar^F), 129.5 (qq, ²J_{FC} = 32, ³J_{CB} = 3, Ar^F), 125.2 (q, ¹J_{FC} = 271, Ar^F), 123.7 (s, py), 121.2 (s, NCH), 121.2 (s, NCH), 118.0 (sept., ³J_{FC} = 4, Ar^F), 56.2 (d, ³J_{RhC} = 2.4, pyCH₂), 49.8 (s, NCH₂), 31.5 (s, CH₂), 29.4 (s, CH₂), 29.3 (s, CH₂), 28.8 (s, CH₂), 28.4 (s, CH₂), 28.3 (s, CH₂), 26.0 (s, CH₂).

HR ESI-MS (positive ion, 4 kV): 592.2520, $[M]^+$ (calcd 592.2517) m/z , 564.2566, $[M-C_2H_4]^+$ (calcd 564.2568) m/z .

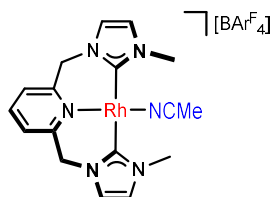
Elemental Anal. Calcd for $C_{63}H_{59}BF_{24}N_5Rh$ ($1455.88 \text{ g}\cdot\text{mol}^{-1}$): C, 51.98; H, 4.08; N, 4.81. Found: C, 51.85; H, 4.01; N, 4.85.

5.3 Compounds prepared in chapter 3

5.3.1. Quenching reactions

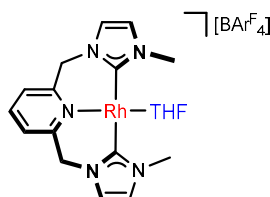
Complex **11-Me** (6 mg, 0.005 mmol) was dissolved in the chosen quenching agent (0.4 mL) and conversion monitored by ^1H NMR using Ar^{F} signals as an internal standard.

$[\text{Rh}(\text{CNC-Me})(d_3\text{-MeCN})][\text{BAr}^{\text{F}}_4]$, **12-Me**



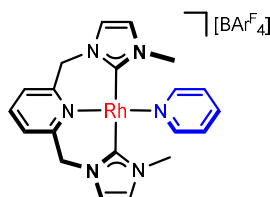
^1H NMR (400 MHz, $d_3\text{-MeCN}$): δ 7.75 (t, $^3J_{\text{HH}} = 7.7$, 1H, py), 7.71 – 7.68 (m, 8H, Ar^{F}), 7.67 (s, 4H, Ar^{F}), 7.39 (d, $^3J_{\text{HH}} = 7.7$, 2H, py), 7.19 (d, $^3J_{\text{HH}} = 1.9$, 2H, NCH), 6.94 (d, $^3J_{\text{HH}} = 1.9$, 2H, NCH), 5.33 (d, $^2J_{\text{HH}} = 14.5$, 2H, pyCH_2), 5.09 (d, $^2J_{\text{HH}} = 14.3$, 2H, pyCH_2), 3.76 (s, 6H, CH_3).

$[\text{Rh}(\text{CNC-Me})(\text{THF})][\text{BAr}^{\text{F}}_4]$, **13-Me**



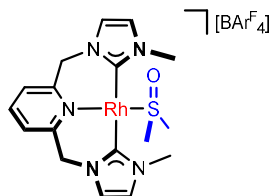
^1H NMR (400 MHz, THF): δ 8.23 (t, $^3J_{\text{HH}} = 7.7$, 1H, py), 8.14 – 8.07 (m, 8H, Ar^{F}), 7.91 (d, $^3J_{\text{HH}} = 7.8$, 2H, py), 7.88 (s, 4H, Ar^{F}), 7.58 (d, $^3J_{\text{HH}} = 1.8$, 2H, NCH), 7.28 (d, $^3J_{\text{HH}} = 1.8$, 2H, NCH), 5.84 (br s, 4H, pyCH_2). (other peaks obscured by solvent signals)

$[\text{Rh}(\text{CNC-Me})(d_5\text{-pyridine})][\text{BAr}^{\text{F}}_4]$, **14-Me**



¹H NMR (400 MHz, *d*₅-pyridine): δ 8.47 – 8.29 (m, 8H, Ar^F), 7.84 (s, 4H, Ar^F), 7.42 (d, ³*J*_{HH} = 1.9, 2H, NCH), 7.31 (d, ³*J*_{HH} = 7.7, 2H, py), 7.01 (d, ³*J*_{HH} = 1.8, 2H, NCH), 5.74 (d, ²*J*_{HH} = 14.1, 2H, pyCH₂), 5.30 (d, ²*J*_{HH} = 14.2, 2H, pyCH₂), 3.08 (s, 6H, CH₃).

[Rh(CNC-Me)(DMSO)][BAr^F₄]. **11-Me**



DMSO (1 μL, 0.01 mmol) was added to a stirring solution of **11-Me** (15 mg, 0.012 mmol) in CH₂Cl₂ (2 mL) and reacted for 30 minutes. The orange solution was concentrated and washed with hexane. Recrystallisation from a CH₂Cl₂/hexane layer gave the desired product as a red crystalline solid. Yield = 12 mg (77%). Crystals grown in this way were suitable for X-ray analysis.

¹H NMR (400 MHz, *d*₆-DMSO): δ 7.90 (t, ³*J*_{HH} = 7.7, 1H, py), 7.71 (s, 4H, Ar^F), 7.64 – 7.59 (m, 8H, Ar^F), 7.57 (d, ³*J*_{HH} = 7.7, 2H, py), 7.46 (d, ³*J*_{HH} = 1.9, 2H, NCH), 7.16 (d, ³*J*_{HH} = 1.8, 2H, NCH), 5.42 (br s, 4H, pyCH₂), 3.80 (s, 6H, CH₃).

¹H NMR (500 MHz, CD₂Cl₂): δ 7.86 – 7.65 (m, 9H, py + Ar^F), 7.55 (s, 4H, Ar^F), 7.34 (d, ³*J*_{HH} = 7.7, 2H, py), 7.08 (d, ³*J*_{HH} = 1.9, 2H, NCH), 6.81 (d, ³*J*_{HH} = 1.9, 2H, NCH), 5.88 (s, 2H, pyCH₂), 4.95 (s, 2H, pyCH₂), 3.83 (s, 6H, NCH₃), 3.29 – 2.98 (m, 6H, SCH₃).

¹³C{¹H} NMR (126 MHz, CD₂Cl₂): δ 186.7 (d, ¹*J*_{RhC} = 45, NCN), 162.3 (q, ¹*J*_{CB} = 50, Ar^F), 157.7 (s, py), 139.4 (s, py), 135.3 (s, Ar^F), 129.4 (qq, ²*J*_{FC} = 32, ³*J*_{CB} = 3, Ar^F), 125.1 (q, ¹*J*_{FC} = 271, Ar^F), 123.3 (s, py), 123.1 (s, NCH), 121.9 (s, NCH), 118.0 (sept., ³*J*_{FC} = 4, Ar^F), 56.4 (d, ³*J*_{RhC} = 2, pyCH₂), 52.8 (br d, ²*J*_{RhC} = 30, SCH₃), 39.0 (s, NCH₃).

Elemental Anal. Calcd for C₄₉H₃₅BF₂₄N₅ORhS (1311.13 g·mol⁻¹): C, 44.87; H, 2.69; N, 5.34. Found: C, 44.81; H, 2.82; N, 5.22).

5.3.2. Terminal alkyne dimerisation studies

Kinetic studies in CD₂Cl₂ using complex **11-Me**

Variable concentration data:

Solutions of **11-Me** (5 or 10 mM) and 3,5-di-*tert*-butylphenylacetylene **16a** (50 or 100 mM) in CD₂Cl₂ (ca. 0.5 mL) were prepared in J. Young's valve NMR tubes

at room temperature and then held at -78 °C until being placed into a NMR spectrometer pre-equilibrated to 298 K and then the reaction progress monitored using ^1H NMR spectroscopy (400 MHz).

Variable temperature data:

To a chilled flask charged with **11-Me** (18.9 mg, 15.0 μmol) and **16a** (64.2 mg, 298 μmol) was added chilled CD_2Cl_2 (3.0 mL) in an argon glove box. The resulting solution was partitioned into chilled J. Young's valve NMR tubes (0.5 mL/ tube), which were sealed and immediately frozen in liquid nitrogen. The samples were then individually thawed and placed into a NMR spectrometer pre-equilibrated to the required temperature and monitored by ^1H NMR spectroscopy (600 MHz, 288 – 308 K).

Kinetic studies in CD_2Cl_2 using complex **15-Me**

A solution of **15-Me** (3.3 mg, 2.5 μmol) and **16a** (10.8 mg, 50.3 μmol) in CD_2Cl_2 (0.5 mL) was prepared in J. Young's valve NMR tubes at room temperature and then held at -78 °C until being placed into a NMR spectrometer pre-equilibrated to 298 K and then monitored by ^1H NMR spectroscopy (400 MHz).

Kinetic studies in 1,2-difluorobenzene using complex **11-Me**

Variable concentration data:

Solutions of **11-Me** (5 or 10 mM) and **16a** (50 or 100 mM) in 1,2-difluorobenzene (ca. 0.5 mL) were prepared in J. Young's valve NMR tubes at -30 °C and then held at -78 °C until being placed into an NMR spectrometer pre-equilibrated to 298 K and then the reaction progress monitored using ^1H NMR spectroscopy (600 MHz).

Variable temperature data:

To a chilled flask containing 1,2-difluorobenzene (2.5 mL), standard solutions of **11-Me** (2.5 mL, 20.0 mM) and **16a** (5 mL, 200 mM) were added chilled in an argon glove box. The resulting solution was partitioned into chilled J. Young's valve NMR tubes (0.5 mL/ tube), which were sealed and immediately frozen in liquid nitrogen. The samples were then individually thawed and placed into an NMR spectrometer pre-equilibrated to the required temperature and monitored by ^1H NMR spectroscopy (600 MHz, 288 – 308 K).

From isolated gem-Ar'CCC(CH₂)Ar':

A standard solution of enyne **18a** (50 mM, 0.5 mL) in 1,2-difluorobenzene was added to a cooled J. Young's valve NMR tube (-30 °C) charged with **11-Me** (3.2 mg, 2.5 μmol) and then held at -78 °C until being thawed immediately before placed into an NMR spectrometer pre-equilibrated to 298 K and the reaction progress monitored using ¹H NMR spectroscopy (600 MHz).

Annulation of *gem*-Ar'CCC(CH₂)Ar' using **11-12**:

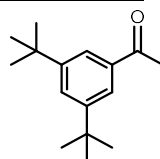
A standard solution of enyne **18a** (50 mM, 0.5 mL) in 1,2-difluorobenzene was added to a J. Young's valve NMR tube charged with **11-12** (3.5 mg, 0.0025 mmol) and held at 50 °C over the reaction period. The progress of the reaction was monitored periodically using ¹H NMR (300 MHz).

Scoping studies using complex **11-Me**

Standard solution of the chosen alkyne (100 mM) in 1,2-difluorobenzene was added to a J. Young's valve NMR tube containing **11-Me** (3 mg, 2 μmol) and the solution frozen at -78 °C. The samples were thawed immediately before placing into an NMR spectrometer pre-equilibrated to 298 K and the reaction progress monitored using ¹H NMR spectroscopy (400 MHz).

5.3.3. Enyne synthesis and isolation

1-(3,5-di-*tert*-butylphenyl)ethan-1-one -**20a**

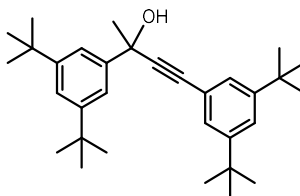


*n*Butyl lithium (5.6 mL, 1 M in hexanes) was added dropwise to a stirring solution of 1-bromo-3,5-di-*tert*-butyl benzene (1.0 g, 3.7 mmol) in THF (50 mL) and TMEDA (0.5 mL) at -78 °C. The reaction was stirred for 30 minutes before the addition of dimethylacetamide (6 mL, 0.07 mmol). The resulting solution was warmed to room temperature and stirred for a further hour. Cold HCl (aq, 2 M) was added and the product extracted into diethyl ether. The crude product was obtained after the organic layer was washed with H₂O, dried over MgSO₄ and solvent removed *in vacuo*. The compound was purified using column chromatography (silica; hexane/ethyl acetate, 48:1). Yield = 410 mg (49%).

¹H NMR (400 MHz, CDCl₃): δ 7.81 (d, ⁴J_{HH} = 1.9, 2H, Ar), 7.65 (t, ⁴J_{HH} = 1.8, 1H, Ar), 2.61 (s, 3H, CH₃), 1.36 (s, 18H, *t*Bu).

*Data consistent with literature values.*¹³

2,4-bis(3,5-di-*tert*-butylphenyl)but-3-yn-2-ol – 21a



*n*Butyl lithium (1.5 mL, 1.475 M, 2.3 mmol) was added dropwise to a chilled solution (0 °C) of diisopropylamine (320 μL, 2.3 mmol) in THF (3 mL). The resulting solution was cooled to -78 °C before the dropwise addition of a solution of 3,5-di-*tert*-butylphenylacetylene (415 mg, 1.94 mmol) in THF (4 mL). After stirring for 4 hours a solution of 1-(3,5-di-*tert*-butylphenyl)ethan-1-one (300 mg, 1.29 mmol) in THF (2 mL) was slowly added. The reaction was warmed to room temperature and stirred for 64 hours before being quenched with saturated NH₄Cl (aq) and the product was extracted into diethyl ether. The organic layer was washed with H₂O before being dried over MgSO₄ and solvent removed *in vacuo*. Purification by column chromatography (silica; ethyl acetate/hexane 1:19) removed residual alkyne starting material affording a 2:3 mixture of **20a** to product. Yield = 61 mg (4%).

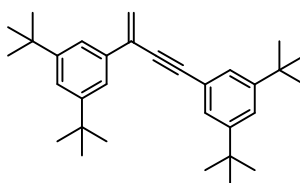
Small quantities of the product could be obtained in higher purity (92%, balance **20a**) following purification using preparatory TLC (hexane) and used to characterise the complex.

¹H NMR (500 MHz, CDCl₃): δ 7.66 (d, ⁴J_{HH} = 1.6, 2H, Ar), 7.41 – 7.38 (m, 2H, Ar), 7.35 (d, ⁴J_{HH} = 1.7, 2H, Ar), 1.89 (s, 3H, CH₃), 1.37 (s, 18H, *t*Bu), 1.32 (s, 18H, *t*Bu).

¹³C{¹H} NMR (126 MHz, CDCl₃): δ 151.0 (s, Ar{C}), 150.9 (s, Ar{C}), 145.2 (s, Ar{C}), 137.0 (s, Ar{C}), 126.1 (s, Ar{CH}), 122.7 (s, Ar{CH} × 2), 119.5 (s, Ar{CH}), 91.8 (s, C≡C-Ar'), 71.2 (s, C≡C-Ar'), 33.4 (s, CH₃), 31.7 (s, *t*Bu), 31.5 (s, *t*Bu).

HR ESI-MS (positive ion, 4 kV): 469.3442 ([M+Na]⁺, calcd 469.3441) *m/z*.

Gem-Ar'CCC(CH₂)Ar' – 18a



Method 1

A solution of **11-Me** (30.0 mg, 23.8 μ mol) and **16a** (102 mg, 475 μ mol) in CH₂Cl₂ (4.8 mL) was stirred at 25 °C for 6 hours. The solution was freeze-pump-thaw degassed and placed under an atmosphere of CO (1 atm) to afford a yellow solution, which was concentrated to dryness and the residue extracted through a short plug (alumina; hexane). The hexane solution was stirred over KHMDS (30.0 mg, 150 μ mol) for 3 hours at room temperature. The resulting suspension was filtered and the filtrate washed with HCl (aq, 2 M) and H₂O before being dried over MgSO₄. Concentration under reduced pressure gave the desired product as a pale-yellow solid. Yield = 74.6 mg (73%).

Method 2

MsCl (2 μ L, 0.02 mmol) was added to a stirring solution of crude 2,4-bis(3,5-di-*tert*-butylphenyl)but-3-yn-2-ol (6 mg, 0.02 mmol) and NEt₃ (0.1 mL) in THF (1 mL) cooled to 0 °C. After 30 minutes the resulting white suspension was filtered and the filtrate reduced to dryness *in vacuo*. The product was purified by preparatory TLC (silica; hexane) to give the product as a pale-yellow solid. Yield = 2.0 mg (57%).

¹H NMR (500 MHz, CD₂Cl₂): δ 7.62 (d, ⁴*J*_{HH} = 1.6, 2H, Ar'), 7.46 – 7.42 (m, 2H, 2 \times Ar'), 7.39 (d, ⁴*J*_{HH} = 1.6, 2H, Ar'), 5.96 (s, 1H, CH₂), 5.71 (s, 1H, CH₂), 1.37 (s, 18H, *t*Bu), 1.33 (s, 18H, *t*Bu).

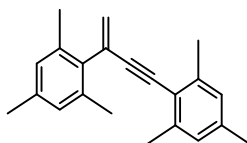
¹³C{¹H} NMR (126 MHz, CD₂Cl₂): δ 151.6 (s, Ar'{C}), 151.5 (s, Ar'{C}), 137.2 (s, Ar'{C}), 132.1 (s, C(CH₂)), 126.4 (s, Ar'{CH}), 123.6 (s, Ar'{CH}), 123.2 (s, Ar'{CH}), 122.7 (s, Ar'{C}), 121.0 (s, Ar'{CH}), 119.8 (s, C(CH₂)), 92.5 (s, C \equiv CAr'), 88.4 (s, C \equiv CAr'), 35.4 (s, *t*Bu{C}), 35.3 (s, *t*Bu{C}), 31.8 (s, *t*Bu), 31.6 (s, *t*Bu).

HR ESI-MS (positive ion, 4 kV): 451.3341 ([M+Na]⁺, calcd 451.3335) *m/z*.

Preparation of *gem*-MesCCC(CH₂)Mes and *E*-MesCCCHCHMes

A standard solution of mesitylacetylene (34 μ L, 0.22 mmol) in 1,2-difluorobenzene (2.1 mL) was added to **11-Me** (13.6 mg, 0.0107 mmol) and the resulting orange solution stirred at 25 °C for 18 hours before being freeze-pump-thaw degassed and quenched with an atmosphere of CO (1 atm). The resulting solution was concentrated to dryness and the organic product mixture extracted into hexane and passed through a short plug (silica; hexane). Yield = 28 mg (90%; 37% *gem*-/63% *E*-). The regioisomers were separated using column chromatography (silica; hexane to toluene/hexane 1:49). Yield = 9 mg (29% *gem*), 15 mg (48% *E*).

Characterisation of *gem*-MesCCC(CH₂)Mes - **18f**



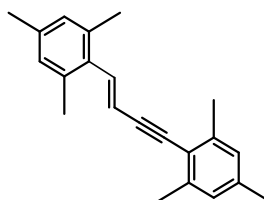
¹H NMR (500 MHz, CDCl₃): δ 6.88 (s, 2H, *m*-Ar), 6.82 (s, 2H, *m*-Ar), 5.88 (d, ²*J*_{HH} = 2.1, 1H, CH₂), 5.30 (d, ²*J*_{HH} = 2.1, 1H, CH₂), 2.35 (s, 6H, *o*-CH₃), 2.32 (s, 6H, *o*-CH₃), 2.28 (s, 3H, *p*-CH₃), 2.25 (s, 3H, *p*-CH₃).

¹³C{¹H} NMR (126 MHz, CD₂Cl₂): δ 140.2 (s, *o*-Ar), 137.8 (s, *p*-Ar), 136.9 (s, *i*-Ar), 136.8 (s, *p*-Ar), 135.5 (s, *o*-Ar), 130.5 (s, C(CH₂)), 128.4 (s, *m*-Ar), 127.6 (s, *m*-Ar), 124.5 (s, C(CH₂)), 120.2 (s, *i*-Ar), 97.2 (s, MesC \equiv C), 87.2 (s, MesC \equiv C), 21.5 (s, *p*-CH₃), 21.2 (s, *p*-CH₃), 21.0 (s, *o*-CH₃), 20.2 (s, *o*-CH₃).

¹H NMR (400 MHz, DiFB) δ 5.79 (d, ²*J*_{HH} = 1.9, 1H, C(CH₂)), 5.14 (d, ²*J*_{HH} = 1.9, 1H, C(CH₂)), 2.28 (s, 6H, *o*-CH₃), 2.20 (s, 6H, *o*-CH₃), 2.06 (s, 3H, *p*-CH₃), 2.06 (s, 3H, *p*-CH₃).

Elemental Anal. Calcd for C₂₂H₂₄ (288.43 g·mol⁻¹): C, 91.61; H, 8.39; N, 0.00. Found: C, 91.70; H, 8.21; N, 0.00.

Characterisation of *E*-MesCCCHCHMes - **17f**

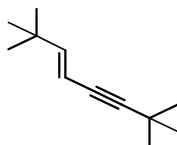


¹H NMR (300 MHz, CDCl₃): δ 7.05 (d, ³J_{HH} = 16.4, 1H, CHCHMes), 6.89 (s, 2H, *m*-Ar), 6.88 (s, 2H, *m*-Ar), 6.01 (d, ³J_{HH} = 16.4, 1H, CHCHMes), 2.44 (s, 6H, *o*-CH₃), 2.35 (s, 6H, *o*-CH₃), 2.28 (s, 6H, 2 × *p*-CH₃).

¹H NMR (300 MHz, DiFB): δ 5.93 (d, ³J_{HH} = 16.4, 1H, CHCHMes), 2.34 (s, 6H, *o*-CH₃), 2.16 (s, 6H, *o*-CH₃), 2.09 (s, 2 × *p*-CH₃). *Selected data only.*

*Data consistent with literature values.*¹⁴

E-tBuCCCHCHtBu – 17b



Prepared using a literature procedure.¹⁵

The product could not be isolated from the catalytic mixtures owing to its high volatility. *In situ* NMR conversions were determined through integration of the associated ¹H NMR spectra using the Ar^F signals as an internal standard.

¹H NMR (400 MHz, CDCl₃): δ 6.09 (d, ³J_{HH} = 16.5, 1H, CHCH), 5.41 (d, ³J_{HH} = 16.1, 1H, CHCH), 1.24 (s, 9H, *t*Bu), 1.01 (s, 9H, *t*Bu).

¹H NMR (300 MHz, *d*₃-MeCN): δ 6.03 (d, ³J_{HH} = 16.2, 1H, CHCH), 5.40 (d, ³J_{HH} = 16.2, 1H, CH), 1.21 (s, 9H, *t*Bu), 1.01 (s, 9H, *t*Bu).

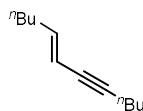
¹H NMR (400 MHz, DiFB): δ 5.95 (d, ³J_{HH} = 16.2, 1H, CHCH), 5.29 (d, ³J_{HH} = 16.1, 1H, CHCH), 1.16 (s, 9H, *t*Bu), 0.83 (s, 9H, *t*Bu).

*Data consistent with literature values.*¹⁶

Preparation of Gem-nBuCCC(CH₂)_nBu and E-nBuCCCHCHnBu

A standard solution of 1-hexyne in 1,2-difluorobenzene (4 mL, 50 mM) was added to **11-Me** (12.6 mg, 9.99 μmol) and the resulting orange solution stirred at 25 °C for 24 hours before being freeze-pump-thaw degassed and quenched with an atmosphere of CO (1 atm). The resulting solution was concentrated to dryness and the organic product mixture extracted into hexane. Yield = 14 mg (85%; of which 75%, *gem*, 15%, *E*; balance trimer).

Characterisation of *E*-*n*BuCCCHCH*n*Bu – 17e

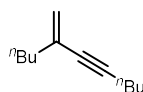


¹H NMR (400 MHz, CDCl₃): δ 6.04 (dt, ³*J*_{HH} = 14.8, 7.0, 1H, CHCH*n*Bu), 5.45 (d, ³*J*_{HH} = 15.8, 1H, CHCH*n*Bu), 2.28 (t, ³*J*_{HH} = 7.1, 2H, CH₂), 2.07 (t, ³*J*_{HH} = 7.1, 2H, CH₂), 1.53 – 1.25 (m, 8H, CH₂), 0.98 – 0.81 (m, 6H, CH₃).

¹H NMR (400 MHz, DiFB): δ 5.90 (dt, ³*J*_{HH} = 14.9, 7.1, 1H, CHCH*n*Bu), 5.35 (d, ³*J*_{HH} = 16.0, 1H, CHCH*n*Bu). *Selected data only.*

*Data consistent with literature values.*¹⁷

Characterisation of *gem*-*n*BuCCC(CH₂)*n*Bu – 18e

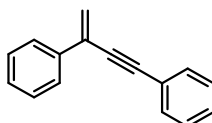


¹H NMR (400 MHz, CDCl₃): δ 5.20 (s, 1H, C(CH₂)), 5.12 (s, 1H, C(CH₂)), 2.31 (t, ³*J*_{HH} = 7.7, 2H, CH₂), 2.12 (t, ³*J*_{HH} = 7.7, 2H, CH₂), 1.55 – 1.25 (m, 8H, CH₂), 0.98 – 0.81 (m, 6H, CH₃).

¹H NMR (400 MHz, DiFB): δ 5.14 (s, 1H, C(CH₂)), 5.02 (s, 1H, C(CH₂)). *Selected data only.*

*Data consistent with literature values.*¹⁸

Gem-PhCCC(CH₂)Ph – 18c



To a solution of **11-Me** (31.2 mg, 24.7 μmol) in CH₂Cl₂ (5 mL) was added phenylacetylene (54.3 μL, 495 μmol). The resulting orange solution stirred at 25 °C for 24 hours and then freeze-pump-thaw degassed and placed under an atmosphere of CO (1 atm). The solution was concentrated *in vacuo* and the residue extracted through a short plug (alumina; hexane) to afford the product as a yellow oil on removal of the solvent. Yield = 32.8 mg (65%).

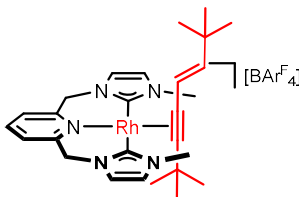
*Data consistent with literature values.*¹⁹

¹H NMR (300 MHz, CDCl₃): δ 7.73 (d, ³*J*_{HH} = 7.6, 2H, Ph), 7.50 – 7.58 (m, 2H, Ph), 7.29 – 7.45 (m, 6H, Ph), 5.99 (s, 1H, C(CH₂)), 5.77 (s, 1H, C(CH₂)).

^1H NMR (400 MHz, DiFB): δ 5.82 (s, 1H, C(CH₂)), 5.61 (s, 1H, C(CH₂)). *Selected data only.*

5.3.4. Isolation of catalytic intermediates

[Rh(CNC-Me)(E-*t*BuCCCHCH*t*Bu)][BAR^F₄] – **19-Me**



A solution of **11-Me** (28.8 mg, 0.0228 mmol) in 1,2-difluorobenzene (1 mL) was added to *E*-enyne **17b** (4.1 mg, 0.025 mmol). The resulting red solution was stirred for 2 hours before volatiles were removed *in vacuo* to afford the crude product which was washed with pentane and dried to obtain the pure product as a bright red solid. Yield = 30.1 mg (94%). Crystals suitable for X-ray diffraction were grown from CH₂Cl₂/hexane at -30 °C.

^1H NMR (500 MHz, CD₂Cl₂): δ 7.76 (t, $^3J_{\text{HH}} = 7.7$, 1H, py), 7.76 – 7.67 (m, 8H, Ar^F), 7.55 (s, 4H, Ar^F), 7.46 (d, $^3J_{\text{HH}} = 7.7$, 1H, py), 7.43 (d, $^3J_{\text{HH}} = 7.7$, 1H, py), 7.07 (d, $^3J_{\text{HH}} = 1.9$, 1H, NCH), 7.02 (d, $^3J_{\text{HH}} = 1.9$, 1H, NCH), 6.71 (d, $^3J_{\text{HH}} = 1.9$, 1H, NCH), 6.67 (d, $^3J_{\text{HH}} = 1.8$, 1H, NCH), 6.38 (d, $^3J_{\text{HH}} = 15.3$, 1H, CHCH*t*Bu), 5.97 (d, $^3J_{\text{HH}} = 15.3$, 1H, CHCH*t*Bu), 5.84 (d, $^2J_{\text{HH}} = 14.5$, 1H, pyCH₂), 5.60 (d, $^2J_{\text{HH}} = 14.4$, 1H, pyCH₂), 5.11 (d, $^2J_{\text{HH}} = 14.6$, 1H, pyCH₂), 5.06 (d, $^2J_{\text{HH}} = 14.4$, 1H, pyCH₂), 3.44 (s, 3H, NCH₃), 3.41 (s, 3H, NCH₃), 1.23 (s, 9H, *t*Bu), 0.96 (s, 9H, *t*Bu).

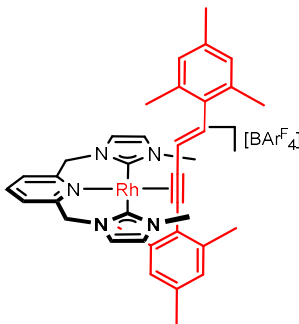
$^{13}\text{C}\{^1\text{H}\}$ NMR (126 MHz, CD₂Cl₂): δ 184.9 (d, $^1J_{\text{RhC}} = 41$, NCN), 184.5 (d, $^1J_{\text{RhC}} = 41$, NCN), 162.3 (q, $^1J_{\text{CB}} = 50$, Ar^F), 155.7 (s, py), 155.5 (s, py), 153.5 (s, $^3J_{\text{RhC}} = 2$, CHCH*t*Bu), 138.5 (s, py), 135.4 (s, Ar^F), 129.4 (qq, $^2J_{\text{FC}} = 32$, $^3J_{\text{CB}} = 3$, Ar^F), 125.1 (q, $^1J_{\text{FC}} = 271$, Ar^F), 124.2 (s, py × 2), 122.4 (s, NCH), 122.3 (s, NCH), 120.8 (s, NCH), 120.3 (s, NCH), 118.0 (sept, $^3J_{\text{FC}} = 4$, Ar^F), 110.8 (d, $^2J_{\text{RhC}} = 1$, CHCH*t*Bu), 97.2 (d, $^1J_{\text{RhC}} = 15$, *t*BuC≡C), 75.1 (d, $^1J_{\text{RhC}} = 12$, *t*BuC≡C), 56.3 (d, $^3J_{\text{RhC}} = 2$, pyCH₂), 56.0 (d, $^3J_{\text{RhC}} = 2$, pyCH₂), 37.0 (s, NCH₃), 36.5 (s, NCH₃), 33.9 (s, *t*Bu{C}), 33.1 (s, *t*Bu{C}), 31.2 (s, *t*Bu), 29.7 (s, *t*Bu).

^1H NMR (300 MHz, DiFB): 8.22 – 8.06 (m, 8H, Ar^F), 7.49 (s, 4H, Ar^F), 5.99 (d, $^3J_{\text{HH}} = 15.1$, 1H, CHCH*t*Bu), 5.67 (d, $^2J_{\text{HH}} = 14.5$, 1H, pyCH₂), 5.40 (d, $^2J_{\text{HH}} = 14.7$, 1H,

pyCH₂), 4.90 (app. t, $J = 14.6$, 2H, pyCH₂), 3.32 (s, 3H, NCH₃), 3.29 (s, 3H, NCH₃), 1.15 (s, 9H, *t*Bu), 0.90 (s, 9H, *t*Bu). *Selected data only.*

Elemental Anal. Calcd for C₅₉H₄₉BF₂₄N₅Rh (1397.75 g mol⁻¹): C, 50.70; H, 3.53; N, 5.01. Found: C, 50.56; H, 3.45; N, 4.99.

[Rh(CNC-Me)(E-MesCCCHCHMes)] [BAr^F₄]



A solution of **11-Me** (45 mg, 0.036 mmol) and **17f** (10.8 mg, 0.0473 mmol) in 1,2-difluorobenzene (2 mL) was stirred for 1 hour. The deep red solution mixture was concentrated to dryness and the residue washed with cold hexane. Recrystallisation from a CH₂Cl₂ solution layered with hexane at -30 °C afforded the pure product as a red crystalline solid. Yield = 31.9 mg (59%).

¹H NMR (500 MHz, CD₂Cl₂): δ 7.85 (t, $^3J_{\text{HH}} = 7.7$, 1H, py), 7.76 – 7.67 (m, 8H, Ar^F), 7.55 (s, 4H, Ar^F), 7.54 – 7.50 (m, 2H, py), 7.42 (d, $^3J_{\text{HH}} = 15.6$, 1H, CHCHMes), 7.05 (s, 1H, NCH), 6.99 (s, 1H, NCH), 6.93 (br s, fwhm = 10.6, 2H, Ar{CH}), 6.88 (s, 2H, Ar{CH}), 6.74 (s, 1H, NCH), 6.62 (s, 1H, NCH), 6.60 (d, $^3J_{\text{HH}} = 15.6$, 1H, CHCHMes), 5.78 (d, $^2J_{\text{HH}} = 14.5$, 1H, pyCH₂), 5.69 (d, $^2J_{\text{HH}} = 15.0$, 1H, pyCH₂), 5.14 (d, $^2J_{\text{HH}} = 14.6$, 1H, pyCH₂), 5.08 (d, $^2J_{\text{HH}} = 15.0$, 1H, pyCH₂), 3.67 (br s, fwhm = 29.8, 3H, NCH₃), 3.47 (s, 3H, *p*-CH₃), 3.38 (s, 3H, *p*-CH₃), 2.45 (br s, fwhm = 27.2, 3H, NCH₃), 2.26 (s, 6H, *o*-CH₃), 2.16 (s, 6H, *o*-CH₃).

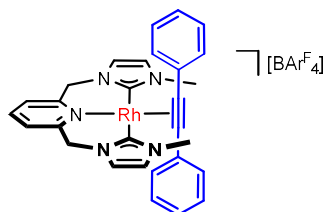
¹³C{¹H} NMR (126 MHz, CD₂Cl₂): δ 182.8 (d, $^1J_{\text{RhC}} = 41$, NCN), 182.6 (d, $^1J_{\text{RhC}} = 41$, NCN), 162.3 (q, $^1J_{\text{CB}} = 50$, Ar^F), 155.8 (s, py), 155.6 (s, py), 139.6 (s, py), 138.1 (s, ArC), 138.0 (s, Ar{C}), 137.9 (d, $^2J_{\text{RhC}} = 3$, CHCHMes), 137.6 (s, Ar{C}), 136.0 (s, Ar{C}), 135.4 (s, Ar^F), 134.4 (s, Ar{C}), 129.5 (s, Ar{CH}), 129.4 (s, Ar{CH}), 129.4 (qq, $^2J_{\text{FC}} = 32$, $^3J_{\text{CB}} = 3$, Ar^F), 125.1 (q, $^1J_{\text{FC}} = 271$, Ar^F), 124.7 (s, py), 124.6 (s, py), 123.9 (s, Ar{C}), 122.9 (s, NCH), 122.8 (s, NCH), 121.9 (s, CHCHMes), 120.9 (s, NCH), 120.6 (s, NCH), 118.0 (sept., $^3J_{\text{FC}} = 4$, Ar^F), 91.5 (d, $^1J_{\text{RhC}} = 15$, C≡CMes), 85.5

(d, $^1J_{\text{RhC}} = 14$, $\text{C}\equiv\text{CMes}$), 56.6 (s, pyCH_2), 55.9 (s, pyCH_2), 37.0 (s, $p\text{-CH}_3$), 36.7 (s, $p\text{-CH}_3$), 24.2 (s, NCH_3),* 23.6 (s, NCH_3),* 21.4 (s, $o\text{-CH}_3$), 21.4 (s, $o\text{-CH}_3$). * Located using correlation experiments.

HR ESI-MS (positive ion, 4 kV): 658.2407 $[\text{M}]^+$ (calcd 658.2412) m/z .

Elemental Anal. Calcd for $\text{C}_{69}\text{H}_{53}\text{BF}_{24}\text{N}_5\text{Rh}$ ($1521.90 \text{ g}\cdot\text{mol}^{-1}$): C, 54.46; H, 3.51; N, 4.60. Found: C, 54.53; H, 3.46; N, 4.43.

$[\text{Rh}(\text{CNC-Me})(\text{PhCCPh})][\text{BAr}^{\text{F}}_4]$



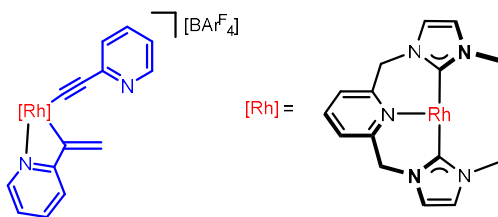
A solution of **11-Me** (13 mg, 0.010 mmol) and diphenylacetylene (2 mg 0.01 mmol) in 1,2-difluorobenzene (0.5 mL) was reacted for 15 minutes before being concentrated to dryness. The resulting bright red residue was washed with pentane (*ca.* 0.5 mL) and volatiles removed *in vacuo* to afford the desired product as a bright red powder. Yield = 12 mg (85%).

^1H NMR (500 MHz, CD_2Cl_2): δ 7.91 (br s, fwhm = 18, 4H, Ph), 7.85 (t, $^3J_{\text{HH}} = 7.7$, 1H, py), 7.77 – 7.70 (m, 8H, Ar^{F}), 7.58 – 7.51 (m, 6H, Ar^{F} + py), 7.43 – 7.29 (m, 6H, Ph), 6.99 (d, $^3J_{\text{HH}} = 1.9$, 2H, NCH), 6.55 (d, $^3J_{\text{HH}} = 1.8$, 2H, NCH), 5.87 (d, $^2J_{\text{HH}} = 14.7$, 2H, pyCH_2), 5.18 (d, $^2J_{\text{HH}} = 14.8$, 2H, pyCH_2), 3.26 (s, 6H, NCH_3).

$^{13}\text{C}\{^1\text{H}\}$ NMR (126 MHz, CD_2Cl_2): δ 183.1 (d, $^1J_{\text{RhC}} = 41$, NCN), 162.1 (q, $^1J_{\text{CB}} = 50$, Ar^{F}), 155.6 (s, py), 139.5 (s, py), 135.2 (s, Ar^{F}), 131.0 (s, $\text{Ph}\{\text{CH}\}$), 129.4 (d, $^2J_{\text{RhC}} = 6$, $\text{Ph}\{\text{C}\}$), 129.1 (s, $\text{Ph}\{\text{CH}\}$), 129.1 (qq, $^2J_{\text{FC}} = 32$, $^3J_{\text{CB}} = 3$, Ar^{F}), 128.5 (s, $\text{Ph}\{\text{CH}\}$), 125.0 (q, $^1J_{\text{FC}} = 272$, Ar^{F}), 124.6 (s, py), 122.7 (s, NCH), 120.4 (s, NCH), 118.0 (sept., $^3J_{\text{FC}} = 4$, Ar^{F}), 88.8 (br, $\text{PhC}\equiv\text{CPh}$), 56.4 (s, pyCH_2), 36.6 (s, CH_3).

Elemental Anal. Calcd for $\text{C}_{61}\text{H}_{39}\text{BF}_{24}\text{N}_5\text{Rh}$ ($1411.70 \text{ g}\cdot\text{mol}^{-1}$): C, 51.90; H, 2.78; N, 4.96. Found: C, 51.63; H, 2.69; N, 4.85.

[Rh(CNC-Me)(CCpy)(C(CH₂)py)][BAr^F₄] – **23-Me**



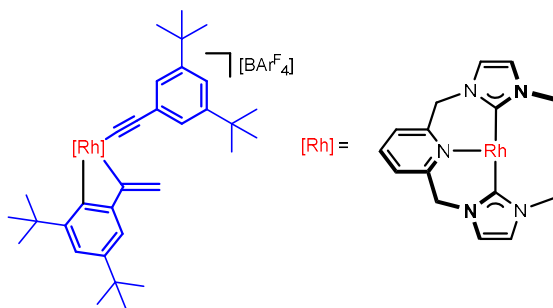
2-ethynylpyridine (9.6 μ L, 0.096 mmol) was added to a stirring solution of **11-Me** (60 mg, 0.048 mmol) in 1,2-difluorobenzene (4 mL) and the reaction stirred for 18 hours at 65 °C before the removal of volatiles *in vacuo*. The product was isolated through recrystallisation from a CH₂Cl₂/hexane layer at -30 °C. Yield = 46.8 mg (72%, mixture of isomers). Crystals grown from a CH₂Cl₂/hexane layer at -30 °C were suitable for X-ray diffraction.

¹H NMR (500 MHz, CD₂Cl₂): δ 8.30 (d, ³J_{HH} = 4.9, 1H, py), 8.01 (d, ³J_{HH} = 5.2, 1H, py), 7.95 (t, ³J_{HH} = 7.7, 1H, py), 7.77 – 7.70 (m, 8H, Ar^F), 7.59 (d, ³J_{HH} = 7.6, 1H, py), 7.57 (d, ³J_{HH} = 7.8, 1H, py), 7.55 (s, 4H, Ar^F), 7.45 (td, ³J_{HH} = 7.7, ⁴J_{HH} = 1.9, 1H, py), 7.39 (d, ³J_{HH} = 8.1, 1H, py), 7.18 – 7.11 (m, 2H, py), 7.09 (s, 1H, NCH), 7.07 (d, ³J_{HH} = 8.1, 1H, py), 7.00 – 6.92 (m, 2H, pyCH₂ + NCH), 6.89 (s, 1H, NCH), 6.78 (s, 1H, NCH), 6.47 (d, ²J_{HH} = 4.0, 1H, C(CH₂)py), 5.96 (d, ²J_{HH} = 2.3, 1H, C(CH₂)py), 5.37 (d, ²J_{HH} = 15.3, 1H, pyCH₂), 5.11 (d, ²J_{HH} = 15.2, 1H, pyCH₂), 5.05 (d, ²J_{HH} = 15.1, 1H, pyCH₂), 4.18 (s, 3H, NCH₃), 3.06 (s, 3H, NCH₃).

¹³C{¹H} NMR (126 MHz, CD₂Cl₂): δ 173.0 (d, ²J_{Rh} = 5, py), 172.5 (d, ¹J_{Rh} = 37, NCN), 171.8 (d, ¹J_{Rh} = 37, NCN), 162.1 (q, ¹J_{CB} = 50, Ar^F), 157.1 (s, py), 155.3 (s, py), 149.9 (s, py), 149.1 (s, py), 146.7 (s, py), 140.6 (s, py), 138.1 (s, py), 137.0 (d, ¹J_{RhC} = 25, C(CH₂)py), 136.0 (s, py), 135.2 (s, Ar^F), 129.1 (qq, ²J_{FC} = 32, ³J_{CB} = 3, Ar^F), 126.2 (s, py), 125.5 (s, py), 125.2 (s, py), 125.0 (q, ¹J_{FC} = 272, Ar^F), 124.4 (NCH), 124.3 (s, py + NCH), 122.4 (s, NCH), 122.3 (s, NCH), 120.7 (s, py), 119.8 (s, C(CH₂)py), 118.0 (sept., ³J_{FC} = 4, Ar^F), 114.4 (s, py), 106.4 (d, ²J_{RhC} = 12, C \equiv Cpy), 98.8 (d, ¹J_{RhC} = 56, C \equiv Cpy), 56.5 (s, pyCH₂), 55.5 (s, pyCH₂), 39.0 (s, NCH₃), 36.4 (s, NCH₃).

HR ESI-MS (positive ion, 4 kV): 576.1373, [M]⁺ (calcd 576.1377) *m/z*.

Characterisation of the [Rh(CNC-Me)(CCAr')(C(CH₂)Ar')][BAR^F₄] – **22-Me**



0.5 mL of CD₂Cl₂ cooled to -30 °C was added to a pre-cooled J. Young's valve NMR tube (-30 °C) containing **15-Me** (13.2 mg, 10.0 μmol) and **16a** (6.4 mg, 30 μmol) and the resulting solution immediately frozen in liquid nitrogen. The sample was thawed immediately before insertion into an NMR spectrometer pre-equilibrated to 5 °C.

¹H NMR (600 MHz, CD₂Cl₂): δ 7.94 (t, ³J_{HH} = 7.8, 1H, py), 7.77 – 7.70 (m, 8H, Ar^F), 7.57 (d, ³J_{HH} = 7.7, 1H, py), 7.55 (s, 4H, Ar^F), 7.52 (d, ³J_{HH} = 7.7, 1H, py), 7.24 (s, 1H, NCH), 7.22 (s, 2H, Ar'), 7.16 – 7.18 (m, 2H, Ar'), 7.06 (s, 1H, NCH), 7.04 (s, 1H, NCH), 7.02 (s, 1H, NCH), 6.79 (s, 2H, Ar'), 6.22 (d, ²J_{HH} = 14.9, 1H, pyCH₂), 5.95 (d, ²J_{HH} = 15.4, 1H, pyCH₂), 5.10 (d, ²J_{HH} = 15.0, 1H, pyCH₂), 4.88 (d, ²J_{HH} = 15.5, 1H, pyCH₂), 4.79 (d, ²J_{HH} = 2.9, 1H, C(CH₂)Ar'), 4.48 (s, 3H, NCH₃), 4.04 (s, 3H, NCH₃), 3.21 (d, ²J_{HH} = 2.1, 1H, C(CH₂)Ar'), 1.23 (s, 18H, tBu), 1.20 (s, 18H, tBu).

¹³C{¹H} NMR (151 MHz, CD₂Cl₂): δ 177.0 (d, ¹J_{RhC} = 40, NCN), 176.6 (d, ¹J_{RhC} = 40, NCN), 162.1 (q, ¹J_{CB} = 50, Ar^F), 157.2 (s, py), 155.6 (s, py), 153.8 (d, ¹J_{RhC} = 36, C(CH₂)Ar'), 150.8 (s, Ar'), 149.5 (s, Ar'), 140.3 (s, py), 135.2 (br, Ar^F), 129.1 (qq, ²J_{FC} = 32, ³J_{CB} = 3, Ar^F), 126.4 (s, py), 125.6 (s, py), 125.0 (q, ¹J_{FC} = 272, Ar^F), 124.6 (s, Ar'), 123.6 (s, NCH), 121.7 (s, NCH), 121.5 (s, NCH), 120.2 (s, Ar'), 119.9 (s, C(CH₂)Ar'), 118.0 (sept., ³J_{FC} = 4, Ar^F), 111.8 (d, ²J_{RhC} = 11, C≡CAr'), 101.9 (d, ¹J_{RhC} = 55, C≡CAr'), 55.7 (s, pyCH₂), 55.3 (s, pyCH₂), 39.4 (s, NCH₃), 38.8 (s, NCH₃), 35.0 (s, tBu{C}), 34.9 (s, tBu{C}), 31.8 (s, tBu), 31.6 (s, tBu).

¹H NMR (600 MHz, DiFB): δ 8.17 (s, 8H, Ar^F), 7.56 (t, ³J_{HH} = 7.7, 1H, py), 7.46 (s, 4H, Ar^F), 6.38 (d, ²J_{HH} = 14.7, 1H, pyCH₂), 5.89 (d, ²J_{HH} = 15.4, 1H, pyCH₂), 5.02 (d, ²J_{HH} = 14.9, 1H, pyCH₂), 4.82 (s, 1H, C(CH₂)), 4.67 (d, ²J_{HH} = 15.5, 1H, pyCH₂), 4.53 (s, 3H, NCH₃), 4.00 (s, 1H, NCH₃), 3.21 (s, 1H, C(CH₂)). *Selected data only.*

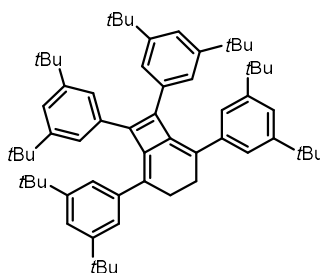
HR ESI-MS (positive ion, 4 kV): 798.3985 ([M]⁺, 798.3977 calcd) *m/z*.

5.3.5. Synthesis of bicyclo[4.2.0]octa-1,5,7-trienes

General procedure

A standard solution of the chosen terminal alkyne (5 mL, 100 mM) was added to **11-Me** (31.5 mg, 5 mol%) under an argon atmosphere. The resulting red solution was reacted at 65 °C until complete consumption of alkyne before being placed under an atmosphere of CO (1 atm).

2,5,7,8-tetrakis(3,5-di-*tert*-butylphenyl)bicyclo[4.2.0]octa-1,5,7-triene – 24a



(3,5-di-*tert*-butylphenyl)acetylene (107 mg, 0.499 mmol) in 1,2-difluorobenzene (5 mL) was reacted with **11-Me** (31.5 mg, 0.0250 mmol) for 4 hours according to the general procedure. The solution was then concentrated to dryness *in vacuo* and the product extracted into cold TMS (0 °C). The product was isolated as a pale-yellow solid on removal of volatiles under reduced pressure. Yield = 101 mg (94%). Crystals suitable for X-ray diffraction were grown from slow evaporation of a solution in TMS.

¹H NMR (500 MHz, CD₂Cl₂): δ 7.22 (t, ³J_{HH} = 1.9, 2H, *p*-Ar), 7.18 (t, ³J_{HH} = 1.9, 2H, *p*-Ar), 7.05 (d, ³J_{HH} = 1.9, 4H, *o*-Ar), 7.02 (d, ³J_{HH} = 1.9, 4H, *o*-Ar), 2.97 (s, 4H, CH₂), 1.11 (s, 32H, *t*Bu), 1.08 (s, 32H, *t*Bu).

¹³C{¹H} NMR (126 MHz, CD₂Cl₂): δ 150.8 (s, *m*-C), 150.5 (s, *m*-C), 149.0 (s, C^{7/8}), 139.2 (s, *i*-C), 135.5 (s, C^{1/6}), 133.0 (s, *i*-C), 123.5 (s, *o*-CH), 123.0 (s, *o*-CH), 122.9 (s, *p*-CH), 121.3 (s, *p*-CH), 118.7 (s, C^{2/5}), 35.1 (s, *t*Bu{C}), 35.0 (s, *t*Bu{C}), 31.6 (s, *t*Bu), 31.6 (s, *t*Bu), 30.0 (s, CH₂).

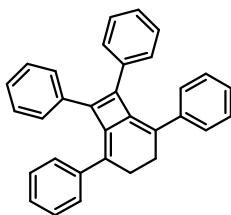
¹H NMR (600 MHz, DiFB): 2.87 (s, 4H, CH₂), 1.11 (s, 32H, *t*Bu), 1.03 (s, 32H, *t*Bu).

Selected data only.

HR ESI-MS (positive ion, 4 kV): 879.6775 ([M+Na]⁺, calcd 879.6778) *m/z*.

Elemental Anal. Calcd for C₃₂H₂₄ (857.41 g·mol⁻¹): C, 89.65; H, 10.35; N, 0.00. Found: C, 89.61; H, 10.35; N, 0.00.

2,5,7,8-tetraphenylbicyclo[4.2.0]octa-1,5,7-triene – 24c



Phenylacetylene (51 mg, 0.50 mmol) in 1,2-difluorobenzene (5 mL) was reacted with

11-Me (31.5 mg, 0.0250 mmol) for 4 hours according to the general procedure. Following concentrating to dryness the crude product was extracted into hexane. Recrystallisation from a saturated hexane solution cooled to 4 °C afforded the pure product as pale-yellow needles. Yield = 39 mg (76%).

¹H NMR (500 MHz, CD₂Cl₂): δ 7.27 – 7.02 (m, 20H, Ph), 2.98 (s, 4H, CH₂).

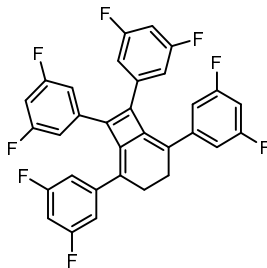
¹³C{¹H} NMR (126 MHz, CD₂Cl₂): δ 148.7 (s, C^{7/8}), 139.9 (s, *i*-C), 135.6 (s, C^{1/6}), 133.6 (s, *i*-C), 129.2 (s, CH), 128.8 (s, CH), 128.6 (s, CH), 128.4 (s, CH), 128.2 (s, CH), 127.3 (s, CH), 118.7 (s, C^{2/5}), 29.5 (s, CH₂).

¹H NMR (400 MHz, DiFB): δ 2.79 (s, 4H, CH₂). *Selected data only.*

HR ESI-MS (positive ion, 4 kV): 447.1511 ([M+K]⁺, calcd 447.1510) *m/z*.

Elemental Anal. Calcd for C₃₂H₂₄ (408.54 g·mol⁻¹): C, 94.08; H, 5.82; N, 0.00. Found: C, 94.08; H, 5.84; N, 0.00.

2,5,7,8-tetrakis(3,5-difluorophenyl)bicyclo[4.2.0]octa-1,5,7-triene – 24g



(3,5-difluorophenyl)acetylene (59 μL, 0.50 mmol) in 1,2-difluorobenzene (5 mL) was reacted with **11-Me** (31.5 mg, 0.0250 mmol) for 8 hours according to the general procedure. The resulting solution was concentrated to dryness and the residues washed with cold diethyl ether (0 °C) to afford the product as a yellow powder. Yield = 68.6 mg (75%). Crystals suitable for X-ray diffraction were grown from slow evaporation of a CH₂Cl₂ solution at 18 °C.

^1H NMR (500 MHz, CD_2Cl_2): δ 6.81 (tt, $^3J_{\text{FH}} = 9.0$, $^4J_{\text{HH}} = 2.3$, 1H, *p*-Ar), 6.75 (tt, $^3J_{\text{FH}} = 8.9$, $^4J_{\text{HH}} = 2.3$, 1H, *p*-Ar), 6.75 – 6.68 (m, 4H, *o*-Ar), 6.66 – 6.59 (m, 4H, *o*-Ar), 2.93 (s, 4H, CH_2).

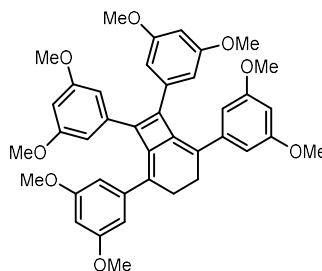
$^{13}\text{C}\{^1\text{H}\}$ NMR (126 MHz, CD_2Cl_2): δ 163.3 (dd, $^1J_{\text{FC}} = 248$, $^3J_{\text{FC}} = 24$, CF), 163.2 (dd, $^1J_{\text{FC}} = 248$, $^3J_{\text{FC}} = 23$, CF), 147.7 (t, $^4J_{\text{FC}} = 3$, $\text{C}^{7/8}$), 142.2 (t, $^3J_{\text{FC}} = 10$, *i*-C), 135.6 (s, $\text{C}^{1/6}$), 135.1 (t, $^3J_{\text{FC}} = 10$, *i*-C), 119.1 (t, $^4J_{\text{FC}} = 3$, $\text{C}^{2/5}$), 112.0 (dd, $^2J_{\text{FC}} = 20$, $^4J_{\text{FC}} = 6$, *o*-Ar), 111.5 (dd, $^2J_{\text{FC}} = 20$, $^4J_{\text{FC}} = 6$, *o*-Ar), 104.9 (t, $^2J_{\text{FC}} = 26$, *p*-Ar), 103.2 (t, $^2J_{\text{FC}} = 26$, *p*-Ar), 28.9 (s, CH_2).

$^{19}\text{F}\{^1\text{H}\}$ NMR (377 MHz, CD_2Cl_2): δ -109.7 (s, 4F), -111.1 (s, 4F).

^1H NMR (400 MHz, D_2O): δ 2.67 (s, 4H, CH_2). *Selected data only.*

Elemental Anal. Calcd for $\text{C}_{32}\text{H}_{16}\text{F}_8$ (552.47 $\text{g}\cdot\text{mol}^{-1}$): C, 69.57; H, 2.92; F, 28.51. Found: C, 69.72; H, 2.85; F, 28.51.

2,5,7,8-tetrakis(3,5-dimethoxyphenyl)bicyclo[4.2.0]octa-1,5,7-triene – 24h



(3,5-dimethoxyphenyl)acetylene (81 mg, 0.50 mmol) in 1,2-difluorobenzene (5 mL) was reacted with **11-Me** (31.5 mg, 0.0250 mmol) for 7 hours according to the general procedure. The dark yellow solution was concentrated to dryness and the crude compound. The pure compound was isolated after washing with cold diethyl ether and removing volatiles under reduced pressure. Yield = 53 mg (64%). Crystals suitable for X-ray diffraction were grown from slow evaporation of a CH_2Cl_2 solution at 18 °C.

^1H NMR (500 MHz, CD_2Cl_2): δ 6.40 (d, $^4J_{\text{HH}} = 2.2$, 4H, *o*-Ar), 6.37 (d, $^4J_{\text{HH}} = 2.2$, 4H, *o*-Ar), 6.36 – 6.35 (m, 2H, *p*-Ar), 6.32 (t, $^4J_{\text{HH}} = 2.2$, 2H, *p*-Ar), 3.52 (s, 12H, OCH_3), 3.49 (s, 12H, OCH_3), 2.94 (s, 4H, CH_2).

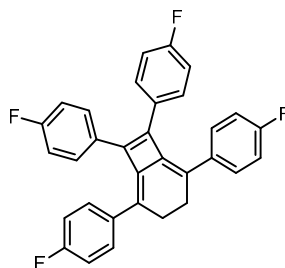
$^{13}\text{C}\{^1\text{H}\}$ NMR (126 MHz, CD_2Cl_2): δ 160.9 (s, *m*-Ar), 160.7 (s, *m*-Ar), 148.9 (s, $\text{C}^{7/8}$), 141.7 (s, *i*-C), 135.5 (s, $\text{C}^{1/6}$), 134.9 (s, *i*-C), 119.2 (s, $\text{C}^{2/5}$), 106.9 (s, *o*-Ar), 106.8 (s, *o*-Ar), 101.9 (s, *p*-Ar), 100.3 (s, *p*-Ar), 55.7 (s, OCH_3), 55.5 (s, OCH_3), 29.5 (s, CH_2).

¹H NMR (400 MHz, DiFB): δ 3.42 (s, 12H, CH₃), 3.36 (s, 12H, CH₃), 2.83 (s, 4H, CH₂). *Selected data only.*

HR ESI-MS (positive ion, 4 kV): 671.2607 ([M+Na]⁺, calcd 671.2615) *m/z*.

Elemental Anal. Calcd for C₄₀H₄₀O₈ (648.75 g·mol⁻¹): C, 74.06; H, 6.22; N, 0.00. Found: C, 73.82; H, 6.30; N, 0.00.

2,5,7,8-tetra(4-fluorophenyl)bicyclo[4.2.0]octa-1,5,7-triene – 24i



4-fluorophenylacetylene (60 mg, 0.50 mmol) in 1,2-difluorobenzene (5 mL) was reacted with **11-Me** (31.5 mg, 0.0250 mmol) for 6 hours according to the general procedure. Following concentrating to dryness the crude product was extracted into diethyl ether and passed through a short plug (silica; diethyl ether). Recrystallisation from a saturated diethyl ether solution cooled to 4 °C afforded the pure product as pale-yellow needles. Yield = 49.1 mg (82%).

¹H NMR (500 MHz, CD₂Cl₂): δ 7.18 (app. dd, *J* = 8, 6, 4H, *o*-Ar), 7.07 (app. dd, *J* = 8, 6, 4H, *o*-Ar), 6.90 (app. td, *J* = 9, 6, 8H, 2× *m*-Ar), 2.93 (s, 4H, CH₂).

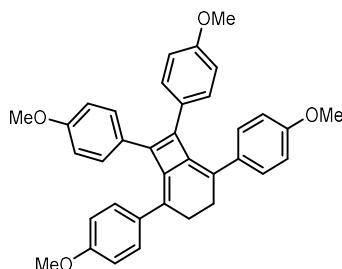
¹³C{¹H} NMR (126 MHz, CD₂Cl₂): δ 163.1 (d, ¹*J*_{FC} = 248, CF), 162.5 (d, ¹*J*_{FC} = 246, CF), 147.2 (s, C^{7/8}), 135.9 (d, ⁴*J*_{FC} = 3, *i*-Ar), 135.2 (s, C^{1/6}), 131.1 (d, ³*J*_{FC} = 8, *o*-Ar), 130.3 (d, ³*J*_{FC} = 8, *o*-Ar), 129.5 (d, ⁴*J*_{FC} = 4, *i*-Ar), 117.7 (s, C^{2/5}), 115.6 (d, ²*J*_{FC} = 22, *m*-Ar), 115.1 (d, ²*J*_{FC} = 21, *m*-Ar), 29.5 (s, CH₂).

¹⁹F{¹H} NMR (376 MHz, CD₂Cl₂): δ -112.93 (s, 2F), -115.85 (s, 2F).

¹H NMR (300 MHz, DiFB): δ 2.71 (s, 4H, CH₂). *Selected data only.*

Elemental Anal. Calcd for C₃₂H₂₀F₄ (480.51 g·mol⁻¹): C, 79.99; H, 4.20; N, 0.00. Found: C, 79.90; H, 4.15; N, 0.00.

2,5,7,8-tetra(4-methoxyphenyl)bicyclo[4.2.0]octa-1,5,7-triene – **24j**



4-Methoxyphenylacetylene (66 mg, 0.50 mmol) in 1,2-difluorobenzene (5 mL) was reacted with **11-Me** (31.5 mg, 0.0250 mmol) for 6.5 hours according to the general procedure. The resulting solution was concentrated to dryness and the residue washed with cold diethyl ether. The pure product was obtained as a pale-yellow solid on removal of volatiles *in vacuo*. Yield = 52 mg (79%)

¹H NMR (500 MHz, CD₂Cl₂): δ 7.15 (d, ³J_{HH} = 8.6, 4H, *o*-Ar), 7.07 (d, ³J_{HH} = 8.7, 4H, *o*-Ar), 6.74 (d, ³J_{HH} = 8.7, 4H, *m*-Ar), 6.71 (d, ³J_{HH} = 8.7, 4H, *m*-Ar), 3.78 (s, 12H, 2 × OCH₃), 2.90 (s, 4H, CH₂).

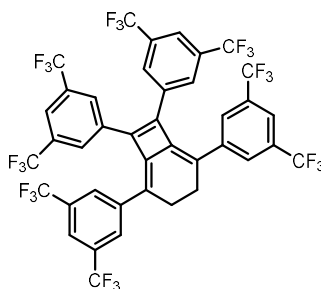
¹³C{¹H} NMR (126 MHz, CD₂Cl₂): δ 160.0 (s, *p*-Ar), 159.1 (s, *p*-Ar), 146.9 (s, C^{7/8}), 134.9 (s, C^{1/6}), 132.8 (s, *i*-C), 130.7 (s, *o*-Ar), 129.9 (s, *o*-Ar), 126.5 (s, *i*-C), 117.0 (s, C^{2/5}), 113.7 (s, *m*-Ar), 113.6 (s, *m*-Ar), 55.8 (s, OCH₃), 55.8 (s, OCH₃), 29.7 (s, CH₂).

¹H NMR (300 MHz, DiFB): δ 3.56 (s, 6H, OCH₃), 3.51 (s, 6H, OCH₃), 2.80 (s, 4H, CH₂). *Selected data only.*

HR ESI-MS (positive ion, 4 kV): 551.2188 ([M+Na]⁺, calcd 551.2193) *m/z*.

Elemental Anal. Calcd for C₃₆H₃₂O₄ (528.65 g·mol⁻¹): C, 81.79; H, 6.10; N, 0.00. Found: C, 81.67; H, 5.94; N, 0.00.

2,5,7,8-tetrakis(3,5-di(trifluoromethyl)phenyl)bicyclo[4.2.0]octa-1,5,7-triene – **24k**



Reaction of 3,5-bis(trifluoromethyl)phenylacetylene (119 mg, 0.500 mmol) with **11-Me** (31.5 mg, 0.0250 mmol) in 1,2-difluorobenzene (5 mL) was conducted according to the general procedure for 5.5 hours. After quenching the resulting orange gel was concentrated to dryness and the crude product extracted into hexane. The pure compound was isolated as a pale-yellow solid following purification using flash column chromatography (silica; hexane). Yield = 94.4 mg (79%).

^1H NMR (600 MHz, CDCl_3): δ 7.83 (s, 2H, *p*-CH), 7.79 (s, 2H, *p*-CH), 7.59 (s, 4H, *o*-CH), 7.43 (s, 4H, *o*-CH), 3.11 (s, 4H, CH_2).

$^{13}\text{C}\{^1\text{H}\}$ NMR (151 MHz, CDCl_3): δ 146.8 (s, $\text{C}^{7/8}$), 139.7 (s, *i*-C), 135.2 (s, $\text{C}^{1/6}$), 132.8 (s, *i*-C), 132.6 (q, $^2J_{\text{FC}} = 34$, $\underline{\text{CCF}_3}$), 132.0 (q, $^2J_{\text{FC}} = 34$, $\underline{\text{CCF}_3}$), 128.0 (s, *o*-Ar), 127.9 (s, *o*-Ar), 123.1 (q, $^1J_{\text{FC}} = 273$, CF_3), 123.1 (s, *p*-Ar), 122.7 (q, $^1J_{\text{FC}} = 273$, CF_3), 121.8 (s, *p*-Ar), 119.2 (s, $\text{C}^{2/5}$), 28.5 (s, CH_2).

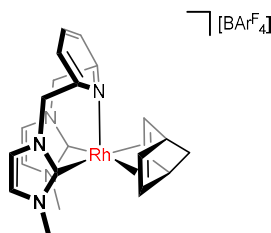
$^{19}\text{F}\{^1\text{H}\}$ NMR (377 MHz, CDCl_3): δ -63.42 (s, 12F), -63.73 (s, 12F).

^1H NMR (300 MHz, DiFB): δ 2.92 (s, 4H, CH_2). *Selected data only.*

Elemental Anal. Calcd for $\text{C}_{40}\text{H}_{16}\text{F}_{24}$ (952.53 $\text{g}\cdot\text{mol}^{-1}$): C, 50.44; H, 1.69; F, 47.87. Found: C, 50.29; H, 1.69; F, 47.87.

5.3.6. Mechanistic probes

$[\text{Rh}(\text{CNC-Me})(\text{NBD})][\text{BAr}^{\text{F}}_4] - \mathbf{26-Me}$



Norbornadiene (4 μL , 0.04 μmol) was added to a stirring solution of **11-Me** (45 mg, 0.036 μmol) in 1,2-difluorobenzene (4 mL). The solution was stirred for 10 minutes before being concentrated to dryness and the resulting yellow residue washed with pentane (2 mL) and dried *in vacuo*. Recrystallisation from a CH_2Cl_2 solution layered with excess pentane at 18 $^\circ\text{C}$ afforded the clean product as a

yellow crystalline solid. Yield = 35.1 mg (76%). Crystals grown in this way were suitable for X-ray diffraction.

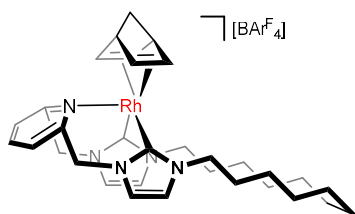
^1H NMR (500 MHz, CD_2Cl_2): δ 7.82 (t, $^3J_{\text{HH}} = 7.7$, 1H, py), 7.77 – 7.70 (m, 8H, Ar^{F}), 7.55 (s, 4H, Ar^{F}), 7.45 (d, $^3J_{\text{HH}} = 7.7$, 2H, py), 7.07 (d, $^3J_{\text{HH}} = 1.8$, 2H, NCH), 6.90 (d, $^3J_{\text{HH}} = 1.8$, 2H, NCH), 5.13 (d, $^2J_{\text{HH}} = 14.0$, 2H, pyCH_2), 4.97 (d, $^2J_{\text{HH}} = 14.1$, 2H, pyCH_2), 4.10 (s, 6H, NCH₃), 3.51 (s, 2H, NBD), 3.13 (s, 4H, NBD), 1.16 (s, 2H, NBD). **$^{13}\text{C}\{^1\text{H}\}$ NMR** (126 MHz, CD_2Cl_2): δ 187.4 (d, $^1J_{\text{RhC}} = 51$, NCN), 162.1 (q, $^1J_{\text{CB}} = 50$, Ar^{F}), 157.0 (s, py), 139.6 (s, py), 135.2 (br, Ar^{F}), 129.1 (qq, $^2J_{\text{FC}} = 32$, $^3J_{\text{CB}} = 3$, Ar^{F}), 125.0 (q, $^1J_{\text{FC}} = 272$, Ar^{F}), 123.9 (s, py), 123.1 (s, NCH), 122.6 (s, NCH), 118.0 (sept., $^3J_{\text{FC}} = 4$, Ar^{F}), 60.9 (d, $^3J_{\text{RhC}} = 5$, NBD), 56.5 (s, pyCH_2), 48.3 (d, $^2J_{\text{RhC}} = 2$, NBD), 43.6 (d, $^1J_{\text{RhC}} = 8$, NBD), 39.7 (s, NCH₃).

^1H NMR (300 MHz, DiFB): δ 8.20 – 8.03 (m, 8H, Ar^{F}), 7.52 (t, $^3J_{\text{HH}} = 8.2$, 1H, py), 7.50 (s, 4H, Ar^{F}), 4.94 (d, $^3J_{\text{HH}} = 14.0$, 2H, pyCH_2), 4.78 (d, $^3J_{\text{HH}} = 14.1$, 2H, pyCH_2), 3.90 (s, 6H, NCH₃), 3.19 (s, 2H, NBD), 2.78 (s, 4H, NBD), 0.88 (s, 2H, NBD).

HR ESI-MS (positive ion, 4 kV): 462.1159 ($[\text{M}]^+$, 462.1160 calcd) m/z .

Elemental Anal. Calcd for $\text{C}_{54}\text{H}_{37}\text{BF}_4\text{N}_5\text{Rh}$ (1325.60 $\text{g}\cdot\text{mol}^{-1}$): C, 48.93; H, 2.81; N, 5.28. Found: C, 49.04; H, 2.63; N, 5.30.

$[\text{Rh}(\text{CNC-12})(\text{NBD})][\text{BAr}^{\text{F}}_4] - \mathbf{26-12}$



Norbornadiene (1.1 μL , 0.010 mmol) was added to a stirring solution of **11-12** (14 mg, 0.010 mmol) in 1,2-difluorobenzene (0.5 mL). The solution was stirred for 3 hours before being concentrated to dryness and the resulting yellow residue washed with pentane (2 mL) and dried *in vacuo*. Yield = 10.1 mg (69%). Crystals suitable for X-ray diffraction were grown from a 1,2-difluorobenzene/hexane layer at $-30\text{ }^\circ\text{C}$.

^1H NMR (500 MHz, CD_2Cl_2): δ 7.82 (t, $^3J_{\text{HH}} = 7.7$, 1H, py), 7.77 – 7.70 (m, 8H, Ar^{F}), 7.55 (s, 4H, Ar^{F}), 7.45 (d, $^3J_{\text{HH}} = 7.7$, 2H, py), 7.10 (d, $^3J_{\text{HH}} = 1.9$, 2H, NCH), 6.95 (d, $^3J_{\text{HH}} = 1.8$, 2H, NCH), 5.19 (d, $^2J_{\text{HH}} = 14.1$, 2H, pyCH_2), 5.04 (app. td, $J = 12.2$, 6.1,

2H, NCH₂), 4.99 (d, $^2J_{\text{HH}} = 14.1$, 2H, pyCH₂), 3.92 (app. td, $J = 12.1$, 4.7, 2H, NCH₂), 3.54 – 3.43 (m, 2H, NBD), 3.17 – 3.03 (m, 4H, NBD), 2.05 – 1.94 (m, 2H, CH₂), 1.94 – 1.82 (m, 2H, CH₂), 1.67 – 1.38 (m, 16H, CH₂), 1.20 – 1.15 (m, 2H, NBD).

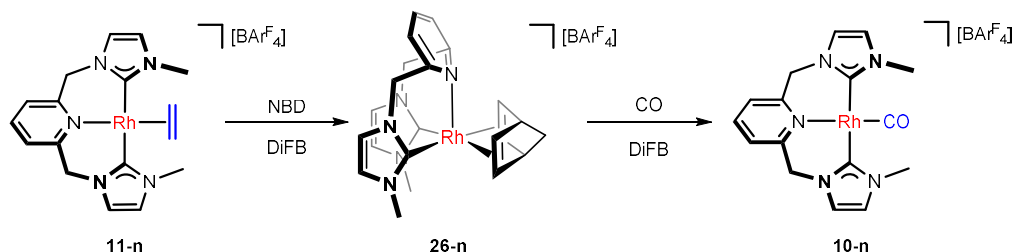
$^{13}\text{C}\{^1\text{H}\}$ NMR (126 MHz, CD₂Cl₂): δ 186.6 (d, $^1J_{\text{RhC}} = 51$, NCN), 162.1 (q, $^1J_{\text{CB}} = 50$, Ar^F), 157.2 (s, py), 139.6 (s, py), 135.2 (br, Ar^F), 129.1 (qq, $^2J_{\text{FC}} = 32$, $^3J_{\text{CB}} = 3$, Ar^F), 125.0 (q, $^1J_{\text{FC}} = 272$, Ar^F), 123.8 (s, py), 123.6 (s, NCH), 120.4 (s, NCH), 118.0 (sept., $^3J_{\text{FC}} = 4$, Ar^F), 60.8 (d, $^3J_{\text{RhC}} = 5$, NBD), 56.5 (s, pyCH₂), 52.2 (s, NCH₂), 48.4 (d, $^2J_{\text{RhC}} = 2$, NBD), 43.1 (d, $^1J_{\text{RhC}} = 8$, NBD), 31.8 (s, CH₂), 26.9 (s, CH₂), 26.7 (s, CH₂), 26.0 (s, CH₂), 24.9 (s, CH₂).

^1H NMR (300 MHz, DiFB): δ 8.20 – 8.03 (m, 8H, Ar^F), 7.52 (t, $^3J_{\text{HH}} = 7.9$, 1H, py), 7.50 (s, 4H, Ar^F), 5.02 (d, $^3J_{\text{HH}} = 14.2$, 2H, pyCH₂), 4.92 (app. td, $J = 12.1$, 6.2, 2H, NCH₂), 4.81 (d, $^3J_{\text{HH}} = 14.2$, 2H, pyCH₂), 3.72 (app. td, $J = 11.8$, 4.9, 2H, NCH₂), 3.36 (s, 4H, CH₂), 2.96 (s, 4H, NBD), 1.82 (s, 2H, NBD), 1.73 (br s, fwhm = 41, 4H, CH₂), 1.49 – 1.20 (m, 12H, CH₂), 1.03 (s, 2H, NBD).

HR ESI-MS (positive ion, 4 kV): 600.2563 ([M]⁺, 600.2568 calcd) m/z .

Elemental Anal. Calcd for C₆₄H₅₅BF₂₄N₅Rh (1463.86 g·mol⁻¹): C, 52.51; H, 3.79; N, 4.78. Found: C, 52.64; H, 3.72; N, 4.65.

Reactions of NBD complexes with CO



From **11-Me** to **26-Me**

NBD (1.1 μL , 0.010 mmol) was added to a solution of **11-Me** (12.6 mg, 0.0999 mmol) in 1,2-difluorobenzene (0.5 mL). The reaction was mixed *via* inversion (*ca.* 30 rpm) and its progress monitored using ^1H NMR spectroscopy using the Ar^F signals as an internal standard. ($t = 2.75$ hours)

From **11-12** to **26-12**

NBD (1.1 μL , 0.010 mmol) was added to a solution of **11-12** (14 mg, 0.010 mmol) in 1,2-difluorobenzene (0.5 mL). The reaction was periodically mixed *via*

inversion (*ca.* 30 rpm) and its progress monitored using ^1H NMR spectroscopy using the Ar^{F} signals as an internal standard. ($t = 2$ hours)

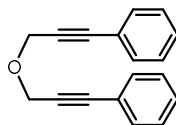
From 26-Me to 10-Me

A solution of **26-Me** (13 mg, 0.098 mmol) in 1,2-difluorobenzene (0.5 mL) was freeze-pump-thaw degassed and placed under an atmosphere of carbon monoxide (1 atm). The reaction was periodically mixed *via* inversion (*ca.* 30 rpm) and its progress monitored using ^1H NMR spectroscopy using the Ar^{F} signals as an internal standard. ($t = 5$ hours)

From 26-12 to 10-12

A solution of **26-12** (10 mg, 0.0068 mmol) in 1,2-difluorobenzene (0.5 mL) was freeze-pump-thaw degassed and placed under an atmosphere of carbon monoxide (1 atm). The reaction was periodically mixed *via* inversion (*ca.* 30 rpm) and its progress monitored using ^1H NMR spectroscopy using the Ar^{F} signals as an internal standard. ($t = 30$ minutes)

(Oxybis(prop-1-yne-3,1-diyl))dibenzene – 27

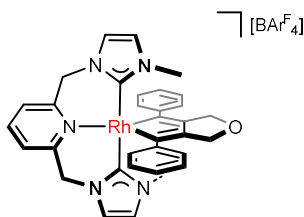


Prepared using a modified literature procedure.²⁰ A suspension of propargyl ether (1 g, 0.01 mol), iodobenzene (4.3 g, 0.021 mol), $[\text{Pd}(\text{PPh}_3)_4]$ (120 mg, 0.104 mmol, 1 mol%) and CuI (40 mg, 0.21 mmol, 2 mol%) in triethylamine (8.5 mL) and THF (20 mL) was stirred for 18 hours at room temperature. The product extracted into diethyl ether and washed with H_2O before the combined organic fraction were dried over MgSO_4 . Purification using column chromatography (silica; $\text{CHCl}_3/\text{hexane}$ 1:1) afforded the pure product as a colourless oil. Yield = 1.63 g (66%).

^1H NMR (300 MHz, CDCl_3): 7.53 – 7.43 (m, 4H, Ph), 7.36 – 7.28 (m, 6H, Ph), 4.55 (s, 4H, OCH_2).

*Data consistent with literature values.*²⁰

[Rh(CNC-Me)(Ph₂C₄(CH₂)₂O)][BARF₄] – 28



27 (2.5 mg, 0.010 mmol) was added to a stirring solution of **11-Me** (12.6 mg, 0.0999 mmol) in 1,2-difluorobenzene (0.5 mL). The resulting solution was stirred for 1 hour to afford a green solution which was concentrated to dryness and washed with pentane to give the desired product as a green solid. Yield = 14.4 mg (97%). Crystals suitable for X-ray diffraction were grown from a 1,2-difluorobenzene solution layered with excess hexane at 18 °C.

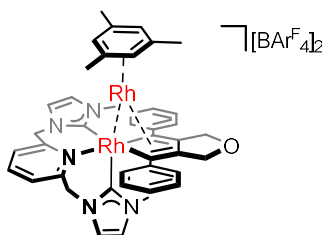
¹H NMR (500 MHz, CD₂Cl₂): δ 7.87 (t, ³J_{HH} = 7.7, 1H, py), 7.77 – 7.70 (m, 8H, Ar^F), 7.55 (s, 4H, Ar^F), 7.43 (d, ³J_{HH} = 7.7, 2H, py), 7.16 (d, ³J_{HH} = 1.8, 2H, NCH), 7.10 – 7.02 (m, 6H, Ph), 6.90 (d, ³J_{HH} = 1.8, 2H, NCH), 6.54 (d, ³J_{HH} = 6.1, 4H, Ph), 5.17 (d, ²J_{HH} = 15.7, 2H, pyCH₂), 4.98 (d, ²J_{HH} = 15.7, 2H, pyCH₂), 4.73 (d, ²J_{HH} = 12.6, 2H, OCH₂), 4.54 (d, ²J_{HH} = 12.7, 2H, OCH₂), 3.53 (s, 6H, NCH₃).

¹³C{¹H} NMR (126 MHz, CD₂Cl₂): δ 175.9 (d, ¹J_{RhC} = 44, NCN), 162.1 (q, ¹J_{CB} = 50, Ar^F), 155.6 (s, py), 155.5 (d, ²J_{RhC} = 3, OCH₂C), 150.8 (d, ¹J_{RhC} = 41, RhCPh), 145.1 (d, ²J_{RhC} = 2, Ph{C}), 141.2 (s, py), 135.2 (s, Ar^F), 129.1 (qq, ²J_{FC} = 32, ³J_{CB} = 3, Ar^F), 129.1 (s, Ph{CH}), 126.4 (s, Ph{CH}), 125.5 (s, Ph{CH}), 125.3 (s, py), 125.0 (q, ¹J_{FC} = 272, Ar^F), 124.3 (s, NCH), 122.3 (s, NCH), 118.0 (sept., ³J_{FC} = 4, Ar^F), 68.0 (d, ³J_{RhC} = 2, OCH₂), 55.7 (s, pyCH₂), 37.8 (s, NCH₃).

HR ESI-MS (positive ion, 4 kV): 616.1581 ([M]⁺, 616.1578 calcd) *m/z*.

Elemental Anal. Calcd for C₆₅H₄₃BF₂₄N₅ORh (1479.77 g·mol⁻¹): C, 52.76; H, 2.93; N, 4.73. Found: C, 52.34; H, 2.46; N, 4.29.

[Rh(CNC-Me)(Ph₂C₄(CH₂)₂O)·Rh(Mes)][BAR^F₄]₂ – **30**



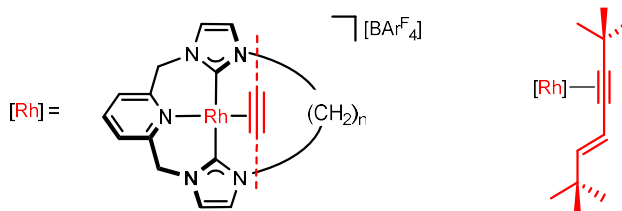
[Rh(Mes)(C₂H₄)₂][BAR^F₄] (11.4 mg, 0.00998 mmol) was added to a solution of **30** (14.4 mg, 0.00973 mmol) in 1,2-difluorobenzene (0.5 mL). The resulting solution was heated at 85 °C for 5 days to afford a deep purple solution which was concentrated to dryness. The residue was dissolved in diethyl ether (1 mL) and addition of toluene (3 mL) afforded a purple oily residue. The solvent was decanted and the resulting oil dried *in vacuo* to give the desired product as a purple/pink solid. Yield = 17.7 mg (67%).

¹H NMR (500 MHz, CD₂Cl₂): δ 7.88 (t, ³J_{HH} = 7.7, 1H, py), 7.77 (d, ³J_{HH} = 7.8, 1H, py), 7.77–7.70 (m, 16H, Ar^F), 7.55 (s, 8H, Ar^F), 7.32 (t, 1H, ³J_{HH} = 7.6, Ph), 7.29 (d, ³J_{HH} = 1.8, 1H, NCH), 7.24 (t, ³J_{HH} = 7.5, 1H, Ph), 7.21 – 7.13 (m, 4H, Ph), 7.04 (d, 1H, ³J_{HH} = 7.8, Ph), 6.93 (d, ³J_{HH} = 2.0, 1H, NCH), 6.85 (d, ³J_{HH} = 2.1, 1H, NCH), 6.79 (d, ³J_{HH} = 7.7, 1H, Ph), 6.75 (t, ³J_{HH} = 7.7, 1H, Ph), 6.60 (d, ³J_{HH} = 1.8, 1H, NCH), 6.27 (d, ³J_{HH} = 7.8, 1H, Ph), 6.19 (d, ²J_{HH} = 13.9, 1H, pyCH₂), 5.94 (s, 3H, Mes), 5.76 (d, ²J_{HH} = 13.8, 1H, pyCH₂), 5.12 (d, ²J_{HH} = 13.9, 1H, OCH₂), 5.03 (d, ²J_{HH} = 13.9, 1H, OCH₂), 4.43 (d, 1H, ²J_{HH} = 13.9, OCH₂), 4.41 (d, ²J_{HH} = 16.4, 1H, pyCH₂), 4.32 (d, ²J_{HH} = 13.9, 1H, OCH₂), 3.60 (d, ²J_{HH} = 16.4, 1H, pyCH₂), 3.55 (s, 3H, NCH₃), 2.45 (s, 3H, NCH₃), 1.87 (s, 9H, Mes).

¹³C{¹H} NMR (126 MHz, CD₂Cl₂): δ 182.9 (d, ¹J_{RhC} = 39, NCN), 162.1 (q, ¹J_{CB} = 50, Ar^F), 161.1 (dd, ¹J_{RhC} = 71, ²J_{RhC} = 5, NCN), 155.7 (s, py × 2), 145.3 (s, Ph{C}), 145.0 (d, ²J_{RhC} = 1, Ph{C}), 143.8 (dd, ¹J_{RhC} = 24, 16, RhCC), 141.0 (s, py), 137.1 (dd, ¹J_{RhC} = 36, 16, RhCC), 135.2 (s, Ar^F), 131.9 (s, Ph{CH}), 130.3 (s, Ph{CH}), 129.7 (s, Ph{CH}), 129.5 (s, Ph{CH}), 129.1 (qq, ²J_{FC} = 32, ³J_{CB} = 3, Ar^F), 129.1 (s, Ph{CH}), 128.7 (s, Ph{CH}), 125.8 (s, Ph{CH}), 125.4 (s, py), 125.1 (s, NCH), 125.0 (q, ¹J_{FC} = 272, Ar^F), 125.0 (s, NCH × 2), 124.9 (s, py), 124.6 (s, Ph{CH}), 124.3 (dd, ¹J_{RhC} = 39, 7, RhCPh), 121.6 (br s, NCH + Ph{CH}), 119.4 (d, ¹J_{RhC} = 4, Mes{C}), 118.0 (sept., ³J_{FC} = 4, Ar^F), 106.5 (d, ¹J_{RhC} = 4, Mes{CH}), 67.7 (s, OCH₂), 67.3 (s, OCH₂), 58.7 (s, pyCH₂), 53.6 (s, pyCH₂), 39.8 (s, NCH₃), 36.4 (s, NCH₃), 19.3 (s, Mes{CH₃}).

5.4 Compounds prepared in chapter 4

5.4.1. 5.4.1 Homocoupling of *t*BuCCH through a ring



[Rh(CNC-12)](*E*-*t*BuCCCHCH*t*Bu)][BAR^F₄] – 19-12

Compound prepared by **Dr Matthew Gyton** (Chaplin group, University of Warwick).²¹

¹H NMR (300 MHz, *d*₃-MeCN): δ 7.91 (t, ³*J*_{HH} = 7.7, 1H, py), 7.73 – 7.65 (m, 12H, Ar^F), 7.63 (d, ³*J*_{HH} = 8.3, 1H, py), 7.58 (d, ³*J*_{HH} = 7.6, 1H, py), 7.50 (d, ³*J*_{HH} = 15.3, 1H, CHCH*t*Bu), 7.16 (s, 2H, NCH), 6.87 (s, 1H, NCH), 6.83 (s, 1H, NCH), 6.04 (d, ³*J*_{HH} = 15.4, 1H, CHCH*t*Bu), 5.78 (d, ²*J*_{HH} = 15.1, 1H, pyCH₂), 5.47 – 5.20 (m, 3H, pyCH₂), 4.29 – 4.04 (m, 2H, NCH₂), 3.70 – 3.53 (m, 1H, NCH₂), 3.41 (td, ²*J*_{HH} = 12.5, ³*J*_{HH} = 6.0, 1H, NCH₂), 1.86 – 1.39 (m, 20H, CH₂), 1.36 (s, 9H, *t*Bu), 1.03 (s, 9H, *t*Bu).

[Rh(CNC-14)](*E*-*t*BuCCCHCH*t*Bu)][BAR^F₄] – 19-14

To a stirring solution of **11-14**, (15 mg, 0.01 mmol) dissolved in 1,2-difluorobenzene (0.4 mL) was added *tert*-butylalkyne (3 μL, 0.022 mmol). The resulting red solution was stirred at room temperature for 18 hours before being concentrated *in vacuo*. After washing with neohexane and drying *in vacuo* the desired product was obtained as a bright red powder. Yield = 14 mg (81%). Crystals grown from CH₂Cl₂/hexane at RT were suitable for X-ray diffraction.

¹H NMR (500 MHz, CD₂Cl₂): δ 7.80 (t, ³*J*_{HH} = 7.7, 1H, py), 7.74 – 7.70 (m, 8H, Ar^F), 7.55 (s, 4H, Ar^F), 7.49 (d, ³*J*_{HH} = 7.7, 1H, py), 7.45 (d, ³*J*_{HH} = 7.7, 1H, py), 7.05 (d, ³*J*_{HH} = 1.9, 2H, NCH), 6.91 (d, ³*J*_{HH} = 15.3, 1H, CHCH*t*Bu), 6.75 (dd, ³*J*_{HH} = 8.1, ³*J*_{HH} = 1.9, 2H, NCH), 6.07 (d, ³*J*_{HH} = 15.2, 1H, CHCH*t*Bu), 5.92 (d, ²*J*_{HH} = 14.5, 1H, pyCH₂), 5.54 (d, ²*J*_{HH} = 14.5, 1H, pyCH₂), 5.11 (d, ²*J*_{HH} = 14.6, 1H, pyCH₂), 5.05 (d, ²*J*_{HH} = 14.5, 1H, pyCH₂), 4.20 – 3.99 (m, 2H, NCH₂), 3.49 (app. td, *J* = 12.1, 5.6, 1H, NCH₂),

3.35 (app. td, $J = 12.7, 5.6$, 1H, NCH₂), 1.76 – 1.59 (m, 2H, CH₂), 1.57 – 1.31 (m, 18H, CH₂), 1.30 (s, 9H, *t*Bu), 1.02 (s, 9H, *t*Bu).

¹³C{¹H} NMR (126 MHz, CD₂Cl₂): δ 184.6 (d, $^1J_{\text{RhC}} = 41$, NCN), 182.2 (d, $^1J_{\text{RhC}} = 42$, NCN), 162.3 (q, $^1J_{\text{CB}} = 50$, Ar^F), 156.2 (s, *t*BuCHCH), 155.8 (s, py), 155.6 (s, py), 138.9 (s, py), 135.3 (s, Ar^F), 129.5 (qq, $^2J_{\text{FC}} = 32$, $^3J_{\text{CB}} = 3$, Ar^F), 125.1 (q, $^1J_{\text{FC}} = 271$, Ar^F), 124.3 (s, py), 124.2 (s, py), 121.1 (s, NCH), 121.0 (s, NCH), 120.8 (s, NCH), 120.3 (s, NCH), 118.0 (sept., $^3J_{\text{FC}} = 4$, Ar^F), 112.2 (s, *t*BuCHCH), 93.2 (d, $^1J_{\text{RhC}} = 15$, *t*BuCC), 74.3 (d, $^1J_{\text{RhC}} = 11$, *t*BuCC), 56.3 (d, $^3J_{\text{RhC}} = 3$, pyCH₂), 56.0 (d, $^3J_{\text{RhC}} = 3$, pyCH₂), 49.6 (s, NCH₂), 49.4 (s, NCH₂), 34.3 (s, *t*Bu{C}), 33.4 (s, *t*Bu{C}), 32.0 (s, CH₂), 32.0 (s, *t*Bu), 31.8 (s, CH₂), 30.0 (s, CH₂), 29.8 (s, *t*Bu), 29.6 (s, CH₂), 29.4 (s, CH₂), 29.4 (s, CH₂), 29.1 (s, CH₂), 29.1 (s, CH₂), 28.8 (s, CH₂), 28.6 (s, CH₂), 26.1 (s, CH₂), 25.7 (s, CH₂).

¹H NMR (300 MHz, *d*₃-MeCN): δ 7.88 (t, $^3J_{\text{HH}} = 7.7$, 1H, py), 7.73 – 7.65 (m, 12H, Ar^F), 7.65 – 7.50 (m, 2H, py), 7.18 (s, 1H, NCH), 6.98 (d, $^3J_{\text{HH}} = 15.2$, 1H, CH), 6.88 (s, 1H, NCH), 6.85 (s, 1H, NCH), 6.06 (d, $^3J_{\text{HH}} = 15.3$, 1H, CH), 5.82 (d, $^2J_{\text{HH}} = 14.8$, 1H, pyCH₂), 5.47 (d, $^2J_{\text{HH}} = 14.8$, 1H, pyCH₂), 5.34 (d, $^2J_{\text{HH}} = 14.9$, 1H, pyCH₂), 5.27 (d, $^2J_{\text{HH}} = 14.8$, 1H, pyCH₂), 4.23 – 3.98 (m, 2H, NCH₂), 3.62 – 3.47 (m, 1H, NCH₂), 3.40 (td, $^2J_{\text{HH}} = 12.5$, $^3J_{\text{HH}} = 5.2$, 1H, NCH₂), 1.82 – 1.58 (m, 2H, CH₂), 1.56 – 1.32 (m, 22H, CH₂), 1.29 (s, 9H, *t*Bu), 1.02 (s, 9H, *t*Bu).

HR ESI-MS (positive ion, 4 kV): 700.3822 [M]⁺ (calcd 700.3820) *m/z*.

Elemental Anal. Calcd for C₇₁H₇₁BF₂₄N₅Rh (1564.06 g·mol⁻¹): C, 54.52; H, 4.58; N, 4.48. Found: C, 54.38; H, 4.44; N, 4.46.

[Rh(CNC-16)(*E*-*t*BuCCCHCH*t*Bu)][BAR^F₄] – 19-16

A standard solution of *tert*-butylalkyne (50 mM) in 1,2-difluorobenzene (0.5 mL) was added to **11-16** (14.3 mg, 0.0982 mmol) and the resulting red solution stirred at room temperature for 1 hour before being concentrated *in vacuo*. After washing with TMS and drying *in vacuo* the desired product was obtained as a bright red powder. Yield = 15 mg (94%). Crystals grown from diethyl ether/hexane at RT were suitable for X-ray diffraction.

¹H NMR (500 MHz, CD₂Cl₂): δ 7.77 (t, $^3J_{\text{HH}} = 7.7$, 1H, py), 7.74 – 7.70 (m, 8H, Ar^F), 7.55 (s, 4H, Ar^F), 7.46 (d, $^3J_{\text{HH}} = 7.7$, 1H, py), 7.42 (d, $^3J_{\text{HH}} = 7.7$, 1H, py), 7.05 (app.

dd, $J = 3.5, 1.9$, 2H, NCH), 6.77 (d, $^3J_{\text{HH}} = 1.9$, 1H, NCH), 6.75 (d, $^3J_{\text{HH}} = 1.9$, 1H, NCH), 6.60 (d, $^3J_{\text{HH}} = 15.2$, 1H, CHCHtBu), 6.00 (d, $^3J_{\text{HH}} = 15.2$, 1H, CHCHtBu), 5.92 (d, $^2J_{\text{HH}} = 14.5$, 1H, pyCH₂), 5.59 (d, $^2J_{\text{HH}} = 14.6$, 1H, pyCH₂), 5.11 (d, $^2J_{\text{HH}} = 14.5$, 1H, pyCH₂), 5.05 (d, $^2J_{\text{HH}} = 14.4$, 1H, pyCH₂), 4.16 – 4.04 (m, 2H, NCH₂), 3.49 – 3.41 (m, 1H, NCH₂), 3.37 (app. td, $J = 12.8, 5.2$, 1H, NCH₂), 1.80 – 1.55 (m, 4H, CH₂), 1.48 – 1.28 (m, 24H, CH₂), 1.26 (s, 9H, tBu), 1.01 (s, 9H, tBu).

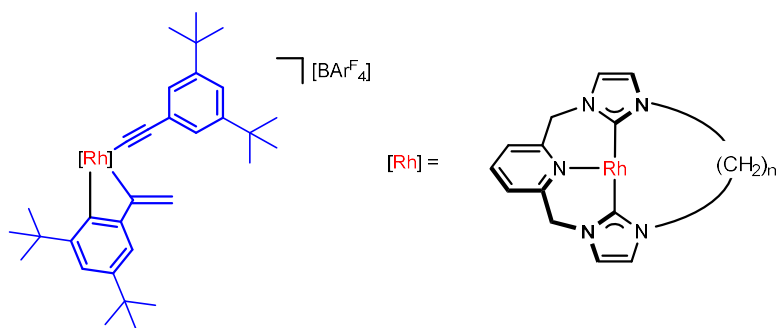
¹H NMR (400 MHz, *d*₃-MeCN): δ 7.86 (t, $^3J_{\text{HH}} = 7.7$, 1H, py), 7.73 – 7.65 (m, 12H, Ar^F), 7.58 (d, $^3J_{\text{HH}} = 7.8$, 1H, py), 7.54 (d, $^3J_{\text{HH}} = 7.8$, 1H, py), 7.20 (s, 2H, NCH), 6.88 (s, 1H, NCH), 6.86 (s, 1H, NCH), 6.67 (d, $^3J_{\text{HH}} = 15.2$, 1H, CHCHtBu), 6.00 (d, $^3J_{\text{HH}} = 15.2$, 1H, CHCHtBu), 5.82 (d, $^2J_{\text{HH}} = 14.7$, 1H, pyCH₂), 5.52 (d, $^2J_{\text{HH}} = 14.6$, 1H, pyCH₂), 5.34 (d, $^2J_{\text{HH}} = 14.7$, 1H, pyCH₂), 5.28 (d, $^2J_{\text{HH}} = 14.7$, 1H, pyCH₂), 4.12 (app. td, $J = 12.9, 4.7$, 1H, NCH₂), 4.03 (app. td, $J = 11.7, 5.6$, 1H, NCH₂), 3.48 (app. td, $J = 11.2, 5.3$, 1H, NCH₂), 3.41 (app. td, $J = 12.7, 4.9$, 1H, NCH₂), 1.47 – 1.27 (m, 28H, CH₂), 1.26 (s, 9H, tBu), 1.01 (s, 9H, tBu).

¹³C{¹H} NMR (126 MHz, CD₂Cl₂): δ 185.0 (d, $^1J_{\text{RhC}} = 41$, NCN), 182.8 (d, $^1J_{\text{RhC}} = 41$, NCN), 162.3 (q, $^1J_{\text{CB}} = 50$, Ar^F), 155.8 (s, py), 155.6 (s, py), 154.5 (s, tBuCHCH), 138.8 (s, py), 135.3 (s, Ar^F), 129.5 (qq, $^2J_{\text{FC}} = 32$, $^3J_{\text{CB}} = 3$, Ar^F), 125.1 (q, $^1J_{\text{FC}} = 271$, Ar^F), 124.1 (s, py), 124.0 (s, py), 121.0 (s, NCH), 120.8 (s, NCH), 120.7 (s, NCH), 120.1 (s, NCH), 118.0 (sept., $^3J_{\text{FC}} = 4$, Ar^F), 111.3 (s, CHCHtBu), 95.4 (d, $^1J_{\text{RhC}} = 16$, tBuC≡C), 75.6 (d, $^1J_{\text{RhC}} = 12$, tBuC≡C), 56.3 (d, $^3J_{\text{RhC}} = 2$, pyCH₂), 56.0 (d, $^3J_{\text{RhC}} = 2$, pyCH₂), 49.6 (s, NCH₂), 49.4 (s, NCH₂), 34.1 (s, tBu{C}), 33.3 (s, tBu{C}), 31.7 (s, tBu), 31.6 (s, CH₂), 31.3 (s, CH₂), 29.8 (s, tBu), 29.7 (s, CH₂), 29.6 (s, CH₂), 29.6 (s, CH₂), 29.5 (s, CH₂), 29.4 (s, CH₂), 29.1 (s, CH₂), 29.1 (s, CH₂), 28.5 (s, CH₂), 26.3 (s, CH₂), 26.2 (s, CH₂).

HR ESI-MS (positive ion, 4 kV): 728.4135 [M]⁺ (calcd 728.4133) *m/z*.

Elemental Anal. Calcd for C₇₃H₇₅BF₂₄N₅Rh (1592.12 g·mol⁻¹): C, 55.07; H, 4.75; N, 4.40. Found: C, 55.18; H, 4.82; N, 4.47.

5.4.2. Homocoupling of Ar'CCH through a ring



[Rh(CNC-14)(CCAr')(C(CH₂)Ar')][BAr₄] – 22-14

A solution of **11-14** (33 mg, 0.023 mmol) and 3,5-di-*tert*-butylphenylacetylene **16a** (10 mg, 0.046 mmol) in 1,2-difluorobenzene (1 mL) was stirred for 1 hour before being concentrated to dryness and the resulting residue washed with cold hexane (*ca.* 0.5 mL, -30 °C) and thoroughly dried *in vacuo* to obtain the product as an orange powder. Yield = 31 mg (73%).

¹H NMR (500 MHz, CD₂Cl₂, 298 K): δ 7.87 (t, ³J_{HH} = 7.7, 1H, py), 7.74 – 7.70 (m, 8H, Ar^F), 7.55 (s, 4H, Ar^F), 7.50 (s, 1H, Ar'), 7.24 – 7.18 (m, 1H, NCH), 7.21 (s, 1H, Ar'), 7.06 (br s, fwhm = 32, 2H, NCH), 6.99 (d, ³J_{HH} = 1.6, 2H, Ar'), 6.73 (s, 2H, Ar'), 6.25 (br s, fwhm = 113, pyCH₂), 5.74 (d, ²J_{HH} = 2.5, 1H, C(CH₂)), 5.66 (s, 1H, C(CH₂)), 5.60 (br s, pyCH₂), 5.13 (br s, pyCH₂), 4.51 (br s, fwhm = *ca.* 210, 1H, pyCH₂), 3.98 (br s, fwhm = *ca.* 250, 1H, NCH₂), 3.21 (br s, fwhm = 160, 1H, NCH₂), 2.14 – 2.02 (m, 2H, NCH₂), 1.86 (br s, fwhm = 116, 1H, CH₂), 1.43 – 1.06 (m, 23H, CH₂), 1.18 (s, 18H, *t*Bu), 0.93 (s, 18H, *t*Bu).

¹H NMR (500 MHz, CD₂Cl₂, 185 K): δ 7.84 (t, ³J_{HH} = 7.7, 1H, py), 7.74 – 7.70 (m, 8H, Ar^F), 7.61 (d, ³J_{HH} = 7.8, 1H, py), 7.55 (s, 4H, Ar^F), 7.33 (d, ³J_{HH} = 7.7, 1H, py), 7.25 (s, 2H, Ar'), 7.19 (s, 1H, Ar'), 7.12 (s, 1H, Ar'), 7.09 (s, 3H, Ar'), 7.05 (s, 1H, NCH), 6.94 (s, 1H, NCH), 6.87 (s, 1H, NCH), 6.03 – 5.78 (m, 2H, pyCH₂ + NCH₂), 5.67 (d, ²J_{HH} = 16.6, 1H, pyCH₂), 5.36 – 5.28 (m, 1H, pyCH₂), 5.20 (br s, 2H, NCH + C(CH₂)), 5.00 (br s, 1H, C(CH₂)), 4.86 (d, ²J_{HH} = 15.4, 1H, pyCH₂), 4.58 (br, fwhm = 30, 1H, NCH₂), 3.81 (br, 1H, NCH₂), 3.37 (br s, fwhm = 46, 1H, NCH₂), 2.31 – 2.07 (m, 2H, CH₂), 1.93 (br s, fwhm = 30, 1H, CH₂), 1.79 (br s, fwhm = 30, 1H, CH₂), 1.70 – 0.85 (m, 4H, CH₂), 1.19 (s, 18H, *t*Bu), 1.13 (s, 9H, *t*Bu), 0.59 (s, 9H, *t*Bu).

¹H NMR (400 MHz, DiFB): δ 8.21 – 8.08 (m, 8H, Ar^F), 7.63 (s, 1H, Ar'), 7.60 (t, ³J_{HH} = 7.6, 1H, py), 7.50 (s, 4H, Ar^F), 5.74 (s, 1H, C(CH₂)), 5.71 (s, 1H, C(CH₂)), 5.53 (br

s, fwhm = 31, 1H, NCH₂), 4.93 (d, ²J_{HH} = 14.1, 1H, pyCH₂), 4.69 (br s, fwhm = 29, 1H, NCH₂), 4.33 (d, ²J_{HH} = 15.3, 1H, pyCH₂), 4.22 – 3.98 (m, 1H, NCH₂), 3.78 – 3.56 (m, 1H, NCH₂), 2.79 (d, ²J_{HH} = 14.8, 1H, pyCH₂), 2.29 – 1.88 (m, 3H, CH₂), 1.74 – 1.57 (m, 1H, CH₂), 1.56 – 1.04 (m, CH₂), 1.16 (s, 18H, *t*Bu), 0.97 (s, 18H, *t*Bu).

¹³C{¹H} NMR (126 MHz, CD₂Cl₂): δ 162.3 (q, ¹J_{CB} = 50, Ar^F), 156.8 (d, ¹J_{RhC} = 25.1, C(CH₂)Ar'), 155.8 (s, py), 155.6 (br, Ar'{C}), 151.1 (s, Ar'{C}), 141.1 (s, py), 135.3 (s, Ar^F), 129.5 (qq, ²J_{FC} = 32, ³J_{CB} = 3, Ar^F), 127.2 (s, Ar'{C}), 125.5 (s, Ar'{CH}), 125.1 (s, Ar'{CH}), 125.1 (q, ¹J_{FC} = 271, Ar^F), 125.0 (s, Ar'{CH}), 120.1 (s, Ar'{CH}), 118.0 (sept., ³J_{FC} = 4, Ar^F), 114.5 (s, C(C(CH₂)Ar'), 104.9 (d, ²J_{RhC} = 16, C≡C(Ar')), 85.7 (C≡C(Ar'))*, 50.7 (br, NCH₂), 35.5 (s, *t*Bu{C}), 35.1 (s, *t*Bu{C}), 32.2 (s, CH₂), 31.7 (s, *t*Bu), 31.3 (s, *t*Bu), 28.7 (br, CH₂), 28.7 (br, CH₂), 28.3 (br, CH₂). *Selected data only.*

* Located using correlation experiment.

HR ESI-MS (positive ion, 4 kV): 964.5699 [M]⁺ (calcd 964.5698) *m/z*.

Elemental Anal. Calcd for C₉₁H₉₅BF₂₄N₅Rh (1828.47 g·mol⁻¹): C, 59.78; H, 5.24; N, 3.83. Found: C, 59.77; H, 5.22; N, 3.80.

[Rh(CNC-16)(CCAr')(C(CH₂)Ar')][BAr^F₄] – 22-16

A solution of **11-16** (134 mg, 0.0920 mmol) and 3,5-di-*tert*-butylphenylacetylene **16a** (41 mg, 0.19 mmol) in 1,2-difluorobenzene was stirred for 1 hour before being concentrated to dryness and the resulting residue washed with cold hexane (*ca.* 1 mL, -30 °C) and thoroughly dried *in vacuo* to obtain the product as an orange powder. Yield = 157 mg (90%).

¹H NMR (500 MHz, CD₂Cl₂, 298 K): δ 7.87 (t, ³J_{HH} = 7.8, 1H, py), 7.76 – 7.68 (m, 8H, Ar^F), 7.55 (s, 4H, Ar^F), 7.45 (s, 1H, Ar'), 7.42 (br s, fwhm = 150, 4H, NCH + py), 7.22 (s, 1H, Ar'), 7.05 (br s, fwhm = 68, 3H, NCH + py), 7.03 (d, ⁴J_{HH}, 1.9, 2H, Ar'), 6.71 (s, 2H, Ar'), 6.32 (br s, fwhm = 65, 1H, pyCH₂), 5.70 (d, ²J_{HH} = 2.9, 1H, C(CH₂)), 5.67 (s, 1H, C(CH₂)), 5.63 (br s, fwhm = 65, 1H, pyCH₂), 5.13 (br s, fwhm = 70, 1H, pyCH₂), 4.54 (br s, fwhm = 80, 2H, pyCH₂ + NCH₂), 4.03 (br s, fwhm = 85, 2H, NCH₂), 3.62 (br s, fwhm = 85, 1H, NCH₂), 1.98 (br s, fwhm = 35, 2H, CH₂), 1.84 (br s, fwhm = 82, 2H, CH₂), 1.30 – 1.22 (m, 24H, CH₂), 1.27 (s, 18H, *t*Bu), 1.03 (s, 18H, *t*Bu).

$^{13}\text{C}\{^1\text{H}\}$ NMR (126 MHz, CD_2Cl_2): δ 162.3 (q, $^1J_{\text{CB}} = 50$, Ar^{F}), 156.3 (br s, py), 155.6 (br s, $\underline{\text{C}}(\text{CH}_2)$), 155.2 (br s, $\text{Ar}'\{\text{C}\}$), 151.2 (s, $\text{Ar}'\{\text{C}\}$), 141.1 (s, py), 135.4 (s, Ar^{F}), 129.4 (qq, $^2J_{\text{FC}} = 32$, $^3J_{\text{CB}} = 3$, Ar^{F}), 127.6 (s, $\text{Ar}'\{\text{C}\}$), 125.4 (s, $\text{Ar}'\{\text{CH}\}$), 125.1 (q, $^1J_{\text{FC}} = 271$, Ar^{F}), 124.6 (s, $\text{Ar}'\{\text{CH}\}$), 120.8 (s, $\text{Ar}'\{\text{CH}\}$), 118.0 (sept., $^3J_{\text{FC}} = 4$, Ar^{F}), 115.3 (s, $\text{C}(\underline{\text{C}}\text{H}_2)$), 114.0 (s, $\text{Ar}'\{\text{C}\}$), 105.4 (d, $^2J_{\text{RhC}} = 15$, $\text{C}\equiv\text{C}\text{Ar}'$), 86.6 ($\text{C}\equiv\text{C}\text{Ar}'$),* 56.5 (pyCH₂),* 50.6 (br, NCH₂), 35.5 (s, $t\text{Bu}\{\text{C}\}$), 35.1 (s, $t\text{Bu}\{\text{C}\}$), 31.7 (s, $t\text{Bu}$), 31.3 (s, $t\text{Bu}$), 28.9 (s, CH₂), 28.8 (s, CH₂), 28.7 (s, CH₂), 28.5 (s, CH₂), 26.7 (br, CH₂).

Selected data only. * Located using correlation experiments.

^1H NMR (500 MHz, CD_2Cl_2 , 185 K): δ 7.90 (t, $^3J_{\text{HH}} = 7.6$, 1H, py), 7.76 – 7.68 (m, 8H, Ar^{F}), 7.65 (d, $^3J_{\text{HH}} = 7.8$, 1H, py), 7.55 (s, 4H, Ar^{F}), 7.42 (d, $^3J_{\text{HH}} = 7.7$, 1H, py), 7.26 (s, 1H, Ar'), 7.18 (s, 1H, Ar'), 7.17 (s, 1H, NCH), 7.12 (s, 1H, Ar'), 7.08 (s, 2H, Ar'), 7.00 (s, 1H, NCH), 6.89 (s, 1H, NCH), 6.82 (s, 1H, NCH), 5.82 (d, $^2J_{\text{HH}} = 16.5$, 1H, pyCH₂), 5.68 (d, $^2J_{\text{HH}} = 15.0$, 1H, pyCH₂), 5.51 (br s, fwhm = 26, 1H, NCH₂), 5.31 (d, $^2J_{\text{HH}} = 16.2$, pyCH₂), 5.23 (s, 1H, $\text{C}(\text{CH}_2)$), 5.09 (s, 1H, NCH), 5.02 (s, 1H, $\text{C}(\text{CH}_2)$), 4.88 (d, $^2J_{\text{HH}} = 15.2$, 1H, pyCH₂), 4.58 – 4.44 (m, 1H, NCH₂), 3.73 (br s, fwhm = 27, 1H, NCH₂), 3.09 (br s, fwhm = 30, 1H, NCH₂), 2.63 (br s, fwhm = 34, 1H, CH₂), 1.74 (br s, fwhm = 38, 2H, CH₂), 1.64 – 0.82 (m, 26H, CH₂), 1.19 (s, 18H, $t\text{Bu}$), 1.13 (s, 9H, $t\text{Bu}$), 0.56 (s, 9H, $t\text{Bu}$).

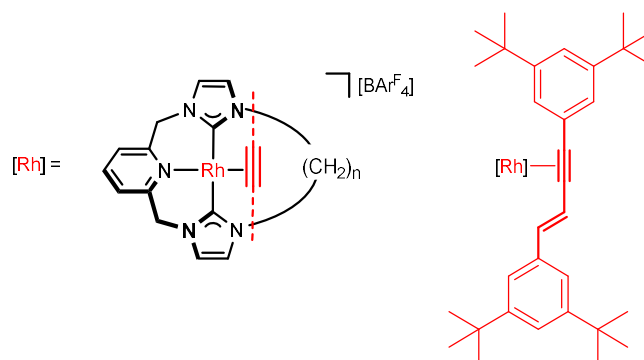
^1H NMR (400 MHz, DiFB): δ 8.21 – 8.08 (m, 8H, Ar^{F}), 7.63 (s, 1H, Ar'), 7.61 (t, $^3J_{\text{HH}} = 7.6$, 1H, py), 7.50 (s, 4H, Ar^{F}), 5.78 (s, 1H, CCH₂), 5.71 (s, 1H, CCH₂), 5.57 (br t, $^3J_{\text{HH}} = 13$, 1H, NCH₂), 4.96 (d, $^2J_{\text{HH}} = 14.8$, 1H, pyCH₂), 4.65 (br t, $^3J_{\text{HH}} = 13$, 1H, NCH₂), 4.37 (d, $^2J_{\text{HH}} = 15.1$, 1H, pyCH₂), 4.07 (br t, $^3J_{\text{HH}} = 13$, 1H, NCH₂), 3.74 (br t, $^3J_{\text{HH}} = 13$, 1H, NCH₂), 3.07 (d, $^2J_{\text{HH}} = 16.2$, 1H, pyCH₂), 1.98 (br s, 3H, CH₂), 1.74 – 1.57 (m, 1H, CH₂), 1.56 – 1.04 (m, CH₂), 1.19 (s, 18H, $t\text{Bu}$), 0.98 (s, 18H, $t\text{Bu}$).

Selected data only.

HR ESI-MS (positive ion, 4 kV): 992.6016 [M]⁺ (calcd 992.6011) *m/z*.

Elemental Anal. Calcd for $\text{C}_{93}\text{H}_{99}\text{BF}_{24}\text{N}_5\text{Rh}$ (1856.53 g·mol⁻¹): C, 60.17; H, 5.38; N, 3.77. Found: C, 60.06; H, 5.25; N, 3.89.

5.4.3. Synthesis of interlocked Ar' enyne systems



Characterisation of $[\text{Rh}(\text{CNC-12})(E\text{-Ar}'\text{CCCHCHAr}')][\text{BAr}^{\text{F}}_4]$ – **32-12**

Prepared according to literature procedure.²²

¹H NMR (300 MHz, *d*₃-MeCN): δ 8.21 (s, 2H, Ar'), 8.13 (d, $^3J_{\text{HH}} = 15.4$, 1H, CHCHAr'), 8.00 (t, $^3J_{\text{HH}} = 7.8$, 1H, py), 7.73 – 7.65 (m, 12H, Ar^F + 2 \times py), 7.49 (s, 1H, NCH), 7.44 (s, 3H, NCH + Ar'), 7.16 (s, 1H, NCH), 7.13 (s, 1H, NCH), 6.99 (d, $^3J_{\text{HH}} = 15.3$, CHCHAr'), 6.78 (s, 2H, Ar'), 5.80 (app. t, $J = 13.9$, 2H, pyCH₂), 5.56 – 5.30 (m, 1H, pyCH₂), 4.16 (app. t, $J = 13.1$, 1H, NCH₂), 3.65 (app. t, $J = 13.0$, 1H, NCH₂), 3.56 – 3.34 (m, 2H, NCH₂), 2.40 – 2.15 (m, 2H, CH₂), 1.87 – 1.63 (m, 8H, CH₂), 1.63 – 1.41 (m, 8H, CH₂), 1.19 – 1.09 (m, 2H, CH₂).

$[\text{Rh}(\text{CNC-14})(E\text{-Ar}'\text{CCCHCHAr}')][\text{BAr}^{\text{F}}_4]$ – **32-14**

A solution of **22-14** (91 mg, 0.05 mmol) in 1,2-difluorobenzene (2.5 mL) was heated at 85 °C for 18 hours to afford a deep red solution. Concentration to dryness *in vacuo* and recrystallisation from hot hexane afforded the compound as a deep red solid. Yield = 76 mg (84%).

¹H NMR (500 MHz, CD₂Cl₂): δ 8.02 (d, $^4J_{\text{HH}} = 1.8$, 2H, *o*-Ar'), 7.29 (d, $^3J_{\text{HH}} = 15.2$, 1H, CHCHAr'), 7.86 (t, $^3J_{\text{HH}} = 7.7$, 1H, py), 7.75 – 7.70 (m, 8H, Ar^F), 7.58 – 7.53 (m, 6H, py + Ar^F), 7.44 (app. q, $J = 1.8$, 2H, *p*-Ar'), 7.37 (d, $^4J_{\text{HH}} = 1.7$, 2H, *o*-Ar'), 7.04 (d, $^3J_{\text{HH}} = 1.8$, 1H, NCH), 7.00 (d, $^3J_{\text{HH}} = 15.1$, 1H, CHCHAr'), 7.00 (d, $^3J_{\text{HH}} = 1.8$, 1H, NCH), 6.68 (d, $^3J_{\text{HH}} = 1.8$, 1H, NCH), 6.65 (d, $^3J_{\text{HH}} = 1.8$, 1H, NCH), 5.99 (d, $^2J_{\text{HH}} = 14.5$, 1H, pyCH₂), 5.95 (d, $^2J_{\text{HH}} = 14.6$, 1H, pyCH₂), 5.22 (d, $^2J_{\text{HH}} = 14.6$, 1H, pyCH₂), 5.17 (d, $^2J_{\text{HH}} = 14.5$, 1H, pyCH₂), 4.16 (app. td, $J = 13.0, 3.0$, 1H, NCH₂), 3.78 (app. td, $J = 12.4, 4.6$, 1H, NCH₂), 3.43 – 3.27 (m, 2H, NCH₂), 1.92 – 0.72 (m, 24H, CH₂), 1.36 (s, 18H, *t*Bu), 1.35 (s, 18H, *t*Bu).

$^{13}\text{C}\{^1\text{H}\}$ NMR (126 MHz, CD_2Cl_2): δ 182.4 (d, $^1J_{\text{RhC}} = 42$, NCN), 182.0 (d, $^1J_{\text{RhC}} = 42$, NCN), 162.3 (q, $^1J_{\text{CB}} = 50$, Ar^{F}), 155.8 (s, $2 \times \text{py}$), 152.4 (s, $\text{Ar}\{\text{C}\}$), 151.6 (s, $\text{Ar}\{\text{C}\}$), 143.0 (d, $^2J_{\text{RhC}} = 2$, CHCHAr'), 139.7 (s, py), 136.6 (s, $\text{Ar}\{\text{C}\}$), 135.3 (s, Ar^{F}), 129.5 (qq, $^2J_{\text{FC}} = 32$, $^3J_{\text{CB}} = 3$, Ar^{F}), 128.9 (s, $\text{Ar}\{\text{C}\}$), 126.6 (s, $\text{Ar}\{\text{CH}\}$), 125.1 (q, $^1J_{\text{FC}} = 271$, Ar^{F}), 124.5 (s, py), 124.5 (s, py), 123.8 (s, $\text{Ar}\{\text{CH}\}$), 123.2 (s, $\text{Ar}\{\text{CH}\}$), 121.6 (s, $\text{Ar}\{\text{CH}\}$), 121.3 (s, NCH), 121.2 (s, NCH), 121.0 (s, NCH), 120.9 (s, NCH), 118.0 (sept., $^3J_{\text{FC}} = 4$, Ar^{F}), 114.5 (s, CHCHAr'), 91.0 (d, $^1J_{\text{RhC}} = 14$, $\text{Ar}'\text{C}\equiv\text{C}$), 83.4 (d, $^1J_{\text{RhC}} = 13$, $\text{Ar}'\text{C}\equiv\text{C}$), 56.2 (s, pyCH_2), 56.2 (s, pyCH_2), 49.9 (s, NCH_2), 49.8 (s, NCH_2), 35.5 (s, $t\text{Bu}\{\text{C}\}$), 35.4 (s, $t\text{Bu}\{\text{C}\}$), 33.5 (s, CH_2), 32.2 (s, CH_2), 31.9 (s, $t\text{Bu}$), 31.8 (s, $t\text{Bu}$), 31.4 (s, CH_2), 29.8 (s, CH_2), 29.4 (s, CH_2), 29.1 (s, CH_2), 29.1 (s, CH_2), 28.7 (s, CH_2), 28.5 (s, CH_2), 28.5 (s, CH_2), 25.6 (s, CH_2), 25.6 (s, CH_2).

HR ESI-MS (positive ion, 4 kV): 964.5702 $[\text{M}]^+$ (calcd 964.5698) m/z .

Elemental Anal. Calcd for $\text{C}_{91}\text{H}_{95}\text{BF}_{24}\text{N}_5\text{Rh}$ ($1828.47 \text{ g}\cdot\text{mol}^{-1}$): C, 59.78; H, 5.24; N, 3.83. Found: C, 59.69; H, 5.27; N, 3.47.

Preparation of $[\text{Rh}(\text{CNC-16})(E\text{-Ar}'\text{CCCHCHAr}')][\text{BAr}^{\text{F}}_4]$ and $[\text{Rh}(\text{CNC-16})(\text{Ar}'\text{CCC}(\text{CH}_2)\text{Ar}')][\text{BAr}^{\text{F}}_4]$

A solution of **22-16** (111 mg, 0.0600 mmol) in 1,2-difluorobenzene (3 mL) was heated at 85°C for 18 hours to afford mixture of the two products as a deep red solution (43% *E*, 57% *gem*). Concentrating to dryness and washing with cold TMS (-78°C) afforded the mixture of isomers as a red solid. Yield = 93.4 mg (83%). These isomers can be separated by crystallisation of **33-16** from a diethyl ether/hexane layer at room temperature followed by crystallisation of **32-16** from a saturated hexane solution at -4°C . Yield = 45 mg (40% *gem*), 28 mg (25% *E*).

Characterisation of $[\text{Rh}(\text{CNC-16})(E\text{-Ar}'\text{CCCHCHAr}')][\text{BAr}^{\text{F}}_4]$ – **32-16**

Crystals suitable for X-ray diffraction were grown from a saturated hexane solution at 4°C .

^1H NMR (500 MHz, CD_2Cl_2): δ 7.87 – 7.83 (m, 3H, $\text{Ar}' + \text{py}$), 7.81 (d, $^3J_{\text{HH}} = 15.8$, 1H, CHCHAr'), 7.76 – 7.68 (m, 8H, Ar^{F}), 7.55 (s, 6H, $\text{Ar}^{\text{F}} + 2 \times \text{py}$), 7.46 – 7.40 (m, 2H, Ar'), 7.33 (s, 2H, Ar'), 7.04 (d, $^3J_{\text{HH}} = 1.8$, 1H, NCH), 7.03 (d, $^3J_{\text{HH}} = 1.8$, 1H, NCH), 6.95 (d, $^3J_{\text{HH}} = 15.3$, 1H, CHCHAr'), 6.70 (d, $^3J_{\text{HH}} = 1.8$, 1H, NCH), 6.66 (d, $^3J_{\text{HH}} = 1.9$,

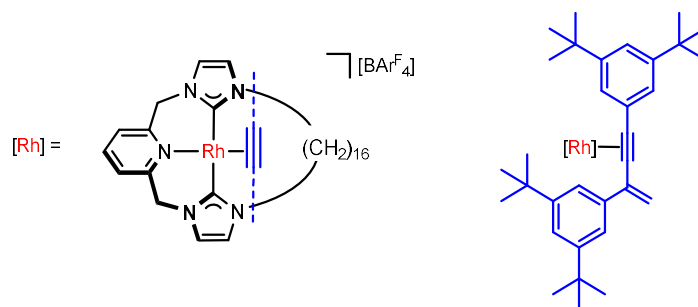
1H, NCH), 5.97 (d, $^2J_{\text{HH}} = 14.5$, 1H, pyCH₂), 5.97 (d, $^2J_{\text{HH}} = 14.6$, 1H, pyCH₂), 5.22 (d, $^2J_{\text{HH}} = 15.1$, 1H, pyCH₂), 5.18 (d, $^2J_{\text{HH}} = 15.6$, 1H, pyCH₂), 4.05 (app. td, $J = 13.2$, 3.6, 1H, NCH₂), 3.88 (app. dt, $J = 13.1$, 7.7, 1H, NCH₂), 3.41 (app. td, $J = 12.2$, 4.9, 1H, NCH₂), 3.34 (app. dt, $J = 13.2$, 7.7, 1H, NCH₂), 1.61 – 0.70 (m, 28H, CH₂), 1.36 (s, 36H, *t*Bu).

$^{13}\text{C}\{^1\text{H}\}$ NMR (126 MHz, CD₂Cl₂): δ 182.8 (d, $^1J_{\text{RhC}} = 41$, NCN), 182.5 (d, $^1J_{\text{RhC}} = 41$, NCN), 162.3 (q, $^1J_{\text{CB}} = 50$, Ar^F), 155.8 (s, py), 155.5 (s, py), 152.3 (s, Ar'^{C}), 151.6 (s, Ar'^{C}), 142.3 (s, CH₂CHAr'), 139.6 (s, py), 136.6 (s, Ar'^{C}), 135.4 (s, Ar^F), 129.5 (qq, $^2J_{\text{FC}} = 32$, $^2J_{\text{CB}} = 3$, Ar^F), 128.7 (s, Ar'^{C}), 126.1 (s, Ar'^{CH}), 125.2 (q, $^1J_{\text{FC}} = 271$, Ar^F), 124.5 (s, py), 124.4 (s, py), 123.7 (s, Ar'^{CH}), 123.1 (s, Ar'^{CH}), 121.4 (s, Ar'^{CH}), 121.1 (s, NCH), 121.0 (s, NCH), 121.0 (s, NCH), 120.9 (s, NCH), 118.0 (sept., $^3J_{\text{FC}} = 4$, Ar^F), 114.3 (s, CH₂CHAr'), 92.3 (d, $^1J_{\text{RhC}} = 14$, C \equiv CHAr'), 84.0 (d, $^1J_{\text{RhC}} = 14$, C \equiv CHAr'), 56.3 (s, pyCH₂), 49.8 (s, NCH₂), 35.4 (s, CH₂), 35.3 (s, CH₂), 32.5 (s, *t*Bu{C}), 32.2 (s, *t*Bu{C}), 31.9 (s, *t*Bu), 31.8 (s, *t*Bu), 29.6 (s, CH₂), 29.6 (s, CH₂), 29.4 (s, CH₂), 29.3 (s, CH₂), 29.3 (s, CH₂), 29.2 (s, CH₂), 29.2 (s, CH₂), 29.2 (s, CH₂), 29.0 (s, CH₂), 28.8 (s, CH₂), 26.9 (s, CH₂), 26.3 (s, CH₂).

HR ESI-MS (positive ion, 4 kV): 992.6007 [M]⁺ (calcd 992.6011) *m/z*.

Elemental Anal. Calcd for C₉₃H₉₉BF₂₄N₅Rh (1856.53 g·mol⁻¹): C, 60.17; H, 5.38; N, 3.77. Found: C, 60.09; H, 5.43; N, 3.75.

Characterisation of [Rh(CNC-16)(Ar'CCC(CH₂)Ar')][BAR^F₄] – 33-16



Crystals suitable for X-ray diffraction were grown from slow diffusion of hexane into a solution in diethyl ether at RT.

^1H NMR (500 MHz, CD₂Cl₂): δ 7.90 (s, 2H, Ar'), 7.77 (t, $^3J_{\text{HH}} = 7.7$, 1H, py), 7.76 – 7.68 (m, 8H, Ar^F), 7.62 (s, 2H, Ar'), 7.55 (s, 4H, Ar^F), 7.48 (d, $^3J_{\text{HH}} = 7.7$, 1H, py), 7.44 (s, 2H, Ar'), 7.30 (d, $^3J_{\text{HH}} = 7.7$, 1H, py), 7.09 (s, 1H, NCH), 6.75 (s, 1H, NCH), 6.69 (s, 1H, NCH), 6.65 (s, 1H, NCH), 6.13 (s, 1H, C(CH₂)), 5.83 (d, $^2J_{\text{HH}} = 14.5$, 1H,

pyCH₂), 5.73 (s, 1H, C(CH₂)), 5.16 (d, ²J_{HH} = 14.7, 1H, pyCH₂), 4.53 (app. td, J = 12.9, 3.9, 1H, NCH₂), 4.26 (d, ²J_{HH} = 14.7, 1H, pyCH₂), 3.94 (d, ²J_{HH} = 14.7, 1H, pyCH₂), 3.90 – 3.80 (m, 1H, NCH₂), 3.64 (app. td, J = 12.6, 5.7, 1H, NCH₂), 3.24 (app. td, J = 12.6, 5.2, 1H, NCH₂), 1.65 – 1.25 (m, 24H, CH₂), 1.35 (s, 18H, *t*Bu), 1.15 (s, 18H, *t*Bu).

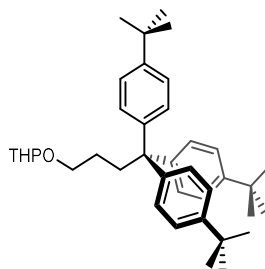
¹³C{¹H} NMR (126 MHz, CD₂Cl₂): δ 181.8 (d, ²J_{RhC} = 42, NCN), 181.0 (d, ²J_{RhC} = 42, NCN), 162.3 (q, ¹J_{CB} = 50, Ar^F), 155.7 (s, py), 155.5 (s, py), 151.5 (s, Ar'{C}), 151.2 (s, Ar'{C}), 142.4 (s, Ar'{C}), 139.4 (s, py), 138.7 (d, ²J_{RhC} = 1, C(CH₂)), 135.4 (s, Ar^F), 129.5 (qq, ²J_{FC} = 32, ²J_{CB} = 3, Ar^F), 128.2 (s, Ar'{C}), 126.7 (s, Ar'{CH}), 125.2 (q, ¹J_{FC} = 271, Ar^F), 124.3 (s, py), 124.2 (s, py), 123.2 (s, Ar'{CH}), 122.7 (s, Ar'{CH}), 122.0 (s, C(CH₂)), 121.2 (s, NCH), 121.0 (s, NCH), 120.9 (s, NCH), 120.3 (s, NCH), 118.0 (sept., ³J_{FC} = 4, Ar^F), 89.4 (d, ¹J_{RhC} = 14, Ar'C≡C), 84.6 (d, ¹J_{RhC} = 14, Ar'C≡C), 56.3 (s, pyCH₂), 54.5 (s, pyCH₂), 50.2 (s, NCH₂), 50.0 (s, NCH₂), 35.4 (s, CH₂), 32.5 (s, *t*Bu{C}), 32.2 (s, CH₂), 32.1 (s, *t*Bu{C}), 31.9 (s, *t*Bu), 31.6 (s, *t*Bu), 30.4 (s, CH₂), 30.0 (s, CH₂), 29.9 (s, CH₂), 29.8 (s, CH₂), 29.8 (s, CH₂), 29.7 (s, CH₂), 29.6 (s, CH₂), 29.5 (s, CH₂), 27.4 (s, CH₂), 27.0 (s, CH₂), 23.2 (s, CH₂).

HR ESI-MS (positive ion, 4 kV): 992.5992 [M]⁺ (calcd 992.6011) *m/z*.

Elemental Anal. Calcd for C₉₃H₉₉BF₂₄N₅Rh (1856.53 g·mol⁻¹): C, 60.17; H, 5.38; N, 3.77. Found: C, 60.03; H, 5.42; N, 3.69.

5.4.4 Synthesis of trityl-type stopper - 16m

2-(4,4,4-tris(para-*tert*-butylphenyl)butoxy)tetrahydro-2H-pyran - 37



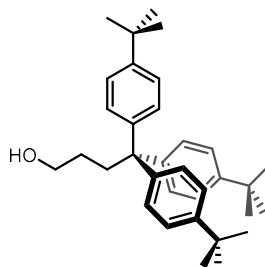
*n*Butyl lithium (10 mL, 0.8 M in hexanes) was then added dropwise over 30 minutes to a stirring solution of tris-(*p-tert*-butylphenyl)methane **36** (3.0 g, 7.3 mmol), in THF (150 mL) and HMPA (30 mL) at -78 °C. The resulting deep red solution was allowed to warm to room temperature over 30 minutes and left stirring for an hour. 2-(3-chloropropoxy)tetrahydropyran (1.8 mL, 11 mmol) was then added and the pale yellow solution stirred for a further 15 hours. The

reaction was then quenched with slow addition of HCl (5 mL, aq, 2 M) and the product extracted into diethyl ether (80 mL) and washed with HCl (aq, 2 M) and H₂O, dried over MgSO₄ and volatiles removed *in vacuo*. The resulting residue was dissolved in a minimum of CH₂Cl₂ and on addition of excess MeOH the crude product was obtained as a white solid following filtration and removal of volatiles *in vacuo*. The product was purified by chromatography (silica; CH₂Cl₂/hexane, 4:1) to give a white powder. Yield = 1.74 g (43%).

¹H NMR (400 MHz, CDCl₃): δ 7.24 (d, ³J_{HH} = 8.7, 6H, Ar), 7.18 (d, ³J_{HH} = 8.7, 6H, Ar), 4.54 (t, ³J_{HH} = 3.5, 1H, CH₂), 3.93 – 3.79 (m, 1H, CH₂), 3.78 – 3.66 (m, 1H, CH₂), 3.52 – 3.43 (m, 1H, CH₂), 3.40 – 3.30 (m, 1H, CH₂), 2.60 (dd, ³J_{HH} = 10.2, 4.5, 2H, CH₂), 1.95 – 1.48 (m, 7H, CH₂), 1.46 – 1.35 (m, 2H, CH₂), 1.29 (s, 27H, *t*Bu).

HR ESI-MS (positive ion, 4 kV): 577.4017 [M+Na]⁺ (calcd 577.4016) *m/z*.

4,4,4-tris((para-*tert*-butyl)phenyl)butan-1-ol – 38



A solution of **37** (800 mg, 1.44 mmol) in THF/MeOH (30 mL, 6:1), H₂O (1.5 mL) and HCl (1 mL, 36% w/w) was stirred for 20 hours resulting in a white suspension. The product was extracted into CH₂Cl₂ and the combined organic layers washed with H₂O and saturated NH₄Cl (aq) before being dried over MgSO₄. The product was obtained as a white solid after the removal of volatiles *in vacuo*. Yield = 680 mg (100%).

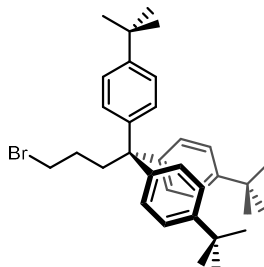
¹H NMR (500 MHz, CDCl₃): δ 7.24 (d, ³J_{HH} = 8.5, 6H, Ar), 7.17 (d, ³J_{HH} = 8.5, 6H, Ar), 3.62 (t, ³J_{HH} = 6.4, 2H, CH₂OH), 2.62 – 2.50 (m, 2H, CH₂C(Ar)₃), 1.42 – 1.32 (m, 2H, CH₂CH₂CH₂), 1.29 (s, 27H, *t*Bu), 1.17 (br s, 1H, OH).

¹³C{¹H} NMR (126 MHz, CDCl₃): δ 148.3 (s, Ar{C}), 144.6 (s, Ar{C}), 128.9 (s, Ar{CH}), 124.6 (s, Ar{CH}), 63.7 (s, CH₂OH), 55.1 (s, C(Ar)₃), 36.6 (s, CH₂C(Ar)₃), 34.4 (s, *t*Bu{C}), 31.5 (s, *t*Bu), 29.4 (s, CH₂CH₂CH₂).

HR ESI-MS (positive ion, 4 kV): 493.3443 [M+Na]⁺ (calcd 493.3441) *m/z*.

Elemental Anal. Calcd for $C_{34}H_{46}O$ (470.74 g mol⁻¹): C, 86.75; H, 9.85; N, 0.00. Found: C, 86.69; H, 9.97; N, 0.00.

1-bromo-4,4,4-tris((para-*tert*-butyl)phenyl)butane – 39



Method 1

Triphenyl phosphine (507 mg, 1.93 mmol) was added to a stirring solution of **38** (700 mg, 1.49 mmol) and carbon tetrabromide (800 mg, 2.41 mmol) in THF (15 mL). After 1 hour a white precipitate had formed. H₂O (10 mL) was added and the product extracted with diethyl ether. The combined organic extracts were washed with H₂O and brine and dried over MgSO₄. The solution was concentrated to dryness under reduced pressure to give the crude product as a white powder. The pure product was obtained by running through a plug (silica; CH₂Cl₂/hexane; 1:1) and subsequent removal of volatiles *in vacuo*. Yield = 825 mg (100%).

Method 2

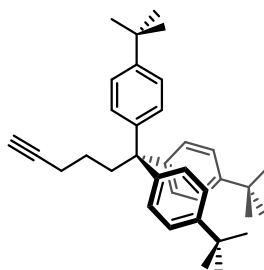
A solution of *n*butyl lithium (4.5 mL, 1.6 M in hexanes) was added dropwise to a solution of **36** (3.0 g, 7.3 mmol) in THF (150 mL) at -78 °C. The solution turned a deep red colour which intensified on warming to room temperature. 1,3-dibromopropane (0.80 mL, 7.3 mmol) was added and the pale-yellow solution stirred for 16 hours. The reaction was then quenched with HCl (5 mL, aq, 2 M) and the crude product was extracted into diethyl ether (80 mL). The organic extracts were washed with HCl (aq, 2 M) and H₂O and dried over MgSO₄. On removal of volatiles *in vacuo* the crude product was obtained as a white solid (630 mg). Purification by column chromatography (silica; CH₂Cl₂/hexane 1:19) and removal of solvents resulted in the desired product as a white powder. Yield = 460 mg (36%).

^1H NMR (500 MHz, CDCl_3): δ 7.26 (d, $^3J_{\text{HH}} = 8.6$, 6H, Ar), 7.17 (d, $^3J_{\text{HH}} = 8.6$, 6H, Ar), 3.35 (t, $^3J_{\text{HH}} = 6.5$, 2H, CH_2Br), 2.77 – 2.57 (m, 2H, $\text{CH}_2\text{C}(\text{Ar})_3$), 1.81 – 1.56 (m, 2H, $\text{CH}_2\text{CH}_2\text{CH}_2$), 1.30 (s, 27H, *t*Bu).

$^{13}\text{C}\{^1\text{H}\}$ NMR (126 MHz, CDCl_3): δ 148.5 (s, Ar{C}), 144.4 (s, Ar{C}), 128.8 (s, Ar{CH}), 124.7 (s, Ar{CH}), 55.1 (s, $\text{C}(\text{Ar})_3$), 39.2 (s, $\text{CH}_2\text{C}(\text{Ar})_3$), 35.1 (s, CH_2Br), 34.4 (s, *t*Bu{C}), 31.5 (s, *t*Bu), 29.1 (s, $\text{CH}_2\text{CH}_2\text{CH}_2$).

Elemental Anal. Calcd for $\text{C}_{34}\text{H}_{45}\text{Br}$ (533.64 $\text{g}\cdot\text{mol}^{-1}$): C, 76.53; H, 8.50; N, 0.00. Found: C, 76.46; H, 8.62; N, 0.00.

6,6,6-tris((para-*tert*-butyl)phenyl)hex-1-yne – 16m



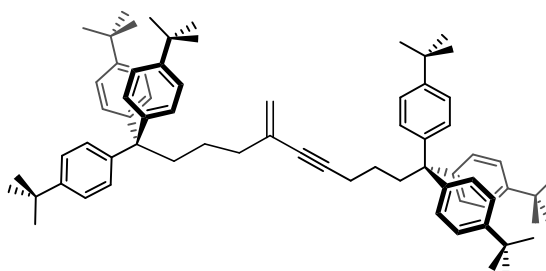
A solution of lithium acetylide (200 mg, 2.25 mmol) in THF (6 mL) and HMPA (0.6 mL) was stirred for 10 minutes. Subsequently, **39** (450 mg, 0.84 mmol) was added and the mixture heated to 65 °C for 3 hours. The reaction was cooled to room temperature and after stirring for 14 hours the solution was passed through a short plug (silica; hexane) to obtain the crude product as a colourless oil. Purification *via* column chromatography (silica; CH_2Cl_2 /hexane 0.5:99.5) and removal of volatiles *in vacuo* gave the desired product as a white powder. Yield = 204 mg (51%).

^1H NMR (500 MHz, CDCl_3): δ 7.25 (d, 6H, $^3J_{\text{HH}} = 8.6$, Ar), 7.18 (d, 6H, $^3J_{\text{HH}} = 8.6$, Ar), 2.69 – 2.55 (m, 2H, CH_2), 2.17 (td, $^3J_{\text{HH}} = 6.9$, $^4J_{\text{HH}} = 2.6$, 2H, CH_2), 1.99 (t, $^4J_{\text{HH}} = 2.6$, 1H, $\text{C}\equiv\text{CH}$), 1.39 – 1.30 (m, 2H, CH_2), 1.30 (s, 27H, *t*Bu).

$^{13}\text{C}\{^1\text{H}\}$ NMR (126 MHz, CDCl_3): δ 148.3 (s, Ar{C}), 144.7 (s, Ar{C}), 128.9 (s, Ar{CH}), 124.6 (s, Ar{CH}), 84.7 (s, $\text{C}\equiv\text{CCH}_2$), 68.6 (s, $\text{HC}\equiv\text{C}$), 55.2 (s, $\text{C}(\text{Ar})_3$), 39.7 (s, $\text{CH}_2\text{C}(\text{Ar})_3$), 34.4 (s, *t*Bu{C}), 31.5 (s, *t*Bu), 24.7 (s, $\text{CH}_2\text{CH}_2\text{CH}_2$), 19.1 (s, $\text{C}\equiv\text{CCH}_2$).

Elemental Anal. Calcd for $\text{C}_{36}\text{H}_{46}$ (478.76 $\text{g}\cdot\text{mol}^{-1}$): C, 90.32; H, 9.68; N, 0.00. Found: C, 90.48; H, 9.67; N, 0.00.

5.4.4. Gem-Ar*CCC(CH₂)Ar* - 18m



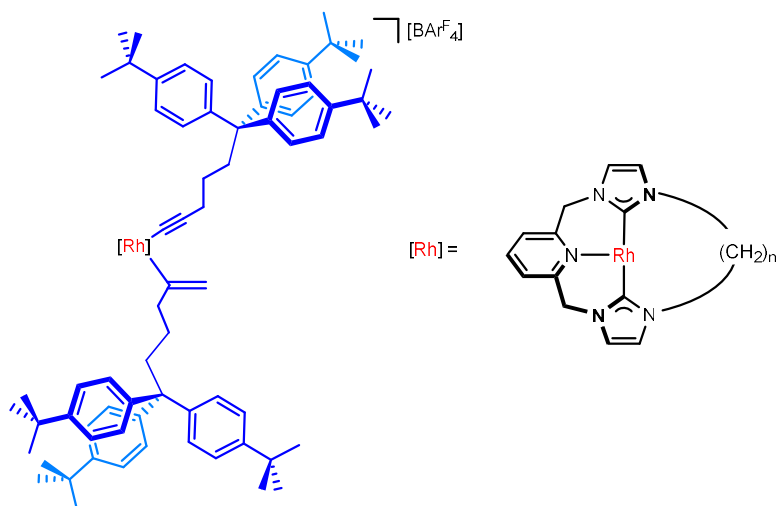
Alkyne **16m** (30 mg, 62 μ mol) was reacted with **11-Me** (4.0 mg, 3.2 μ mol, 5 mol%) in 1, 2-difluorobenzene (2 mL) for 24 hours before being quenched with an atmosphere of CO (1 atm). The reaction was then concentrated to dryness and the crude product extracted into hexane. The product was purified using column chromatography (silica; hexane/CH₂Cl₂, 3:2). Yield = 26.2 mg (87%).

¹H NMR (600 MHz, CDCl₃): δ 7.24 – 7.09 (m, Ar, 24H), 5.26 (d, ²*J*_{HH} = 2.0, 1H, C(CH₂)), 5.09 (d, ²*J*_{HH} = 1.6, 1H, C(CH₂)), 2.64 – 2.56 (m, 2H, CH₂), 2.54 – 2.48 (m, 2H, CH₂), 2.25 (t, ³*J*_{HH} = 6.7, 2H, CH₂), 2.10 (t, ³*J*_{HH} = 7.1, 2H, CH₂), 1.39 – 1.32 (m, 2H, CH₂), 1.28 (s, 27H, *t*Bu), 1.27 (s, 27H, *t*Bu).

¹³C{¹H} NMR (151 MHz, CDCl₃): δ 148.2 (s, Ar{C}), 148.1 (s, Ar{C}), 144.9 (s, Ar{C}), 144.7 (s, Ar{C}), 132.0 (s, C(CH₂)), 129.0 (s, Ar{CH}), 128.9 (s, Ar{CH}), 124.6 (s, Ar{CH}), 124.5 (s, Ar{CH}), 120.1 (s, C(CH₂)), 90.4 (s, C \equiv CAr*), 81.5 (s, C \equiv CAr*), 58.8 (s, CH₂), 55.4 (s, CAr₃), 55.2 (s, CAr₃), 39.8 (s, CH₂), 39.6 (s, CH₂), 38.2 (s, CH₂), 34.5 (s, CH₂), 31.6 (s, *t*Bu), 31.5 (s, *t*Bu), 24.9 (s, *t*Bu{C}), 23.8 (s, *t*Bu{C}), 19.9 (s, CH₂).

Elemental Anal. Calcd for C₇₂H₉₂ (957.53 g·mol⁻¹): C, 90.32; H, 9.68; N, 0.00. Found: C, 90.15; H, 9.53; N, 0.00.

5.4.5. Homocoupling of Ar^{*}CCH through a ring



[Rh(CNC-12)(CCAr^{*})(C(CH₂)Ar^{*})] [BARF₄] – 40-12

A solution of **16m** (9.6 mg, 0.020 mmol) and **11-12** (14 mg, 0.010 mmol) in 1,2-difluorobenzene (0.5 mL) was added to a J. Young's valve NMR tube. The formation of **40-12** was confirmed using *in situ* reaction monitoring by ¹H NMR spectroscopy.

¹H NMR (400 MHz, DiFB): δ 8.18 – 8.09 (m, 8H, Ar^F), 7.62 (t, ³J_{HH} = 7.7, 1H, py), 7.50 (s, 4H, Ar^F), 5.72 (br s, fwhm = 112, 2H, pyCH₂), 4.93 (app. dt, *J* = 14.9, 7.7, 1H, NCH₂), 4.65 (br s, fwhm = *ca.* 180, 1H, C(CH₂)), 4.39 (br s, fwhm = 71, 1H, pyCH₂), 4.09 (br s, fwhm = *ca.* 75, 1H, pyCH₂), 3.93 (app. dt, *J* = 12.5, 5.9, 1H, NCH₂), 3.81 (br s, fwhm = *ca.* 85, 1H, C(CH₂)), 2.44 – 2.37 (m, 2H, CH₂), 2.29 (t, ³J_{HH} = 7.5, 2H, CH₂), 2.19 (t, ³J_{HH} = 7.0, 2H, CH₂), 1.18 (s, 27H, *t*Bu), 1.12 (s, 27H, *t*Bu). *Selected data only.*

HR ESI-MS (positive ion, 4 kV): 1464.9148 [M]⁺ (calcd 1464.9141) *m/z*.

[Rh(CNC-14)(CCAr^{*})(C(CH₂)Ar^{*})] [BARF₄] – 40-14

A solution of **16m** (9.6 mg, 0.020 mmol) and **11-14** (14.3 mg, 0.0100 mmol) in 1,2-difluorobenzene (0.5 mL) was reacted for 4 hours at RT before being concentrated to dryness. The resulting residue was washed with HMDSO to afford the product as an orange powder after thoroughly drying *in vacuo*. Yield = 16 mg (67%). 85% *gem* 15% *E* by ¹H NMR integration of isolated material.

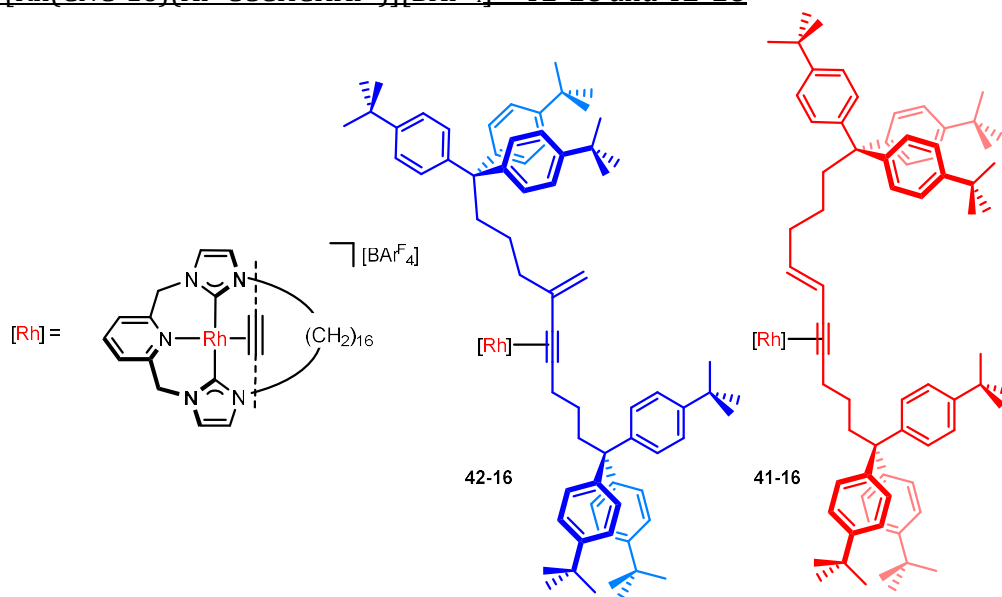
^1H NMR (500 MHz, CD_2Cl_2): δ 7.89 (t, $^3J_{\text{HH}} = 7.7$, 1H, py), 7.74 – 7.70 (m, 8H, Ar^{F}), 7.55 (s, 4H, Ar^{F}), 7.52 (d, $^3J_{\text{HH}} = 7.7$, 1H, py), 7.46 (d, $^3J_{\text{HH}} = 7.7$, 1H, py), 7.32 – 7.08 (m, 27H, Ar + NCH), 7.01 (d, $^3J_{\text{HH}} = 1.9$, 1H, NCH), 5.99 (app. ddd, $J = 12.6, 9.7, 5.4$, 1H, NCH₂), 5.66 (d, $^2J_{\text{HH}} = 15.4$, 1H, pyCH₂), 5.61 (d, $^2J_{\text{HH}} = 15.7$, 1H, pyCH₂), 5.12 (d, $^2J_{\text{HH}} = 15.9$, 1H, pyCH₂), 4.84 (d, $^2J_{\text{HH}} = 15.4$, 1H, pyCH₂), 4.46 (td, $^2J_{\text{HH}} = 13.4$, $^3J_{\text{HH}} = 4.4$, 1H, NCH₂), 4.03 (td, $^2J_{\text{HH}} = 13.2$, $^3J_{\text{HH}} = 4.7$, 1H, NCH₂), 3.70 (s, 1H, C(CH₂)), 3.68 – 3.65 (m, 1H, NCH₂), 3.13 – 3.04 (m, 1H, CH₂), 2.67 – 2.60 (m, 1H, CH₂), 2.62 (s, 1H, C(CH₂)), 2.58 – 2.47 (m, 4H, CH₂), 2.48 – 2.29 (m, 2H, CH₂), 2.22 – 2.09 (m, 1H, CH₂), 2.20 – 2.13 (m, 1H, CH₂), 2.06 – 1.82 (m, 2H, CH₂), 1.81 – 1.63 (m, 2H, CH₂), 1.58 – 1.43 (m, 2H, CH₂), 1.61 – 1.45 (m, 2H, CH₂), 1.46 – 1.13 (m, 12H, CH₂), 1.29 (s, 27H, *t*Bu), 1.28 (s, 27H, *t*Bu), 1.12 – 1.02 (m, 6H, CH₂).

$^{13}\text{C}\{^1\text{H}\}$ NMR (126 MHz, CD_2Cl_2): δ 176.7 (d, $^1J_{\text{RhC}} = 40$, NCN), 175.5 (d, $^1J_{\text{RhC}} = 41$, NCN), 162.3 (q, $^1J_{\text{CB}} = 50$, Ar^{F}), 157.2 (d, $^1J_{\text{RhC}} = 36$, C(CH₂)), 156.9 (s, py), 149.1 (s, *p*-Ar), 149.1 (s, *p*-Ar), 145.3 (s, CAr₃), 145.1 (s, CAr₃), 140.7 (s, py), 135.3 (s, Ar^{F}), 129.5 (qq, $^2J_{\text{FC}} = 32$, $^3J_{\text{CB}} = 3$, Ar^{F}), 129.2 (s, Ar{CH}), 129.2 (s, Ar{CH}), 126.6 (s, py), 125.8 (s, py), 125.2 (s, Ar{CH}), 125.1 (s, Ar{CH}), 125.1 (q, $^1J_{\text{FC}} = 271$, Ar^{F}), 122.6 (s, NCH), 121.8 (s, NCH), 121.6 (s, NCH), 118.0 (sept., $^3J_{\text{FC}} = 4$, Ar^{F}), 113.0 (s, C(CH₂)), 87.5 (d, $^1J_{\text{RhC}} = 57$, C \equiv CCH₂), 68.9 (s, C \equiv CCH₂), 56.1 (s, pyCH₂), 55.8 (s, pyCH₂), 51.7 (s, NCH₂), 50.3 (s, NCH₂), 50.1 (d, $^2J_{\text{RhC}} = 3$, CH₂), 49.7 (s, CH₂), 39.7 (s, CH₂), 34.8 (s, *t*Bu{C}), 34.7 (s, *t*Bu{C}), 31.7 (s, *t*Bu), 31.6 (s, *t*Bu), 29.7 (s, CH₂), 29.7 (s, CH₂), 29.5 (s, CH₂), 29.4 (s, CH₂), 29.3 (s, CH₂), 29.3 (s, CH₂), 29.0 (s, CH₂), 27.8 (s, CH₂), 27.6 (s, CH₂), 27.5 (s, CH₂), 26.0 (s, CH₂), 25.7 (s, CH₂), 25.1 (s, CH₂), 24.0 (s, CH₂), 19.3 (s, CH₂).

HR ESI-MS (positive ion, 4 kV): 1493.9513 [M]⁺ (calcd 1493.9487) *m/z*.

Elemental Anal. Calcd for C₉₃H₉₉BF₂₄N₅Rh·C₆H₁₄ (2443.48 g·mol⁻¹): C, 67.34; H, 6.48; N, 2.87. Found: C, 67.89; H, 6.20; N, 2.83.

[Rh(CNC-16)(Ar*CCCHCHAR*)][BAR^F₄] – **41-16** and **42-16**



A solution of **11-16** (100 mg, 0.069 mmol) and **16m** (80 mg, 0.17 mmol) in 1,2-difluorobenzene (80 mL) was stirred for 18 hours at 65 °C. The resulting red solution was concentrated to dryness and the residue washed with TMS (*ca.* 5 mL). The isolated product mixture was obtained as a red-orange solid on removal of volatiles *in vacuo*. Yield = 138 mg (84%).

Characterisation of **42-16**

¹H NMR (500 MHz, CD₂Cl₂): δ 7.76 – 7.70 (m, 8H, Ar^F), 7.56 (s, 4H, Ar^F), 7.38 (d, ³*J*_{HH} = 7.8, 1H, py), 7.31 (d, ³*J*_{HH} = 7.8, 1H, py), 7.26 (t, ³*J*_{HH} = 7.8, 12H, Ar{CH}), 7.17 (t, ³*J*_{HH} = 8.6, 12H, Ar{CH}), 6.97 (d, ³*J*_{HH} = 1.8, 1H, NCH), 6.94 (d, ³*J*_{HH} = 1.9, 1H, NCH), 6.71 (d, ³*J*_{HH} = 1.9, 1H, NCH), 6.66 (d, ³*J*_{HH} = 1.8, 1H, NCH), 5.62 (s, 1H, C(CH₂)), 5.52 (d, ²*J*_{HH} = 14.6, 1H, pyCH₂), 5.23 (d, ²*J*_{HH} = 14.5, 1H, pyCH₂), 5.03 (s, 1H, C(CH₂)), 4.97 (d, ²*J*_{HH} = 14.6, 1H, pyCH₂), 4.65 (d, ²*J*_{HH} = 14.6, 1H, pyCH₂), 3.86 (app. ddd, *J* = 13.4, 9.6, 5.9, 1H, NCH₂), 3.68 (app. td, *J* = 13.2, 3.8, 1H, NCH₂), 3.35 – 3.26 (m, 1H, NCH₂), 3.21 (app. td, *J* = 12.4, 5.1, 1H, NCH₂), 2.84 (app. ddd, *J* = 16.1, 12.4, 4.5, 1H, CH₂), 2.68 (app. td, *J* = 12.7, 3.9, 1H, CH₂), 2.63 – 2.49 (m, 2H, CH₂), 2.46 – 2.33 (m, 4H, CH₂), 1.76 – 0.94 (m, 32H, CH₂), 1.27 (s, 27H, *t*Bu), 1.26 (s, 27H, *t*Bu).

¹³C{¹H} NMR (126 MHz, CD₂Cl₂): δ 183.8 (d, ¹*J*_{RhC} = 41, NCN), 183.4 (d, ¹*J*_{RhC} = 41, NCN), 162.3 (q, ¹*J*_{CB} = 50, Ar^F), 155.6 (s, py), 155.5 (s, py), 149.2 (s, Ar{C}), 149.2 (s, Ar{C}), 145.1 (s, Ar{CH}), 145.0 (s, Ar{C}), 138.9 (s, py), 136.1 (s, C(CH₂)),

135.4 (s, Ar^F), 129.5 (qq, $^2J_{FC} = 32$, $^2J_{CB} = 3$, Ar^F), 125.2 (q, $^1J_{FC} = 271$, Ar^F), 124.1 (s, py), 123.9 (s, py), 120.9 (s, 2 × NCH), 120.8 (s, NCH), 120.3 (s, NCH), 118.6 (s, C(CH₂)), 118.0 (sept., $^3J_{FC} = 4$, Ar^F), 89.6 (d, $^1J_{RhC} = 14$, C≡CCH₂), 77.3 (d, $^1J_{RhC} = 14$, C≡CCH₂), 56.1 (s, pyCH₂), 56.0 (s, pyCH₂), 55.9 (s, C(Ar₃)), 55.8 (s, C(Ar₃)), 49.7 (s, 2 × NCH₂), 40.8 (s, CH₂), 40.5 (s, CH₂), 37.9 (s, CH₂), 34.8 (s, tBu{C}), 31.8 (s, CH₂), 31.7 (s, tBu), 31.6 (s, tBu), 30.0 (s, CH₂), 29.8 (s, CH₂), 29.5 (s, CH₂), 29.4 (s, CH₂), 29.3 (s, CH₂), 29.3 (s, CH₂), 29.2 (s, CH₂), 29.1 (s, CH₂), 29.0 (s, CH₂), 28.9 (s, CH₂), 28.6 (s, CH₂), 27.0 (s, CH₂), 26.7 (s, CH₂), 26.5 (s, CH₂).

HR ESI-MS (positive ion, 4 kV): 1520.9798 [M]⁺ (calcd 1520.9767) *m/z*.

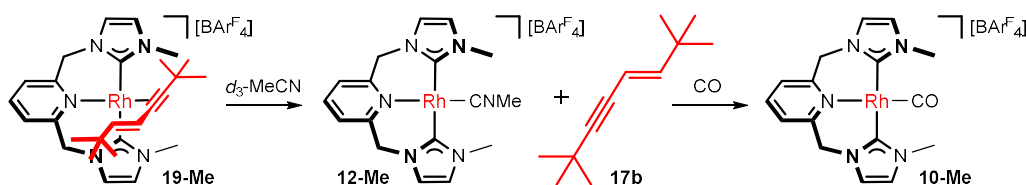
Elemental Anal. Calcd for (2385.35 g·mol⁻¹): C, 66.97; H, 6.21; N, 2.94. Found: C, 66.78; H, 5.98; N, 2.87.

Characterisation of **41-16**

¹H NMR (500 MHz, CD₂Cl₂): δ 7.76 – 7.70 (m, 8H, Ar^F), 7.56 (s, 4H, Ar^F), 6.68 (d, $^3J_{HH} = 1.9$, 1H, NCH), 6.56 (d, $^3J_{HH} = 1.9$, 1H, NCH), 6.31 (dt, $^3J_{HH} = 14.5$, 7.2, 1H, CHCH), 5.95 (d, $^3J_{HH} = 14.9$, 1H, CHCH), 5.54 (d, $^2J_{HH} = 14.2$, 1H, pyCH₂), 5.42 (d, $^2J_{HH} = 14.6$, 1H, pyCH₂), 4.88 (d, $^2J_{HH} = 14.3$, 1H, pyCH₂), 4.79 (d, $^2J_{HH} = 14.6$, 1H, pyCH₂). *Selected data only.*

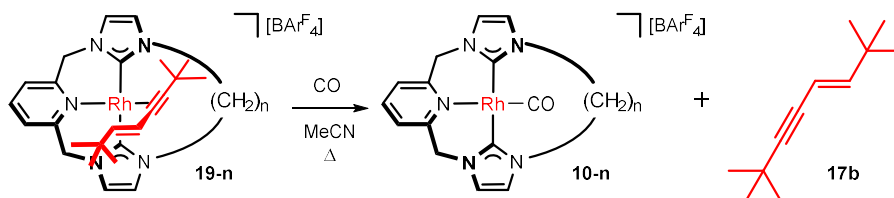
5.4.6. Axle dethreading reactions

[Rh(CNC-Me)(*E*-tBuCCCHCHtBu)][BAR^F₄] – **19-Me**



19-Me (14 mg, 0.010 mmol) was dissolved in *d*₃-MeCN (0.5 mL) and the progress of the reaction determined by ¹H NMR spectroscopy. The NMR taken after 5 minutes showed exclusive formation of **12-Me** and free **17b** through comparison with authentic samples (*vide supra*). The resulting mixture was freeze-pump-thaw degassed and placed under an atmosphere of CO (1 atm) to give the exclusive formation of **10-Me**.

Macrocyclic analogues



General Procedure

A solution of chosen interlocked compound **19-n** (0.01 mmol) in d_3 -MeCN (0.5 mL) in a J. Young's valve NMR tube was freeze-pump-thaw degassed and placed under an atmosphere of CO (1 atm). The sample was then heated at 85 °C and the reaction progress monitored periodically using ^1H NMR spectroscopy through comparison of spectra with spectra obtained of authentic samples of **10-n** and **17b** (d_3 -MeCN, CO). On completion the samples were concentrated to dryness and the resulting yellow residues dissolved in d_3 -MeCN to further confirm the exclusive formation of the carbonyl products.

[Rh(CNC-12)(*E*-*t*BuCCCHCH*t*Bu)][BArF₄]

Compound **19-12** (15.4 mg, 0.0100 mmol) was reacted according to the general procedure for 26 days.

Intermediate 43-12

^1H NMR (300 MHz, d_3 -MeCN, CO): δ 7.92 (t, $^3J_{\text{HH}} = 7.8$, 1H, py), 7.73 – 7.65 (m, 12H, Ar^F), 7.61 (d, $^3J_{\text{HH}} = 7.8$, 2H, py), 7.40 (d, $^3J_{\text{HH}} = 15.2$, 1H, CHCH), 7.17 (s, 2H, NCH), 6.86 (s, 2H, NCH), 6.08 (d, $^3J_{\text{HH}} = 15.4$, 1H, CHCH), 5.52 (d, $^2J_{\text{HH}} = 15.0$, 2H, pyCH₂), 5.35 (d, $^2J_{\text{HH}} = 15.0$, 2H, pyCH₂), 4.00 – 3.72 (m, 4H, NCH₂), 1.87 – 1.37 (m, 20H, CH₂), 1.34 (s, 9H, *t*Bu), 1.04 (s, 9H, *t*Bu).

[Rh(CNC-14)(*E*-*t*BuCCCHCH*t*Bu)][BArF₄]

Compound **19-14** (15.6 mg, 0.0997 mmol) was reacted according to the general procedure for 40 days.

Intermediate 43-14

^1H NMR (300 MHz, d_3 -MeCN, CO): δ 8.04 (t, $^3J_{\text{HH}} = 7.7$, 1H, py), 7.73 – 7.65 (m, 12H, Ar^F), 7.30 (s, 2H, NCH), 7.02 (s, 2H, NCH), 6.53 (d, $^3J_{\text{HH}} = 15.1$, 1H, CHCH), 6.35 (d, $^3J_{\text{HH}} = 15.2$, 1H, CHCH), 5.46 (d, $^2J_{\text{HH}} = 15.1$, 2H, pyCH₂), 5.37 (d, $^2J_{\text{HH}} = 15.1$,

2H, pyCH₂), 3.86 – 3.52 (m, 2H, NCH₂), 1.73 – 1.26 (m, 24H, CH₂), 1.20 (s, 9H, *t*Bu), 1.12 (s, 9H, *t*Bu).

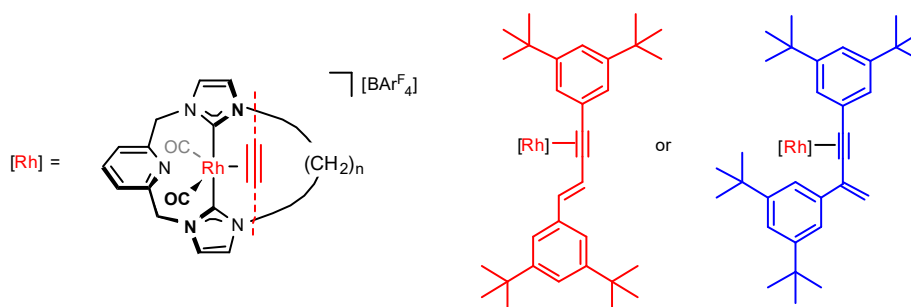
[Rh(CNC-16)(*E*-*t*BuCCCHCH*t*Bu)][BAr^F₄]

Compound **19-16** (15.9 mg, 0.0999 mmol) was reacted according to the general procedure for 1 hour at 85 °C.

Intermediate 43-16

¹H NMR (400 MHz, *d*₃-MeCN, CO): δ 7.93 (t, ³*J*_{HH} = 7.7, 1H, py), 7.73 – 7.65 (m, 12H, Ar^F), 7.30 (d, ³*J*_{HH} = 1.9, 2H, NCH), 7.15 (d, ³*J*_{HH} = 1.9, 2H, NCH), 6.12 (s, 2H, CHCH), 5.14 (s, 2H, pyCH₂), 5.13 (s, 2H, pyCH₂), 4.31 – 4.20 (m, 2H, NCH₂), 4.19 – 3.99 (m, 2H, NCH₂), 1.81 – 1.17 (m, 28H, CH₂), 1.15 (s, 9H, *t*Bu), 0.92 (s, 9H, *t*Bu).

Reactions of 32-*n* and 33-16 with CO



[Rh(CNC-12)(*E*-Ar'CCCHCHAr')(CO)₂][BAr^F₄]

Compound **32-12** (15.9 mg, 0.0883 mmol) was reacted according to the general procedure for 72 hours.

LR ESI-MS (positive ion, 4 kV): 992.5 [M+(CO)₂]⁺ (calcd 992.53) *m/z*.

[Rh(CNC-14)(*E*-Ar'CCCHCHAr')(CO)₂][BAr^F₄]

Compound **32-14** (15 mg, 0.082 mmol) was reacted according to the general procedure for 16 hours.

¹H NMR (400 MHz, *d*₃-MeCN, CO): δ 8.06 (s, 2H, Ar{CH}), 7.96 (t, ³*J*_{HH} = 7.7, 1H, py), 7.73 – 7.65 (m, 12H, Ar^F), 7.30 (s, 2H, NCH), 7.02 (s, 2H, NCH), 6.53 (d, ³*J*_{HH} = 15.1, 1H, CHCH), 6.35 (d, ³*J*_{HH} = 15.2, 1H, CHCH), 5.46 (d, ²*J*_{HH} = 15.1, 2H, pyCH₂), 5.37 (d, ²*J*_{HH} = 15.1, 2H, pyCH₂), 3.86 – 3.52 (m, 2H, NCH₂), 1.73 – 1.26 (m, 24H, CH₂), 1.20 (s, 9H, *t*Bu), 1.12 (s, 9H, *t*Bu).

LR ESI-MS (positive ion, 4 kV): 1020.5 $[M+(CO)_2]^+$ (calcd 1020.56) m/z .



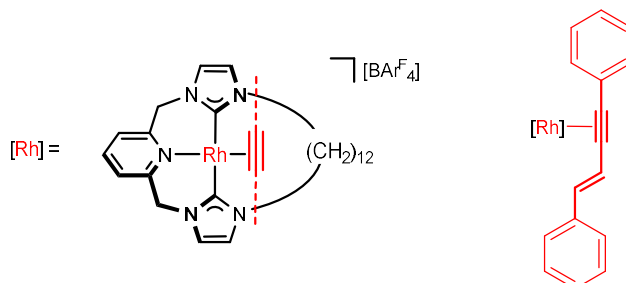
Compound **32-16** (18 mg, 0.097 mmol) was reacted according to the general procedure for 60 hours.

LR ESI-MS (positive ion, 4 kV): 1048.6 $[M+(CO)_2]^+$ (calcd 1048.59) m/z .



Compound **33-16** (18.5 mg, 0.0996 mmol) was reacted according to the general procedure for 60 hours.

LR ESI-MS (positive ion, 4 kV): 1020.6 $[M+CO]^+$ (calcd 1020.60), 1048.6 $[M+(CO)_2]^+$ (calcd 1048.59) m/z .



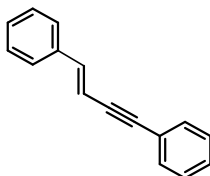
A solution of phenylacetylene **16c** (27.2 μ L, 0.248 mmol) and **11-12** (172 mg, 0.118 mmol) in CH_2Cl_2 (12 mL) was heated to 50 $^{\circ}C$ for 5 hours. The resulting red solution was concentrated to dryness and the resulting residue washed with hexane (10 mL) and dried *in vacuo* to afford the product as a red solid. Yield = 156 mg (84%).

1H NMR (300 MHz, CD_2Cl_2): δ 8.37 (d, $^3J_{HH} = 7.3$, 2H, Ph{CH}), 7.94 (d, $^3J_{HH} = 15.6$, 1H, CHCH), 7.92 (t, $^3J_{HH} = 7.6$, 1H, py), 7.76 – 7.67 (m, 8H, Ar^F), 7.59 (d, $^3J_{HH} = 7.9$, 1H, py), 7.55 (s, 4H, Ar^F), 7.59 (d, $^3J_{HH} = 7.9$, 1H, py), 7.44 – 7.31 (m, 4H, Ph{CH}), 7.27 – 7.16 (m, 4H, Ph{CH}), 7.05 (d, $^3J_{HH} = 15.4$, 1H, CHCH), 7.03 (d, $^3J_{HH} = 1.7$, 1H, NCH), 6.94 (d, $^3J_{HH} = 1.8$, 1H, NCH), 6.67 (d, $^3J_{HH} = 1.7$, 1H, NCH), 6.63 (d, $^3J_{HH} = 1.6$, 1H, NCH), 5.84 (d, $^2J_{HH} = 14.9$, 1H, pyCH₂), 5.81 (d, $^2J_{HH} = 14.7$, 1H, pyCH₂), 5.20 (d, $^2J_{HH} = 14.7$, 1H, pyCH₂), 5.14 (d, $^2J_{HH} = 15.0$, 1H, pyCH₂), 4.13 (app. t, $J = 14$, 2H,

NCH₂), 3.81 – 3.53 (m, 2H, NCH₂), 3.52 – 3.24 (m, 1H, CH₂), 2.05 – 1.81 (m, 4H, CH₂), 1.77 – 1.38 (m, 19H, CH₂).

HR ESI-MS (positive ion, 4 kV): 712.2880 [M]⁺ (calcd 712.2881) *m/z*.

***E*-PhCCCHCHPh – 17c**



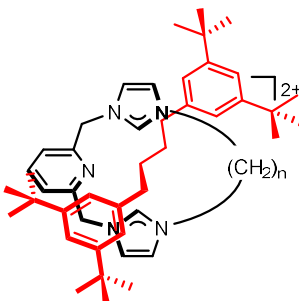
To a solution of **11-12** (172 mg, 118 μmol) in CH₂Cl₂ (12 mL) was added **16c** (27.2 μL, 248 μmol). The resulting orange solution was stirred at 50 °C for 5 hours and then cooled to room temperature. The resulting red solution was concentrated *in vacuo* and the residue washed with cold hexane (*ca.* 10 mL). The residue was then dissolved in MeCN (*ca.* 15 mL), freeze-pump-thaw degassed and placed under an atmosphere of CO (1 atm) and stirred at 85 °C for 16 hours. The solution was concentrated *in vacuo* and the residue extracted through a short plug (alumina; hexane) to afford the product as a white microcrystalline powder. Yield = 20.3 mg (80% / HCCPh, 84% / Rh).

*Data consistent with literature values.*²³

¹H NMR (300 MHz, CDCl₃): δ 7.28 – 7.57 (m, 10H, Ph), 7.05 (d, ³*J*_{HH} = 16.3, 1H, CHCH), 6.39 (d, ³*J*_{HH} = 16.2, 1H, CHCH).

5.4.7. Hydrogenation attempts

General procedure



A solution of chosen interlocked compound in 1,2-difluorobenzene was freeze-pump-thaw degassed and placed under a hydrogen (4 atm) and heated to reflux (95 °C), until complete consumption of starting material indicated by LR ESI-MS.



Compound **32-12** (50 mg, 0.01 mmol) in 1,2-difluorobenzene (3 mL) was reacted according to the general procedure for 48 hours.

LR ESI-MS (positive ion, 4 kV): 418.2 [M-Rh]²⁺ (calcd 417.82), 1698.6 [M-Rh][BAR^F₄]⁺ (calcd 1698.71) *m/z*.



Compound **32-14** (18 mg, 0.01 mmol) in 1,2-difluorobenzene (2 mL) was reacted according to the general procedure for 72 hours.

LR ESI-MS (positive ion, 4 kV): 434.9 [M+(8H)-Rh]²⁺ (calcd 434.86), 1732.6 [M+(8H)-Rh][BAR^F₄]⁺ (calcd 1732.79) *m/z*.



Compound **32-16** (10 mg, 0.01 mmol) in 1,2-difluorobenzene (1 mL) was reacted according to the general procedure for 60 hours.

LR ESI-MS (positive ion, 4 kV): 449.2 [M+(8H)-Rh]²⁺ (calcd 448.88); 1760.8 [M+(8H)-Rh][BAR^F₄]⁺ (calcd 1760.82) *m/z*.



Compound **33-16** (15 mg, 0.01 mmol) in 1,2-difluorobenzene (1 mL) was reacted according to the general procedure for 60 hours.

LR ESI-MS (positive ion, 4 kV): 448.2 [M+(8H)-Rh]²⁺ (calcd 448.88); 1758.7 [M+(6H)-Rh][BAR^F₄]⁺ (calcd 1758.81) *m/z*.

5.5 Crystallographic Data

Crystallographic data for complexes; **4-12**, **6-14**, **6-16**, **7-12**, **8-14**, **9-12**, **9-14**, **11-Me**, **11-12**, **10-Me**, **10-14**, **10-16**, **15-Me**, **19-Me**, **19-14**, **19-16**, **23-Me**, **24a**, **24g**, **26-Me**, **26-12**, **28**, **32-16** and **33-16** were collected on either an Oxford diffraction Agilent SuperNova AtlasS2 CCD diffractometer with either a micro-focus SuperNova Mo K α ($\lambda = 0.71073$) X-ray source or a micro-focus Cu K α ($\lambda = 1.54184$) X-ray source or on an Oxford diffraction xcalibur Gemini Ruby CCD diffractometer with an Enhance Mo K α ($\lambda = 0.71073$) X-ray source and a graphite monochromator and all associated data are summarised in Tables 5.5.1 to 5.5.6.

Data for all structures were collected and reduced using CrysAlisPro. All non-hydrogen atoms were refined anisotropically using SHELXL,²⁴ through the Olex2 interface.²⁵ Hydrogen atoms were placed in calculated positions using the riding model.

For compounds with CCDC codes reported the full crystallographic details are documented in CIF format and have been deposited with the Cambridge Crystallographic Data Centre. These data can be accessed free of charge *via* www.ccdc.cam.ac.uk/data/request/cif

Table 5.5.1.

CCDC/ ID code		4-12	6-14	6-16	7-12	9-12
Figure		2.2.1	-	-	1470497	1849622
Formula		C ₂₅ H ₃₅ N ₅ S ₂	C ₅₉ H ₅₁ BClF ₂₄ N ₅ Pd	C ₆₁ H ₅₅ BClF ₂₄ N ₅ Pd	C ₅₇ H ₄₇ BClF ₂₄ N ₅ Ni	C ₅₈ H ₄₉ BCl ₂ CuF ₂₄ N ₅
<i>M</i>		469.70	1438.71	1466.76	1362.96	1417.27
Crystal system		Monoclinic	Monoclinic	Monoclinic	Triclinic	Monoclinic
Space group		P2 ₁ /c	P2 ₁	P2 ₁ /c	P1	P2 ₁ /c
T / K		150(2)	150(2)	150(2)	150(2)	150(2)
a / Å		17.82145(13)	9.9316(3)	14.73088(16)	9.7990(4)	20.5595(4)
b / Å		6.51664(3)	41.4638(12)	17.04901(19)	14.7487(6)	17.9203(2)
c / Å		23.12534(18)	15.8061(4)	24.9662(3)	21.7093(12)	16.8629(3)
α / °		90	90	90	101.223(4)	90
β / °		111.3725(9)	104.960(3)	98.8059(12)	99.989(4)	99.2412(17)
γ / °		90	90	90	101.393(3)	90
V / Å ³		2500.99(3)	6288.4(3)	6196.27(13)	2942.7(2)	6132.19(17)
Z(Z')		4(1)	4(2)	4(1)	2(1)	4(1)
Density/ gcm ⁻³		1.247	1.520	1.572	1.538	1.535
μ / mm ⁻¹		2.091	3.793	0.459	0.494	2.352
θ range / °		7.1 ≤ θ ≤ 70.07	6.404 ≤ θ ≤ 66.599	2.95 ≤ θ ≤ 29.574	3.233 ≤ θ ≤ 25.682	3.6110 ≤ θ ≤ 72.5320
Reflections collected		35247	58076	115935	13369	10808
R _{int}		0.0315	0.0691	0.0556	0.1528	0.0694
Completeness / %		99.9	99.8	99.9	99.8	99.8
No. of data/restr/param		4728/0/289	22078/3285/1750	17371/382/909	13369/342/858	10808/342/876
R ₁ / I > 2σ(I)		0.0285	1227	0.0424	0.0643	0.0582
wR ₂ / I > 2σ(I)		0.0724	0.3183	0.0953	0.1415	0.1469
R ₁ / all data		0.0303	0.1508	0.0651	0.0811	0.0865
wR ₂ / all data		0.0740	0.3484	0.1053	0.1479	0.1680
Goof		1.020	1.052	1.012	1.048	1.027
F ₀₀₀		1008.0	2896.0	2960.0	1380.0	2864
Largest diff. pk and hole / e Å ⁻³		0.22/-0.27	1.38/-1.00	0.91/-0.46	0.53/-0.47	0.738/-0.545
Flack (x)		n/a	0.51(2)	n/a	n/a	n/a

Table 5.5.2.

8-14		9-14	11-Me ^a	11-12 ^b
CCDC/ ID code	-	-	1849620	1849621
Figure	2.5.1	2.5.2	2.6.1	2.6.1
Formula	C ₅₄ H ₇₈ Br ₄ Cu ₄ N ₁₀	C ₅₉ H ₅₁ BCuF ₂₄ N ₅	C ₄₉ H ₃₃ BF ₂₄ N ₅ Rh	C ₅₉ H ₅₁ BF ₂₄ N ₅ Rh
<i>M</i>	1441.06	1360.40	1261.52	1399.77
Crystal system	Triclinic	Monoclinic	Triclinic	Triclinic
Space group	<i>P</i> 1	C2/c	<i>P</i> 1	<i>P</i> 1
T/ K	150(2)	150(2)	150(2)	150(2)
a/ Å	8.5472(3)	24.5598(4)	12.7811(2)	13.9521(2)
b/ Å	10.9164(4)	24.7381(3)	13.0076(2)	16.3879(2)
c/ Å	16.0160(6)	42.3671(8)	16.4419(4)	17.2510(3)
α/ °	97.990(3)	90	95.0738(17)	108.5400(10)
β/ °	90.817(3)	106.0594(19)	97.8097(17)	110.0690(10)
γ/ °	105.735(3)	90	110.5406(17)	103.4960(10)
V/ Å ³	1422.28(9)	24736.1(7)	2508.53(9)	3242.43(9)
Z(Z')	1(0.5)	16(2)	2(1)	2(1)
Density/ gcm ⁻³	1.682	1.461	1.670	1.434
μ/ mm ⁻¹	4.330	1.531	0.472	0.373
θ range/ °	3.459 ≤ θ ≤ 25.68	6.343 ≤ θ ≤ 70.074	2.8170 ≤ θ ≤ 34.2000	3.5070 ≤ θ ≤ 30.3780
Reflections collected	13254	121686	23237	30484
R _{int}	0.0304	0.0527	0.0307	0.0649
Completeness/ %	95.4	99.8	99.9	99.8
No. of data/restr/param	5164/0/325	23472/1153/1788	10248/540/835	13255/ 524/ 872
R ₁ / I > 2σ(I)	0.0273	0.0488	0.0357	0.0429
wR ₂ / I > 2σ(I)	0.0540	0.1197	0.0907	0.1060
R ₁ / all data	0.0372	0.0658	0.0405	0.0523
wR ₂ / all data	0.0575	0.1321	0.0940	0.1117
Goof	1.035	1.021	1.039	1.030
F ₀₀₀	728.0	11040.0	1256	1412
Largest diff. pk and hole/ e Å ⁻³	0.40/-0.42	0.60/-0.48	0.744/-0.466	0.728/-0.499
Flack (x)	n/a	n/a	n/a	n/a

a) Crystals grown by Dr Rhiann Andrew; b) Crystals grown by Dr Matthew Gyton

Table 5.5.3.

	10-Me ^a	10-14	10-16	15-Me	26-Me
CCDC/ID code	1849623	-	-	1849624	-
Figure	2.6.3	2.6.2	2.6.2	3.2.1	3.4.4
Formula	C ₄₈ H ₂₉ BF ₂₄ N ₅ ORh	C ₆₀ H ₅₁ BF ₂₄ N ₅ ORh	C ₆₂ H ₅₅ BF ₂₄ N ₅ ORh	C ₄₉ H ₃₅ BF ₂₄ N ₅ ORhS	C ₅₄ H ₃₇ BF ₂₄ N ₅ Rh
<i>M</i>	1261.48	1427.78	1455.83	1311.60	1325.60
Crystal system	Triclinic	Monoclinic	Triclinic	Triclinic	Monoclinic
Space group	<i>P</i> 1	<i>P</i> 2 ₁	<i>P</i> 1	<i>P</i> 1	<i>C</i> 2/ <i>c</i>
<i>T</i> / K	150(2)	150(2)	150(2)	150(2)	150(2)
<i>a</i> / Å	12.4768(2)	9.76168(12)	10.02760(17)	12.3645(2)	16.95902(18)
<i>b</i> / Å	13.1965(3)	41.8114(6)	15.9101(2)	13.2233(2)	18.45666(19)
<i>c</i> / Å	16.2071(4)	15.70553(18)	42.1004(7)	18.5030(4)	34.7576(3)
α / °	93.7157(17)	90	89.6838(12)	76.3934(17)	90
β / °	99.2679(16)	104.4405(12)	84.9118(14)	78.8007(17)	98.7133(10)
γ / °	107.8854(17)	90	74.5895(13)	77.7247(15)	90
<i>V</i> / Å ³	2487.76(9)	6207.69(14)	6448.55(18)	2839.80(10)	10753.81(19)
<i>Z</i> (<i>Z'</i>)	2(1)	4(2)	4(2)	2(1)	8(1)
Density / g cm ⁻³	1.684	1.528	1.500	1.534	1.638
μ / mm ⁻¹	0.477	3.279	3.168	0.456	0.444
θ range / °	3.1160 ≤ θ ≤ 34.0210	6.352 ≤ θ ≤ 70.075	6.334 ≤ θ ≤ 66.6	3.7990 ≤ θ ≤ 34.3110	3.032 ≤ θ ≤ 29.574
Reflections collected	23690	73127	24216	31197	128904
<i>R</i> _{int}	0.0295	0.0403	0.2812	0.0324	0.0385
Completeness / %	99.9	99.8	99.2	99.8	99.9
No. of data/restr/param	10163/612/807	23372/1103/1782	24216/3102/1888	11598/639/883	15104/540/880
<i>R</i> ₁ / <i>I</i> > 2 σ (<i>I</i>)	0.0398	0.0686	0.1327	0.0346	0.0519
<i>wR</i> ₂ / <i>I</i> > 2 σ (<i>I</i>)	0.1009	0.1759	0.3341	0.0885	0.1098
<i>R</i> ₁ / all data	0.0443	0.0694	0.1433	0.0381	0.0573
<i>wR</i> ₂ / all data	0.1042	0.1766	0.3406	0.0910	0.1126
Goof	1.045	1.064	1.043	1.036	1.145
<i>F</i> ₀₀₀	1252	2880.0	2944.0	1308	5296.0
Largest diff. pk and hole / e Å ⁻³	0.837/-0.602	1.22/-0.67	1.43/-2.13	0.785/-0.555	0.80/-0.86
Flack (<i>x</i>)	n/a	0.468(10)	n/a	n/a	n/a

a) Crystals grown by Dr Rhiann Andrew

Table 5.5.4.

CCDC/ ID code		24g	24a	23-Me	28	19-Me
Figure		3.4.2	3.4.2	3.3.5	3.4.6	3.3.2
Formula	$C_{32}H_{16}F_8$	$C_{64}H_{88}$	$C_6H_{39}BF_{24}N_7Rh$	$C_{60}H_{51}BCl_2F_{24}N_5Rh$		
<i>M</i>	552.45	857.34	1439.71	1536.81		1482.68
Crystal system	Triclinic	Triclinic	Triclinic	Triclinic	Triclinic	Monoclinic
Space group	<i>P</i> 1	<i>P</i> 1	<i>P</i> 1	<i>P</i> 1	<i>P</i> 1	<i>C</i> c
T/ K	150(2)	150(2)	150(2)	150(2)	150(2)	150(2)
a/ Å	10.7497(5)	14.6350(7)	12.9083(7)	13.01044(8)	19.4406(3)	
b/ Å	11.1750(4)	18.1373(9)	14.2464(8)	20.05043(13)	17.1714(3)	
c/ Å	11.5688(3)	22.0161(10)	20.1480(15)	26.99316(16)	19.5160(3)	
$\alpha/^\circ$	96.962(2)	79.631(4)	74.898(6)	90.7652(5)	90	
$\beta/^\circ$	96.945(3)	75.201(4)	79.351(5)	97.9088(5)	103.0795(16)	
$\gamma/^\circ$	116.711(4)	74.120(4)	89.459(4)	106.6364(5)	90	
V/ Å ³	1207.93(8)	5396.2(5)	3512.7(4)	6672.31(7)	6345.89(18)	
Z(Z')	2(1)	4(2)	2(1)	4(2)	4(1)	
Density/ gcm ⁻³	1.519	1.055	1.361	1.530	1.552	
μ / mm ⁻¹	1.138	0.431	2.905	3.124	0.467	
θ range/ °	6.556 $\leq \theta \leq$ 70.071	6.326 $\leq \theta \leq$ 66.598	6.433 $\leq \theta \leq$ 39.96	6.421 $\leq \theta \leq$ 70.075	3.197 $\leq \theta \leq$ 29.572	
Reflections collected	20046	31197	9021	208069	99593	
<i>R</i> _{int}	0.0412	0.0864	0.0402	0.0294	0.0304	
Completeness/ %	99.8	99.8	97.8	99.8	99.9	
No. of data/restr/param	4575/0/361	31197/90/1202	4155/1977/1045	25285/1785/2237	17717/602/969	
<i>R</i> ₁ / <i>I</i> > 2 σ (<i>I</i>)	0.0400	0.1066	0.0997	0.0348	0.0383	
w <i>R</i> ₂ / <i>I</i> > 2 σ (<i>I</i>)	0.1068	0.2653	0.2466	0.0901	0.0953	
<i>R</i> ₁ / all data	0.0466	0.1246	0.1176	0.0363	0.0415	
w <i>R</i> ₂ / all data	0.1124	0.2812	0.2619	0.0918	0.0976	
Goof	1.032	1.106	1.040	1.015	1.025	
<i>F</i> ₀₀₀	560.0	1888.0	1440.0	3084.0	2984.0	
Largest diff. pk and hole/ e Å ⁻³	0.27/-0.22	1.02/-0.34	2.95/-0.71	0.78/-0.55	0.67/-0.48	
Flack (x)	n/a	n/a	n/a	n/a	-0.023(19)	

Table 5.5.5.

	26-12	19-14	19-16	32-16	33-16
CCDC/ ID code	-	-	-	-	-
Figure	3.4.4	4.2.2	4.2.2	4.3.3	4.3.3
Formula	C ₆₇ H ₆₂ BF ₂₄ N ₅ Rh	C ₇₁ H ₇₁ BF ₂₄ N ₅ Rh	C ₇₆ H ₈₂ BF ₂₄ N ₅ Rh	C ₉₃ H ₉₉ BF ₂₄ N ₅ Rh	C ₉₃ H ₉₉ BF ₂₄ N ₅ Rh
<i>M</i>	1506.93	1564.04	1635.18	1856.49	1856.49
Crystal system	Triclinic	Monoclinic	Triclinic	Triclinic	Triclinic
Space group	<i>P</i> 1	<i>P</i> 2 ₁ / <i>c</i>	<i>P</i> 1	<i>P</i> 1	<i>P</i> 1
<i>T</i> / K	150(2)	150.03(10)	150(2)	150(2)	150(2)
<i>a</i> / Å	11.7452(4)	20.0457(10)	13.08351(16)	15.87677(19)	17.21212(14)
<i>b</i> / Å	16.7896(5)	18.9314(7)	15.17260(17)	18.4083(2)	18.05180(16)
<i>c</i> / Å	18.5777(7)	19.6860(7)	20.1851(2)	18.9532(2)	18.19599(18)
α / °	84.062(3)	90	98.9729(9)	110.0871(12)	60.6826(9)
β / °	73.668(3)	107.089(5)	105.9301(10)	96.1227(10)	66.6042(8)
γ / °	70.038(3)	90	93.7107(10)	113.3779(12)	80.9541(7)
<i>V</i> / Å ³	3304.3(2)	7140.8(5)	3781.46(8)	4581.78(11)	4519.37(8)
<i>Z</i> (<i>Z'</i>)	2(1)	4(1)	2(1)	2(1)	2(1)
Density/ gcm ⁻³	1.515	1.455	1.436	1.346	1.364
μ / mm ⁻¹	3.100	2.890	2.753	2.339	2.371
θ range/ °	6.653 ≤ θ ≤ 70.076	6.509 ≤ θ ≤ 39.972	6.567 ≤ θ ≤ 70.076	6.331 ≤ θ ≤ 70.074	6.393 ≤ θ ≤ 70.076
Reflections collected	39054	22281	74217	96691	176178
<i>R</i> _{int}	0.564	0.2119	0.0321	0.0554	0.0417
Completeness/ %	99.7	98.9	99.9	99.8	99.8
No. of data/restr/param	12524/1045/1108	4285/1716/1037	14343/723/1109	17357/2014/1414	17125/1187/1362
<i>R</i> ₁ / <i>I</i> > 2 σ (<i>I</i>)	0.0561	0.0977	0.0357	0.0563	0.0469
<i>wR</i> ₂ / <i>I</i> > 2 σ (<i>I</i>)	0.1408	0.2548	0.0940	0.1515	0.1317
<i>R</i> ₁ / all data	0.0676	0.1281	0.0369	0.0606	0.0494
<i>wR</i> ₂ / all data	0.1481	0.2827	0.0951	0.1566	0.1353
Goof	1.036	1.059	1.058	1.035	1.037
<i>F</i> ₀₀₀	1530.0	3192.0	1678.0	1916.0	1916.0
Largest diff. pk and hole/ e Å ⁻³	0.76/-1.96	0.81/-0.95	1.09/-0.83	1.21/-0.72	0.92/-0.56
Flack (<i>x</i>)	n/a	n/a	n/a	n/a	n/a

5.6 References

- 1 W. E. Buschmann, J. S. Miller, K. Bowman-Jamoes and C. N. Miller, in *Inorg. Synth.*, John Wiley & Sons, Ltd, 2002, pp. 83–91.
- 2 R. Cramer, J. A. McCleverty and J. Bray, in *Inorg. Synth.*, John Wiley & Sons, Ltd, 1990, pp. 86–88.
- 3 J. A. McCleverty, G. Wilkinson, L. G. Lipson, M. L. Maddox and H. D. Kaesz, in *Inorg. Synth.*, John Wiley & Sons, Ltd, 2007, pp. 84–86.
- 4 S. Gründemann, M. Albrecht, J. A. Loch, J. W. Faller and R. H. Crabtree, *Organometallics*, 2001, **20**, 5485–5488.
- 5 R. Zhang, X. Hao, X. Li, Z. Zhou, J. Sun and R. Cao, *Cryst. Growth Des.*, 2015, **15**, 2505–2513.
- 6 H. W. Gibson, S. H. Lee, P. T. Engen, P. Lecavalier, J. Sze, Y. X. Shen and M. Bheda, *J. Org. Chem.*, 1993, **58**, 3748–3756.
- 7 N. V. Shvydkiy, E. A. Trifonova, A. M. Shved, Y. V. Nelyubina, D. Chusov, D. S. Perekalin and A. R. Kudinov, *Organometallics*, 2016, **35**, 3025–3031.
- 8 M. Zarska, F. Novotny, F. Havel, M. Sramek, A. Babelova, O. Benada, M. Novotny, H. Saran, K. Kuca, K. Musilek, Z. Hvezdova, R. Dzijak, M. Vancurova, K. Krejciakova, B. Gabajova, H. Hanzlikova, L. Kyjaccova, J. Bartek, J. Proska and Z. Hodny, *Bioconjug. Chem.*, 2016, **27**, 2558–2574.
- 9 R. E. Andrew and A. B. Chaplin, *Dalton Trans.*, 2014, **43**, 1413–1423.
- 10 R. Patchett, R. C. Knighton, J. D. Mattock, A. Vargas and A. B. Chaplin, *Inorg. Chem.*, 2017, **56**, 14345–14350.
- 11 R. E. Andrew, C. M. Storey and A. B. Chaplin, *Dalton Trans.*, 2016, **45**, 8937–8944.
- 12 R. E. Andrew and A. B. Chaplin, *Inorg. Chem.*, 2015, **54**, 312–322.
- 13 G. Oss, J. Ho and T. V. Nguyen, *Eur. J. Org. Chem.*, 2018, **2018**, 3974–3981.
- 14 S. Ventre, E. Derat, M. Amatore, C. Aubert and M. Petit, *Adv. Synth. Catal.*, 2013, **355**, 2584–2590.
- 15 C. Yang and S. P. Nolan, *J. Org. Chem.*, 2002, **67**, 591–593.
- 16 C. Jahier, O. V. Zatolochnaya, N. V. Zvyagintsev, V. P. Ananikov and V. Gevorgyan, *Org. Lett.*, 2012, **14**, 2846–2849.
- 17 C. Moberg and C. Moberg, *Org. Lett.*, 2008, **10**, 2505–2508.
- 18 C. Xu, W. Du, Y. Zeng, B. Dai and H. Guo, *Org. Lett.*, 2014, **16**, 948–951.
- 19 R. E. Islas, J. Cárdenas, R. Gaviño, E. García-Ríos, L. Lomas-Romero and J. A. Morales-Serna, *RSC Adv.*, 2017, **7**, 9780–9789.
- 20 S. Moulin, H. Dentel, A. Pagnoux-Ozherelyeva, S. Gaillard, A. Poater, L. Cavallo, J.-F. Lohier and J.-L. Renaud, *Chem. Eur. J.*, 2013, **19**, 17881–17890.
- 21 R. E. Andrew, University of Warwick, 2016.
- 22 C. M. Storey, M. R. Gyton, R. E. Andrew and A. B. Chaplin, *Angew. Chem. Int. Ed.*, 2018, **57**, 12003–12006.
- 23 M. J. Dabdou, V. B. Dabdou and J. V. Comasseto, *Tetrahedron Lett.*, 1992, **33**, 2261–2264.
- 24 G. Sheldrick, *Acta Crystallogr. Sect. A*, 2008, **64**, 112–122.
- 25 O. V. Dolomanov, L. J. Bourhis, R. J. Gildea, J. A. K. Howard and H. Puschmann, *J. Appl. Crystallogr.*, 2009, **42**, 339–341.

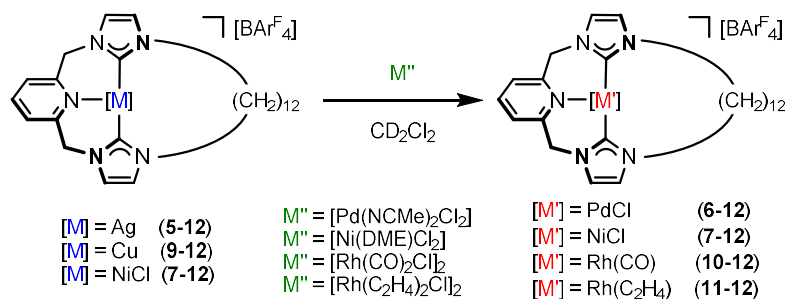
Chapter 6 – Summary of findings

The objective of this project was to elucidate the mechanistic organometallic chemistry of terminal alkyne dimerisation reactions, promoted by a series of rhodium CNC pincer complexes, with the ultimate aim of using this reaction for the formation of mechanically interlocked molecules. Through comparison of the chemistry of acyclic and macrocyclic variants, a number of factors which influence the selectivity of alkyne homocoupling reactions have been identified.

6.2 Chapter 2

This chapter begins by outlining the synthesis and coordination chemistry of macrocyclic NHC-based pincer proligands **3-14** and **3-16**, which feature a lutidine backbone tethered by tetradecamethylene and hexadecamethylene spacers, respectively. The corresponding palladium(II) chloride complexes (**6-n**; $n = 14, 16$) notably extend a previously described homologous series ($n = 8, 10, 12$).¹ Examination of the solution dynamics and solid-state structures of **6-14** and **6-16** highlights their expanded apertures relative to the smaller ringed congeners, comfortably accommodating the chloride ligand with additional space to spare. This indicates that that they are well suited to performing reactions within the macrocyclic interior.

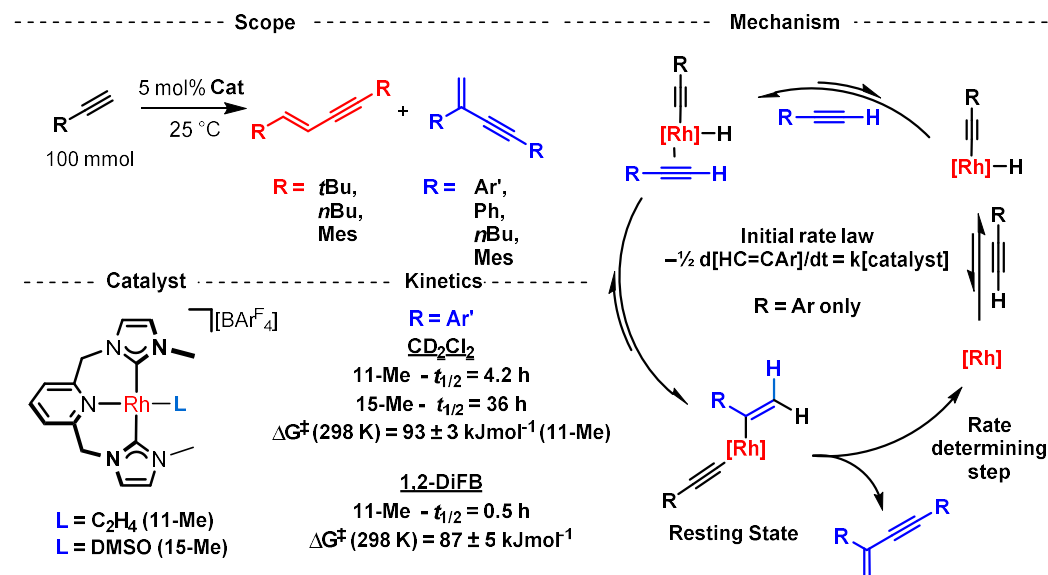
Transmetallation studies evaluating the effectiveness of Ag(I), Cu(I) and Ni(II) complexes for the formation of a range of d^8 -metal complexes (Scheme 6.2.1) identified copper complexes (*viz.* **9-12**) as being well suited for the transfer of CNC pincer ligands to Rh(I). A mild procedure was subsequently developed for the preparation of labile Rh(I) ethylene complexes **11-n** ($n = \text{Me}, 12, 14, 16$). Avoiding difficulties associated with more traditional silver-based transfer agents, this methodology has significant potential for achieving carbene complexation to synthetically challenging metal fragments. Indeed, this strategy has been employed in the group for the isolation of five-coordinate rhodium and iridium biphenyl complexes.²



Scheme 6.2.1. Transmetalation studies of complexes of a CNC macrocycle

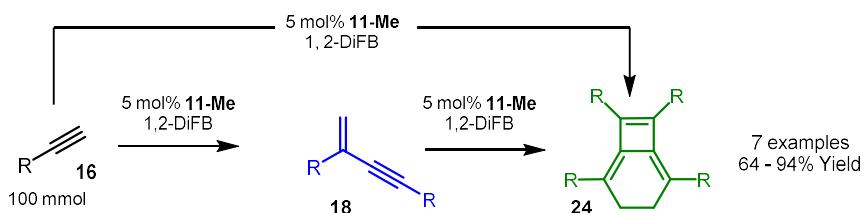
6.3 Chapter 3

This chapter focuses on the catalytic performance of acyclic complex **11-Me** in terminal alkyne homocoupling reactions (Scheme 6.3.1). Following brief examination of the scope of this reaction, detailed mechanistic investigations focused on $\text{Ar}'\text{C}\equiv\text{CH}$ ($\text{Ar}' = 3,5\text{-di}(\text{tert-butyl})\text{phenyl}$), that exclusively results in the corresponding *gem*-enyne product, were conducted. Performing this reaction using the weakly coordinating 1,2-difluorobenzene solvent leads to a marked improvement in catalyst stability and an order of magnitude rate enhancement relative to CH_2Cl_2 . This observation is reconciled by solvent coordination to the Rh(III) alkenyl alkynyl resting state, which attenuates subsequent reductive elimination. The result of kinetic investigations and intermediate trapping experiments confirm that the reaction proceeds *via* a hydrometallation pathway with a rate-limiting reductive elimination step.



Scheme 6.3.1. Summary of terminal alkyne coupling reactions using **11-Me** and **15-Me**

During these mechanistic investigations, additional metal catalysed reactivity of the aromatic *gem*-enynes products was discovered, involving an unusual annulation into bicyclo[4.2.0]octa-1,5,7-trienes (Scheme 6.3.2). Investigation into the scope of this step, whilst not exhaustive, found it to be tolerant to a variety of substituents in either the *meta* or *para* positions of the aromatic ring, but inoperative for alkyl alkynes.



Scheme 6.3.2. Tetramerisation of terminal aryl alkynes catalysed by **11-Me**

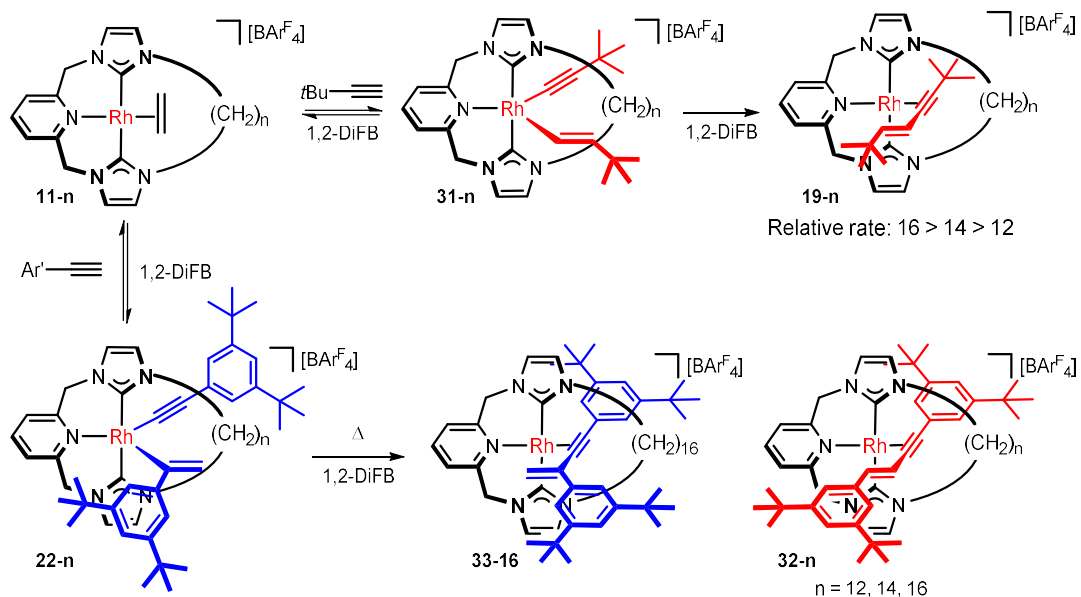
Kinetic modelling of the combined tandem reaction sequence indicates a first-order dependence in enyne and second-order dependence in metal for the annulation step. Using a range of reaction mimics in conjunction with computational simulations, a plausible mechanism has been proposed. The auto-tandem catalytic behaviour of **11-Me** is believed to be enabled by facile isomerisation between *fac* and *mer* coordination modes of the flexible pincer ancillary. The promotion of mechanistically distinct transformations autonomously in this way, represents a new and potentially widely applicable concept for tandem catalysis.

6.4 Chapter 4

Following the findings highlighted above and previous investigations in the Chaplin group, the last chapter details the exploration of terminal alkyne dimerisation reactions using macrocyclic congeners **11-n** ($n = 12, 14, 16$). Using alkynes bearing sterically cumbersome stoppering groups, *t*Bu and Ar', this reaction was found to be an effective active metal template approach for the formation of a series of rotaxanates **19-n** and **32-n**, which have been characterised both in solution and the solid-state (Scheme 6.4.1).

Notably, reaction of macrocyclic complexes **11-n** with Ar'C≡CH led to exclusive formation of Rh(III) alkenyl alkynyl intermediates **22-n** for all ring sizes ($n = 12,$

14, 16) in-line with the catalytic process (*vide supra*). However, contrasting **22-Me**, onwards reactivity of **22-12** and **22-14** showed orthogonal selectivity, generating the corresponding interlocked *E*-enyne products **32-12** and **32-14**. Exhibiting comparable electronic profiles across the ligand series, it has been concluded that the modifications in ligand topology, brought about by the presence of the macrocyclic tether, are responsible for perturbing the direct reductive elimination step and thus enforcing this switch in selectivity.



Scheme 6.4.1. Terminal alkyne coupling reactions through rings

It was thought that expansion of the macrocyclic annulus would reduce the steric congestion at the metal centre and therefore related metal-based reactivity would start to emulate the acyclic congener. Indeed, reductive elimination in the largest ring system saw the formation of a mixture of the two isomers (47% *E* and 53% *gem*). These results represent a proof-of concept demonstration of how metal-based reactivity can be controlled or adapted by augmentation in the periphery of the metal coordination sphere.

The presence of a robust mechanical bond in rotaxanates **32-n** and **33-16** was confirmed using axle dethreading studies, highlighting the potential of terminal alkyne coupling reactions for the successful active metal templated syntheses of interlocked molecules. To this end, a trityl terminated alkyne featuring a flexible propylene linker between the alkyne functionality and the bulky stopper group

was prepared and its reactivity explored. Unfortunately, the spatial confinement of the smaller macrocycles ($n < 16$) prevented direct reductive elimination of the *gem*-isomer and unlike **22-n** these systems were unable to isomerise to allow the alternate reductive elimination of the *E*-enyne product. Only with the largest was reductive elimination observed, but a mixture of interlocked *E*- and *gem*-enyne products was obtained. Reflecting on these results, it would appear that whilst **11-n** do enable C(sp)–C(sp²) bond formation reaction to be conducted through the macrocyclic annuli, high selectivity is limited to specific combinations of alkyne and ring size. In some cases these systems offer a trade-off between activity and selectivity, with the larger ring permitting a broader scope of interlocked species at the expense of the high selectivity evoked by the smaller rings.

With subtle changes in the alkyne functionality and ligand ring size influencing the selectivity of these reactions, the universal applicability of this methodology in combination with the CNC macrocycles used in this investigation is improbable. Nevertheless, with a number of pincer complexes reported to catalyse this transformation selectively, terminal alkyne coupling has undoubted potential for the active template formation of supramolecular structures comprising a pincer macrocycle and an interlocked hydrocarbon axle. Indeed, work within the Chaplin group is currently exploring the use of the terminal alkyne dimerisation approach in the formation of interlocked architectures featuring phosphine-based macrocycles.

References

- 1 R. E. Andrew and A. B. Chaplin, *Dalton Trans.*, 2014, **43**, 1413–1423.
- 2 M. R. Gyton, B. Leforestier and A. B. Chaplin, *Organometallics*, 2018, **37**, 3963–3971.